



**Improved biosensing applications using
lab-on-a-chip and other platforms**

Mariana Medina Sánchez

PhD Thesis

PhD in Biotechnology

Directors:

Prof. Arben Merkoçi and Dr. Sandrine Miserere

Department of Genetic and Microbiology

Bioscience Faculty

2013

The present work entitled “Improved biosensing applications using lab-on-a-chip and other platforms”, presented by Mariana Medina Sánchez to obtain the degree of doctor by Universitat Autònoma de Barcelona, was performed at the Nanobioelectronics and Biosensors Group in the Institut Català de Nanociència i Nanotecnologia (ICN2), under the supervision of Prof. Arben Merkoçi, ICREA Professor and Group Leader, and Dr. Sandrine Miserere.

Bellaterra, September 2013

The supervisors

Prof. Arben Merkoçi

Dr. Sandrine Miserere

The present thesis was performed also under the doctoral program studies “Doctorado en Biotecnología” at Faculty of Biosciences, Universitat Atunònoma de Barcelona, under the tutorship of Professor Antonio Villaverde.

The University tutor

Prof. Antonio Villaverde Corrales

The present PhD Thesis was carried out at Nanobioelectronics and Biosensors Group at Catalan Institute of Nanoscience and Nanotechnology (ICN2) under the doctoral program of Biotechnology at Autonomous University of Barcelona (UAB). The research work accomplished, resulted in several publications and manuscripts that were submitted to international peer-reviewed scientific journals, and also in a book chapter by invitation of the editor.

“New trends in DNA sensors for environmental applications. Nanomaterials, miniaturization and lab-on-a-chip technology”. A. de la Escosura, M. Medina-Sánchez, and A. Merkoçi. *Nucleic Acid Biosensors for Environmental Monitoring, Editorial: Royal Society of Chemistry (Ed. I. Palchetti and M. Mascini)*. Chapter 8, **2011**, 143-166.

“Micro and nanomaterials based detection systems applied in lab-on-a-chip technology”. M. Medina-Sánchez, and A. Merkoçi. *Handbook of Green Analytical Chemistry (Ed. M. de la Guardia and S. Garrigues)*, John Wiley & Sons, Ltd, Chichester, UK. Chapter 18, **2011**, DOI 10.1002/9781119940722.

“Nanomaterials and lab-on-a-chip technologies”. M. Medina-Sánchez, S. Miserere, and Arben Merkoçi, *Lab Chip*, **2012**, 12, 1932-1943. Impact factor: 5.67.

“On-chip electrochemical detection of CdS quantum dots using normal and multiple recycling flow through modes”. M. Medina-Sánchez, S. Miserere, S. Marín, G. Aragay, and A. Merkoçi. *Lab Chip*, **2012**, 12, 2000–2005. Impact factor: 5.67.

“On-chip electrochemical detection of Alzheimer’s disease biomarker using QDs as labels in a magneto-immunoassay”, M. Medina-Sánchez, S. Miserere, E. Morales, and A. Merkoçi, *Submitted*, **2013**.

“Electrochemical determination of atrazine by magnetoimmunoassay strategy with Pt-NPs modified boron-doped diamond electrode integrated into microfluidic platform”. M. Medina-Sánchez, C. Mayorga, W. Takeshi, I. Tribidasari, Y. Einaga and A. Merkoçi. *Submitted*, **2013**.

“Inkjet printed FET for biosensing applications”. M. Medina-Sánchez, C. Martínez-Domingo, E. Ramón, S. Miserere, A. Alcalde-Aragón, J Carrabina and A. Merkoçi. *16th International Conference on Miniaturized Systems for Chemistry and Life Sciences MICROTAS*, Okinawa, Japan, **2012**, 1837-1839.

Additional publications and manuscripts for annexes:

“Paper-based electrodes for nanoparticles detection”, C. Parolo, M. Medina-Sánchez, H. Montón, A. de la Escosura and A. Merkoçi. *Part. Part. Syst. Charact.*, **2013**, 30, 662–666.

“Simple paper architecture modifications lead to enhanced sensitivity in nanoparticle based lateral flow immunoassay”, C. Parolo, M. Medina-Sánchez, A. de la Escosura and A. Merkoçi., *Lab Chip*, **2013**, 13, 386-390. Impact factor: 5.67.

“Nano/micromotor Enhanced Microarray Technology for Protein Detection”, E. Morales-Nárvaez, Maria Guix, Mariana Medina-Sánchez, C. Mayorga-Ramírez. *Submitted*, **2013**.

ACKNOWLEDGMENTS

In this section, I would like to thank all the people who have supported me during this Thesis; it has really been a very important stage in my life. I want to express my acknowledgments to all the people who in one way or another have accompanied me during this time.

First of all I would like to thank Prof. Meyya Meyyappan, who was the person who trusted and supported me to continue my PhD studies when we met in Colombia in a Congress. He recommended me the group of Prof. Arben Merkoçi as well as he has been aware of my personal and professional progress. Of course his suggestion to come here was the proper one, because Prof. Arben opened me the doors to his group. He gave me the opportunity to start the PhD in a totally new field for me, he trusted me and he gave me all the support to complete it. Prof Arben has been as a father in this time and for me it has been an honor to be part of his fantastic group, where I have learnt a lot of things, to meet people from different nationalities and cultures and have been part of this great family. Now I can say that there is a big difference since I arrived until now, because I feel I have growth professionally and personally thanks to Prof. Arben's support, suggestions and direction as well as the time shared with my friends and colleagues in the group.

I want to thank also to my group, the Nanobioelectronics & Biosensors group, with whom I lived for about four years. I have learnt from all of you, science, traditions, different ways to think and see the world, and different cultures and it has an invaluable sense. The first day in the group, I remember I met Anna and Marisa; they were very kind, after that I talked with Arben and I felt that everything was amazing but I had also a lot of fear because I faced something totally different and new for me. After that I was feeling more comfortable thanks to all people and especially to Maria and Sergi, who taught me how the lab worked. With them I shared a lot of things. I never will forget our great "metacrilate's team" and our "salsa's tutorial". I want to say some words to each of you for your friendship and shared time. Sandrine: thank you very much for your suggestions and support, though we had our differences, we have learnt a lot from each other and the most important, we have formed a beautiful friendship. Alfredo was a reference to follow for his dedication and research background. Anna, thanks for your work, as Claudio mentioned in his Thesis, you are the motor of the group. Carmen and Lulu, thanks for your friendship, for the afternoons conversations, for the support and words of encouragement in complicated situations, thanks for the lived moments, with you I feel really at home. Miquel, thank you also for your friendship, you are an excellent person, I have learnt a lot from you. You have also listened to me and supported me in my bad moments as well as in the good ones, also thanks for the coffee. Marisol, with your smile you give us gladness everyday. Adaris, the salsa's girl, thanks for your friendship. Eden, the beer's guy thank

you for the shared moments. Helena, we should have worked together from the beginning, I'm sure we would have done amazing things. You are very dedicated and organized person, I have learnt a lot from you and we have taken long chat conversations trying to organize the world. Pino San, I will never forget your quarrels, but I want to tell you that you are a very nice person and also you have a lot of qualities. Luisiño thanks for sharing with me your cheer everyday in the lab. Claudio, as you write to me in your Thesis, you were as a brother in my first years, and we shared a lot of moments, thanks for your friendship. Chamo, since I know you, I'm surprised because you are a very kind person with a very nice and noble personality, you always think in the people and you are the most collaborative person in the group. Bricita thank you very much for your friendship, the moments lived with you and Gillaume, thank you for your advices for helping me when I needed it. Thanks to the people who are not now in the lab, Marisa, Sergi, and Gemma.

I want also thank to the visitors, because I shared a lot of moments and it was for me a pleasure to know all of you: Gina, Pinar, Jihane, Yuki, Serdar1, Serdar2, Misa, Welter, Wilanee, Maelle, Irene, Lenka 1, Lenka2, Anna, Amal, Andrejz, Sevinç, Abdelmoneim, Joan, Natalia, Thiago, Giselle, Erika, Ruslan, André, and Denis.

Also thanks to Rosa, Anabel, Montse, Belen, Carlos, and Marcos for your collaboration and good disposition to help and support me in different things.

Thanks to the Printed Electronics Group – CAIAC, especially to Eloi for your inspiration and for supporting me with the BioFET idea, you are an excellent person, researcher and professor, thank you so much for all the things. I want thanks also to Carme because was a great collaborator and friend, thank you for your important support and the afternoons testing hundreds of BioFETs. Finally thank to Ana for her collaboration in the device fabrication.

I want to express my acknowledgment to the Einaga's group for its hospitality in Japan. Especially thank to Prof. Einaga for your welcome and support. To Takeshi for your friendship and for support me all the time. Also thanks to Ivandinni, for your kindness. Prof. Yamamoto, Dr. Stephane Fierro, Yuki, Akahori, Ai, Namba, Mukuda and all the people for your kindness, really I felt like at home.

A mi familia, que a pesar de la distancia siempre han estado orgullosos de mí y siempre han depositado toda su confianza en mí. A mis amigas Margarita y Lili porque siempre han estado pendientes de mí y son como mis hermanas. A mi tía Consuelo, la artista de la familia, por la preciosa obra de arte que ha pintado para la portada de esta Tesis.

A mi Berg quiero expresarle mi agradecimiento por estar siempre junto a mí, apoyándome en todo momento, brindándome todo su amor y paciencia.

ACKNOWLEDGEMENTS FOR THE FINANCING SUPPORT



Simple and miniaturized micro / nanofluidic platforms are especially interesting due to their advantages like the reduction of sample and reagent volumes, the decrease of the analysis time, the possibility of portability and the integration of conventional analytical techniques. Furthermore it is important to point out the role that nanomaterials can play in terms of enhancing electrochemical properties after being integrated into the microfluidic platform or even in the electrode, where the detection event will be performed. Combined together, nanotechnology, electrochemistry and microfluidics could provide a really powerful biosensor platform, thus in the present Thesis different microfluidic platforms with integrated electrodes as transducers in biosensing applications were evaluated.

General aspects and experimental results are exposed, starting from a General Introduction that describes various aspects related with the use of nanomaterials and lab-on-a-chip technologies as a promising synergy for a wide range of applications. The electrochemical detection of proteins (ex. Apolipoprotein-E, ApoE) by using CdS or CdSe@ZnS Quantum Dots (QDs) as labels has been one of the main objectives of this Thesis. The immunocomplex was performed by using tosylactivated magnetic beads as preconcentration platform into the same microfluidic system.

Due to the need to achieve a lower limit of detection of the immunoassays, different strategies for electrochemical signal enhancing are proposed. The first one is the use of a magnetic field to immobilize magnetic beads in a controllable way into a microfluidic channel in order to obtain a stable magnetic plug where the immunoassay is performed. The second strategy is the use of a home-made recycling system. In this part, the increasing signal of QDs is demonstrated by using an external peristaltic pump connected to a microfluidic chip forming a loop system. After this demonstration, a micro-peristaltic pump with integrated valves is also proposed. All the fabrication steps have been optimized and the software for sequential control of the valves also has been developed. Finally, bismuth is used as it is a well-known material that agglomerates with heavy metals. We took advantages of this property for improving the electrochemical signal of QDs, due to the cadmium content that QDs have in their core. Optimization of the bismuth concentration has been done in order to achieve the highest signal. This detection has been performed in batch system as well as in microfluidic mode.

In addition, another novel platform for electrochemical determination of a pesticide (atrazine) based on magneto-immunoassay using boron-doped diamond (BDD) electrode is presented. BDD electrode has been modified by electroreduction of potassium tetrachloroplatinate (K_2PtCl_4) in order to grow platinum nanoparticles (Pt-NPs) onto the

electrode surface. The immunoassay was based on a direct competitive assay using horseradish peroxidase (HRP) as enzymatic label and magnetic microparticles as preconcentration platform.

A flexible organic double gate Bio-Field Effect Transistor (Bio-FET) developed by inkjet technology onto a flexible substrate is also presented. This kind of organic transducers has important advantages for biosensors in terms of fabrication cost and biocompatibility as well as their integration into microchannels. To demonstrate the applicability of this device in the biological field, its functionalization with a capture antibody, in order to detect a model protein in a label-free mode was performed. The device fabrication, its structure, materials composition optimization, electrical characteristics and other functionalities are also discussed.

Finally, the general conclusions are exposed including some opinions / recommendations for further continuation of the research in the field.

Las plataformas Micro / Nanofluídicas, simples y miniaturizadas son especialmente interesantes debido a sus ventajas como la reducción de los volúmenes de muestra y reactivos, la disminución del tiempo de análisis, la posibilidad de portabilidad y la integración de técnicas analíticas convencionales. Además, es importante señalar el papel que pueden jugar los nanomateriales en términos de mejora de las propiedades electroquímicas después de ser integrados en plataformas microfluídicas, o incluso modificaciones superficiales de los transductores. Así, la combinación de la nanotecnología, la electroquímica y la microfluídica, podría proporcionar una plataforma de detección muy potente, por lo que, en esta Tesis se estudian diferentes dispositivos microfluídicos con transductores electroquímicos integrados para aplicaciones bioanalíticas.

En esta Tesis se exponen también los aspectos generales y los resultados experimentales, a partir de una introducción general, la cual presenta los trabajos más recientes relacionados con el uso de nanomateriales y tecnologías lab-on-a-chip como una sinergia prometedora para una amplia gama de aplicaciones. Después se presenta la detección electroquímica de proteínas mediante el uso de puntos cuánticos como marcadores. En primera instancia, se describe un chip microfluídico híbrido compuesto por una canal de polidimetilsiloxano flexible (PDMS) y policarbonato (PC) como substrato. Este substrato a su vez tiene impreso electrodos serigrafados integrados de carbono (SCPE). El dispositivo desarrollado combina las ventajas de los chips microfluídicos flexibles, tales como su bajo coste, la posibilidad de ser desechables y la susceptibilidad de ser producidos en masa con las ventajas de la electroquímica por su facilidad de integración y la posibilidad de ser miniaturizables. En la segunda parte, se realizó la detección electroquímica de puntos cuánticos como marcadores en un ensayo para la determinación de un biomarcador de la enfermedad de Alzheimer: Apolipoproteína E (ApoE). El inmunocomplejo se llevó a cabo mediante el uso de partículas magnéticas tosilactivadas, las que fueron a su vez utilizadas como plataforma de preconcentración de muestra dentro de un canal microfluídico.

Debido a la necesidad de lograr límites inferiores de detección en inmunoensayos, en esta Tesis se han propuesto diferentes estrategias para mejorar la sensibilidad de los dispositivos. La primera de ellas es el uso de un campo magnético para inmovilizar una mayor cantidad de partículas magnéticas en una disposición controlable dentro de un canal microfluídico con el fin de obtener una zona de precocentración, donde se lleva a cabo el inmunoensayo. La segunda estrategia que se presenta en esta Tesis es el uso de un sistema de reciclaje de fabricación propia. En esta parte, el incremento de la señal de los puntos cuánticos se demuestra mediante el uso de una bomba peristáltica externa conectada a un chip microfluídico que forma un sistema cerrado. Después de esta demostración, se propuso una micro-bomba peristáltica con válvulas integradas. Todas las etapas de fabricación se

optimizaron así como también se desarrolló un software para su control. Por último, el bismuto, que es un material bien conocido para aglomerar los metales pesados, fue usado para aglomerar los puntos cuánticos cuyo núcleo está formado por cadmio II, de esta forma se pudo mejorar la señal electroquímica mediante la reducción de los QDs junto con el Bismuto III. Diferentes optimizaciones fueron hechas usando canales microfluídicos.

Adicionalmente, se presentan otras nueva plataforma basada en diamante dopado con boro, transductor utilizado para la determinación electroquímica de la atrazina basado en el desarrollo de un magneto-inmunoensayo. Este inmunoensayo se realizó mediante un ensayo competitivo con peroxidasa de rábano silvestre (HRP) como marcador enzimático y micropartículas magnéticas como plataforma de preconcentración.

Otra plataforma propuesta es el transistor orgánico de efecto campo de doble puerta, como transductor para biosensores, desarrollado por la tecnología de inyección de tinta sobre un sustrato flexible. Este tipo de transistores orgánicos tiene ventajas importantes para biosensores en términos de coste de fabricación y biocompatibilidad, así como su posibilidad de integración en microcanales. Para demostrar la aplicabilidad de este dispositivo en el campo biológico, se ha funcionalizado su capa externa con un anticuerpo de captura que detecta una proteína modelo sin ningún marcador. Se realiza la fabricación del dispositivo, teniendo en cuenta su estructura, los materiales que lo componen, sus características eléctricas y posibles aplicaciones.

Por último, se exponen las conclusiones generales y futuras propuestas.

GLOSSARY OF TERMS, ACRONYMS AND ABBREVIATIONS

1-ethyl-3-(dimethylaminopropyl)carbodiimide	EDC
3-Aminopropyltriethoxysilane	APTES
Acid orange	AO
Antibody	Ab
Antigen	Ag
Bio organic thin field effect transistor	BioOTFT
Bio thin field effect transistor	BioTFT
Bio-field effect transistor	BioFET
Bismuth	Bi
Bismuth film electrode	BiFE
Boron doped diamond electrode	BDD
Bovine serum albumin	BSA
Cadmium sulfide	CdS
Carbon nanotubes	CNTs
Carcinoembryonic antigen	CEA
Chemical vapor deposition	CVD
Computer assisted design	CAD
Confocal fluorescence microscopy	CLSM
Cyclic voltammetry	CV
Cycloolefin copolymer	COC
Desoxyribonucleic acid	DNA
Differential interference contrast	DIC
Electrochemiluminescence	ECL
Electro-osmotic flow	EOF
Environmental protection agency	EPA
Flow injection analysis	FIA
Fluorescence resonance energy transfer	FRET
Focus ion beam	FIB
Gold nanowires	AuNWs
Graphene oxide	GO
Horseradish peroxidase	HRP
Human Immunoglobulin G	HIgG
Ink-jetted printed electrodes	IPE
Lab-on-a-chip	LOC
Lead-sulphide nanoparticles	PbS NPs
Limit of detection	LOD
Liquid gate field effect transistor	LG-FET
Localized surface plasmon resonance	LSPR
Magnetic bead	MB

Magnetic nanoparticles	MNPs
Magnetic resonance	MRX
Metal-insulator-semiconductor	MIS
Metil methacrylate	MMA
Micro total analysis system	μ TAS
Nanocrystals	NCs
Nanomaterials	NMs
N-hydroxysuccinimide	NHS
P-aminothiophenol	p-ATP
Paper screen printed electrodes	pSPE
Phosphate saline buffer	PBS
Phosphate saline buffer (Tween 20)	PBST
Platinum nanoparticles	Pt-NPs
Point of care	POC
Poly(3,4-ethylenedioxythiophene)	PEDOT
Polycarbonate	PC
Polydimethylsiloxane	PDMS
Polyethylene naphthalate	PEN
Polyethylene terephthalate	PET
Polymetacrylate	PMMA
Prostate-specific antigen	PSA
Quantum dots	QDs
Reduce graphene oxide	rGO
Relative standard deviation	RSD
Resistive pulse sensor	RPS
Scanning electron microscopy	SEM
Screen printed carbon electrodes	SPCE
Silica nanoparticles	SNPs
Silver nanoparticles	AgNPs
Silver / silver chloride	Ag/AgCl
Single wall carbon nanotubes	SWCNT
Spin valve	SV
Square wave anodic stripping voltammetry	SWASV
Square wave voltammetry	SWV
Surface raman spectroscopy	SERS
Thin field effect transistor	TFT
Total internal reflection	TIRF
Transmission electron microscopy	TEM

TABLE OF CONTENTS

THESIS OVERVIEW	1
INTRODUCTION	9
1.1. Lab-on-a-chip devices.....	11
1.1.1. Definitions and general overview.....	11
1.1.2. Fabrication processes.....	13
1.2. Nanomaterials and Lab-on-a-chip technology.....	15
1.2.1. Nanomaterials in LOC technologies.....	16
1.2.2. Nanomaterials as labels in microfluidics.....	24
1.2.3. Nanomaterials for process improvement.....	27
1.2.4. In-chip production and characterization of nanomaterials	29
1.2.5. Other applications.....	32
1.2.6. Perspectives	33
1.3. References.....	34
OBJECTIVES.....	47
FABRICATION METHODOLOGIES.....	53
3.1. Microchannels design.....	56
3.2. Fabrication of the microfluidic device.	56
3.2.1 Reagents.....	56
3.2.2 Experimental details	57
3.2.3. PDMS replica.....	59
3.2.4. Device bonding.....	61
3.3. Electrochemical detectors for microfluidic devices.	63
3.3.1. Screen Printed Carbon Electrodes (SPCE)	63
3.3.2. Inkjet Printed Electrodes (IPE)	64
3.3.3. Photolithography-based electrodes	67
3.3.4. Composite-based Electrodes for microchannels.....	71
3.4. Conclusions	72
3.5. References	73

QUANTUM DOTS AS ELECTROCHEMICAL REPORTERS IN LAB-ON-A-CHIP DEVICES 77

4.1. Introduction 79

4.2. On-chip electrochemical detection of CdS quantum dots 81

 4.2.1. Experimental details. 81

 4.2.2. Results and discussions..... 82

4.3. On-chip magneto-immunoassay for Alzheimer’s biomarker electrochemical detection by using Quantum Dots as labels..... 89

 4.3.1. Experimental Section..... 89

 4.3.2. Results and Discussion..... 92

4.4. Conclusions..... 97

4.5. Futures perspectives..... 98

4.6. References..... 99

NOVEL STRATEGIES TO OBTAIN ELECTROCHEMICAL LOCs WITH HIGHER SENSITIVITY 105

5.1. Introduction 107

5.2. Magnetic plug-based platform development 109

 5.2.1. Experimental details 110

 5.2.2. Results and discussion 113

5.3. Design and fabrication of a recycling flow micro-system..... 120

 5.3.1. Experimental details. 120

 5.3.2. Results and discussions..... 122

5.4. Enhanced detection sensitivity of quantum dots labeled protein by bismuth electrodeposition into microfluidic channel. 130

 5.4.1. Experimental details 131

 5.4.2. Results and discussions..... 133

5.5. Conclusions 139

5.6. Reference..... 140

..... 145

DIAMOND BASED PLATFORMS..... 147

6.1. Introduction 149

6.2. Experimental details 150

6.2.1. Reagents.....	150
6.2.2. Apparatus	150
6.2.3. Preparation of BDD electrode.....	151
6.2.4. Microfluidic channel fabrication and BDD electrode integration	151
6.2.5. Platinum nanoparticles electro-deposition onto BDD electrode.....	152
6.2.6. Atrazine derivatization.....	152
6.2.7. Biosensor variables optimization.....	152
6.2.8. ELISA magneto-immunoassay for atrazine detection	152
6.2.9. On-chip ELISA magneto-immunoassay for Atrazine detection	153
6.3. Results and discussions	155
6.3.1. Morphological characterization of BDD electrode.....	155
6.3.2. Optimization of experimental variables of the biosensor for atrazine detection based on ELISA immunoassay.	156
6.3.3. Electrochemical magneto-immunosensing strategy	157
6.3.4. Implementation of the ELISA magnetic immunoassay for atrazine detection by using a microfluidic chip with BDD Pt-NPs electrode as detection platform.	159
6.3.5. Implementation of the complete ELISA magnetic immunoassay for atrazine detection by using a micromixer coupled to the BDD Pt-NPs based detection platform.	161
6.4. Conclusions	162
6.5. References	164
INK-JET BASED BIOSENSING PLATFORM.....	169
7.1. Introduction	171
7.1.1. Operation principle	172
7.2. Experimental Section.....	174
7.2.1. Reagents.....	174
7.2.2. Instruments.....	174
7.2.3. Dielectric layer optimization	174
7.2.4. OTFTs Fabrication.....	175
7.2.5. MMAcoMAA functionalization and label-free immunoassay	176
7.3. Results and Discussion	177
7.3.1. BioOTFT fabrication	177

7.3.2. Dielectric layer optimization	179
7.3.3. SEM Characterization of the different TFT layers	182
7.3.4. Electrical characterization of OTFT	183
7.3.5. MMA Functionalization	184
7.3.6. Label free immunoassay	186
7.4. Conclusions	190
7.5. References	191
.....	194
CHAPTER 8.....	195
CONCLUDING REMARKS.....	195
Considering the objectives previously described in Chapter 2, along with the obtained results presented from Chapter 3 to Chapter 7, the following specific conclusions on this PhD thesis can be given for each chapter:	197
8.1. Fabrication methodologies	197
8.2. Quantum Dots as electrochemical reporters in lab-on-a-chip devices	197
8.3. Novel strategies to obtain electrochemical LOCs with higher sensitivity.....	198
8.4. Boron-doped diamond based platforms.....	199
8.5. Ink-jet based biosensing platform.....	199
ANNEXES	201

THESIS OVERVIEW

Electrochemical detection exhibits great advantages such as low power requirements, low limits of detection, high sensitivity. The last years, the use of microfluidic platforms for electroanalysis has increased in a remarkable way. This trend can be explained by the fact that most of microdevices work under certain hydrodynamic conditions which enhance mass transport toward the detector surface (working electrode) resulting in an increase of the obtained current and sensitivity compared to the classical static measurement modes. Thus, the combination of the electrochemistry, microfluidics and also nanotechnology could provide a really powerful biosensor platform, so, in this PhD thesis different microfluidic platform with integrated electrodes as transducers in biosensing applications were designed and evaluated.

General aspects and experimental results related to the present PhD Thesis are divided into eight chapters, including the introduction, thesis objectives, results and discussions and general conclusions and perspectives.

Chapter 1, entitled “*Introduction*” hereby presents the use of nanomaterials and lab-on-a-chip technologies as a promising synergy for a wide range of applications. Two points of view are described and discussed: microfluidic for nanomaterials production and characterization, and nanomaterials to enhance microfluidic process in addition to their various applications in biosensing and other fields.



Scheme 1. Graphical representation of a microchannel including nanomaterials.

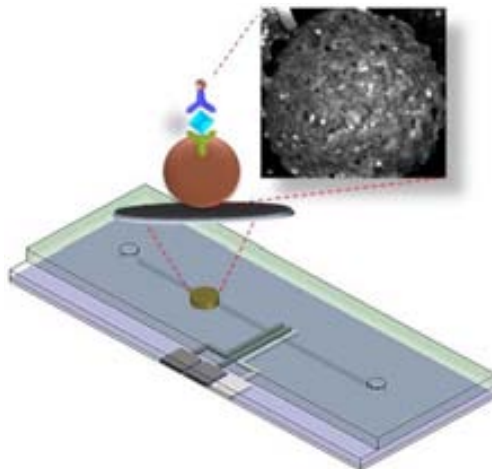
Chapter 2, entitled “*Objectives of the thesis*”, presents the different objectives of the PhD Thesis. The main objective was to study the implementation of nano / micromaterials in different miniaturized platforms with the aim of obtaining robust, sensitive and more efficient (bio) sensing platforms for point-of-care applications.

Chapter 3, entitled “*Fabrication methodologies*”, summarizes the optimization of the microfluidic channels fabrication as well as the integration of different transducers, especially screen printed carbon electrodes (SPCE), for the better performance in the

THESIS OVERVIEW

various applications as shown in the next chapters (including new topics with interest for other collaborations in the research group).

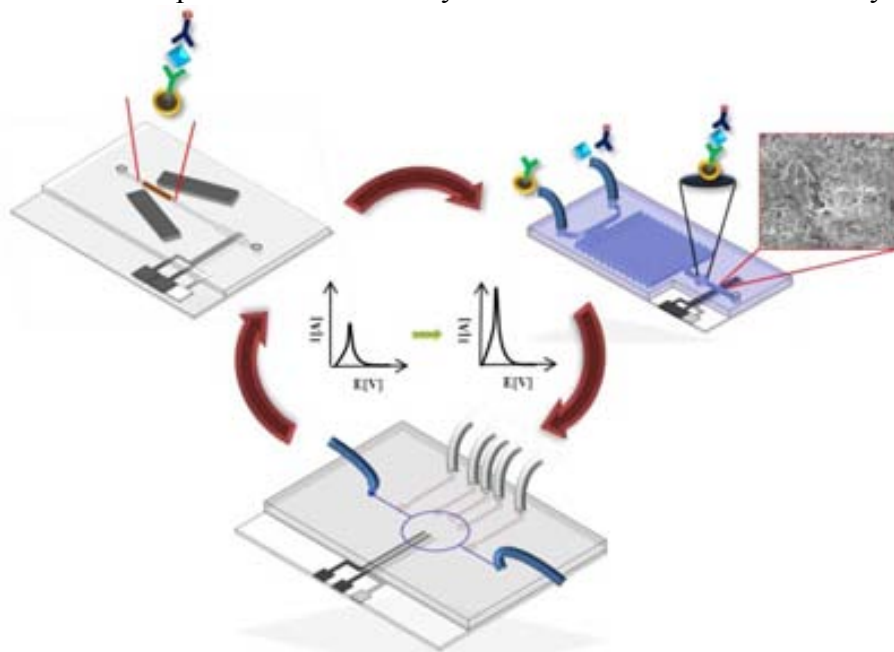
Chapter 4, entitled “*Quantum dots as electrochemical reporters in lab-on-a-chip devices*”, is divided in two parts. The first part describes how a flexible hybrid polydimethylsiloxane (PDMS)/Polycarbonate (PC) microfluidic chip with integrated screen printed carbon electrodes (SPCE) has been applied for electrochemical Quantum Dots (QDs) detection. In the second part, electrochemical detection of quantum dots (cadmium-selenide/zinc-sulfide, CdSe@ZnS) as labeling carriers in an assay for apolipoprotein E (ApoE) detection has been also evaluated. The immunocomplex was performed by using tylosylactivated magnetic beads as preconcentration platform into the same microfluidic platform. All the immunoassay was conducted into a microfluidic channel with a magnetic preconcentration zone.



Scheme 2. Microchannel with integrated screen printed electrode for magneto-immunoassay application.

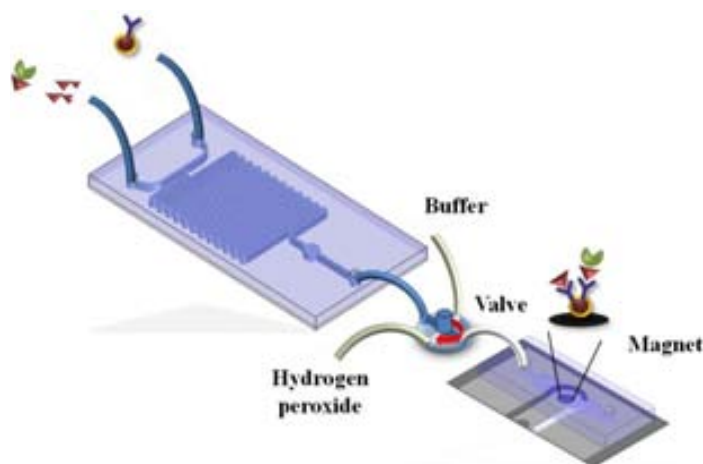
In Chapter 5, entitled “*Novel strategies to obtain electrochemical LOCs with higher sensitivity*”, includes three different strategies to improve the electrochemical signal of Quantum dots (QDs) as labels in immunoassays. The first one is the use of a magnetic field to immobilize magnetic beads in a controllable configuration into a microfluidic channel in order to obtain a stable magnetic plug where the immunoassay is performed. The second strategy is the use of a home-made recycling system. In this part, the QDs increasing signal is demonstrated by recirculation using an external peristaltic pump connected with a microfluidic chip forming a loop system. After this demonstration, the fabrication of a micro-peristaltic pump with in-chip integrated valves is proposed. All the fabrication steps have been optimized and the software for valves control has been also developed. Finally, bismuth is used as it is a well-known material to agglomerate heavy metals. We took advantages of this property for improving the electrochemical signal of CdS QDs due to the cadmium ions reduction enhanced by bismuth ions presence onto the working electrode.

Optimization of the bismuth concentration has been done in order to achieve the highest signal. The detection is performed in batch system as well as in microfluidic systems.



Scheme 3. Different strategies to improve the sensitivity of immunoassay performed into microfluidic channel.

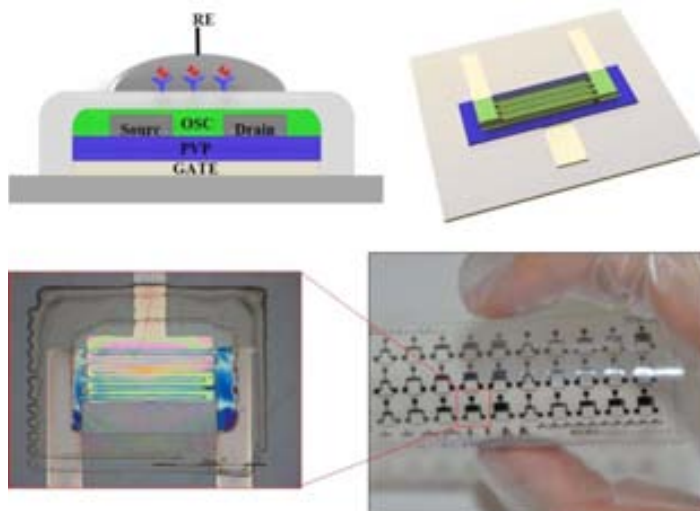
In **Chapter 6**, entitled “*Diamond based platforms*”, electrochemical determination of atrazine based on magneto-immunoassay using boron-doped diamond (BDD) electrode is performed into a microfluidic platform. BDD electrode was modified by electroreduction using potassium tetrachloroplatinate (K_2PtCl_4) in PBS buffer, in order to grow platinum nanoparticles (Pt-NPs) onto its surface. Immunoassay has been performed by direct competitive assay using horseradish peroxidase (HRP) as enzymatic label and magnetic microparticles as preconcentration platform.



Scheme 4. Micromixer coupled to a detection chip based on boron doped diamond electrode.

THESIS OVERVIEW

In **Chapter 7**, entitled “*Inkjet based Biosensing platform*”, a flexible organic double gate Bio-Field Effect Transistor (BioFET) developed by inkjet technology onto a flexible substrate is presented. This kind of organic transducers has important advantages for biosensors in terms of fabrication cost and biocompatibility as well as their integration into microchannels. To demonstrate the applicability of this device in biosensing, we have functionalized it with a capture antibody which detects a model protein without any label. The device fabrication, its structure, materials optimization, electrical characteristics and functionalities are also discussed.



Scheme 5. Schema and pictures of the BioFET fabricated by inkjet technology.

Concluding remarks of the present Thesis in addition to future perspectives regarding the different results and research fields explored are enclosed in **Chapter 8**.

CHAPTER 1. INTRODUCTION.....	9
1.1. Lab-on-a-chip devices.....	10
1.1.1. Definitions and general overview.....	11
1.1.2. Fabrication processes.....	13
1.2. Nanomaterials and Lab-on-a-chip technology.....	15
1.2.1. Nanomaterials in LOC technologies.....	16
1.2.2. Nanomaterials as labels in microfluidics.....	24
1.2.3. Nanomaterials for process improvement.....	27
1.2.4. In-chip production and characterization of nanomaterials	29
1.2.5. Other applications.....	32
1.2.6. Perspectives	33
1.3. References.....	34

CHAPTER 1

INTRODUCTION

Related Publications

“New trends in DNA sensors for environmental applications. Nanomaterials, miniaturization and lab-on-a-chip technology”. A. de la Escosura, M. Medina-Sánchez, and A. Merkoçi. *Nucleic Acid Biosensors for Environmental Monitoring*, Editorial: Royal Society of Chemistry (Ed. I. Palchetti and M. Mascini). Chapter 8, **2011**, 143-166. (Annex 1).

“Micro and nanomaterials based detection systems applied in lab-on-a-chip technology”. M. Medina-Sánchez, and A. Merkoçi. *Handbook of Green Analytical Chemistry (John Wiley & Sons, Ltd, Chichester)*. Chapter 18, **2011**, DOI 10.1002/9781119940722. (Annex 1).

M. Medina-Sánchez, S.Miserere and A. Merkoçi, “Nanomaterials and lab-on-a-chip technologies”. *Lab Chip*, 2012, 12, 1932-1943. (Annex 1).

1.1. Lab-on-a-chip devices

1.1.1. Definitions and general overview

One of the trends in the analytical chemistry field is oriented to miniaturization and automation of analytical systems. These include classic operation like filtration, extraction, mixing, separation and detection, giving origin to lab-on-a-chip systems (LOC) or micro total analysis systems (μ TAS)¹.

The first reported microsystem using integrated circuit technology was for gas chromatography. It was created by 1975 by S.C. Terry, from Stanford University, although, its high growth was at 90's with the development of micropumps, flow sensors and the concept of the integrated systems probing the possibility to integrate steps of treatment, separation and sample cleaning, obtaining a whole analysis in a single device².

Years later, Manz et al. in the year 1990³ introduced the term micro TAS (μ TAS), also known as lab-on-a-Chip (LOC). The benefits of μ TAS are mainly in the possibility to manage complex samples and to introduce different steps for a complete functional device⁴. On the other hand, small amount of sample and reagents (down to picoliters) is needed, and the fast reaction times decrease considerably when molecular diffusion lengths are of the order of the microchannel dimensions. The miniaturization also takes advantages of different physicochemical phenomena that are not dominant at larger scales, like laminar flow⁵, diffusion phenomena at microscale, electrokinetics⁶, surface tension-driven flows⁷, acoustic streaming⁸, etc. These phenomena can improve the performance of the systems.

While the fluids in the macroscale present a chaotic movement, in microfluidic systems they present a laminar flow behavior, since the fluid viscosity dominates instead of its inertial behavior and thus Reynolds number values below one are common. A fluid with a laminar flow is very predictable and can be used together with other fluids to create gradients of physicochemical properties⁹. Diffusion can be used to mix liquids, or special structures that increase the turbulence can be designed and fabricated in order to reduce the mixing time. Another characteristic of the miniaturized devices is that the ratio between the liquid volume and the wall surface of the LOC are decreased and the interactions between the walls and the analytes that are found in the liquids get more efficient. This is important for processes like immunoassays, protein immobilizations etc. However, this property can facilitate the nonspecific adsorption, making necessary to do some kind of surface modifications to avoid these not desirable absorptions¹⁰.

In addition, some research works are taking advantage of hydrodynamics for sample handling, including several microfluidic-platforms designs, such as spiral geometries following conventional centrifugal separation based on size, taking advantage of inertial

INTRODUCTION

forces and dean rotation forces¹¹. By others channel features like microchannel constriction, bending channel, bifurcation, the ratio between diameter and length it is possible to reach the separation of analytes by physical effects, including Fahraeus and Fahraeus-Lindqvist effects, the Zweifach-Fung bifurcation law and the cell-free layer phenomenon, between others^{12,13}. Herringbone chaotic mixers could also be of interest for further application on sorting mechanisms and spinning trajectories¹⁴. A well-known device is the microfluidic platform based on pillars, used to isolate cells or proteins from real samples being one example the separation of rare circulating tumor cells in the peripheral blood of patient with metastatic cancer¹⁵. Other works had been performed in the same field by sorting and detecting label-free biomarkers from whole blood, concluding that a quantitative detection of a 20 μ L biomarker sample in less than 20 min was possible¹⁶. Membranes had also been focused into tasks like reproducing cells cultures using two-layers platforms, where the top channel contains the cells while the bottom channel transfers the nutrients through the membrane allowing its grown. In addition, membranes are used as scaffolds to localize and sustained drugs^{17,18}. A possible novel approach for these membranes could be taking advantage of its different size pores in order to filter and separate analytes by size.

Not least, electronic, magnetic and optical separations have been studied for microfluidic devices. Some research groups have reported microelectronic chips, integrating electrodes and sensors arrays to allow cell and proteins separation, as for example electrophoresis, traditional method for analyte separation, used for example in neurotransmitters separation and detection by an electrical field application¹⁹, genes separation from saliva samples²⁰ beside others. A variant of electrophoresis is the dielectrophoresis, which uses electrodes array to manipulate drops by alternative voltage application. One of the work in this field, was the fabrication of over 100.000 independent electrodes, used to manipulate up to 10.000 cells applying an electrical alternative field, where the change of frequency and amplitude make possible translate and move each cell on a 2D grid, maintaining their viability and reproducibility²¹. Conductive membranes²², magnetic particles. super paramagnetic particles could be also of interest in microfluidic platforms to concentrate and to purificate samples²³.

Another possible alternative to separate and manipulate cells is by using sound effect²⁴. The authors introduced a method of continuous particle separation through standing surface acoustic wave (SSAW)-induced acoustophoresis in a microfluidic channel.

In general, manipulation of fluids in microfluidic channels has shown a great potential for different applications such as chemical synthesis, biological analysis, environment studies, etc., although this area is still in progress, many challenges should be solved for real applications²⁵.

Nowadays, a wide range of different structures are ready to be included in LOCs in order to carry out all the required steps in analytical processes, such as channels, reactors, mixers,

pumps, chromatographic columns or detectors. LOC research field is inherently multidisciplinary, combining the knowledge of different areas for their design, fabrication and application. Physics provides the understanding of the fluid dynamics at the microscale²⁶. Microtechnology assures high precision for LOC components²⁷. Chemistry studies the composition and properties of the matter as well as the changes it undergoes during chemical reactions²⁸, and biology is also important since many of the applications are biomedical and the development of biosensors requires the incorporation of biological agents as recognition element²⁹.

Other important area that contributes specially in the LOCs production is the Materials field. Traditionally materials such as silicon and glass have been used for microfluidic devices; however these materials are being displaced in part by plastics and elastomers. Silicon, in particular is expensive and is not useful for some optical applications because is opaque to visible and ultraviolet light. Also, some of the microfluidic platforms like valves, pumps, porous membranes require flexible materials such elastomers and thermoplastics. Much of the research in microfluidic systems has been carried out in a polymer poly (dimethylsiloxane) (PDMS)³⁰. PDMS is an optically transparent, soft elastomer. Whether the microfluidic devices that ultimately become widely used will use PDMS or one of the engineering polymers (such as polycarbonate or polyolefin) remains to be seen. PDMS is a very useful material for the testing of new concepts, for exploratory research at the early stages of development, while plastic materials are widely used for mass production by injection and thermoforming technologies.

In summary, microfluidics have generated extensive development in materials, manufacturing processes, integration³¹, etc., providing an infinite range of possibilities for application especially in life sciences or environmental field. However, its impact on science has not yet been revolutionary. This technology requires a broad range of components, integration of different areas. Although many technological developments are already available, there is still a long way to obtain fully functional devices, user friendly and robust for real bioanalytical applications.

1.1.2. Fabrication processes

Microchannel Fabrication

Several chip fabrication methodologies that allow obtaining different geometries according to the micro and nanofluidics have been reported. A brief description of the most important technologies is given in the next sections.

Photolithography is an optical based methodology that allows transferring of patterns onto certain substrates. It is essentially the same process used in lithographic printing. This

INTRODUCTION

technique consists in transferring a landlord from a photomask to the surface of a substrate. 3D structures fabricated by using this process have potential applications in MEMS sensors/actuators, optical devices, and microfluidics³².

Soft Lithography is a manufacturing technique using elastomers, molds and conformable photomasks. It is called “Soft” because elastomeric materials are used, especially poly (dimethylsiloxane) (PDMS) and recently poly [(3-mercaptopropyl)-methylsiloxane] (PMMS), demonstrating the successful pattern replication from the micrometer to sub-100 nm scale³³. Generally it is used to build devices at micro and nano-scale. The process includes technology of impression by micro contact, molding by replica, molding by micro transference and micromolding in capillaries³⁴.

Micro manufacturing is based on the use of a cutting tool to obtain predefined material geometries³⁵. Although the sizes obtained by this technique are not as small as those obtained using lithography, it allows the fabrication of platforms for the integration with smaller devices.

Ink-Printing Technology; initially, this technology was used for computer science and decorative objects. Now it is widely used to print on different surfaces, such as aluminum, glass, plastic and paper. Nowadays special inks like graphite inks, silver, carbon nanotubes inks and polymers inks, among others are used. These allow printing geometries with certain thicknesses and roughness to create three-dimensional structures, without masks³⁶.

Polymerization based prototyping is a layer by layer fabrication technique through a computer aided design (CAD). Resin is deposited in crud and then using laser traces or an agglutinant cartridge it is polymerized and solidified onto the surface. It allows the construction of 3D structures and assembled pieces³⁷.

Other processes used to fabricate microfluidic systems are: X-rays lithography³⁸, molding by high precision, hot embossing³⁹, micro-injection molding⁴⁰, and roll-to-roll embossing⁴¹. This technology allows building three-dimensional complex structures with a great variety of materials.

Electrode/detector fabrication methods.

Screen-printed technology is based on the sequential transfer of different conductive or non-conductive inks on a variety of inert substrates through a mask with the desired geometry. Nowadays, screen-printing microfabrication technology is a well-established technology for mass production of thick film electrodes and it is widely applied to build biological or chemical sensors⁴². Screen-printed electrodes (SPE) represent one of the most important products of this technology because has high mass production capability and low cost.

Generally, inert substrates used in screen-printed processes are ceramic or polymeric ones. In case of polymeric substrates, polyester substrate is the most commonly used for its durability, thermal and hygroscopic stability, clarity and stiffness. Exact composition of printing inks usually is uncertain (patented and commercially available).

Ink-jet printing is also being used as an alternative to screen-printing technology. Other micro / nanofabrication techniques based on photolithography and imprinting techniques are also extended for electrode/detector fabrication.

1.2. Nanomaterials and Lab-on-a-chip technology

While the term “Nanotechnology” is widely used, its definition due to involvement of many research fields is rather open. Nanotechnology is the technical capability to manipulate and modify the matter with the possibility to produce new materials through the re-organization or self-assembly of atoms and molecules, in order to obtain functional structures at nano-scale⁴³.

There is a strong relation between nanotechnology and miniaturized (bio) analytical or biosensing systems. The advantages of miniaturized (bio) systems stand on the reduction of the sample and reagents consume, detection facility, minimal handling of hazardous materials and in parallels multiple sample detection. It is well known that nanomaterials (NMs) are bringing a series of advantages in the improvement of biosensing systems. DNA^{44,45,46}, proteins⁴⁷, and even cells detection⁴⁸ using electrochemical, optical and other techniques have been reported to gain impressive advantages by using NMs. Micro and nanomaterials are recently shown to be important building blocks for improvement of environmental monitoring systems such as those for heavy metals analysis⁴⁹. Given the advantages of NMs in the design of novel biosensing systems or improvements of the existing ones, it is logical to see a strong interaction between these novel materials and lab on a chip (LOC) platforms. NMs are being used in microfluidic platforms as detectors (or detectors modifiers)⁵⁰, tools for microreactors⁵¹, and others. In addition LOCs are being used for NMs synthesis^{52,115,127}.

Several NM based accessories for flow control, such as particle positioning platforms (i.e. an optical method to manipulate nanosized particles in suspensions within confined microfluidic devices⁵³) also have been reported.

LOC technology already is an established research field where scientists of different areas of knowledge are working together to achieve new synergies of this technology with nanotechnology in general and NMs in particular. This is a continuous growing field where

INTRODUCTION

the development of novel “nanobiosensors” is opening the way to cost-effective devices that would be the perfect candidate to be integrated into LOC systems.

M. Pumera recently has put emphasis to the mutual benefits of microfluidics and nanomaterials. His review is focused on in-chip separation and detection of analytes, microfluidics use for synthesis and as platform for nanomotors and other applications⁵⁴. In the following introduction part we provide now an overview of the various strategies related to the use of nanoparticles and nanostructures for microfluidics as well as of microfluidics platforms for synthesis, toxicity studies and characterization of NMs. The integration of NMs into analytical devices for both detection and in-chip process improvement will also be discussed.

1.2.1. Nanomaterials in LOC technologies

Transducers involving nanomaterials

The application of nanomaterials (NMs) in the development of sensors and biosensors represents one of the main focusing of the nowadays nanotechnology. Their interesting optical and electrical properties are making NMs new building blocks for the design of various kinds of sensing and biosensing devices with improved performances. In the last decade NMs have been very attractive for the modification of transducers which are the most important part of the (bio) sensing systems to be integrated into LOCs. The transducer’s modification through NMs can improve the electrochemical (amperometric, impedimetric, potentiometric), the optical (light absorbance, dispersion, fluorescence) or other mixed signals (i.e. electrochemiluminescence) based measurements. These works have been reported and discussed in the following sections.

Electrochemical detection

Various NMs based electrochemical detectors integrated within the LOC systems have been reported. Among these, carbon nanotubes (CNTs) are the most reported^{55,56,57,58}. Indeed they present interesting properties like extraordinary thermal and electrical conductivity as well as excellent mechanical resistance. CNTs can be easily deposited or grown onto different surfaces through simple dropping, chemical vapor deposition (CVD) or plasma enhanced CVD. The CNTs modified transducers show higher surface area which increases the current density besides offering an increased surface for biomolecules attachment. This can improve the current stability and increase the sensitivity of the detector. The electrical behavior of such platforms depends on CNTs chirality, the number of carbon layers, defects and their functionalization, which must be carefully considered during their application. All these CNTs properties are useful in catalysis⁵⁹, enzyme immobilization⁶⁰, protein detection⁶¹ and metal detection⁶².

Okuno *et al.* have developed a label-free immunosensor modified with CNTs to enhance the detection of total prostate-specific antigen (T-PSA) (Figure 1.1A)⁶³. An array of platinum microelectrodes was modified by CVD with single-wall carbon nanotubes (SWCNTs). CNTs allow a better electron transfer, improving the limit of detection (LOD) in relation to the non-modified electrodes, obtaining a LOD of 0.25ng mL⁻¹.

CNTs are widely used in the fabrication of field effect transistors (FET); Javey *et al.* have obtained a CNTs based FET by combining ohmic metal-tube contacts, high-dielectric-constant films as gate insulators, and electrostatically doped nanotube segments as source/drain electrodes⁶⁴. This approach looks like those of MOSFETs (Metal Oxide Semiconductor Field Effect Transistor) and can provide excellent ON-OFF states to nanotube based FETs under aggressive vertical scaling.

Tey *et al.* described a liquid gate field effect transistor (LG-FET) that integrates SWCNTs⁶⁵. The electrical detection was performed by using CNTs as contact electrodes and semiconductive channel. A limit of detection of 1 pM of poly-L-lysine was achieved. The SWCNTs were used as “channel modulation labels” to sense changes in their immediate environment as a result of specific interactions with biomolecules. In this design the electrolyte replaces the dielectric in normal operation; also the electrical double layer capacitance created by the electrolyte and high surface area of the SWCNT network yields gives a total gate capacitance increasing in an order of magnitude in comparison with the typical Si/SiO₂ bottom gate configuration.

A non-enzymatic carbon nanotube sensor for sugars detection was developed by Vlandas *et al.*⁶⁶. The sensor was also assembled as a LG-FET (Liquid Gate Field Effect Transistor). The semiconductive channel is based on SWCNTs functionalized with boronic acid receptors. This sensor is capable to detect glucose in a range of concentration from 5 to 30 mM by measuring the change of impedance at different frequencies and gate voltages, which is in the range of physiological glucose detection. However, the conventional impedance detector, based on the uses of screen printed electrodes (SPEs) modified with bimetallic nanowires, has been able to achieve a limit of detection of 20 μM⁶⁷, being an excellent alternative for in lab-on-a-chip application.

LG-FET with CNTs to detect herbicides via competitive immunoassay was also reported⁶⁸. This system could detect concentrations lower than 500fM of 2,4-dichlorophenoxyacetic acid herbicides by conductimetric methods by reading the current in the drain contact.

Graphene is another interesting NM which has recently attracted significant attention due to its interesting inputs for electrochemical detection. It offers higher electron transference and is easy to be functionalized with (bio) molecules. This material, easy to be produced from graphite⁶⁹ seems to be much cheaper than CNTs and consequently a good alternative. Chua *et al.* reported a microfluidic graphene oxide based amperometric detector which showed

INTRODUCTION

higher peak sensitivity, resolution and separation efficiency than the same device without modification⁷⁰. Figure 1.1B represents a graphene FET-based device⁷¹ where the drain and source pads were made with graphene oxide and the channel with reduced graphene (rGO). The detection of fibronectin was demonstrated as proof of concept, with a detection limit of 0.5 nM.

Finally, nanostructured electrodes are attracting the attention for biological samples analysis at very low concentrations where the reduction of the sensor size seems to facilitate the detection of reaction products at the similar scale⁷².

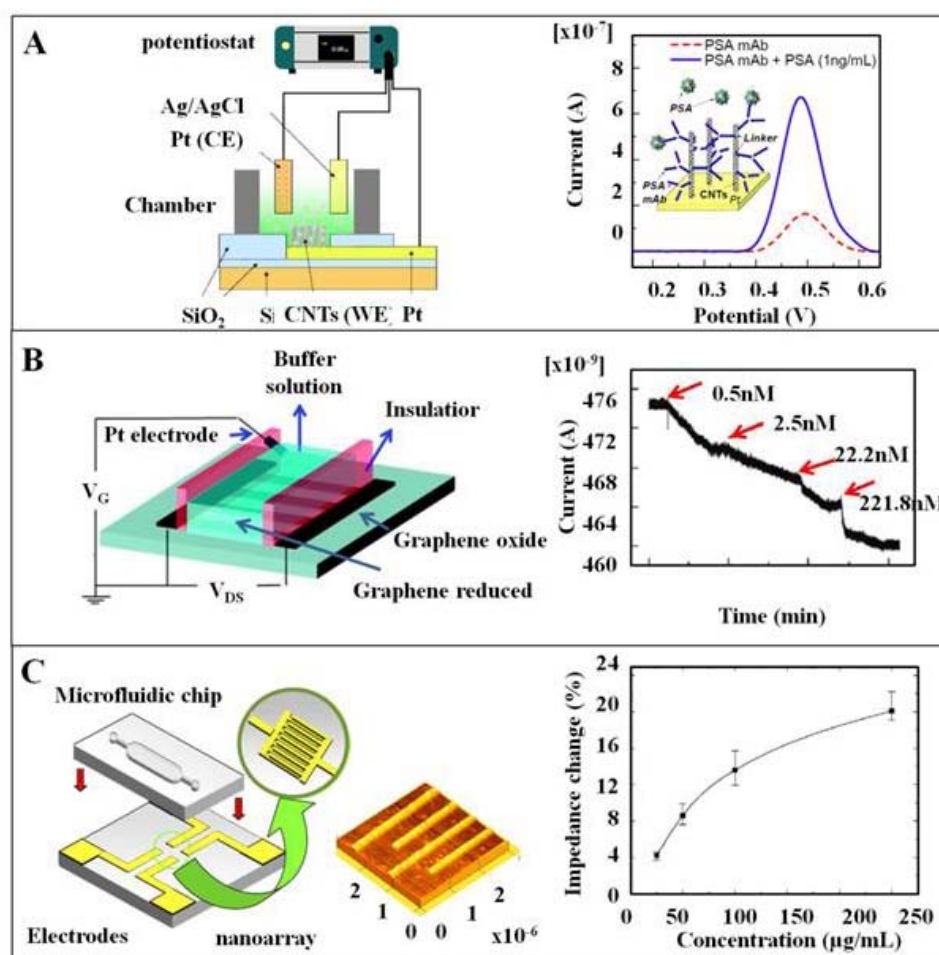


Figure 1.1. Electrochemical readout technologies. (A) Amperometric sensor modified with SWCNTs for PSA detection, (B) Bio-field effect transistor (BioFET) fabricated with graphene oxide (source-drain contacts) and reduced graphene (conductive channel) integrated into microfluidic system for fibronectine detection, and (C) Impedimetric gold nanoarray for protein detection. Adapted with permissions from [62, 70, and 72] respectively.

Ahn's group reported the functionalization of nano interdigitated electrodes array fabricated onto cyclic olefin copolymer (COC) substrate for direct bio-affinity sensing (see Figure

1.1C)⁷³. The protein immobilization was based on the self-assembly of alkanethiol groups on the electrode surface. Different concentrations of mouse monoclonal anti-rabbit immunoglobulin were used as analyte for the biomolecular binding sensing tests. The protein was covalently immobilized on the alkanethiols SAMs which recognize amino groups of protein. Finally the variations of impedance to the electrode were measured for different protein concentrations. In this example, the scale and thickness of the electrode play an important role, due to the possibility to be integrated in microfluidic platforms as well as the improving of the sensitivity when the analyte is detected at the same scale as the detection platform.

These kinds of electrodes could also be modified with nanoparticles as Lee *et al.*,⁷⁴ reported in 2011. Indium oxide and silica nanoparticles (SNP) were selectively assembled onto multi-site channel area of the resistors, using layer-by-layer self-assembly. Glucose oxidase was immobilized onto the SNPs layer and glucose detection was performed by conductimetry. A current dependence upon different glucose concentrations with a sensitivity that depends on the channel and resistors dimensions was observed. The sensitivity for glucose detection was between 4 and 12 nA mM⁻¹.

In general, modifying transducing platforms with nanoparticles allows generating really high-conductive surface area interfaces that enables the sensitive / catalytic detection of ionic, molecular and biomolecular analytes. These high sensitive sensors are easy to be integrated and become good candidates for LOCs.

Optical detection

The integration of photonics and microfluidics is a well-known strategy that provides enhanced sensing and simplification of microsystems. Various optofluidic detections such as those based on surface enhanced raman spectroscopy (SERS), fluorescence and absorbance and related with the use of NMs modified detectors have been reported.

SERS is a surface-sensitive technique that enhances raman scattering by molecules adsorbed onto rough metal surfaces. For this reason, the use of NMs provides a wide range of possibilities for sensitive detection.

The use of gold nanowires (NWs) (diameter of 170 nm) synthesized by electrocrystallization method into a polycarbonate microchannel has been reported⁷⁵. Gold nanowires produce large increases in a raman cross-section. This kind of SERS-active dielectric polymer / NWs itself is a good candidate for in-microchip integration (Figure 1.2A). An increased sensitivity was also observed by detection of isonicotinic acid in perchloric acid due to the higher surface to volume ratio.

Different SERS spectra for a microfluidic separation chip with an integrated chromatographic column based on pillars array were evaluated⁷⁶. Diffusive mixing of silver nanoparticles (AgNPs) solution with the eluent stream in a laminar flow to induce SERS

INTRODUCTION

signals due to their advantages as relative easy preparation, manipulation and possibility to have high SERS reproducibility has been reported. Interesting information about complex mixtures without complete resolution of chromatography bands was obtained. Analysis of mixing kinetics effect on efficiency was also performed.

The combination of localized surface plasmon resonance (LSPR) and SERS has also been reported by Astilean's group⁷⁷. LSPR provides detection of molecular adsorption in both transmission and reflectivity modes, and SERS gives the analysis of the adsorbed molecule and its structure and orientation on the metal surface. The optical and spectroscopy properties of regular arrays of subwavelength holes in a thin gold film by combining SPR and SERS was demonstrated by the binding of the p-aminothiophenol (*p*-ATP) monolayer, observing a shift in SPR. A change in SERS related to the orientation of the adsorbed molecule, with a greater sensitivity of 300 nm / RIU and spectral shift of 16 nm was also observed.

The glass surface of a glass-PDMS microfluidic channel was modified by immobilization of QDs to develop a solid-phase assay for nucleic acid determination⁷⁸ (Figure 1.2B). QDs served as energy donors in fluorescence resonance energy transfer (FRET) for transduction of nucleic acid hybridization. A selective detection of femtomole quantities of target using 20 % formamide was reported.

A novel alternative for fluorescence detection by using on-chip superlocalization and super-resolution imaging of single molecules and nanoparticles under different microscopy modes was reported by Luo *et al*⁷⁹. The detection was performed by using epi-fluorescence and differential interference contrast (DIC) modes at the same time. The performance was validated by precisely mapping micronecklaces made of fluorescent microtubules and gold nanoparticles (40 nm of diameter) and by demonstrating the activation and excitation cycles of single Alexa Fluor 647 dyes for direct stochastic optical. In chip measurements of light absorbance are also reported by Demming *et al*. Nanoparticles can be used to modify the index of reflection of the material and by this way increase the obtained signal⁸⁰. A PDMS matrix involving Cu and Ag nanoparticles for microfluidic devices was also performed. These nanoparticles were suspended in PDMS to obtain a permanent modification. The antiseptic behavior of each nanoparticle was studied by observing the absorption of *saccharomyces cerevisiae* culture cells.

Gold nanoparticles embedded in a polymeric waveguide for localized surface plasmon resonance (Figure 1.2C), capable to capture minor variations in the refractive index of its microenvironment have been demonstrated⁸¹. A linear behaviour of refractive index changes of SU8 waveguide bound to gold nanoparticles was also observed.

Optical characterization should also be performed in microfluidic platforms, mainly by SERS detection. Qu *et al.*, reported the development of disposable screen printed SERS

arrays by using silver nanoparticles ink (AgNPs). This nanostructured surface was characterized by detecting rhodamine 6G with a LOD of $1.6 \times 10^{-13} \text{M}$ ⁸².

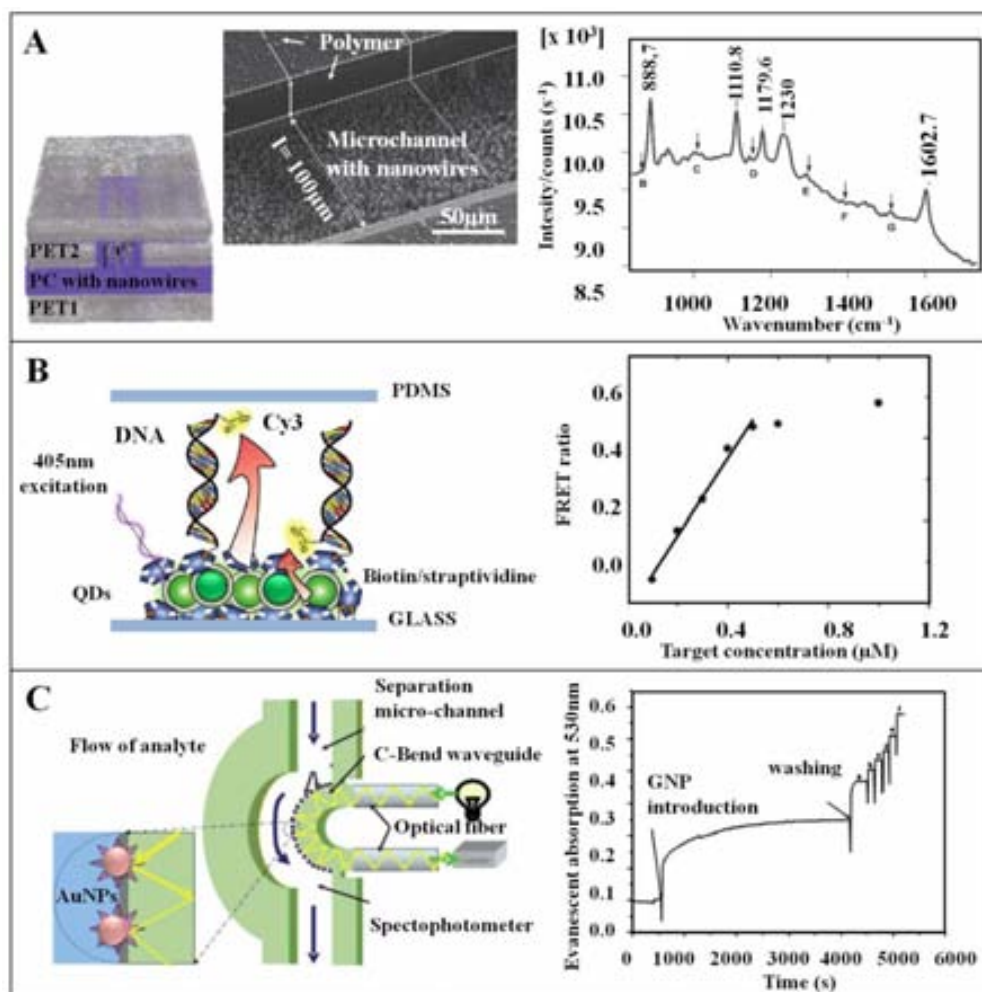


Figure 1.2. Optical readout technologies. (A) Schematic and SEM images of a microchannel with embedded gold and the corresponding typical SERS response. (B) Assay for the transduction of nucleic acid hybridization using FRET and CdSe/ZnS QDs, and (C) Scheme of optical set-up with gold nanoparticles (GNPs) modified waveguide coupled microchannel, and its typical curves of absorbance vs. time. Adapted with permissions from [74, 77 and 80].

The combination between quantum dots labeled nerve growth factor (QDs-NGF), microfluidic chambers for neuronal culture, and pseudo total internal reflection (TIRF) microscopy provided a single molecule detection and analysis⁸³. Chu's group developed a platform to detect retrograde axonal transport of NGF signals which is critical for the survival, differentiation, and maintenance of peripheral sympathetic and sensory neurons and basal forebrain cholinergic neurons. QD-NGF was used to track the movement of NGF in real time in compartmentalized culture of rat dorsal root ganglion (DRG) neurons. They obtained quantitative analysis at the single molecule level demonstrating that the majority

INTRODUCTION

of NGF containing endosomes had only a single NGF dimer. Electron microscopic analysis of axonal vesicles carrying QD-NGF confirmed this finding. Kuyper *et al.* proposed real-time nanoparticles synthesis (quantum dots, gold colloids, fluorescent and non-fluorescent beads) allowing the possibility to optimize reactions on the basis of real-time readout of particle dimensions⁸⁴. Confocal correlation spectroscopy (CCS) for on chip sizing of both fluorescent and no fluorescent nanoparticles was used. This technique can be advantageous powerful tool to characterize colloids, polymer beads, and biological particles such as vesicles, viruses, and DNA molecules.

In summary, optical detection is the most common detection method in microfluidic analyses. Fluorescence-based detection can be considered more usual for its facility to be integrated onto microfluidic devices (i.e. fluorescence excitation and detection components), as well as its ability to detect low volume samples.

SERS technique is also a potential tool to carry out qualitative and quantitative characterization of analytes; however its integration with microfluidic still needs more efforts. In the same way, fluorescence and absorbance detection are moving towards information-improving techniques, such as fluorescence lifetime-imaging microscopy or multicolor analyses. NMs enter to play an important role in the fluorescence as labeling and surface modification materials in order to improve the sensitivity and the sensibility of already existing methods.

Other detections

Other detection principles like electrochemiluminescence (ECL) and mass detection using nanoresonators are also applied in lab-on-a-chip technologies.

Electrochemiluminescence is a kind of luminescence produced during electrochemical reactions. A material emits light in response to an electric current or electrical field (see Figure 1.3A).

Nanoparticles could be used to improve the sensitivity of ECL. An enzymatic biosensor based on MWCNT surface modified with cadmium sulfide nanocrystals (CdS NCs)⁸⁵ (Figure 1.3B). The MWCNT-CdS can react with H₂O₂ generating strong and stable ECL emission in neutral solution. By following the same procedure, a biosensor based on CdS-graphene has shown promising results for H₂O₂ sensing with acceptable linear response from 5 μ M up to 1 mM with a detection limit of 1.7 μ M⁸⁶.

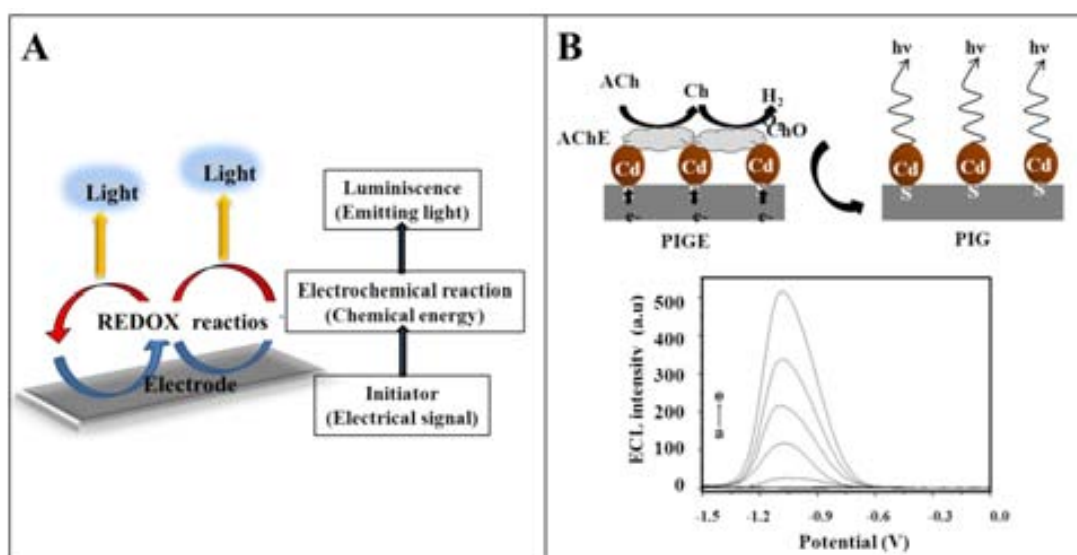


Figure 1.3. Electroluminescence (ECL) based measurement. (A) Principle of operation, and (B) scheme of multi wall carbon nanotubes (MWCNT)-Cadmium sulfide (CdS) modified with acetylcholine esterase (AChE), used for detection of acetylcholine neurotransmitter. Adapted with permission from [84].

Nanomechanical biosensors^{87,88,89} could also be integrated into microfluidics. A variation of the mass onto the cantilever will produce a change in the length by material deformation. This deformation can be detected by different transducers (i.e. optical, piezoelectrical, electrical by field effect transistor principle, etc.) (Figure 1.4A).

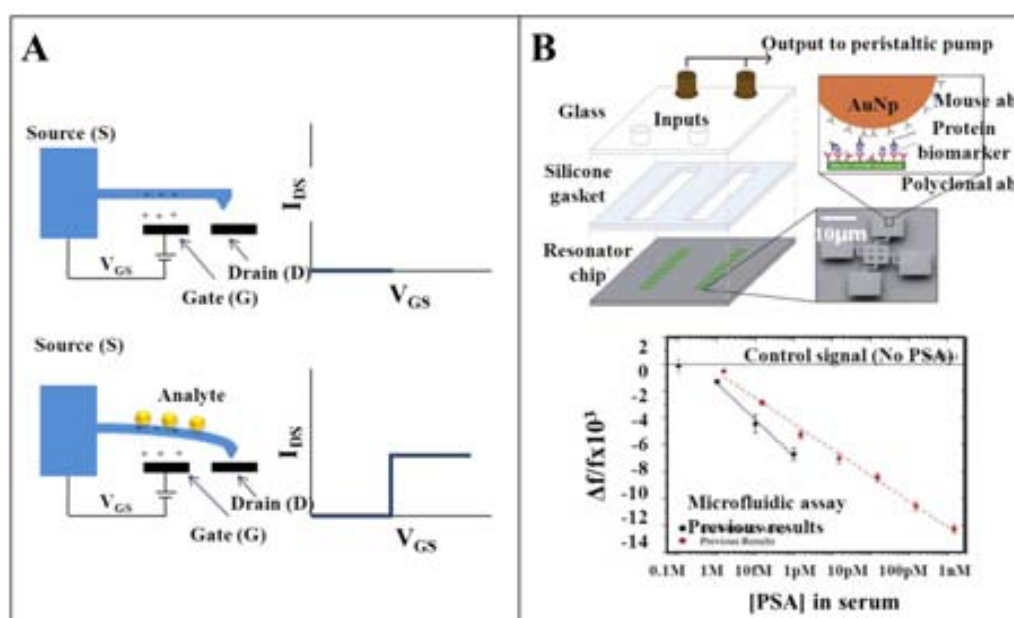


Figure 1.4. (A) Scheme of a resonator operation, and (B) scheme of a microfluidic-resonator device, with its respective frequency shift graph, applied for PSA detection in serum. Adapted with permission from [89].

INTRODUCTION

Waggoner *et al.* were able to detect concentrations of 1-100 fM of prostate-specific antigen (PSA) in serum, using a gold nanoparticle-based mass-labeling sandwich assay⁹⁰. A reduced time of analysis with microfluidic assay was observed. Such a platform using nanoparticles allows multiplexed protein analysis with a very high sensitivity offering many new alternatives of applications in clinical and biological studies for the early detection of diseases (Figure 1.4B).

Nanowires or nanotubes could also be employed as mass detectors. Hwang *et al.* have developed a nanocantilever-based sensor with a field effect transistor as a transducer. The signal from the gate changes when the cantilever is deflected due to specific binding of biomolecules on its surface⁹¹.

1.2.2. Nanomaterials as labels in microfluidics

Biomarkers related to various diseases are present at very low concentrations. For this reason, enhancement strategies such as nanoparticles-labeling besides labeling with fluorescence dyes, enzymes etc. have been demonstrated with interest for lab-on-a-chip diagnostics applications. Some examples related to nanoparticles used as labels in different lab-on-a-chip applications are showed in Table 1.1.

Quantum dots are the most common nanoparticles used as labeling platforms in microfluidics. They could be attached to antibodies, aptamers, oligonucleotides, or peptides⁹². The increased and stable fluorescence properties are of special interest to develop ultrasensitive and robust LOCs. Furthermore they have also interesting electrochemical / electrocatalytic properties which could be very useful for the integration of electrochemical detection for lab-on-a-chip applications with high sensitivity and selectivity.

A nanoparticles-labeling based LOC platforms involving different detection principles including electrochemical detection by using QDs as biotracers / labels for tumor marker protein detection is reported⁹³. Cadmium sulphide quantum dots (CdS QDs) were synthesized based on a modification of the procedure reported by Wang *et al.*⁹⁴, with anti-carcinoembryonic antibody (α CEA) and detected by square wave anodic stripping voltammetry (SWASV). The electrode surface was modified with carbon nanoparticles enhancing the performance of the electrochemical reaction while the QDs labels allow the amplification of the signal, improving the sensitivity and selectivity of the detection system.

Another interesting application involving QDs as biomarkers is the development of nano-bio-microfluidic chips for multiplexed protein detection in serum and saliva⁹⁵. Fluorescence detection of carcinoembryonic antigen (CEA), cancer antigen 125 (CA125) and Her-2/Neu

(C-erbB-2) was achieved. The platform used to capture the antigen is a microporous agarose bead array where an antibody labeled with QDs is captured. An amplification of 30 times higher in comparison to the standard molecular fluorophores is observed. In addition the use of different sized QDs with a wide range of wavelength emissions for multiple detections is also possible.

Zhang *et al.* reported the use of QDs as fluorescent labels for virus detection and genotyping⁹⁶. The device could detect 1000 copies mL⁻¹ of hepatitis B virus, in clinical serum samples using in vitro transcribed RNA as target molecules. Based on DNA hybridization with quantum dots labels, on-chip virus genotyping was also described.

A study for virus detection was performed by Ang's group⁹⁷. A microfluidic platform for immunofluorescent detection using quantum dots was also employed. The LOD was improved from 360 ng mL⁻¹ (ELISA assay) to 22 ng mL⁻¹ using these QDs based microfluidic system.

An immunochromatographic strip, based on nanoparticle probe was also demonstrated⁹⁸. This platform allows the determination of cotinine in human serum. In this case the QDs serve as signal vehicles for electrochemical readout with a linear range from 1 to 100 ng mL⁻¹ of cotinine with a detection limit of 1 ng mL⁻¹. This sensor provides a rapid, accurate, and quantitative tool for cotinine detection and shows great promise for in-field and point of care (POC) quantitative screening of tobacco smoke exposure.

Gold nanoparticles (AuNPs) are also good label candidates. They are easy to be produced in various sizes and to be functionalized. AuNP can be used for both fluorescence and electrochemical detection.

PSA in the samples was detected by using AuNPs as labels at concentrations ranging from 40 pM to 40 fM⁹⁹. The reported detection limit of this assay is 10 fM being the entire assay, from sample injection to final data analysis, completed in eighty minutes. Lei *et al.* also developed a biochip for protein detection involving AuNPs¹⁰⁰. AuNPs indicate the presence of protein. The concentration of protein was related with the resistance between interdigitated electrodes, achieving a limit of detection of 50 ng mL⁻¹.

Another detection principle applied in relation to labeling is the magnetoresistance where the sensor is a magnetic field transducer that exhibits a linear change in electrical resistance under an external magnetic field^{101,102}. An integrated microfluidic system incorporating spin valve (SV) sensors has been fabricated allowing cell detection and counting¹⁰³. That detection system can be used as a flow chip cytometer having the same efficiency, for high concentration samples, of the hemocytometer method and less than half of the error (4.5% in comparison to 8.5%). Germano *et al.* reported a platform for biomolecular recognition detection using magnetic nanoparticles (250 nm) achieving a robust detection of up to 20

INTRODUCTION

pM of DNA (20 mer single stranded DNA oligonucleotides hybridization)¹⁰⁴. The signal between complementary and non-complementary controls was possible to be discriminated.

Freitas's group developed a biochip portable platform for bioassay using DNA-DNA oligonucleotides hybridization model¹⁰⁵, where 130 nm magnetic nanoparticles (MNPs) were used for their magnetic resonance contribution, allowing the detection in real-time of 20 mer single stranded DNA sequences.

Table 1.1. Nanomaterials as labels in lab-on-a-chip applications.

Label	Analyte	Detection mode	LOD	Reference
CdSe/ZnS QD565/QD655	Carcinoembryonic antigen (CEA)	Fluorescence	0.02 ng mL ⁻¹	[94]
CdSe/ZnS QD565/QD655	Hepatitis B virus (HBV) in serum samples	Fluorescence	100 copies mL ⁻¹	[95]
CdSe/ZnS QDs	Marine fish iridovirus	Fluorescence	22 ng mL ⁻¹	[96]
CdSe/ZnS QDs	Cotinine	Electrochemical	1 ng mL ⁻¹	[97]
Gold nanoparticles	Prostate specific antigen (PSA)	Fluorescence	10fM	[98]
Gold nanoparticles	Proteins	Electrochemical	50 ng mL ⁻¹	[99]
Magnetic nanoparticles	DNA strands	Magnetoresistance	20 pM	[103]
Magnetic nanoparticles	DNA strands	Magnetoresistance	20 mer single stranded DNA sequences	[104]
PbS nanoparticles	Carcinoembryonic antigen (CEA)	Electrothermal vaporization inductively coupled plasma mass spectroscopy	0.058 ng mL ⁻¹	[105]

The same MNPs were used by Chen *et al.* for both capturing and labeling¹⁰⁶. Their device permitted to determine carcinoembryonic antigen (CEA) in human serum samples. Briefly the immunoassay was performed by immobilizing the CEA onto magnetic NPs modified

with the 1st Ab-CEA. Then, 2nd Ab-CEA labelled with PbS NPs was added. A limit of detection of 0.058 ng mL⁻¹, suitable for CEA determination in human serum samples was possible to be achieved.

NMs as labels give a wide range of possibilities to improve sensibility and selectivity. They also have shown to be of particular interest in developing high sensitive (bio) detection devices with multidetection capability and compatibility with LOCs. Various detection techniques ranging from optical, electrochemical and mass changes can be applied in LOCs while using NMs based labeling technologies.

1.2.3. Nanomaterials for process improvement

NMs could also be employed to improve analytical processes. Electrophoresis separation, capture and cell sorting between others are some of the reported examples improved through the use of NMs.

Concerning electrophoresis, a microchannel used for separation purposes could be modified with nanoparticles in order to control the electro-osmotic flow (EOF). Wang *et al.* modified microfluidic channels by citrate-stabilized gold nanoparticles after coating a layer of linear polyethylenimine (LPEI)¹⁰⁷. This modification was successfully used to separate dopamine and pinephrine, which were difficult to be separated from baseline in native and hybrid PDMS microchannels. Measurements by in-channel amperometric detection with a single carbon fibre cylindrical electrode were performed. Linear responses from 25 to 600 μ M for both compounds with detection limits of 2 μ M for dopamine and 5 μ M for epinephrine respectively were obtained. (Figure 1.5A,a)

The use of nanopore array is also extended for capture and release of bacteria, as described by Zare's group. In this work, conical nanopores on membrane inside a microfluidic device was developed¹⁰⁸, demonstrating the optimal capture of cyanobacterias, (one bacteria per pore) in a defined orientation with viabilities as high as 100%. The platform can discriminate cyanobacteria from a mixed suspension of cyanobacteria and chlamydomonas with a 90% of selectivity. (Figure 1.5A,b)

For filtering and / or capturing process, nanoporous elements have been integrated into microfluidics, in order to manipulate bioparticles. Porous materials have been limited to membranes sandwiched between microchannel layer and polymer monoliths, but Chen *et al.* reported the use of micropatterned carbon-nanotubes confined inside microfluidic channel for mechanically and/or capturing particles ranging over three orders of magnitude in size¹⁰⁹. Nanoparticles with size below the internanotube spacing can penetrate inside the forest and interact with the large surface area of carbon nanotubes. To validate this

INTRODUCTION

platform, specific biomolecular interactions were demonstrated by using cells, bacteria and viral-sized particles.

Carbon nanotubes for lab-on-a-chip applications especially their integration into microfluidic devices to improve superlubricating, microchannels, filtering and separation process also have been also studied by Choong *et al.*¹¹⁰

The use of nanoassembled graphene oxide appears as a novel capture alternative. Yoon *et al.* reported the circulating tumor cell isolation by using this strategy, showing a selective and sensitive detection of cells¹¹¹. The functionalized GO can self-assemble on patterned gold surfaces via electrostatic interactions between functional groups on GO and gold surfaces. This material is attractive for their 2D and 3D electrical conductivity, large surface area, mechanical flexibility, and high chemical and thermal stability.

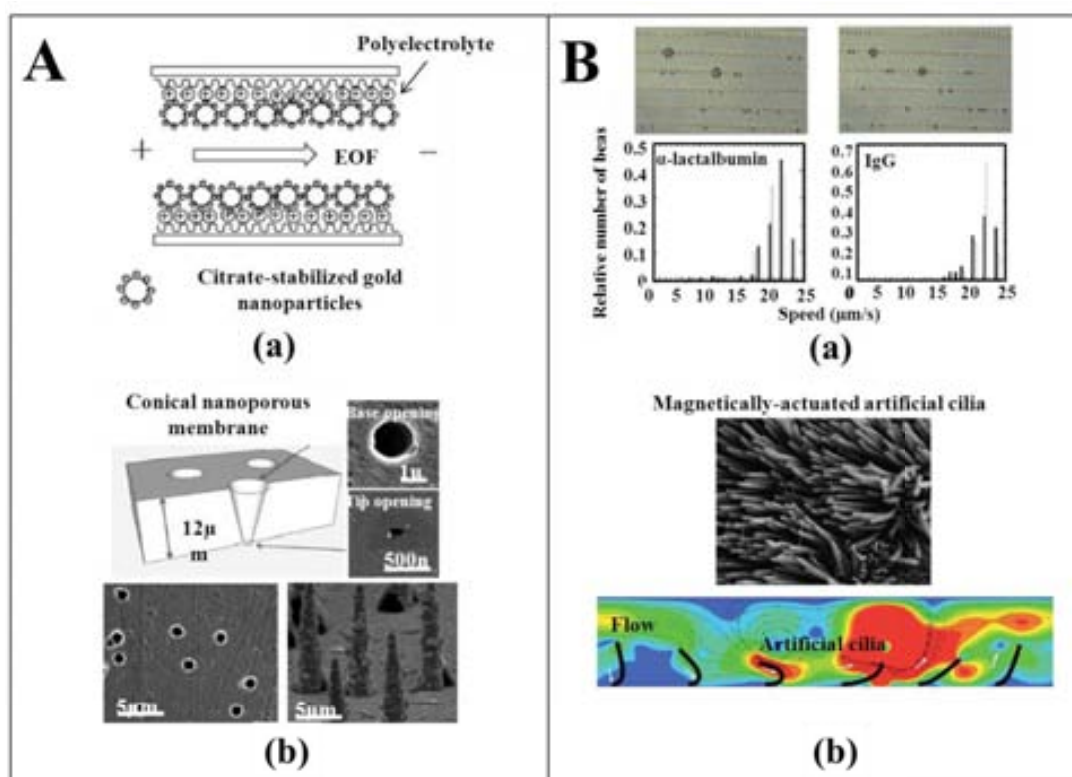


Figure 1.5. Process improving by using nanomaterials: (A) sorting tasks: PDMS-PDMS modification by using gold nanoparticles (13 nm of diameter). (a), schematic of the channel and (b) SEM images of conical nanopore array in PET used to trap cyanobacteria, and (B) capturing and mixing tasks: magnetic bead velocity distribution of protein coated beads (α -lactalbumin, f IgG) (a) and magnetically controlled nano-cilia for flow mixing with their respective simulation (b). Figures adapted with permissions from [106, 107, 111, and 112].

Magnetic nanoparticles used as labels in magnetoresistive sensors are also used as molecule's transport controller, in order to preconcentrate the sample on the detector

chamber. The Oscarsson's group reported a magnetic microchip for controlled transport of attomole levels of proteins. The activity of proteins immobilized on the beads was also demonstrated by injecting antibodies into the channel. Parameters like the sticking forces between beads and substrate during transportation of proteins and the charge interaction in comparison with the hydrophobic forces were also optimized. The performance of the platform was tested by detecting a solution of fluorescein iso-thiocyanate (FITC) labeled anti-HSA, achieving a LOD of 0.02 mg mL^{-1} by fluorescence methods¹¹² (Figure 1.5B,a). Another interesting application for process improvement is microfluidic propulsion by using magnetically-actuated artificial cilia fabricated using thin polymer films with embedded magnetic nano-particles. These artificial cilia were fabricated using thin polymer films with embedded magnetic nanoparticles. Onck's group studied their deformation under different external magnetic fields and flows¹¹³ (Figure 1.5B,b).

1.2.4. In-chip production and characterization of nanomaterials

Synthesis

As already seen in the previous section of this Chapter, NMs are really powerful tools to improve the sensitivity of microfluidic devices, but the contrary is also true. Nanoparticles are usually produced by batch chemical syntheses which are designed for mass production but they are time consuming and suffer from a poor control of the homogeneity and monodispersity. Furthermore they require high volumes of reagents what doesn't make them really environmental friendly. Furthermore for biological and medical applications, the quality and the homogeneity of the NPs is much more important than the amount of produced NPs. The rapid chemical reactions and efficient mixing of microfluidics allows a better control of the synthesis parameters such as the size and the properties of the nanoparticles. The wide varieties of device substrates as also an important flexibility in the solvent employed for the NPs fabrication. Synthesis of a wide range of polymeric and inorganic particulate materials has already been investigated in microfluidics¹¹⁴.

Semiconductors like QDs have been produced by continuous flow. In this case the reaction occurs at the interface of two liquids. Thus CdS ¹¹⁵, CdSe ^{116,117,118} and CdSe-ZnS synthesis have been reported. A better distribution could be obtained by using segmented techniques like droplet based flow synthesis and reactor's features. Droplets are assimilated as microreactors of Nanoliters (nL) volumes size solutions. QDs with better controlled sizes have been produced by this way^{119,120} even at high temperature^{121,122}.

In 2011, Zhao *et al.* generated multifunctional quantum dot barcode particles¹²³. Indeed, the QDs were entrapped in a hydrogel. By melting different QDs or different size of QDs, it is possible to obtain an infinite range of barcodes. The authors also showed the possibility to

INTRODUCTION

have two delimited compartments inside these particles, one of QDs for the detection and one of magnetic particles for magnetic separation and manipulation.

Colloidal nanoparticles synthesis in lab-on-a-chip platforms have been also reported for applications in optical coating, displays, chromatography, and catalyst¹²⁴. The use of microreactors for nanoparticles synthesis allows the flexibility for reagent manipulation, therefore, the possibility to use multichannel depending of the synthesis requirements. Gijs's group reported the synthesis of silica nanoparticles with controllable shape and size, taking advantage of the high monodispersity of on-chip generated microdroplets to produce nanoparticles assemblies with narrow size distribution¹²⁵. By rolling the droplets over a hydrophobic substrate, they could obtain pillar-like assemblies, to be used as a support for catalytically precipitation reaction of fluorescent dye.

The synthesis of magnetic iron oxide nanoparticles (4 nm of diameter) were also demonstrated in a microfluidic system by Frenz, *et al.* The novelty of this work is that all reaction occurs into microdroplets, in this way is possible to reduce the time of reaction being more efficient¹²⁶. During microreactors formation is also possible to integrate a functionalization step for biocompatibility, drug anchoring and cell targeting, giving a better control of synthesis conditions determining in this way their properties.

Jensen *et al.* described basic principles of operation of microfluidic reactors for synthesis of colloidal silica nanoparticles, controlling the particles size, changing the linear velocity and mean residence time¹²⁷. For a given laminar flow reactor design, monodisperse particle distributions are only feasible under conditions that minimize axial dispersion. (Figure 1.6A).

New nanomaterial-conjugated polymer dots were synthesized in a microfluidic platform obtaining a new class of fluorescent nanoprobe with interest to be used in subcellular labelling and sensor field. That is the case for the preparation of highly monodisperse, sub-micrometer conjugated polymer particles reported by Weitz's group¹²⁸. Particle size is tuned between 150 to 2 nm, by emulsification of a conjugated polymer solution on a microfluidic chip followed by solvent evaporation. The obtained particles represent a novel class of photonic materials with a wide spectrum for applications such as coatings, photonic crystals, etc. Other polymeric materials were developed by F. Schütze, *et al.*¹²⁹. Stable fluorescent nanoparticles (between 30 to 60nm) from controlled mixing of a tetrahydrofuran (THF) solution of poly (fluorene ethynylene)-block-poly(ethylene glycol) in a microfluidic laminar flow cross junction were obtained. Due to different conjugation lengths and energy transfer to lower-energy chromophores, fluorescence emission of conjugated polymer nanoparticles is commonly red-shifted vs. polymer solutions in organic solvents.

Toxicity

NMs, even when made of inert elements like gold, become highly active at nanometer dimensions. Nanotoxicological studies are intended to determine whether and to what extent these properties may pose a threat to the environment and to human beings. For instance, some works involving microfluidic platforms have brought an interesting solution to study the NMs behavior in presence of biological elements, taking advantage of the small volume consume, lower time of analysis and sensitivity enhancement.

NMs have many potential biomedical applications, therefore, *in vitro* studies should be performed to analyze and optimize the interaction between these nanoparticles and biological entities.

Faronkhzad, *et al.* in 2005, studied the interaction of polymeric nanoparticles conjugated with aptamers that recognized the transmembrane prostate specific membrane antigen (PSMA), with cells seeded in microchannels. The binding of particles to cells that expressed or did not express the PSMA (LNCaP or PC3, respectively) were evaluated with respect to changes in fluid shear stress, PSMA expression on target cells, and particle size. The presence of ligands on vehicle surface, size of vehicles, and amount of shear stress generated during fluid flow that can affect the *in vitro* targeting efficiency of these vehicles was demonstrated¹³⁰. Also, the shear stress generated from fluid flow can have a significant effect on the binding characteristics. Richter *et al.* developed a microfluidic tool to study cell–nanoparticle interactions and nanoparticle accumulation effects in small cell populations¹³¹. Results of the study showed a 20% and 95% reduction of collagen production following 4 hours exposure to 10 and 1 mg/mL of gold and silver nanoparticles (diameter of 10 nm) respectively (Figure 1.6B).

In 2010, Rhee's group evaluated the cytotoxicity effects of surface-modified QDs on neuron-like PC12 cells cultured inside microfluidic devices¹³². The results suggest that QDs can induce toxicity to neurons depending on the stability of surface ligands on their surface. CTAB/TOPO-QDs were highly toxic to neurons, whereas MPA-QDs were non-toxic. Through the use of the microfluidic neuronal device, the axonal degeneration induced by CTAB/TOPO- QDs was related to the neuronal cell death as well as of direct axonal toxicity. The results indicated that oxidative stress could be a leading cause of QD toxicity. Moreover, the microfluidic neuronal device, which is providing distinguished benefits over the conventional platforms, can be efficiently utilized to study the mechanisms of axonal growth and degeneration, and the protection of axons.

A study done by Safi *et al.* was focused on interactions between magnetic nanowires and living cells, their toxicity and degradation¹³³. The toxicity studies were based on mitochondrial activity, cell proliferation, and production of reactive oxygen species, showing that the wires don't display acute short-time (<100h) toxicity toward the cells. In relation to the nanowires, the cells are able to degrade them and transform them in

INTRODUCTION

aggregates in short time periods (days). This degradation is likely to occur as a consequence of the internal structure of the wires, which is that of a non-covalently bound aggregate.

Characterization

Few works regarding microfluidic for NMs characterization are reported, however, this could be a good approach to understand optical, electrochemical and mechanical behavior of NMs under flow conditions, with interest for further applications in (micro)analytical assays.

One characterization device found in the literature is the CMOS-hall-effect sensor for characterization and detection of magnetic nanoparticles¹³⁴ for biomedical application. This technique was proposed by Liu *et al.* in contrast with the conventional characterization technique: magnetic resonance (MRX). They improved the time of measurement due to the fast magnetic relaxation within short time constant of 64 ns. Three different commercial magnetic nanoparticles were tested with this system showing different time of relaxation, allowing the implication of samples with different magnetic properties. The chip is easy to be integrated with microfluidics for point-of-care applications.

Resistive pulse sensor (RPS) with a submicron sensing gate and dual detecting channels-two stage differential amplifier was also proposed to characterize nanoparticles¹³⁵. This device can achieve a high sensitivity allowing the detection of nanometer size particles. This method is able to detect nanoparticles of 490nm and 220nm using a microfluidic chip. The RPS chip can be divided into upstream section, sensing gate, downstream section, and two detecting channels. The upstream channel, sensing gate, and downstream channel form the main channel between inlet and outlet reservoirs at the two ends. The detecting channels also have two reservoirs at the end of each channel for inserting the sensing electrodes, so when a non-conducting particle passes through a small sensing gate, the resistance of the sensing gate as well as its resistance change. (Figure 1.6C).

1.2.5. Other applications

Other nanostructured platforms have been reported for applications in cell therapy/tissue engineering, cell and developmental biology. Gallego-Pérez *et al.*, developed a micro-nanofabricated platform, consisting in microwells structurally bonded to a sheet of electrospun fibers¹³⁶. Human hepatocytes were used as model cells to demonstrate the ability of the platform to allow controlled cluster formation.

It is well known the recent use of nanostructures (i.e. vesicles, micelles, bilayers) as encapsulation agents for the eventual release of drugs, flavors, and fragrances. Micelle-vesicle transition studies were performed by Lee *et al.* by the development of an integrated microfluidic chip / cryogenic transmission electron microscopy (cryo-TEM) unit¹³⁷, in

order to characterize this phenomenon in specific amphiphilic system where micellar solutions of cetyltrimethylammonium bromide (CTAB) and dodecylbenzene sulfonic acid (HDBS) are mixed to form vesicles. This tool can be applied broadly to study transient structures in nanoscale systems under highly controlled conditions provided by microfluidics.

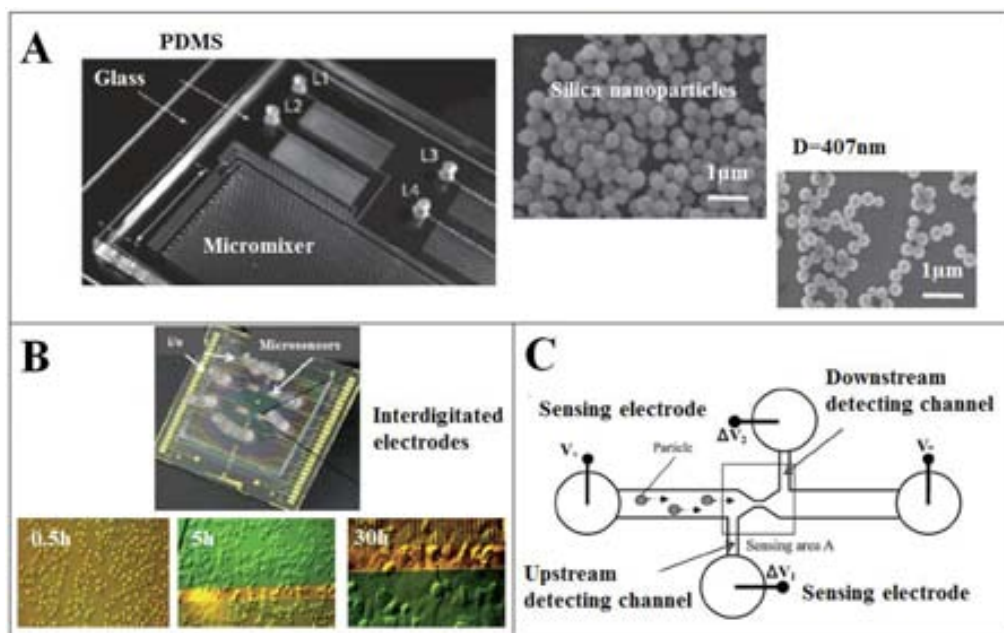


Figure 1.6. In-chip production and characterization of nanomaterials: (A) PDMS/glass based chip that includes a micromixer used for the in-chip synthesis of nanoparticles. Are shown SEM images of silica nanoparticles from the Stober process developed in a gas–liquid segmented microflow. (B) toxicity studies in chip using as a microfluidic biochip consisting of PDMS microchannels bonded to a glass bottom substrate that includes four sample inlets and wastes as well as contactless dielectric microsensors located underneath monitoring chambers. Pictures taken after 0.5 h, 5 h and 30 h after cell seeding show NHDF seeding density, adhesion and spreading processes during cell cultivation are included, and (C) a schematic diagram of a nanoparticle detecting microfluidic chip. Adapted with permissions from [126, 130 and 134].

1.2.6. Perspectives

Nanomaterials (NM)-based lab-on-a-chip technology is showing to be an interesting alternative for a wide range of (bio) analytical devices applications. The integration of NMs into LOC systems seems to bring additional advantages in relation to the system sensitivity and miniaturization beside the versatility of the designs and applications possibilities. NMs application as detectors or detectors' modifiers is improving the performance of the conventional LOCs. Particularly the use of carbon nanotubes and graphene is bringing significant advances in electrical or optical detections. NMs applications as microchannel's

INTRODUCTION

modifier for separation enhancement are offering novel functionalization possibilities for improvements in sample pre-treatment or separation processes.

Microfluidics platform is also being used as a novel strategy for production and characterization of NMs opening new routes for encapsulation and homogenous shell-particles synthesis. Of notable progress are the synthesis of QDs and nanowires using microfluidic devices. Very good reproducibility, reducing of the preparation time and the reagents consume are some of the advantages of in-chip NMs preparation and applications.

NMs are also involved in microanalytical process enhancement. NMs can be used for filtering, sorting, biomolecules capturing and other actuations with interest for various applications.

The in-chip NM application spectra also include applications like tissue nano-scaffolds, and drugs delivery systems. This is a challenging field for future nano-drug-delivery platforms.

Finally, problems such as the application of complicated fabrication and measuring technologies probably not in agreement with mass production and user-friendly technologies need to be resolved so as to bring these devices to the end-users interested in microdevices.

1.3. References

¹J. Hübner, K.B. Mogensen, A.M. Jorgensen, P. Friis, P. Telleman, and J.P. Kutter. *Integrated optical measurement system for fluorescence spectroscopy in microfluidic channels*. Rev. Sci. Instrum. 2001, 72(1), 229-233.

²S. Terry. *A gas chromatography system fabricated on a silicon wafer using integrated circuit technology*. Ph.D. dissertation, department of Electrical, Stanford University, Stanford, California, USA, 1975.

³A. Manz, N. Graber, and H.M. Widmer. *Miniaturized total chemical analysis systems: a novel concept for chemical sensing*. Sens. Actuators, B1. 1990, 244-248.

⁴M.U. Kopp, H.J. Crabtree, and A. Manz. *Developments in technology and applications of microsystems*. Curr. Opin.Chem. Biol. 1997, 1, 410-419.

⁵A.E. Kamholz, and P. Yager. *Theoretical analysis of molecular diffusion in pressure-driven laminar flow in microfluidic channels*. Biophys. J. 2001, 80, 155-160.

-
- ⁶J. Yang, D. Kwok. *Analytical treatment of electrokinetic microfluidics in hydrophobic microchannels*. Anal. Chim. Acta. 2004, 507(1), 39-53.
- ⁷C. Galusinski, and P. Vigneaux. *On stability condition for bifluid flows with surface tension: application to microfluidics*. J. Comput. Phys. 2008, 227(12), 6140-6164.
- ⁸M. Wiklund, R. Green, and M. Ohlin. *Acoustofluidics 14: applications of acoustic streaming in microfluidic devices*. 2012, Lab Chip 12, 2438-2451.
- ⁹T. Kulrattanakul, R.G.M. van der Sman, C.G.P.H. Schroën, and R.M. Boom. *Classification and evaluation of microfluidic devices for continuous suspension fractionation*. Adv. Colloid Interface Sci. 2008, 142, 53-66.
- ¹⁰J. Zhou, A.V. Ellis, and N.H. Voelcker. *Recent developments in PDMS surface modification for microfluidic devices*. 2010, Electrophoresis 31, 2-16.
- ¹¹A. Asgar, S. Bhagat, S. Kuntaegowdanahalli and I. Papautsky. *Continuous particle separation in spiral microchannels using dean flows and differential migration*. Lab Chip. 2008, 8, 1906-1914.
- ¹²M. Kersaudy-Kerhoas and R. Dhariwal. *Hydrodynamic blood plasma separation in microfluidic channels*. Micro Nanofluid. 2010, 8, 105-114.
- ¹³X. Xue, M. K Patel, M. Kersaudy-Kerhoas, C. Baily, et.al. *Effect of Fluid Dynamics and Device Mechanism on Biofluid Behaviour in Microchannel Systems: Modeling Biofluids in a Microchannels Biochip Separator*. IEEE International Conference on Electronic Packaging Technology & High Density Packaging. 2009.
- ¹⁴Y.-J. Yang, H.-H. Liao, K.-H. Huang, et.al. *Novel designs of Herringbone chaotic mixers*. Proceedings of the 1st IEEE International Conference on Nano/Micro Engineered and Molecular Systems. 2006.
- ¹⁵S.Nagrath, L. V. Sequist, S. Maheswaran, et. al., *Isolation of rare circulating tumor cells in cancer patient by microchip technology*. Nature. 2007, 450, 1235-1239.
- ¹⁶E. Stern, A. Vacic, N. K. Rjan, et. al. *Label-free biomarker detection from whole blood*. Nat. Nanotechnol. 5. 2010, 5, 138-142.
- ¹⁷A. Y. Hsiao, Y. Torisawa, Y.-C. Tung, et. al. *Microfluidic system for formation of PC-3 prostate cancer co-culture spheroids*. Biomaterials. 2009, 30(16), 3020-3027.
- ¹⁸M. Chen, H. Huang, E. Pierstorff, et. al. *Parylene-Encapsulated copolymeric membranes as localized and sustained drug delivery platforms*. Ann. Biomed. Eng. 2009, 37(10), 2003-2017.

INTRODUCTION

- ¹⁹ J. Wang, B. Tian, and E. Sahlin, *Integrated Electrophoresis Chips/Amperometric Detection with Sputtered Gold Working Electrodes*. *Anal. Chem.* 1999, 71(17), 3901-3904.
- ²⁰ K-J. Lien, C-J. Liu, et.al. *Microfluidic System for Detection of Thalassemia-1 deletion using saliva samples*. *Anal. Chem.* 2009, 81(11), 4502-4509.
- ²¹ A. B. Fuchs, A. Romani, D. Freida, et. al. *Electronic sorting and recovery of single live cells from microlitre sized samples*. *Lab Chip*. 2005, 6(1), 121-126.
- ²² S.P. Nunes, B. Ruffmann, E. Rikowski, S. Vetter and K. Richau. *Inorganic modification of proton conductive polymer membranes for direct methanol fuel cells*. *J. Membr. Sci.* 2002, 30, 215-225.
- ²³ G. D. Chen, C. J. Alberts, W. Rodríguez, et. al. *Concentration and purification of human immunodeficiency virus type 1 virions by microfluidic separation of superparamagnetic nanoparticles*. *Anal. Chem.* 2009, 82(2), 723-728.
- ²⁴ J. Shi, H. Huang, Z. Stratton, et. al. *Continuous particle separation in a microfluidic channel via standing surface acoustic waves (SSAW)*. *Lab Chip*. 2009, 9(23), 3354-3359.
- ²⁵ GM. Whitesides. *The origins and the future of microfluidics, Insight overview*, *Nature*. 2006, 442, 368-373.
- ²⁶ D.J. Beebe, G.A. Mensing, G.M. Walker. *Physics and applications of microfluidics in biology*. *Annu. Rev. Biomed. Eng.* 4, 2002, 261-286.
- ²⁷ C.J. Kastrupp, M.K. Runyon, E.M. Lucchetta, J.M. Price, R.F. Ismagilov. *Using chemistry and microfluidics to understand the spatial dynamics of complex biological networks*, *Acc. Chem.Res.* 2008, 41(4), 549-558.
- ²⁸ S. Siau, A. Vervaet, E. Schacht, U. Demeter, A.V. Calster. *Epoxy polymer surface modification through wet-chemical organic surface synthesis for adhesion improvement in microelectronics*. *Thin Solid Films*. 2006, 495, 348-356.
- ²⁹ L. De Stefano, E. Orabona, A. Lamberti, I. Rea, I. Rendina. *Microfluidics assisted biosensors for label-free optical monitoring of molecular interactions*. *Sens. Actuators B*. 2013, 179, 157-162.
- ³⁰ A. Mata, A.J. Fleischman, and S. Roy. *Characterization of polydimethylsiloxane (PDMS) properties for biomedical micro/nanosystems*. *Biomed. Microdevices*. 2005, 7(4), 281-293.
- ³¹ S. Alegret, *Integrated analytical systems*. *Comprehensive Analytical Chemistry*, edited by D. Barceló, Wilson and Wilson's, vol. 39, 2003.

-
- ³²A. C. Richards Grayson, R. S. Shawgo, A. M. Johnson, N. T. Flynn, Y. Li, M. J. Cima and R. Langer. *A BioMEMS Review: MEMS technology for physiologically integrated devices*. Proceedings of the IEEE. 2004, 92 (1), 6-21.
- ³³L. M. Campos, T. T. Truong, D. E. Shim, M. D. Dimitriou, D. Shir, I. Meinel, J. A. Gerbec, H. T. Hahn, J. A. Rogers and C. J. Hawker. *Applications of photocurable PMMS thiol-ene stamps in soft lithography*. Chem. Mater. 2009, 21, 5319–5326.
- ³⁴T. Lomas, S. Mongpraneet, A. Wisitsoraat, K. Jaruwongrungeee, A. Sappat, T. Maturos, F. Chevasuvit and A. Tuantranont. *Low cost hot Embossing process for plastics microfluidic chips fabrication*, 6th International Conference on Electrical Engineering/Electronics, Computer, Telecommunications and Information Technology, 2009, 462-464.
- ³⁵P.P. Shiu, G.K. Knopf and M. Ostojic. *Fabrication of metallic micromolds by laser and electro-discharge micromachining*, Microsys. Technol. 2010, 16 (3), 477-485.
- ³⁶S. Roy. *Fabrication of micro- and nano-structured materials using mask-less processes*, J. Phys. D: Appl. Phys. 2007, 40, 413–426.
- ³⁷P. Nath, D. Fung, Y. A. Kunde, A. Zeytun, B. Branch and G. Goddard. *Rapid prototyping of robust and versatile microfluidic components using adhesive transfer tapes*, Lab Chip. 2010, 10, 2286–2291.
- ³⁸S. Mongpraneet, A. Wisitsora, R. Phatthanakun, N. Chomnawang and A. Tuantranont *Low-cost x-ray mask based on micropattern sputtered lead film for x-ray lithography*, AVS. 2010, 27 (3), 1299-1303.
- ³⁹J. Greener, W. Li, J. Ren, D. Voicu, V. Pakhareenko, T. Tang and E. Kumacheva, *Rapid. Cost-efficient fabrication of microfluidic reactors in thermoplastic polymers by combining photolithography and hot embossing*, Lab Chip. 2009, 10, 522–524.
- ⁴⁰S. H. Choi, D. S. Kim and T. H. Kwon. *Microinjection molded disposable microfluidic lab-on-a-chip for efficient detection of agglutination*. Microsyst. Technol. 2009, 15, 309-316.
- ⁴¹L. P. Yeo, S. Huan, Z. Wang, Z. Wang and N. Frans. *Micro-fabrication of polymeric devices using hot roller embossing*, Microelectron. Eng. 2009, 86, 933–936.
- ⁴²P. Fanjul-Bolado, D. Hernández-Santos and P. J. Lamas-Ardisana. *Electrochemical characterization of screen-printed and conventional carbon paste electrodes*, Electrochim. Acta. 2008, 53, 3635-3642.

-
- ⁴³S. C. Currall, E. B. King, N. Lane, J. Madera, and S. Turner, *What drives public acceptance of nanotechnology?*, *Nat.Nanotechnol.* 2006, 1, 153-155.
- ⁴⁴C. M. Niemeyer. *Nanoparticles, Proteins, and Nucleic Acids: Biotechnology Meets Material Science.* *Angew. Chem.* 2001, 40, 4128-4158.
- ⁴⁵N. L. Rosi and CA. Mirkin. *Nanostructures in biodefense and molecular diagnostics*, *Chem. Rev.* 2005, 105, 1547-1562.
- ⁴⁶A. Merkoçi. *Nanoparticles-based strategies for DNA, protein and cell sensors.* *Biosens. Bioelectron.* 2010, 26, 1164–1177.
- ⁴⁷A. de la Escosura-Muñiz, A. Ambrosi, and A. Merkoçi. *Electrochemical analysis with nanoparticle based biosystems.* *Trends Anal. Chem.* 2008, 27, 568-584.
- ⁴⁸M. Perfezou, A. Turner, and A. Merkoçi. *Cancer detection using nanoparticles-based sensors.* *Chem. Soc. Rev.* 41, 2012, 2606-2622.
- ⁴⁹G. Aragay, J. Pons, A. Merkoçi. *Recent trends in macro, micro and nanomaterials based tools and strategies for heavy metals detection.* 2011, *Chem. Rev.* 111 (5), 3433-3458.
- ⁵⁰O. A. Sadik, A.L. Zhou, S. Kikandi, N. Du, Q. Wang, and K. Varner. *Sensors as tools for quantitation, nanotoxicity and nanomonitoring assessment of engineered nanomaterials.* *J. Environ. Monit.* 2009, 11(10), 1782-1800.
- ⁵¹Y. Liu, Y. Xue, J. Ji, X. Chen, J. Kong, P. Yang, H. H. Girault, and B. Liu. *Gold nanoparticle assembly microfluidic reactor for efficient on-line proteolysis.* *Mol. Cell. Proteomics.* 2007, 1428-1436.
- ⁵²C. H. Weng, C. C Huang, C. S. Yeh, and G. B. Lee. *Synthesis of gold nanoparticles using microfluidic reaction systems.* 7th IEEE Conference on Nanotechnology (IEEE NANO), 2007, 462-466.
- ⁵³P. B. Abdallah, A.O. Moctar, B. Ni, N. Aubry, and P. Singh. *Optical manipulation of neutral nanoparticles suspended in a microfluidic channel.* *J. Appl. Phys.* 2006, 99, 1-6.
- ⁵⁴M. Pumera. *Nanomaterials Meet Microfluidics.* *Chem. Commun.*, 2011, 47, 5671–5680.
- ⁵⁵C. L. Choong, W. I. Milne, and K. B. K. Teo. *Review: carbon nanotube for microfluidic lab-on-a-chip application.* *Int. J. Mat. Forming.* 2008, 1, 117-125.
- ⁵⁶A. G. Crevillén, M. Pumera, M. C. González, and A. Escarpa. *Towards lab-on-a-chip approaches in real analytical domains base don microfluidic chips/electrochemical multi-walled carbon nanotube platforms.* *Lab Chip.* 2009, 9, 346-353.

-
- ⁵⁷K. Maehashi and K. Matsumoto. *Label-free electrical detection using carbon nanotube-based biosensors*. *Sensors*. 2009, 9, 5368-5378.
- ⁵⁸J. N. Tey, I. P. M. Wijaya, J. Wei, I. Rodriguez, and S. G. Mhaisalkar. *Nanotubes-/nanowires-based, microfluidic-integrated transistors for detecting biomolecules*. *Micro/Nanofluidics*. 2010, 9, 1185-1214.
- ⁵⁹P. Serp and E. Castillejos. *Catalysis in carbon nanotubes*. *Chem. Cat. Chem.* 2010, 2, 41-47.
- ⁶⁰W. Feng, and P. Ji. *Enzymes immobilized on carbon nanotubes*. *Biotech. Adv.* 2011, 29(6), 889–895.
- ⁶¹Q. Z. Zhang, B. Zhao, J. Yan, SP. Song, R. Min, CH. Fan. *Nanotube-based colorimetric probe for ultrasensitive detection of ataxia telangiectasia mutated protein*. *Anal. Chem.* 2011, 83, , 9191-9196.
- ⁶²J. Morton, N. Havens, A. Mugweru, A. K. Wanekaya. *Detection of trace heavy metal ions using carbon nanotube-modified electrodes*. *Electroanalysis*. 2009, 21(14), 1597–1603.
- ⁶³J. Okuno, K. Maehashi, K. Kerman, Y. Takamura, K. Matsumoto, and E. Tamiya. *Label-free immunosensor for prostate-specific antigen base don single-walled carbon nanotube array-modified microelectrodes*. *Biosens. Bioelectron.* 2007, 22, 2377-81.
- ⁶⁴A. Javey, J. Guo, D. B. Farmer, Q. Wang, D. Wang, R. G. Gordon, M. Lundstrom, and H. Dai. *Self-aligned ballistic molecular transistor and electrically parallel nanotube arrays*. *Nano Lett.* 2004, 4(7), 1319-1322.
- ⁶⁵J. N. Tey, I. P. M. Wijaya, Z. Wang, W. H. Goh, A. Palaniappan, S. G. Mhaisalkar, I. Rodriguez, S. Dunham, and J. a Rogers. *Laminated, microfluidic-integrated carbon nanotube based biosensors*. *Appl. Phys. Lett.* 2009, 94, 1-3.
- ⁶⁶A. Vlandas, T. Kurkina, A. Ahmad, K. Kern, and K. Balasubramanian. *Enzyme-free sugar sensing in microfluidic channel with an affinity-based single-wall carbon nanotube sensor*. *Anal. Chem.* 2010, 82, 6090-6097.
- ⁶⁷C. Mayorga-Martinez, M. Guix, R.E. Madrid and A. Merkoçi. *Bimetallic nanowires as electrocatalysit for nonenzymatic real-time impedancimetric detection of glucose*. *Chem. Commun.* 2012, 48, 1686-1688.
- ⁶⁸I. P. M. Wijaya, T. J. Nie, S. Gandhi, R. Boro, A. Palaniappan, G. W. Hau, I. Rodríguez, C.R. Suri, and S.G. Mhaisalkar. *Femtomolar detection of 2,4-dichlorophenoxyacetic acid*

herbicides via competitive immunoassay using microfluidic based carbon nanotube liquid gate transistor. Lab Chip. 2010, 10, 634-638.

⁶⁹W. S. Hummers, and R. E. Offeman. *Preparation of graphitic oxide*, J. Amer. Chem. Soc. 1958, 80 (6), 1339–1339.

⁷⁰C. K. Chua, A. Ambrosi, and M. Pumera. *Graphene based nanomaterials as electrochemical detectors in lab-on-a-chip devices.* Electrochem. Commun. 2011, 13, 517-519.

⁷¹Q. He, S. Wu, S. Gao, X. Cao, Z. Yin, H. Li, P. Chen, and H. Zhang. *Transparent, flexible, all-reduced graphene oxide thin film transistors.* ACS Nano. 2011, 5 (6), 5038-5044.

⁷²B. J. Plowman, S. K. Bhargava, and A. P. O'Mullane. *Electrochemical fabrication of metallic nanostructured electrodes for electroanalytical applications.* Analyst. 2011, 136, 5107-5119.

⁷³Z. Zou, J. Kai, M. Rust, J. Han, and C. *Functionalized nano interdigitated electrodes arrays on polymer with integrated microfluidics for direct bio-affinity sensing using impedimetric measurements.* Sens. Actuators A: Physical. 2007, 136, 518-526.

⁷⁴D. Lee, J. Ondrake, and T. Cui. *A conductometric indium oxide semiconducting nanoparticle enzymatic biosensor array.* Sensors. 2011, 11, 9300-9312.

⁷⁵J. Gamby, A. Rudolf, M. Abid, H. H. Girault, C. Deslouis, and B. Tribollet. *Polycarbonate microchannel network with carpet of gold nanowires as SERS-active device.* Lab Chip. 2009, 9, 1806-1808.

⁷⁶L. C. Taylor, T. B. Kirchner, N. V. Lavrik, and M. J. Sepaniak. *Surface enhanced raman spectroscopy for microfluidic pillar arrayed separation chips.* Analyst. 2012, 137, 1005-1013.

⁷⁷V. Canpean and S. Astilean. *Multifunctional plasmonic sensor son low-cost subwavelength metallic nanoholes arrays.* Lab Chip. 2009, 9, 3574-3579.

⁷⁸A. J. Tavares, M. O. Noor, C. H. Vannoy, W. R. Algar, and U. J. Krull. *On-chip transduction of nucleic acid hybridization using spatial profiles of immobilized quantum dots and fluorescence resonance energy transfer.* Anal. Chem. 2012, 84 (1), 312-319.

⁷⁹Y. Luo, W. Sun, C. Liu, G. Wang, and N. Fang. *Superlocalization of single molecules and nanoparticles in high-fidelity optical imaging microfluidic devices.* Anal. Chem. 2011, 83, 5073-5077.

-
- ⁸⁰S. Demming, A. Hahn, A. Edlich, E. Franco-Lara, R. Krull, S. Barcikowski, and S. Büttgenbach, *Phys. Status Solidi. A.* 2010, 207, 898-903.
- ⁸¹A. Prabhakar and S. Mukherji. *A novel C-shaped, gold nanoparticle coated, embedded polymer waveguide for localized surface plasmon resonance based detection.* *Lab Chip.* 2010, 10, 3422-3425.
- ⁸²L. L. Qu, D. W. Li, J. Q. Xue, W. L. Zhai, J. S. Fossey, and Y. T. Long. *Batch fabrication of disposable screen printed SERS arrays.* *Lab Chip.* 2012, 12, 876-881.
- ⁸³B. Cui, C. Wu, L. Chen, A. Ramirez, E. L. Bearer, W. P Li, W. C. Mobley, and S. Chu. *One at a time, live tracking of NGF axonal transport using quantum dots.* *PNAS.* 2007, 104 (34), 13666-13671.
- ⁸⁴C. L. Kuyper, K. L. Budzinski, R. M. Lorenz, and D. T. Chiu. *Real-Time Sizing of Nanoparticles in Microfluidic Channels Using Confocal Correlation Spectroscopy.* *J. Am.Chem. Soc.* 2006, 128, 730-731.
- ⁸⁵X. F. Wang, Y. Zhou, J. J. Xu and H. Y. Chen. *Signal-on electrochemiluminescence biosensors base don CdS-carbon nanotube nanocomposite for the sensitive detection of choline and acetylcholine.* *Adv. Funct. Mater.* 2009, 19, 1444-1450.
- ⁸⁶K. Wang, Q. Liu, X. Y. Wu, Q. M. Guan and H. N. Li. *Graphene enhanced electrochemiluminiscence of CdS nanocrystal for H₂O₂ sensing.* *Talanta.* 2010, 82, 372-376.
- ⁸⁷Y. Lu, S. Peng, D. Luo, and A. Lal. *Low-concentration mechanical biosensor base don a photonic crystal nanowire array.* *Nat. Commun.* 2 (578), 2011, DOI: 10.1038/ncomms 1587.
- ⁸⁸A. Y. Joshi, S. C. Sharma, and S. P. Harsha. *Zeptogram scale mass sensing using single walled carbon nanotube based biosensors.* *Sens. Actuators A.* 2011, 168(2), 275-280.
- ⁸⁹I. Mehdipour, A. Barari, and G. Domairry. *Application of a cantilevered SWCNT with mass at the tip as a nanomechanical sensor.* *Comp. Mater. Sci.* 2011. 50(6), 1830-1833.
- ⁹⁰P. S. Waggoner, C. P. Tan, and H. G. Craighead. *Microfluidic integration of nanomechanical resonators for protein analysis in serum.* *Sens. Actuators B.* 2010, 150, 550-555.
- ⁹¹K. S. Hwang, S. M. Lee, S. K. Kim, J. H. Lee, and T. S. Kim. *Micro- and nanocantilever devices and systems for biomolecule detection.* *Annu. Rev. Anal. Chem.* 2009, 2, 77-98.

-
- ⁹²M. K. Wagner, F. Li, J. Li, X. F. Li, and X. C. Le. *Use of quantum dots in the development of assays for cancer biomarker*. *Anal. Bioanal. Chem.* 2010, 397, 3213-24.
- ⁹³J. A. Ho, Y.C. Lin, L. S. Wang, K.C. Hwang, and P. T. Chou. *Carbon nanoparticle-enhanced immunoelectrochemical detection for protein tumor marker with cadmium sulfide biotracers*. *Anal. Chem.* 2009, 81, 1340-1346.
- ⁹⁴S. Wang, N. Mamedova, N. A. Kotov, W. Chen, and J. Studer. *Antigen/antibody immunocomplex from CdTe nanoparticle bioconjugates*. *Nano Lett.* 2002, 2, 817-822.
- ⁹⁵J. V. Jokerst, A. Raamanathan, N. Christodoulides, P. N. Floriano, A. Pollard, G. W. Simmons, J. Wong, C. Gage, W. B. Furmaga, S. W. Redding, and J. T. McDevitt. *Nano-bio-chips for high performance multiplexed protein detection: determinations of cancer biomarkers in serum and saliva using quantum dot bioconjugate labels*. *Biosens. Bioelectron.* 2009, 24, 3622-3629.
- ⁹⁶H. Zhang, T. Xu, C. W. Li, and M. Yang. *A microfluidic device with microbead array for sensitive virus detection and genotyping using quantum dots as fluorescence labels*. *Biosens. Bioelectron.* 2010, 25, 2402-2407.
- ⁹⁷W. T. Liu, L. Zhu, Q. W. Qin, Q. Zhang, H. Feng, and S. Ang. *Microfluidic device as a new platform for immunofluorescent detection of viruses*. *Lab Chip.* 2005, 5, 1327-30.
- ⁹⁸H. Nian, J. Wang, H. Wu, J. G. Lo, K. H. Chiu, J. G. Pounds, and Y. Lin. *Electrochemical immunoassay of cotinine in serum based on nanoparticle probe and immunochromatographic strip*. *Anal. Chim. Acta.* 2012, 713, 50-55.
- ⁹⁹E. D. Goluch, S. I. Stoeva, J-S. Lee, K. A. Shaikh, C. A. Mirkin, and C. Liu. *A microfluidic detection system based upon a surface immobilized biobarcode assay*. *Biosens. Bioelectron.* 2009, 24(8), 2397-2403.
- ¹⁰⁰K. F. Lei, *Quantitative Electrical Detection of the Immobilized Protein using Gold Nanoparticles and Gold Enhancement on a Biochip*. *Meas. Sci. Technol.* 2011, 22, 105802 1-7.
- ¹⁰¹X. Zhi, Q. Liu, X. Zhang, Y. Zhang, J. Feng and D. Cui. *Quick genotyping detection of HBV by giant magnetoresistive biochip combined with PCR and line probe assay*. *Lab Chip.* 2012, 12(4), 741-745.
- ¹⁰²P. P. Freitas, H. A. Ferreira, D. L. Graham, L. A. Clarke, V. Amaral, L. Martins, J. S. Fonseca, J.S. Cabral. *Magnetoelectronics; Chapter 7: Magnetoresistive DNA chips*. Johnson M., Ed.; Elsevier Inc.: Oxford, UK, 2004, 331-374.

-
- ¹⁰³J. Loureiro, P. Z. Andrade, S. Cardoso, C. L. da Silva, J. M. Cabral and P. P. Freitas. *Magneto-resistive chip cytometer*. Lab Chip. 2011, 11, 2255-2261.
- ¹⁰⁴J. Germano, V. C. Martins, F. a Cardoso, T. M. Almeida, L. Sousa, P. P. Freitas, and M. S. Piedade. *A Portable and Autonomous Magnetic Detection Platform for Biosensing*. Sensors. 2009, 9, 4119-4137.
- ¹⁰⁵V. C. Martins, J. Germano, F. a Cardoso, J. Loureiro, S. Cardoso, L. Sousa, M. Piedade, L. P. Fonseca, and P. P. Freitas. *Challenges and trends in the development of a magneto-resistive biochip portable platform*. J. Magn. Mater. 2010, 322, 1655-1663.
- ¹⁰⁶B. Chen, B. Hu, P. Jiang, M. He, H. Peng, and X. Zhang. *Nanoparticle labelling-based magnetic immunoassay on chip combined with electrothermal vaporization-inductively coupled plasma mass spectrometry for the determination of carcinoembryonic antigen in human serum*. Analyst. 2011, 136, 3934-4392.
- ¹⁰⁷A. J. Wang, J. J. Xu, Q. Zhang, H. Y. Chen. *The use of poly(dimethylsiloxane) surface modification with gold nanoparticles for the microchip electrophoresis*. Talanta. 2006, 69(1), 210–215.
- ¹⁰⁸P. Guo, E. W. Hall, R. Schirhagl, H. Mukaibo, C. R. Martin, and R. N. Zare. *Microfluidic capture and release of bacteria in a conical nanopore array*. Lab Chip. 2012, 2(3), 558-561.
- ¹⁰⁹G. D. Chen, F. Fachin, M. Fernandez-Suarez, B. L. Wardle, and M. Toner. *Nanoporous Elements in Microfluidics for Multiscale Manipulation of Bioparticles*. Small. 2011, 7, 1061-1067.
- ¹¹⁰C. L. Choong, W. I. Milne, and K. B. K. Teo. *Review: carbon nanotube for microfluidic lab-on-a-chip application*. Intern. J. Mat.For. 2008, 1, 117-125.
- ¹¹¹H. J. Yoon, K. Lee, Z. Zhang, T. M. Pham, and S. Nagrath. *Nanoassembly of graphene oxide for circulating tumor cell isolation*. μ TAS, 2011, 1098-1100.
- ¹¹²L. Johansson, K. Gunnarsson, S. Bijelovic, K. Eriksson, A. Surpi, E. Göthelid, P. Svedlindh, and S. Oscarsson. *A magnetic microchip for controlled transport of attomole levels of proteins*. Lab Chip. 2010, 10, 654-661.
- ¹¹³S. N. Khaderi, C. B. Craus, J. Hussong, N. Schorr, J. Belardi, J. Westerweel, O. Prucker, J. Rühle, J. M. J. den Toonder, and P. R. Onck. *Magnetically-actuated artificial cilia for microfluidic propulsion*. Lab Chip. 2011, 11, 2002-2010.
- ¹¹⁴J. Park, A. Saffari, S. Kumar, A. G. Unther, and E. Kumacheva. *Microfluidic Synthesis of Polymer and Inorganic Particulate Materials*. Annu. Rev. Mater. Res. 2010, 40, 415–443.

INTRODUCTION

- ¹¹⁵J. B. Edel, R. Fortt, J. C. De Mello, and A. J. De Mello. *Microfluidic routes to the controlled production of nanoparticles*. Chem. Comm. 2002, 1136-1137.
- ¹¹⁶E. M. Chan, R. a. Mathies, and a. P. Alivisatos. *Size-controlled growth of CdSe nanocrystals in microfluidic reactors*. Nano Lett. 2003, 3, 199-201.
- ¹¹⁷H. Nakamura, Y. Yamaguchi, M. Miyazaki, M. Uehara, H. Maeda, and P. Mulvaney. *Continuous Preparation of CdSe Nanocrystals by a Microreactor*. Chem. Lett. 2002, 10, 1072-1073.
- ¹¹⁸H. Nakamura, Y. Yamaguchi, M. Miyazaki, H. Maeda, M. Uehara, and P. Mulvaney. *Preparation of CdSe nanocrystals in a micro-flow-reactor*. Chem. Comm. 2002, 2844-2845.
- ¹¹⁹L.-H. Hung, K. M. Choi, W.-Y. Tseng, Y.-C. Tan, K. J. Shea, and A. P. Lee. *Alternating droplet generation and controlled dynamic droplet fusion in microfluidic device for CdS nanoparticle synthesis*. Lab Chip. 2006, 6, 174-8.
- ¹²⁰I. Shestopalov, J. D. Tice, and R. F. Ismagilov. *Multi-step synthesis of nanoparticles performed on millisecond time scale in a microfluidic droplet-based system*. Lab Chip, 2004, 4, 316-21.
- ¹²¹E. M. Chan, a P. Alivisatos, and R. a Mathies. *High-temperature microfluidic synthesis of CdSe nanocrystals in nanoliter droplets*. J. Am. Chem. Soc, 2005, 127, 13854-61.
- ¹²²B. K. H. Yen, A. Günther, M. a Schmidt, K. F. Jensen, and M. G. Bawendi. *A microfabricated gas-liquid segmented flow reactor for high-temperature synthesis: the case of CdSe quantum dots*. Ang. Chem. (International ed. in English), 2005, 44, 5447-51.
- ¹²³Y. Zhao, H. C. Shum, H. Chen, L. L. a Adams, Z. Gu, and D. a Weitz. *Microfluidic Generation of Multifunctional Quantum Dot Barcode Particles*. J. Am. Chem. Soc, 2011, 133, 8790-8793.
- ¹²⁴G-R. Yi, T. Thorsen, V. N. Manoharan, M.-J. Hwang, S.-J. Jeon, D.J. Pine, S.R. Quake, and S.-M Yang. *Generation of Uniform Colloidal Assemblies in Soft Microfluidic Devices*. Adv. Mater. 2003, 15, 1300-1304.
- ¹²⁵J.B. Wacker, V.K. Parashar, and M.A.M. Gijs. *On-chip synthesis of silica nanoparticle assemblies with controlled shape and size*. Transducers, 2011, 2940-2943.
- ¹²⁶L. Frenz, A. E. Harrak, M. Pauly, S. Bégin-Colin, A. D. Griffiths, and J.C. Baret. *Droplet-Based Microreactors for the Synthesis of Magnetic Iron Oxide Nanoparticles*. Angew. Chem. Int. Ed. 2008, 47, 6817-6820.

-
- ¹²⁷S. A. Khan, A. Günther, M. A. Schmidt, and K. F. Jensen. *Microfluidic Synthesis of Colloidal Silica*. *Langmuir*. 2004, 20 (20), 8604–8611.
- ¹²⁸A. J. C. Kuehne and D. A. Weitz. *Highly monodisperse conjugated polymer particles synthesized with drop-based microfluidics*. *Chem. Commun.* 2011, 47, 12379–12381.
- ¹²⁹F. Schütze, B. Stempfle, C. Jüngst, D. Wöll, A. Zumbusch and S. Mecking. *Fluorescent conjugated block copolymer nanoparticles by controlled mixing*. *Chem. Commun.* 2012, 48, 2104-2106.
- ¹³⁰O. C. Farokhzad, A. Khademhosseini, S. Jon, A. Hermmann, J. Cheng, C. Chin, A. Kiselyuk, B. Teply, G. Eng, and R. Langer. *Microfluidic System for Studying the Interaction of Nanoparticles and Microparticles with Cells*. *Anal. Chem.*, 2005, 77, 5453-5459.
- ¹³¹L. Richter, V. Charwat, C. Jungreuthmayer, F. Bellutti, H. Brueckla and P. Ertl. *Monitoring cellular stress responses to nanoparticles using a lab-on-a-chip*. *Lab Chip*. 2011, 11, 2551-2560.
- ¹³²S. K. Mahto, T. H. Yoon, and S. W. Rhee. *Cytotoxic effects of surface-modified quantum dots on neuron-like PC12 cells cultured inside microfluidic devices*. *BioChip J.* 2010, 4, 82-88.
- ¹³³M. Safi, M. Yan, M.-A. Guedeau-Boudeville, H. Conjeaud, V. Garnier-Thibaud, N. Boggetto, A. Baeza-Squiban, F. Niedergang, D. Averbeck, and J.-F. Berret. *Interactions between magnetic nanowires and living cells: uptake, toxicity, and degradation*. *ACS NANO*. 2011, 5, 5354-64.
- ¹³⁴P. Liu, K. Skucha, M. Megens, and B. Boser. *A cmos hall-effect sensor for the characterization and detection of magnetic nanoparticles for biomedical applications*. *IEEE transactions on magnetics*, 2011, 47, 3449-3451.
- ¹³⁵Y. Song, H. Zhang, C. H. Chon, X. Pan, and D. Li. *Nanoparticle Detection by Microfluidic Resistive Pulse Sensor with a submicron sensing gate and dual detecting channels-two stage differential amplifier*. *Sens. Act. B: Chem.* 2011, 155, 930-936.
- ¹³⁶D. Gallego-Perez, N. Higuera-Castro, S. Sharma, R. K. Reen, A. F. Palmer, K. J. Gooch, L. J. Lee, J. J. Lannutti, and D. J. Hansford. *High throughput assembly of spatially controlled 3D cell clusters on a micro/nanoplatfrom*. *Lab Chip*. 2010, 10, 775-82.
- ¹³⁷J. Lee, A. K. Jha, A. Bose, and A. Tripathi. *Imaging new transient nanostructures using microfluidic chip integrated with a controlled environment vitrification system for cryo-TEM*. *Langmuir*. 2008, 24 (22), 12738–12741.

CHAPTER 2
OBJECTIVES

GENERAL OBJECTIVE

The main objective of the present Thesis is to study the integration of nano / micromaterials in different miniaturized platforms with the aim of obtaining robust, sensitive and more efficient (bio)sensing platforms for point-of-care applications with interest for diagnostics beside other industries. Indeed the development of efficient and miniaturized analytical platforms for proteins or pollutants detection is of great concern nowadays both to address environmental and/or health, safety and security related issues.

More in details, the objectives of the Thesis can be summarized as following:

- The design, fabrication and study of electrochemical lab-on-a-chip devices and their application in protein detection by using quantum dots (QDs) as electrochemical labels.
- The study and development of alternative high sensible microfluidic platforms for immunoassay applications.
- The integration and study of a complete system for pesticide detection into a lab-on-a-chip platform by using boron-doped diamond electrode modified with nanoparticles.
- Design and study of various enhanced electrochemical detection alternatives based on either microfluidic architecture enrichments (i.e. valve integration for recycling, *in-situ* magnetic particles plug formation) or *in-situ* modified detectors (i.e. using bismuth) with interest for LOC applications
- The study and characterization of a novel inkjet-based Bio-Field Effect Transistor (BioFET) printed onto flexible substrate for possible integration into a microfluidic system.

CHAPTER 3. FABRICATION METHODOLOGIES	53
3.1. Microchannels design.....	56
3.2. Fabrication of the microfluidic device.....	56
3.2.1. Reagents.....	56
3.2.2. Experimental details	57
3.2.3. PDMS replica.....	59
3.2.4. Device bonding.....	61
3.3. Electrochemical detectors for microfluidic devices.....	63
3.3.1. Screen Printed Carbon Electrodes (SPCE)	63
3.3.2. Inkjet Printed Electrodes (IPE).....	64
3.3.3. Photolithography-based Electrodes	67
3.3.4. Composite-based Electrodes for microchannels.....	71
3.4. Conclusions	72
3.5. References	73

CHAPTER 3

FABRICATION METHODOLOGIES

This chapter summarizes the results obtained for microfluidic channels design and fabrication as well as the integration of different transducers, especially screen printed carbon electrodes (SPCE), for electrochemical detection of proteins in magnetosandwich immunoassays. This chapter contains the following parts: i) Design, ii) Microchannel and electrode fabrication, and iii) Electrode integration.

Fast and cheap prototyping methods for the design and fabrication of polymeric microfluidic systems have been developed. Traditionally, microfluidic systems have been fabricated in glass, defined by photolithography and micromachining^{1,2}, however, there are limitations with glass substrate, especially for the rapid prototyping. Indeed fabrication process of glass chips is very slow, expensive, and requires special facilities. Instead, polymers (i.e. thermoplastics such as polymethyl methacrylate (PMMA)³ or elastomers as poly (dimethylsiloxane) (PDMS)⁴) offer an attractive alternative to glass as material for fabrication of microfluidic systems.

The microchannel design and fabrication process was performed in four steps: i) design of the microfluidic network and printing onto a transparency mask, ii) master fabrication through photolithography; iii) PDMS channel replication and finally iv) bonding with the substrate. The fabrication steps are explained in the next paragraphs and summarized in the Figure 3.1.

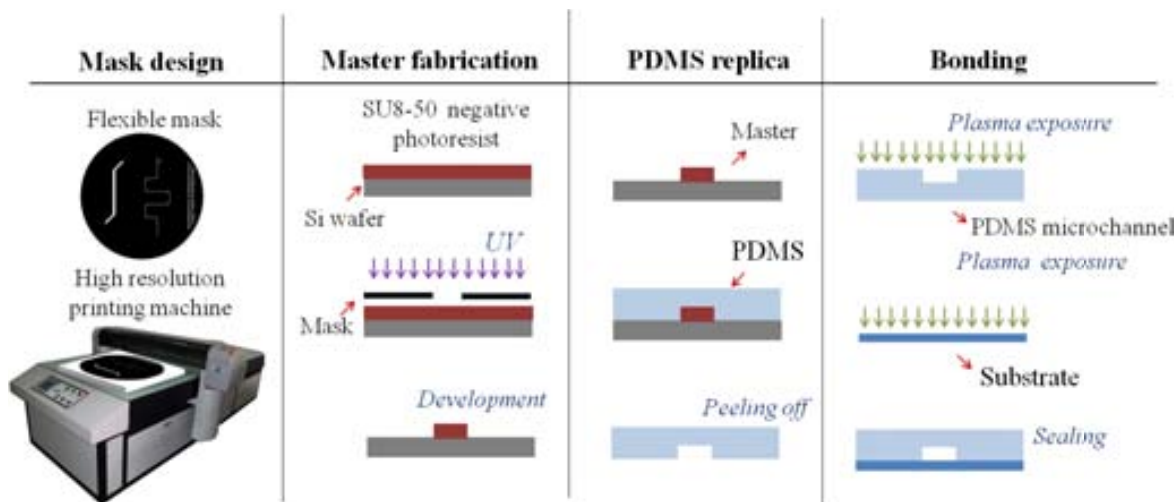


Figure 3.1. Microchannel fabrication steps: mask design, master fabrication, PDMS replication and bonding.

FABRICATION METHODOLOGIES

3.1. Microchannels design

Microchannels features were designed by using a computer assisted design software (QCAD, version 2) with high resolution. The designs were done according to each application described in the Thesis. The most used platforms are showed in Figure 3.2.

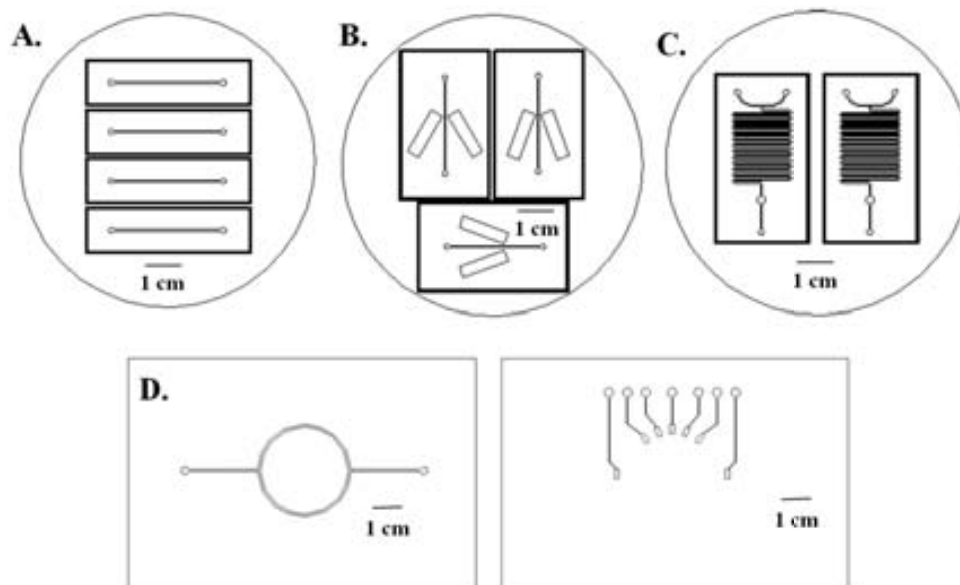


Figure 3.2. Designs of different microfluidic platforms: (A) linear channel for simple immunoassay (diameter of 500 μm), (B) Magnetic plug for magneto immunoassay performance (diameter of 100 - 200 μm), (C) Mixer with turbulent flow in order to decrease the incubation time and mixing of different solutions present in the assay (diameter of 500 μm), and (D) Recycling flow system: flow channel: circular geometry with diameter of 500 μm , and control channel for the valves actuation¹.

3.2. Fabrication of the microfluidic device.

3.2.1 Reagents

The SU8-50 photoresist and XP SU8 Developer were obtained from MicroChem (Newton, MA, USA) while Sylgard 184 Silicone Elastomer (dimethylsiloxane oligomer), Sylgard 184 curing agent (Dimethyl, methylhydrogensiloxane, crosslinking agent) and 2-propanol were purchased from Ellsworth Adhesive Ibérica (Spain). Silicon wafers (4-inch) were obtained from Silicon Inc. (Boise, ID, USA) while borosilicate plates were received from Chemglass (Vineland, NJ, USA), and plastics from Corning (Germany).

¹ Note: Each design will be explained along the Thesis.

3.2.2 Experimental details

The most critical step in the fabrication of PDMS microfluidic device is the manufacture of a high quality master. This involves spin coating of the substrate (usually silicon wafer) with photoresist to ensure uniform thickness of the master, pre-exposure bake to evaporate the excess of the solvent from the photoresist, exposure time of the master through a mask, post-exposure bake to promote polymerization in irradiated areas, and development of the master to remove unexposed photoresist, leaving only the desired positive structure. For this reason, an optimization of the different steps was done as shown in Figure 3.3.

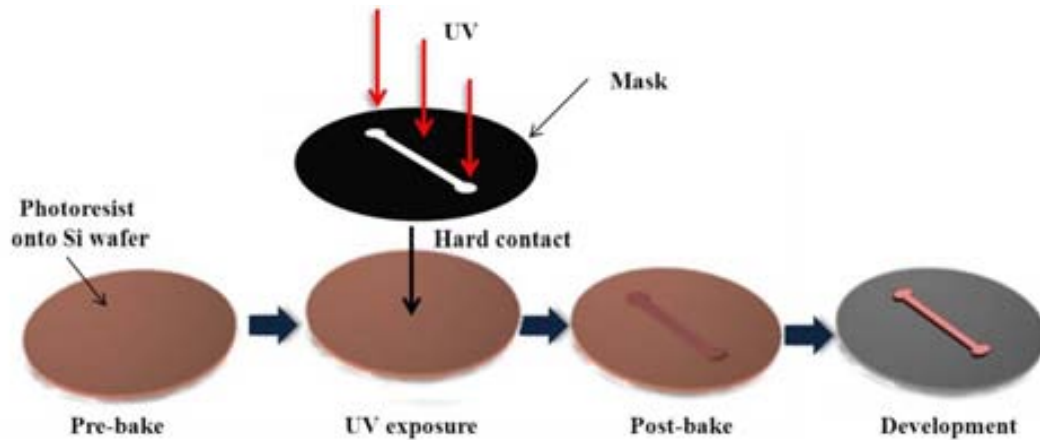


Figure 3.3. Scheme of master fabrication steps: After the step of the spin-coating of the photoresist pre-baking is followed by the UV exposure using a mask, post-baking and finally the development to obtain the master. The detailed parameters of each step are given in the text below.

Optimization of spin coating velocity

Spin coating (Figure 3.4) is an inexpensive and fast method for producing thin films of polymers, with a well-defined thickness. As stated above, the thickness of the master is controlled by velocity of spin (Spincoater SET TP 1100, France). The process is performed in a clean room environment or under laminar hood to avoid dust.

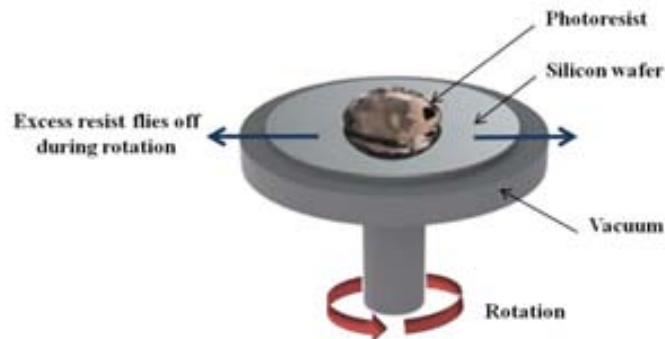


Figure 3.4. A schematic view of spin-coating

FABRICATION METHODOLOGIES

SU8 (5-6 ml) was poured onto the silicon wafer fixed by vacuum application. The plate is spun in at least two stages which may be programmed according to the desired micro channel thickness. During the first stage the plate is spun at a low to moderate speed (500-1000 rpm).

The final thickness of the coating is then determined and controlled during the second stage by spinning the coating at a higher speed (1500 rpm for a thickness of 50 μm) to constant acceleration of 750 rpm sec⁻² (Table 3.1). This information is correlated with the SU8-50 data-sheet.

Table 3.1. Influence of the spinning speed upon the thickness of the SU8-50 resist. Conditions: Spreading stage 30 s at 1000 rpm followed by spinning on described velocity.

Spin velocity (RPM)	Thickness (μm)
3000	39,43
2500	40,66
2200	42,52
2000	47,32
1500	53,93

Optimized parameters were obtained by controlling, step by step, the effect of each parameter in the microfabrication process. Controls were based on the evaluation of shape and thickness of the final pattern by using characterization techniques such as SEM and profilometry.

Pre-exposure / pre-baking time

Pre-baking time was optimized for a time range of 10 to 60 min (by intervals of 10 min) and temperature range from 65°C to 95°C (by intervals of 10°C). This step was performed using an oven. The best condition of temperatures and times were 95°C during 40 min.

Exposure time

The exposure-time was also optimized. Exposure times less than 20 s were considered underexposed for thickness around 50 μm .

According to the Table 3.2, the recommended exposure time was selected to be 50 seconds due to the lower standard deviation of the channel height (the channel width is independent of the exposure time) (7.9 mW/cm², $\lambda=365$ nm; SET MA 750, France).

Table 3.2. Influence of the exposure time upon the width and channel height deviations. A nominal mask width of 100 μm was used. *Deviation was calculated from the data obtained by measuring in middle and end of the channel. Conditions: Intensity of the UV source 7.9 mW cm^{-2} .

Exposure Time (s)	Width of the channel (μm)	Deviation of channel height* (%)
5	106	6.26
10	100	0.27
15	100	0.29
20	100	0.15
25	100	0.10
60	106	0.06

Optimization of post-exposure bake time.

The post-baking time was optimized for interval times from 1 to 25 min. For the first range of time interval studies, the structures were formed according to the design but for higher intervals of times undesirable zones were polymerized making the following development process more complicated. In conclusion, the optimum post-baking time was set at 25 min. See Table 3.3.

Table 3.3. Post-exposure time optimization. Conditions: Intensity of the UV source 7.9 mW/cm^2 ; Pre-exposure bake for 40 min at 95 $^{\circ}\text{C}$. A nominal mask width of 100 μm is used. *Deviation was calculated from the data obtained by measuring in middle and end of the channel.

Post-exposure bake time (min)	Width of the channel (μm)	Deviation of channel height* (%)
0	N/A	N/A
5	100	0.42
10	100	0.02
20	100	0.04
30	100	0.02
45	100	0.02

3.2.3. PDMS replica

Before pouring PDMS onto the silicon wafer, it is important to accurately clean its surface to avoid possible dust that can lead to deformities on the final PDMS microchannel. PDMS oligomer and crosslinking agent were mixed in the weight ratio of 10:1 and degassed. The pattern for the PDMS device is created by pouring the liquid PDMS onto a surface

FABRICATION METHODOLOGIES

containing the negative of the pattern. After pouring it, it is cured for 2 hours at 65°C. Then, the PDMS layer with the pattern of the negative relief was peeled off from the master. The reservoirs were made by punching holes in the structured PDMS plate. (Figure 3.5).

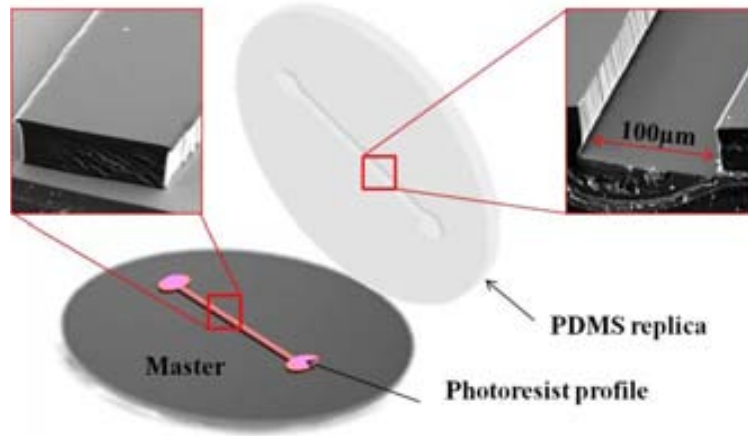


Figure 3.5. PDMS replica and peeling off from the master.

Once the PDMS is peeled off from the master, characterization of PDMS channel by using Scanning Electron Microscopy (SEM) was done in order to confirm the data obtained before with the master profile. As is shown in Figure 3.6 there are different measurements corresponding to different zones along the channel (M1 to M6).

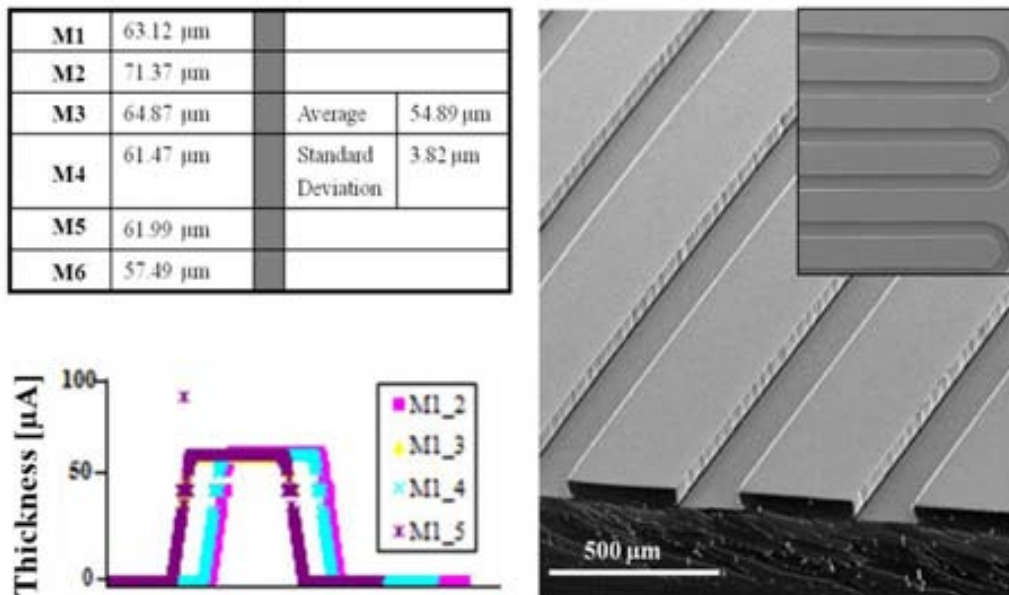


Figure 3.6. Profilometry data of the master and SEM images of the PDMS channel.

3.2.4. Device bonding

After the process described above, solid PDMS that contains the desired pattern of channels is bonded to different substrates. This last step on the microchannel fabrication is crucial as it determines the optimal microchannel termination.

To ensure a good bonding and to prevent dust particles from clogging the channels, substrates must be cleaned prior to bonding. They must be washed with isopropyl alcohol and completely dried by using the nitrogen gun. Any remaining humidity will be taken out by putting the glass into the oven during 15 min at approximately 110°C. After that, cleaned glass should be stored in a petri dish.

On the other hand, any possible dust present in the PDMS device is preserved by the use of a protective tape. For bonding between PDMS and glass, the most common hybrid microfluidic chip, the two parts (PDMS channel and glass substrate) are put into the plasma cleaner (Harrick Plasma cleaner of 60 W). Both glass and PDMS are inserted faced up. The surface of both materials is subjected to high energy plasma which strips away electrons on the surface. This causes the surfaces to become hydrophilic. When these two hydrophilic surfaces come into contact they form a strong bond.

Exposure time should be around 50-60 s. After flipping over the two surfaces, a gently pressure was done to the regions of the device that have difficulty on bonding² (as for example the fluid delivery holes) and put onto a hot-plate at 70°C for 1 h.

Other substrates were used to close our microdevices such as polycarbonate (PC), cyclic olefin copolymer (COC), and polyester (PE). For these thermoplastics, the following protocol was applied (see Table 3.4).

The substrate was cut into small rectangular pieces. PDMS was also cut with nonspecific dimensions (they are not relevant). Both thermoplastic and PDMS were treated under various conditions including; (i) oxygen plasma treatment (60 W, 1 min) and then treatment with 1% v/v aqueous APTES solution for 30 min; (ii) oxygen plasma treatment and then immersed in DI water for 20 min; (iii) oxygen plasma treatment; and (iv) immersed in an aqueous solution of 1% v/v APTES for 30 min without prior oxygen plasma treatment. All the substrates treated were then washed with DI water and dried with a stream of air. Different combinations of the activated thermoplastic and PDMS substrates were kept in conformal contact at room temperature for 1 h and bonding was evaluated by a manual peeling test. The better combination of surface treatments is described in Table 3.4.

² It is important to bond the glass and the PDMS as quickly as possible, as surface become less hydrophilic when they are exposed to air.

FABRICATION METHODOLOGIES

Table 3.4. Summary of the bonding methods between thermoplastics and the PDMS⁵

	Glass	
PDMS	<i>Step 1.</i> Plasma treatment	<i>Step 2.</i> NONE
<i>Step 1.</i> Plasma treatment	PC, COC, PS	
<i>Step 2.</i> None	<i>Step 1.</i> Plasma treatment	<i>Step 2.</i> APTES

Hydrodynamic stability of the device was tested by performing a leakage test under fluid flow conditions. The PDMS with microchannel (depth = 50 μm ; width = 500 μm ; total length = 40 mm) was bonded to a planar piece of thermoplastic. Water was infused through the channel using a syringe pump 11 Elite Infusion/Withdrawal Programmable Dual Syringe (Harvard Apparatus, USA), initially at a flow rate of 5 $\mu\text{L min}^{-1}$ and then increased gradually to 5 mL min^{-1} so as to test the bonding efficiency.

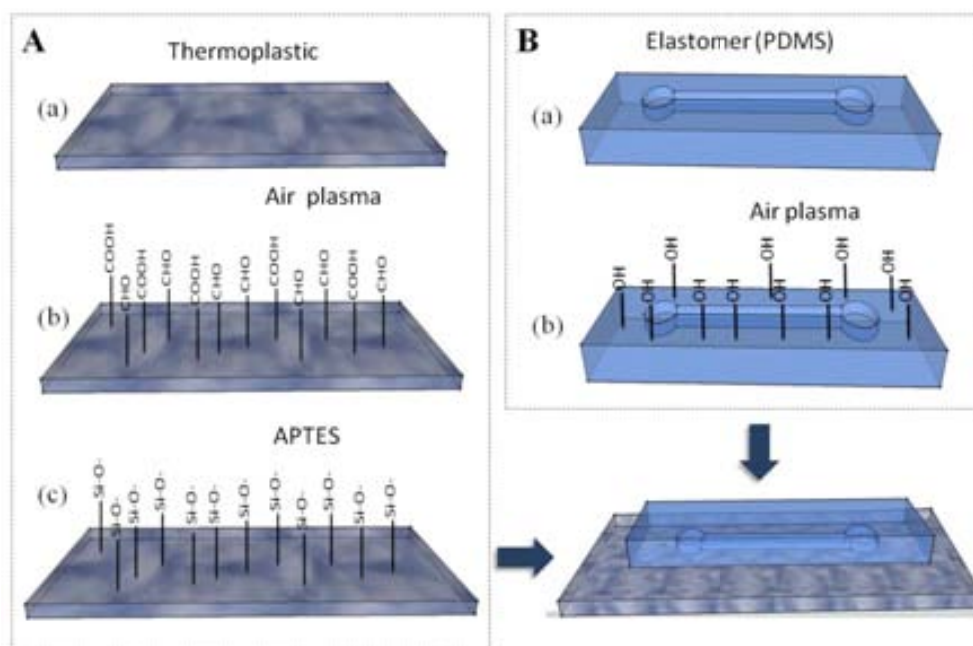


Figure 3.7. Effect of the plasma treatment and APTES treatment onto (A) Thermoplastic and (B) PDMS.

The best bonding between thermoplastics and PDMS was observed with the treatment showed in Figure 3.7. In one hand, the thermoplastic was treated with air plasma to create carboxylic or aldehyde groups onto the surface, then the presence of 3 - Aminopropyl)triethoxysilane (APTES), which has on one side silanes and on the other side

amines, so the amines are bond with the carboxylic / aldehyde groups in a covalent way, left the silanes exposed onto the thermoplastic surface. On the other hand the elastomer, in our case PDMS, was also treated with air plasma generating hydroxilic groups onto the surface. These hydroxilic groups with the silanes are bonded covalently.

3.3. Electrochemical detectors for microfluidic devices.

3.3.1. Screen Printed Carbon Electrodes (SPCE)

Materials and Instrumentation

Polyester sheets were purchased from Autostat HT5 from McDermid Autotype; polycarbonate was purchased from Corning-USA and COC in Topas Advanced Polymers, USA. The carbon ink (Electrodag PF407C) and the silver/silver chloride ink (Electrodag 6037SS) were from Acheson-USA.

The screen printed electrodes were produced by using a semi-automatic screen-printing machine (DEK 248, UK).

Experimental details

Screen printed carbon electrodes (SPCE) were fabricated with carbon ink and silver-chloride / silver ink onto a glass substrate. Three electrodes were located throughout the channel allowing the contact with the solution so as to achieve the electrochemical detection.

Step a: A first layer of graphite was printed using the screen-printing machine with the stencil on a glass substrate. The electrodes were cured for 40 min at 120°C; Step b: A second layer of silver/silver chloride was printed as reference. Another curing step for 40 min at 120°C was needed. The SPCE should be printed onto a wide variety of materials like glass, PC, COC, PE, and paper. For polycarbonate substrate the curing temperature was lower due to its melting temperature (higher than 90°C).

Screen-printing technology offers the opportunity for mass production of low cost biosensors. Several printing steps such as biomolecules (i.e. enzyme) layers as well as other species (i.e. mediators etc.) with interest for the normal operation of biosensors can be applied that makes this technology versatile for a broad range of applications.

In relation with the SPE integration it is necessary to specify that the optimal bonding between the substrate containing the electrode and the PDMS microchannel depends also

FABRICATION METHODOLOGIES

on the electrode geometry (width and thickness). We have observed that for the home-made SPCE (with dimensions around 500 μm width, 500 μm separation and 4 μm thickness), the channel should preferably be with the same dimensions (Figure 3.8). Although the screen printed technology is a very well-known technology, few works related to integrated screen printed electrodes into microfluidic systems have been reported^{6,7,8}.

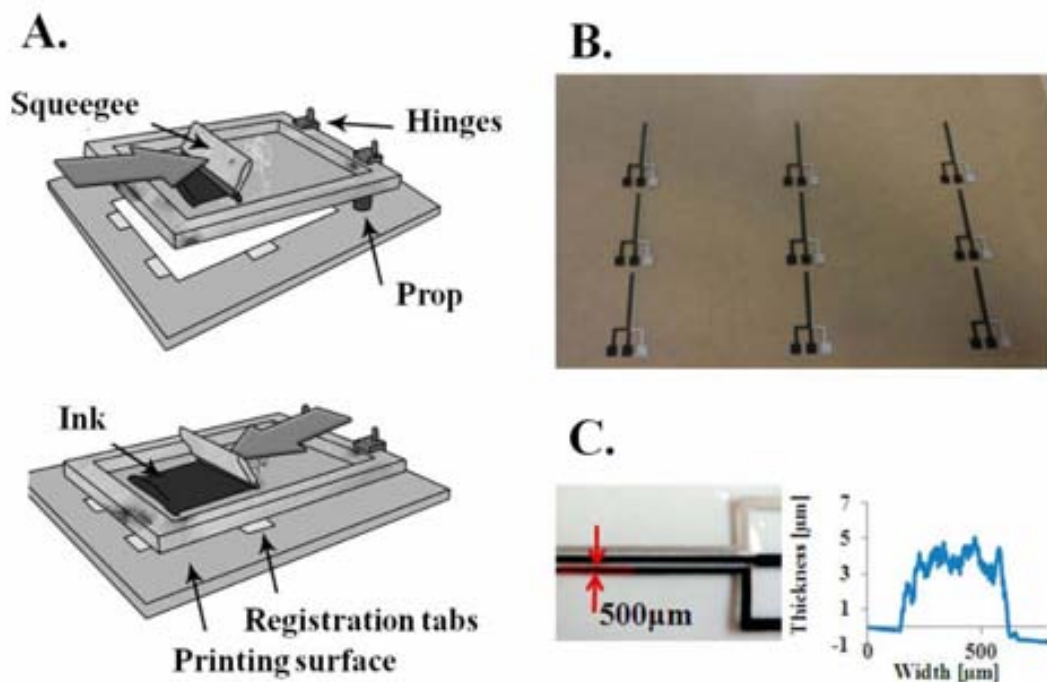


Figure 3.8. Screen printing technology. (A) Scheme of the operation principle, (B) Complete sheet with two layers of printing (carbon and silver/silver chloride), and (C) Details about the size and thickness of the SPCE used for microfluidic chips.

3.3.2. Inkjet Printed Electrodes (IPE)

As an alternative method for fast and easy prototyping of electrodes, the inkjet technology has been used for electrochemical sensors preparation^{9,10}. We have optimized the most important parameters for fabrication of electrochemical related electrodes and other transducers as field effect transistors or capacitance and resistance related ones. Moreover, inkjet technology in comparison to screen printing allows the fabrication of electrodes with thinner layers. The thickness can be decreased from 5 μm to few hundred of nanometers (from 100 to 800 nm), making suitable the electrode integration into small channels (less than 500 μm width until few micrometers).

The inkjet printing setup used in this work to deposit all the inks was a Fujifilm Dimatix DMP2831 desktop printer, USA (Figure 3.9A). It uses one user-fillable piezo-based inkjet print cartridge with 16 nozzles, able to jet 1 pL or 10 pL drops of a wide range of fluids with a variable jetting resolution. The printer includes an alignment system to avoid layer misalignment when sample is moved for curing processes or cartridge change. The steps are divided in: (i) design of the pattern (each layer), (ii) printing of each layer after alignment, and (iii) drying onto the hotplate (the temperature depends of each material).

Design of pattern

The pattern for the inkjet procedure can be obtained in two different ways: using a computer assisted design (CAD) program as QCAD or Autocad or using the Dimatix software. Particular draws (with resolution up to 5080 dpi) have been obtained using CAD programs saving the designs as bitmap file. (Figure 3.9B).

Inks Requirements

Inks have a fundamental part in this deposition process and their formulation has to fulfill some essential requisites: Particles in the fluid should be smaller than 0.2 μm (100 times smaller than the nozzle diameter), solvents with a flash point below 120°C are prohibiting. Ink viscosity should be between 10-12 cPs ($1.0 \times 10^{-2} - 1.2 \times 10^{-2}$ Pa.s). Fluids with viscosity up to 30 cPs can be also injected by at low speed. Surface tension should be between 28 and 33 dynes cm^{-1} ($0.028 - 0.033$ N m^{-1}). Typically a surfactant is added to water-based fluids to achieve this surface tension range.

The printing parameters were optimized for silver nanoparticle ink with less than 150 nm of diameter, and 20 w% dispersion in organic solvents. This ink was purchased in Sigma Aldrich, Spain. A conducting polymer poly (3,4-ethylene dioxythiophene) / poly(styrene sulfonic acid) (PEDOT:PSS) ink is also used for working and counter electrode (Heraeus, Germany). In the case of field effect transistor was necessary to use conductive, semiconductive and insulator inks (details described in Chapter 7). Different substrates (ceramic, polyester, polycarbonate, paper and glass) were also checked.

Finally the adhesion of the PDMS with these different substrates was studied. The best substrates for PDMS chips were glass, polycarbonate and polyester.

Experimental details

Inkjet printed electrodes were fabricated with PEDOT:PSS ink for counter and working electrode and silver nanoparticle ink followed by a treatment with potassium chloride to obtain a pseudo-reference electrode. These inks were printed onto different substrates. Three electrodes were located throughout the channel allowing the contact with the solution so as to achieve the electrochemical detection. (Figure 3.9C).

FABRICATION METHODOLOGIES

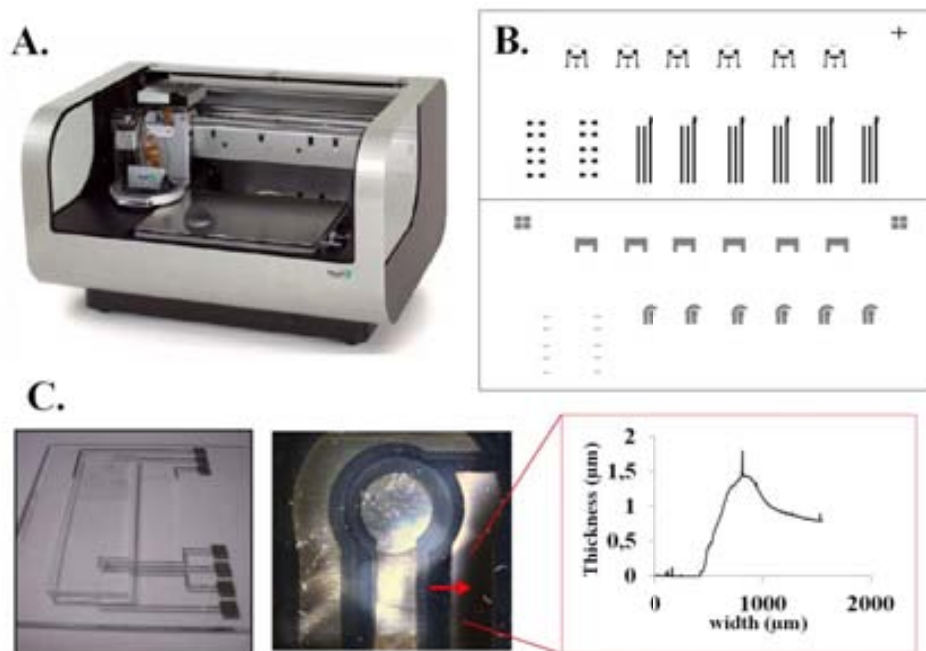


Figure 3.9. Inkjet printed electrodes: (A) DIMATIX inkjet machine, (B) Design of each layer (PEDOT:PSS and silver layer), and (C) Picture of different electrode designs for batch mode and in chip measurements. Inset (C) is the thickness of the inkjet printed electrodes.

Step a: A first layer of PEDOT:PSS is directly printed, reducing the pixels until 50 % by using PAINT.NET (free software) in order to avoid the dispensing of the ink in too much amount onto the surface due to the ink viscosity. The electrodes are cured for 20 minutes at 110°C; Step b: A second layer of nanoparticle silver ink is printed as reference and dried during 30 minutes at 130°C. The major requirements of a reference electrode are that it should be easy to be prepared and maintained, and that its potential be stable. The last requirement essentially means that the concentration of any ionic species involved in the electrode reaction must be held at a fixed value. This electrode usually takes the form of a piece of silver wire coated with AgCl. The coating is done by making the printed silver as anode in an electrolytic cell containing HCl; the Ag^+ ions combine with Cl^- ions as fast as they are formed at the silver surface.

In detail, the electrode is connected in open circuit and immersed in a solution of KCl 2 M with applied potential of 0.5 V during 90 s vs. Pt wire as reference electrode. Once, the set of electrodes is obtained, the PDMS channel can be bonded to the substrate following the bonding procedure described according to the substrate material.

3.3.3. Photolithography-based electrodes

Evaporation and sputtering are more conventional methods to produce thin film electrodes. For this purpose, photolithography process is needed in order to obtain small electrodes (with flexible mask, from 10 μm width), with thickness around 100 or 200 nm, allowing their integration into smaller channels in comparison with the previous methods. The main drawback is the necessity of cleaning room conditions. The materials employed are more expensive (silver, gold, platinum..), and the processes use to be time consuming, however, the resolution, repeatability and electrode surface quality are much better, with roughness of few nanometers.

Reagents and Instrumentation

6512 positive photoresist with its OPD 4262 developer were used to define the geometry of the set of electrodes through photolithography (from MicroChemicals, Germany). Different electrode materials were tested such as gold, silver, platinum, and carbon (these materials were purchased in Monocomp Inc., USA).

A DELTA 20 model BLE spin coater was used with the aim of depositing a thin film of photosensitive resist. For the UV irradiation, a MA6 model KARL SUSS aligner was used. A UNIVEX 450b evaporator was used to perform the evaporation of the materials (silver, gold, platinum and carbon). A sonicator and acetone in room temperature was used for the removal of the resist and the residual deposited metal from the Pyrex[®] wafer (from Corning, Germany). The access to the equipment was obtained as a result from collaboration project with the IMB-CNM (CSIC).

Experimental details

Characterization techniques

A Dektak-150 mechanical profilometer (VEECO, USA) was used for the measurement of the profiles. The tip used presented a diameter of 2.5 μm . The measurable range of the profilometer goes from 0.1 nm to 1000 μm . For the mask and wafer inspection a LEICA DM6000M optical microscope with a capacity of up to 200 magnifications was used.

Design of the masks for transparencies

The design of the masks was done with CAD software with the corresponding alignment marks for each of them, since different photolithography processes were carried out. An example of one of the designs for the fabrication of three electrodes is shown in Figure 3.10A.

FABRICATION METHODOLOGIES

Fabrication of the electrodes over Pyrex[®] wafers

6512 photoresist was deposited by spin coating, obtaining a thin film of approximately 2 μm . Then a prebake process was carried out at 100 °C for 25 min, followed by a UV exposure step (11 mW cm^{-2}) for 30 s. Post-baking was done at 115 °C for 20 min and finally the development to obtain the desired geometry. The pre and post-bakings were performed in an oven avoiding the use of the hot-plate which explains the relatively long time of this process.

Once the photolithography process was done, the evaporation of the previously mentioned metals was carried out (gold, silver, platinum and carbon for the different combination of electrodes), and finally the lift-off process was carried out in an acetone bath, using a sonicator, in 1 min rounds followed by a DI water bath, and repeated three times in order to eliminate the resist and the residues of the evaporated metal. Figure 3.10B,C.

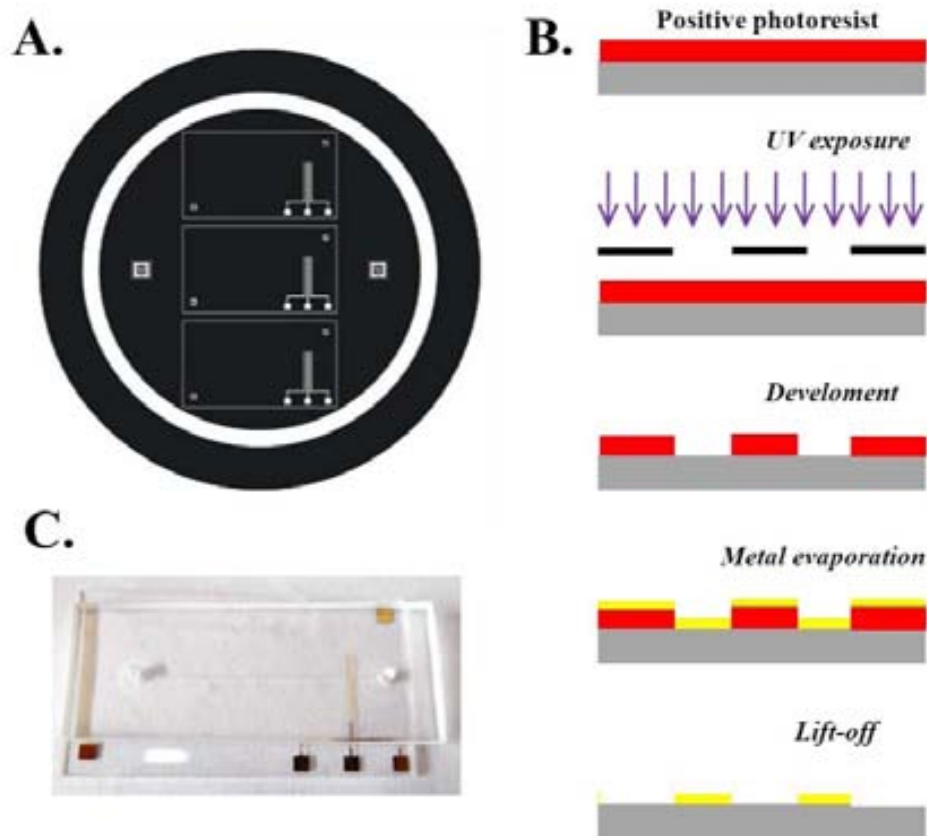


Figure 3.10. (A) Example of a mask design (fabricated electrodes of 50, 100, 200 and 500 μm of wide), (B) Steps for the electrode fabrication by metal evaporation, and (C) Final microfluidic (100 μm wide, 50 μm of thickness and 20 mm of length) device with integrated gold electrodes.

Table 3.5. Applied parameters for the metal evaporation process.

Wafer	Support	Material(s)	Melting pot	Position in the holder	Thickness (Å)	Quartz thickness (Å)
1	1	Cr/Au	V.C/Fab.	$\frac{3}{4}$	150/1000	150/1000
2	2	Ag	Alumina	1	1000	1000

Complementary tests onto flexible substrates.

The evaporation of gold, silver, platinum and carbon were done onto glass, polyamide (Kapton®), polycarbonate, paper and copolymer substrates with the idea to study their adherence, the temperature resistance of the process and its compatibility with the used lift-off process. Metal evaporation onto flexible substrates is of great interest in the microfluidic and biosensing field, for the creation of disposable and flexible devices. Recently many works have been done by using flexible substrates to be integrated into microfluidic platforms for biosensing application^{11,12}. Figure 3.11.

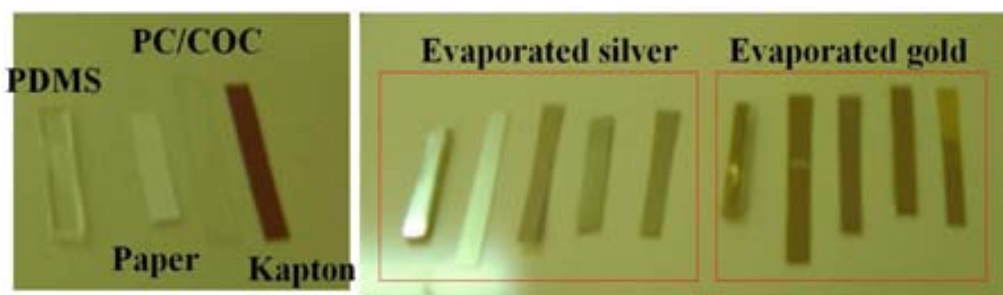


Figure 3.11. Metal evaporation onto different substrates without adherence layer. The used substrates were: PDMS, polycarbonate, COC, cellulose paper, and kapton®.

The metal evaporation on the mentioned flexible substrate doesn't require adherence layer, making it a advantageous also for the fabrication process, as well as, the use of cheaper substrates easy for post-processing.

These metal deposition studies were also carried out at the IMB-CNM (CSIC), under the GICSERV project, formation and collaboration Program.

FABRICATION METHODOLOGIES

Table 3.6. Summary of the performance of the evaporation test onto different substrates.

Substrate	Deposited material			
	Gold	Silver	Platinum	Carbon
PDMS	Fissures are produced on the metal due to material flexibility	Fissures are produced on the metal due to material flexibility	Fissures are produced on the metal due to material flexibility	Improved, due to the thickness of the deposited film, which was thinner (50 nm)
Polyamide	Successful	Successful	Successful	Successful
PC	Successful	Successful	Material deformation due to the temperature	Material deformation due to the temperature
Glass	Successful	Successful	Successful	Successful
Paper	Successful	Successful	Successful	Successful
COC	Successful	Successful	Material deformation due to the temperature	Material deformation due to the temperature

In Figure 3.12, optical images are shown. Microfissures can be observed in the deposited metal on all the substrates except for the paper. Although this does not affect its conductivity, it can contribute to its deterioration during the application.

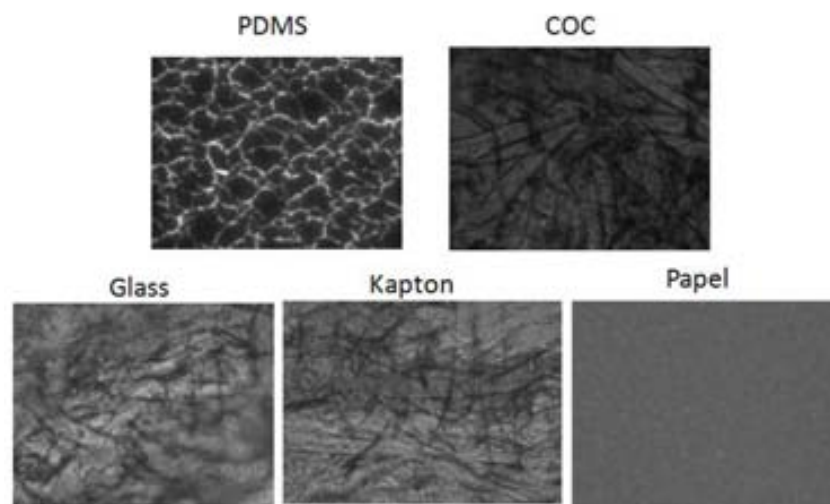


Figure 3.12. Optical microscopy pictures of evaporated gold over the different substrates (50 magnifications).

Finally, tests were carried out for the resistance to the acetone bath in the sonicator during the lift-off process using the different materials. The results are summarized in Table 3.7.

Table 3.7. Results of the material resistance to the lift-off process.

Substrate	Deposited material			
	Gold	Silver	Platinum	Carbon
PDMS	During the first lift-off minute the metal was completely eliminated.			
Kapton®	The lift-off process was successfully done.			
PC	During the second and third minute of the lift-off the PC was deteriorated.			
Glass	The lift-off process was successfully done.			
Paper	The lift-off process eliminated the paper and only its plastified side remained.			
COC	Successfully done	Successfully done	None	None

The lift-off step can be avoided if instead of positive photoresist to define the electrode design, an external hard mask such as aluminum or metallic mask with the micromechanized structure is used, the temperature resistance of the mask material according to the achieved temperature inside the evaporator so as to avoid the mask deformation is necessary to be known.

3.3.4. Composite-based Electrodes for microchannels

Another alternative for microelectrode fabrication, the composite-based electrodes, were prepared for future biological application^{13, 14}. Briefly, the process consists in the development of electrodes inserted in the PDMS channel itself. For this purpose, the same protocol described before for the PDMS replica was done to form the electrodes paths into the PDMS channels. The PDMS part is filled inside the channels (electrodes) with the composite material (i.e. Carbon, silver, nanoparticles, etc.). This kind of electrode can be useful for electrode modification, like enzyme based electrode, or electrode modified with nanomaterials in the same composite based ink. Although not used in this thesis, these electrodes were characterized with Ferri-Ferrocyanide 10 mM in KCl 1 M (results doesn't show in this Thesis).

An important advantage of this kind of electrode is the possibility to have a complete PDMS chip with integrated electrodes. In addition it represents a good alternative to study

FABRICATION METHODOLOGIES

different material composition as working electrode, mixing nanomaterials or biological entities and corresponding studies.

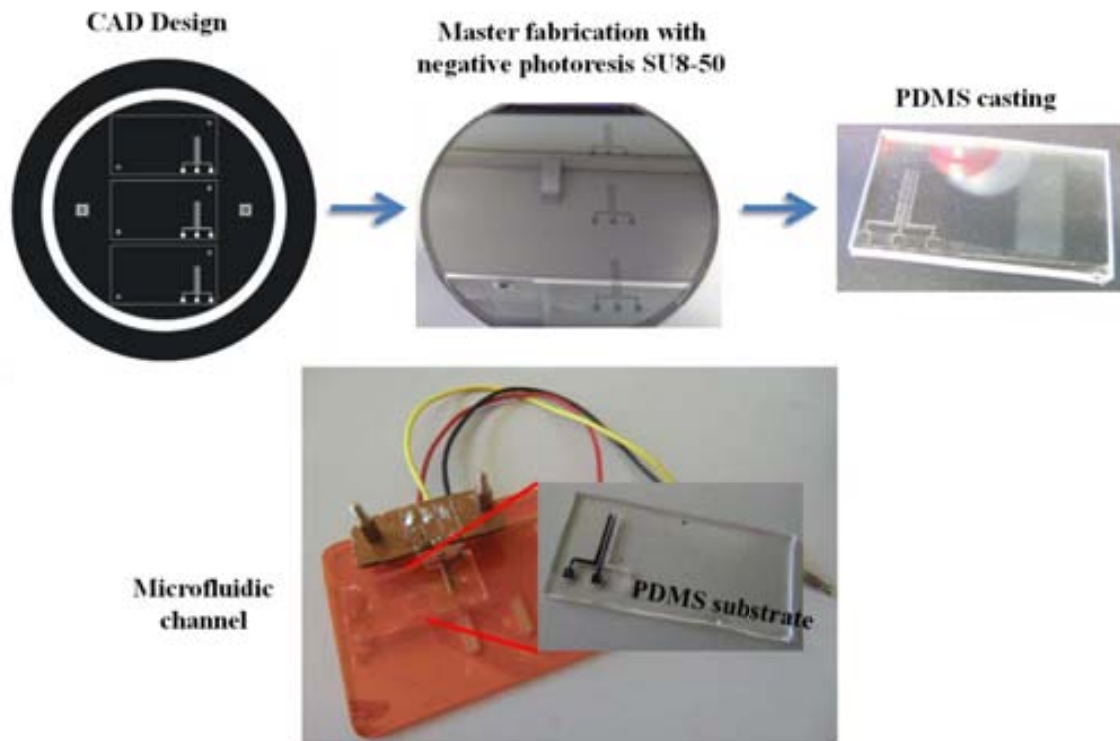


Figure 3.13. Composite based electrodes. The fabrication process started with the mask design and master fabrication with a negative photoresist. After that, PDMS replica is obtained with the electrodes holes, as channels. Finally the carbon composite and silver ink is deposited into the paths by spatula in order to fill them with the electrode materials. After the curing step this substrate is bonded with the PDMS channel by plasma exposure of the two PDMS side during 1 min (as explained before) and put in contact.

3.4. Conclusions

The use of the soft-lithography and PDMS replica for rapid prototyping of microfluidic devices offers several advantages over the conventional photolithography and micromachining in silicon or glass that have been previously used to create masters for molding polymeric microfluidic systems¹⁵: i) transparencies take less time to be produced (hours compared to weeks) and are substantially less expensive (20 EURO vs. 500-1000 EURO for silicon); ii) the development of photoresist to create a relief on silicon is easier and more flexible in the types of patterns that can be produced than the etching needed in micromachining of silicon.

A system for fabricating networks of channels rapidly and at a low cost, based on rapid prototyping of masters using high-resolution printing and contact lithography, molding of PDMS is developed.

Finally, the fabrication procedures for electrode fabrication are optimized although most of the further studies and applications are focused in the use of a home-made SPCE because they are produced faster, offer the possibility to be mass produced with a low cost, and can be easily integrated within the microfluidic device.

3.5. References

¹ J. Wang, M. Pumera, M.P. Chatrathi, A. Escarpa, M. Musameh, A. Mulchandani, G. Collins, Y. Lin, and K. Olsen. *Single-channel microchip for fast screening and detailed identification of nitroaromatic explosives or organophosphate nerve agents*, Anal. Chem., 2002, 74, 1187-1191.

² A. M. García Campaña, W. R. G. Baeyens, H. Y. Aboul-Enein, and X. Zhang *Miniaturization of capillary electrophoresis systems using micromachining techniques*. J. Microcolumn Separations. 1998, 10(4), 339-355.

³ J. Wang, M. Pumera, M.P. Chatrathi, A. Escarpa, R. Konrad, A. Griebel, A. W. Dorner, and H. Lowe. *Towards disposable lab-on-a-chip: poly(methylmethacrylate) microchip electrophoresis device with electrochemical detection*. Electrophoresis. 2002, 23, 596-601.

⁴ D. C. Duffy, J. C. McDonald, O J. A. Schueller, and G.M. Whitesides. *Rapid prototyping of microfluidic systems in poly(dimethylsiloxane)*. Anal. Chem. 1998, 70, 4974-4984.

⁵ V. Sunkara, D-K Park, H. Hyundoo, R Chantiwas, S. A. Soperac and Y-K Cho. *Simple room temperature bonding of thermoplastics and poly(dimethylsiloxane)*. Lab Chip. 2011, 11, 962-965.

⁶ E. S. Fakunle, and I. Fritsch. *Low-temperature co-fired ceramic microchannels with individually addressable screen-printed gold electrodes on four walls for self-contained electrochemical immunoassay*. Anal. Bioanal. Chem. 2010, 398, 2605-2610.

⁷ D-M. Tsai, K-W. Lin, J-M. Zen, H-Y. Chen, and R-H. Hong. *A new fabrication process for a microchip electrophoresis device integrated with a three-electrode electrochemical detector*. Electrophoresis. 2005, 26, 3007-3012.

⁸ H. Dong, C-M. Li, Y-F. Zhang, X-D. Cao, and Y. Gan. *Screen-printed microfluidic device for electrochemical immunoassay*. Lab Chip. 2007, 7, 1752-1758.

- ⁹ N. Komuro, S. Takaki, K. Susuki, and D. Citterio. *Inkjet printed (bio)chemical sensing devices*. Anal. Bioanal. Chem. 2013, 17, 5785-5805.
- ¹⁰ Anni Määttänen, U. Vanamo, P. Ihalainen, P. Pulkkinen, H. Tenhu, J. Bobacka, and J. Peltonen. *A low-cost paper-based inkjet-printed platform for electrochemical analysis*. Sens. Actuators B: Chem. 2013, 177, 153-162.
- ¹¹ P. Ihalainen, H. Majumdar, A. Määttänen, S. Wang, R. Österbacka, and J. Peltonen. *Versatile characterization of thiol-functionalized printed metal electrodes on flexible substrates for cheap diagnostic applications*. Biochim. Biophys. Acta (BBA). 2013, 9, 4391-4397.
- ¹² Z. Zou, J. Kai, M. J. Rust, J. Han, and C. H. Ahn. *Functionalized nano interdigitated electrodes arrays on polymer with integrated microfluidics for direct bio-affinity sensing using impedimetric measurement*. Sens. Actuators, 2007, 136, 518-526.
- ¹³ T. D. Yoshida Kozai, N. B. Langhals, P. R. Patel, X. Deng, H. Zhang, K. L. Smith, J. Lahann, N. A. Kotov, and D. R. Kipke. *Ultrasmall implantable composite microelectrodes with bioactive surfaces for chronic neural interfaces*. Nature Mat. 2012, 11, 1065-1073.
- ¹⁴ J. Kim, R. Surapaneni, and B. K. Gale. *Rapid prototyping of microfluidic systems using a PDMS/polymer tape composite*. Lab Chip. 2009, 9, 1290-1293.
- ¹⁵ C.S. Effenhauser, G. J. M. Bruin, A. Paulus, and M. Ehrat. *Integrated capillary electrophoresis on flexible silicone microdevices: analysis of DNA restriction fragments and detection of single DNA molecules on microchips*. Anal. Chem. 1997, 69, 3451-3457

CHAPTER 4. QUANTUM DOTS AS ELECTROCHEMICAL REPORTERS IN LAB-ON-A-CHIP DEVICES	77
4.1. Introduction	79
4.2. On-chip electrochemical detection of CdS quantum dots	81
4.2.1. Experimental details.	81
4.2.2. Results and discussions.....	82
4.3. On-chip magneto-immunoassay for Alzheimer’s biomarker electrochemical detection by using Quantum Dots as labels.....	89
4.3.1. Experimental Section.....	89
4.3.2. Results and Discussion.....	92
4.4. Conclusions.....	97
4.5. Futures perspectives.....	98
4.6. References.....	99

CHAPTER 4**QUANTUM DOTS AS ELECTROCHEMICAL REPORTERS IN LAB-ON-A-CHIP DEVICES***Related Publications*

M. Medina-Sánchez, W. Miserere, S. Marín, G. Aragay, and A. Merkoçi, “On-chip electrochemical detection of CdS quantum dots using normal and multiple recycling flow-through modes”. *Lab Chip*, 12, 2000-2005. (2012). Annex 1.

M. Medina-Sánchez, S. Miserere, E. Morales, and A. Merkoçi, “On-chip magneto-immunoassay for Alzheimer’s biomarker electrochemical detection by using Quantum Dots as labels”. Submitted (2013). Annex 2.

M. Medina-Sánchez, S. Miserere, E. Morales, and A. Merkoçi. “Lab-on-a-chip for electrochemical magneto-immunoassay for Alzheimer’s biomarker detection”. MICROTAS proceedings, Germany (2013). Annex 1.

In this Chapter, it is described how a flexible hybrid polydimethylsiloxane (PDMS)/Polycarbonate (PC) microfluidic chip with integrated screen printed carbon electrodes (SPCE) was fabricated and applied for electrochemical Quantum Dots (QDs) detection. The developed device combines advantages of flexible microfluidic chips such as their low cost, the possibility to be disposable and amenable to mass production with the advantages of electrochemistry for its facility of integration and the possibility to miniaturize the analytical device. Due to the interest in biosensing applications in general and particularly the great demand for labeling alternative in affinity biosensors the electrochemistry of cadmium sulfide quantum dots (CdS QDs) is evaluated. Square wave anodic stripping voltammetry (SWASV) is the technique used due to its sensitivity and low detection limits that can be achieved. The electrochemical as well as the microfluidic parameters of the developed system were optimized. In the first part, the detection of home-made CdS QDs in the range between 50 to 8000 ng mL⁻¹ with a sensitivity of 0.0009 μA (ng mL⁻¹)⁻¹ has been achieved, as well the comparison between drop and in-flow measurements.

In the second part, electrochemical detection of quantum dots (cadmium-selenide/zinc-sulfide, CdSe@ZnS) as labeling carriers in an assay for apolipoprotein E (ApoE) detection has been also evaluated. The immunocomplex was performed by using tosylactivated magnetic beads as preconcentration platform into the same microfluidic platform. All the immunoassay was conducted in flow mode. ApoE was evaluated for its potential as biomarker for Alzheimer's disease detection, achieving a limit of detection (LOD) of ~12.5 ng mL⁻¹ with a linear range between 0 to 200 ng mL⁻¹ and high accuracy for diluted human plasma.

4.1. Introduction

The microfluidic know-how for itself has been oriented to develop new products and solutions in different areas like, biotechnology, environmental science, medical and pharmaceutical industries¹. The operations that can be developed in these microsystems are basically for analysis and sample treatment, including cells, proteins and virus due to their advantages, like the reduction of sample and reagent volumes, the decrease of analysis time, the possibility of portability and the integration of conventional analytical techniques.

Microfluidic chips must be inexpensive, disposable and amenable to mass production. That is why polymers are increasingly replacing traditional substrates such as glass and silicon. The kinds of substrate, as well as, the detection methods in microfluidics are critical points to be considered for the further integration².

These platforms in combination with nanomaterials offer excellent improvements in properties for many applications, among this wide variety of nanomaterials, quantum dots, also known as semiconductor nanoparticles, which are crystalline clusters of a nanometric size³ have special labeling properties. They are most commonly used as labels in imaging and biosensing for their optical properties and their stability; however, QDs have also interesting electrochemical properties. They can be detected electrochemically either by dissolving them liberating the metal ions⁴ or by direct detection of the QDs⁵. Furthermore, a wide range of commercial QDs are available, with different surface functional groups, allowing their functionalization with biomolecules such as antibodies, biomarkers, enzymes, DNA or cells. Depending on their structure, this interaction should be considered in the design of the experiments and detection strategy. Thereby, we take the advantages of on-chip magnetic bead manipulation⁶ and link it with the great electrochemical properties of QDs as labels for a sensitive and efficient detection of biomarkers and proteins. In this work, Human IgG and ApoE biomarker detection were performed to demonstrate its functionalities.

Neurodegenerative processes have a high incidence and prevalence in our society; most of them have no cure and are generally diagnosed in people over 65 years of age⁷. The evolution of such kind of disease is long and irreversible, whereby the goal of treatment is usually to improve symptoms, relieve pain and increase mobility. One of the most common neurodegenerative illnesses is Alzheimer disease (AD), characterized by pathological changes in the brain, including senile plaques, synapse, neurofibrillary tangles and neuronal loss. AD is usually diagnosed clinically from the patient history, by clinical observation based on neurological features, however there are a wide range of neurological diseases difficult to distinguish, with very long asymptomatic evolution and extensive neurological damages over time that become more difficult to treat it, making essential the use of biomarker-based diagnosis for its early stages detection^{8,9}.

Biomarkers are indicators of biological status; they can give information about biological processes in normal or pathological states, and even during therapy. One biomarker of interest of AD is Apolipoprotein E (ApoE). ApoE is one of the primary AD polymorphisms, associated not only with risk and age of onset, but also brain integrity in AD¹⁰. ApoE is a 34 kD protein present in the lipid transport and lipoprotein metabolism, whose levels are controlled by the gene ApoE. This biomarker is found in plasma lipoprotein particles, in large amounts at sites of neurological damage, and it is also involved in recycling of apoptotic remnants of amyloid aggregates. ApoE is mainly produced in the liver and by macrophages but also by cell types including smooth muscle cells and neuronal cells. It exists in three isoforms: ApoE2, ApoE3, and ApoE4. Ultimately, total ApoE and ApoE4 levels have been reported to be significantly different in AD patients compared to control patients¹¹.

We used magnetic beads as capture / preconcentration platform for improving the immunological reactions^{12,13,14} thanks to their surface area, faster assay kinetics and easy washing steps due to their simple magnetic manipulation by using external magnets.

Magnetic beads into microfluidic platforms for virus,¹⁵ biomolecules,^{16,17} cells¹⁸ and environmental pollutants immobilization¹⁹ have been widely reported in the literature. These analytes have been labeled mainly with enzymatic and fluorescent (fluorophores) labels for their posterior detection.

On the other hand, the combination of microfluidics and electrochemistry enables quasi automated measurements^{20,21,22}. The advantages of this platform in comparison with standard procedures are: reduced time of incubation steps, low volume consumption, possibility to miniaturize the sample treatment as well the readout system. This platform could be easily reusable by flushing the channel to remove the particles and introducing fresh solution of beads.

To the best of our knowledge there are still not reports on Alzheimer biomarker detection in microfluidic platforms by using quantum dots as electrochemical labels. In general AD diagnosis has been done by strategies different from the electrochemical ones^{23,24}. The development of a microfluidic-based Alzheimer's A β aggregates clearance system, suitable for efficient screening of chemical candidates to enhance the clearance of A β amyloide deposits prior to *in vivo* analysis was described,²⁵ and the use of interfacial chemistry in nanoliters droplets for *in vitro* measurements of protein aggregation to understanding the amyloidosis biophysics was also proposed²⁶ However in the proposed work we use micro and nanomaterials to perform a sensitive immunoassay for ApoE detection. In addition all the optimizations were done using a model protein, human IgG (HIgG) and finally the ApoE detection in plasma within a microfluidic platform, making the system easily scalable to a point of care system, is demonstrated discussing also advantages and drawbacks of the microfluidic platform for real samples related to Alzheimer's diseases.

4.2. On-chip electrochemical detection of CdS quantum dots

4.2.1. Experimental details.

Microfluidic device and screen printed electrodes fabrication.

Microchips were fabricated by rapid prototyping and PDMS technologies as described previously in the Chapter 3. Briefly, a 4 inch silicon wafer was spin coated with a negative photoresist (SU-8 from Microchem) and patterned by photolithography. PDMS was poured onto the resulted mold and cured at 65°C for 2 hours. The channels were 500 μm wide by 50 μm depth and 5 cm long (Figure 4.1A,a).

The electrochemical detector consists of a set of three electrodes of 500 μm width separated by 500 μm with an approximate thickness of 4 μm (Figure 4.1A,a). Finally, the PDMS channel and the PC substrate were assembled using a previously reported protocol²⁷. The polycarbonate substrate was treated by air-plasma for 1 min and then immersed into a 2% (v/v) 3-aminopropyltriethoxylane (APTES) (Sigma Aldrich) solution in water for 1 hour, as well as, the surface of the PDMS channel was also activated for 1 min by plasma, and put into contact with the PC sheet to achieve irreversible bonding. Finally, a homemade connector was used for the electrical connection (see Figure 4.1A,b).

CdS QDs electrochemical detection

3 nm CdS-QDs were synthesized by arrested precipitation using water-dispersed cadmium chloride and hexamethyldisilathiane (HMSDT) as sulfide precursor (Figure 4.1B)²⁸.

The procedure for CdS QDs detection has been previously described by our group²⁹. It involves adsorption of CdS QDs onto the surface of the working electrode and the further reduction of Cd^{2+} ions from the QDs surface onto the WE. The further reoxidation of Cd^0 to Cd^{2+} gives the electrochemical response. The electrochemical detection was done in static (batch measurements). The detection was performed in acetate buffer 0.2 M (NaCl 0,05 M, pH=4.6).

The CdS QDs concentrations were determined by SWASV. In order to get maximum sensitivity, the voltammetry parameters (deposition time, conditioning potential, conditioning time and frequency) were optimized using a solution of 1 $\mu\text{g mL}^{-1}$ of CdS QDs in acetate buffer. The flow-through conditions were used during the conditioning and the deposition step, whereas the equilibration step and the square wave scan were performed in a static solution. Before each analysis, SPCE were pretreated by cyclic voltammetry between -0.8 V to 0.8 V in acetate buffer solution (previously mentioned), during 10 cycles.

4.2.2. Results and discussions

A simple and low cost microfluidic platform for CdS QDs electrochemical detection was performed. It consists of a PDMS channel and a polycarbonate sheet onto which surface the carbon and silver/silver chloride electrodes were screen-printed. Screen-printing is a well-known technique to produce low cost electrodes at industrial level. Combining the advantages of PDMS technology and screen-printing allow producing reliable and low-cost microdevices. As shown in Figure 4.1A,a. SPCE are thick electrodes of around 5 μm which could be a problem during the assembly of the chip and some leakage between the electrodes could appear. This problem can be solved if the width of the electrode remains smaller than the width of the channel.

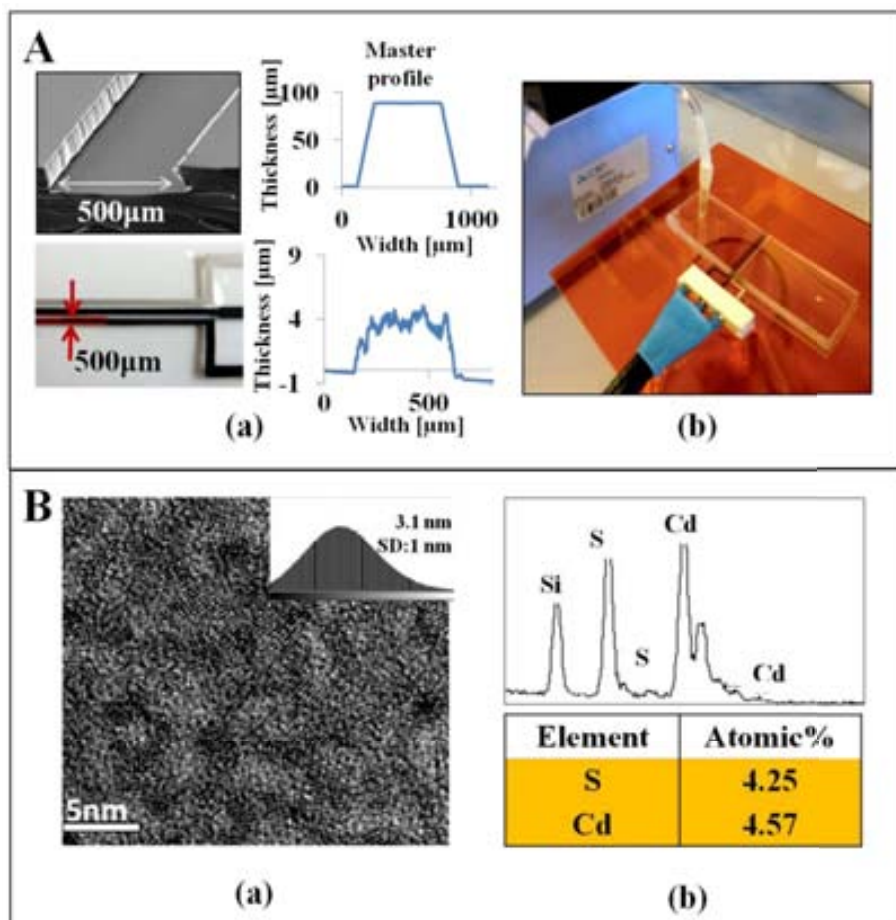


Figure 4.1. (A) Microfluidic platform system: scanning electron microscopy images of microchannel cross section, optical image of SPCE and their respective profiles (a) and microfluidic Set-Up (b). (B) CdS QDs: transmission electron microscopy images of CdS QDs (a) and the corresponding microanalysis data (b).

Out of chip and in-chip cyclic voltammetry studies of SPCE detectors.

In order to validate the use of SPCE as detector in chip, we first investigated cyclic voltammetry responses of the working electrode before and after the bonding procedure (in static and flow through modes). Figure 4.2A shows typical voltammograms obtained with a solution of 5 mM ferrocyanide/ferricyanide in 0.1 M KCl. The obtained electrodes were characterized in order to observe their repeatability and reproducibility. The repeatability studies were performed by studying the electrochemical response of three different electrodes in three consecutive measurements. The electrochemical conditions for the electrodes characterization were: $V_{ini} = -0.2$ V; $V_1 = 0.8$ V; $V_2 = -0.2$ V; scan rate of 50 mV s^{-1} .

The current data can be interpreted according to Levich's equation³⁰. For SPCE inside a channel with a rectangular cross-section, it can be expressed as:

$$I = 0.925nFcv(x_e D)^{2/3} \left(\frac{U}{h^2 d} \right)^{1/3} \quad (1)$$

The presented results prove that the screen-printed electrodes integrated into the microfluidic platform show good performance in a aqueous media and their behavior is in good agreement with Levich's predictions, demonstrating that the bonding process does not affect the electrodes. The developed integrated system shows good adhesion of screen printed electrodes with high resistance to high flow values of the measuring solution. On the other hand, repeatability and reproducibility studies for both drop (SP CE before integration into the channel).

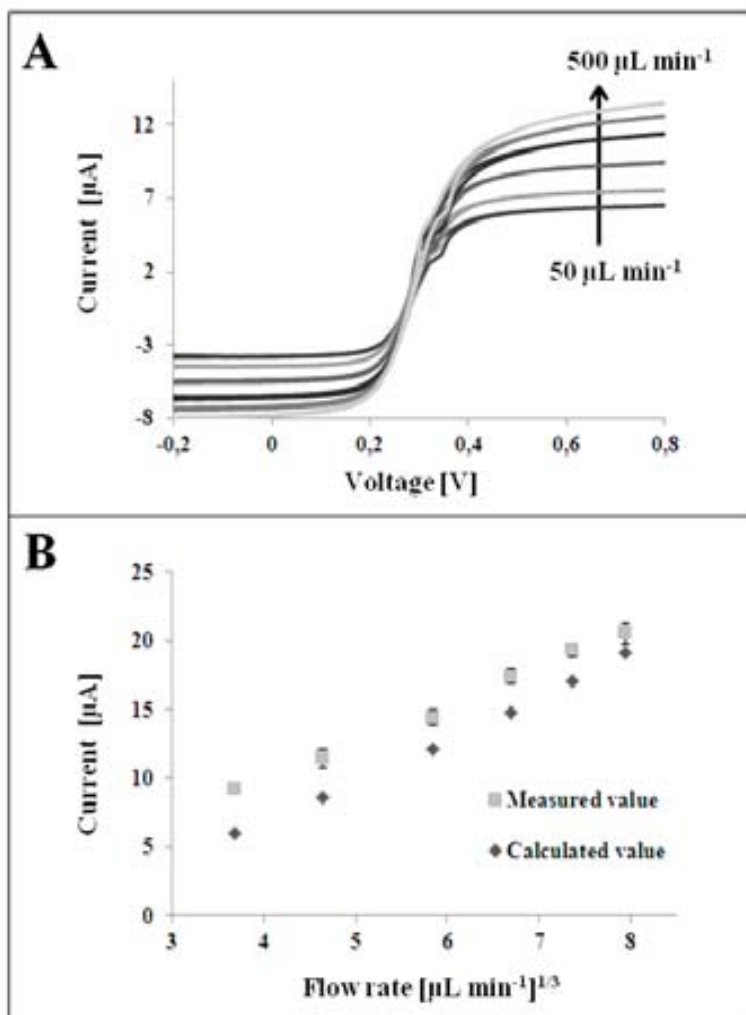


Figure 4.2. (A) Cyclic voltammograms recorded at different flow rates. (50, 100, 200, 300, 400, 500 $\mu\text{L min}^{-1}$) and (B) comparison between the calculated and the measured values of ferrocyanide/ferricyanide using cyclic voltammetry. Range of the measurement from -0.2 V to 0.8 V and scan rate 50 mV s^{-1} .

Where n is the number of exchanged electrons, F is the Faraday constant (96485 C mol^{-1}), c and D are the concentration and the diffusion coefficient of the electroactive species,

respectively, d is the channel width, h is half the height of the channel, x_e and w are the length and the width of the electrode, respectively, and U is the flow rate. In our case, the values used for the diffusion coefficients of ferrocyanide and ferricyanide³¹ were, in both cases, $D = 7.63 \times 10^{-10} \text{ m}^2\text{s}^{-1}$. The electrode dimensions were set to be approximate $w = 500 \text{ }\mu\text{m}$, $x_e = 500 \text{ }\mu\text{m}$, and the channel dimensions to $d = 500 \text{ }\mu\text{m}$ and $2h = 50 \text{ }\mu\text{m}$; according to the SEM images. The experimental data represented for each flow rate correspond to the average limiting current value from at least six consecutive cyclic voltammograms. The experimental limiting current values present a linear dependence with the cubic root of the flow rate, as predicted by the Levich equation, with a standard deviation between the measured values (in laminar flow regime) and calculated values around $1.72 \text{ }\mu\text{A}$. See Figure 4.2B.

QDs electrochemical detection

Until now, our group has demonstrated the electrochemical detection of CdS-QDs in batch measurements using commercial electrodes³² which are mercury-modified carbon electrodes. These electrodes combined with stripping methods lead to really high sensitivities but nowadays, the development of alternative methods less toxic and more environmental friendly than the ones using mercury are subject of interest. This is a reason why we have focused this work on the use of “non-toxic” carbon electrodes detector. However, as it can be seen in Figure 4.3, we are not able to discriminate the QDs signal from the blank. Indeed with commercial electrodes, a mercury-cadmium amalgam is created during the deposition step, which helps to the deposition of cadmium on the electrodes. When the detection is done in chip (in flow) an increase of the signal was observed.

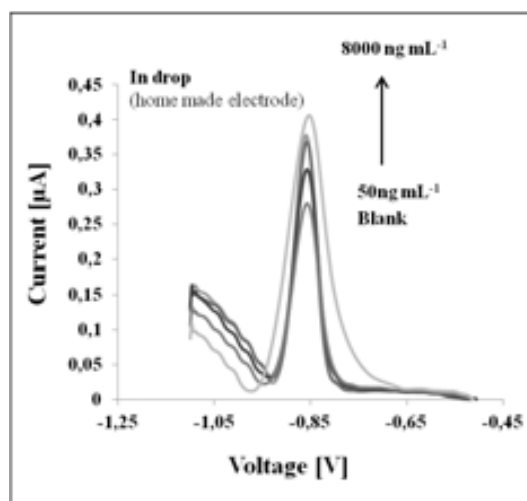


Figure 4.3. Typical voltammetry peak of CdS QDs re-oxidation in batch measurements with homemade carbon screen printed electrodes.

QUANTUM DOTS AS ELECTROCHEMICAL REPORTERS IN LOCs

This increase is related to a faster redox process that occurs in chip in comparison to drop measurement that should be related to the channel dimensions and the more controllable environmental conditions. (Figure 4.4A). Furthermore, as the deposition of QDs is done under flow conditions, we are not limited by the diffusion which leads to a higher enrichment to the electrode.

The repeatability between measurements using one single electrode was studied so as to see its operation behavior. Similar responses in three consecutive measurements with a standard deviation of $2.4 \mu\text{A}$ (Figure 4.4B) were obtained. In addition, the reproducibility between electrodes (chips) was studied giving rise to very similar responses using three different chips with standard deviation of $2.9 \mu\text{A}$ (Figure 4.4C).

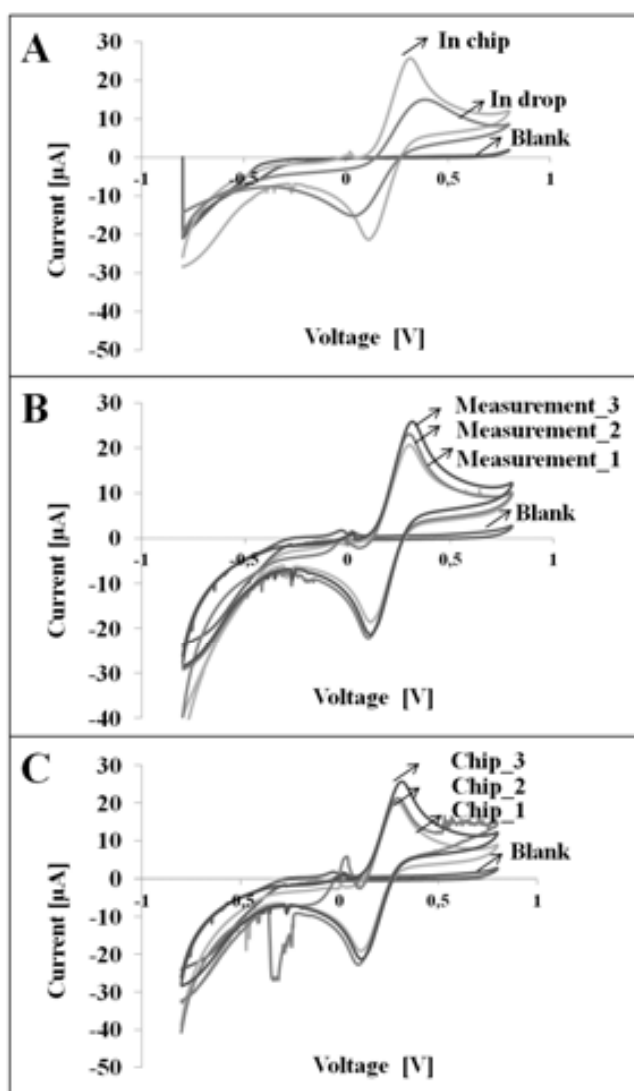


Figure 4.4. Cyclic voltammograms in a solution of 5 mM ferrocyanide/ferricyanide in 0.1 M KCl. Comparison between -in chip- and -in drop- measurements (A), Three consecutive measurements by using the same chip (B), and with three different chips (C). The scan rate for all CVs was 50 mV s^{-1} .

Electrochemical stripping parameters optimization

The electrochemical stripping detection of QDs was studied in different mediums such as phosphate buffer, acetate buffer or HCl (results not shown). Acetate buffer 0.2 M + NaCl 0.05M (pH 4.5) was selected taking into account the lower detection limits achieved.

In Figure 4.5, the different optimizations of the analytical parameters are shown. The best signal to noise relation and the highest sensitive of the detection were the choice criteria. Based on this study the optimal conditions were: conditioning potential: -0.15 V; conditioning time: 60 s; deposition voltage: -1.3 V; deposition time: 120 s; equilibrium time: 30 s; frequency: 10 Hz, and scan rate: 10 mV s⁻¹.

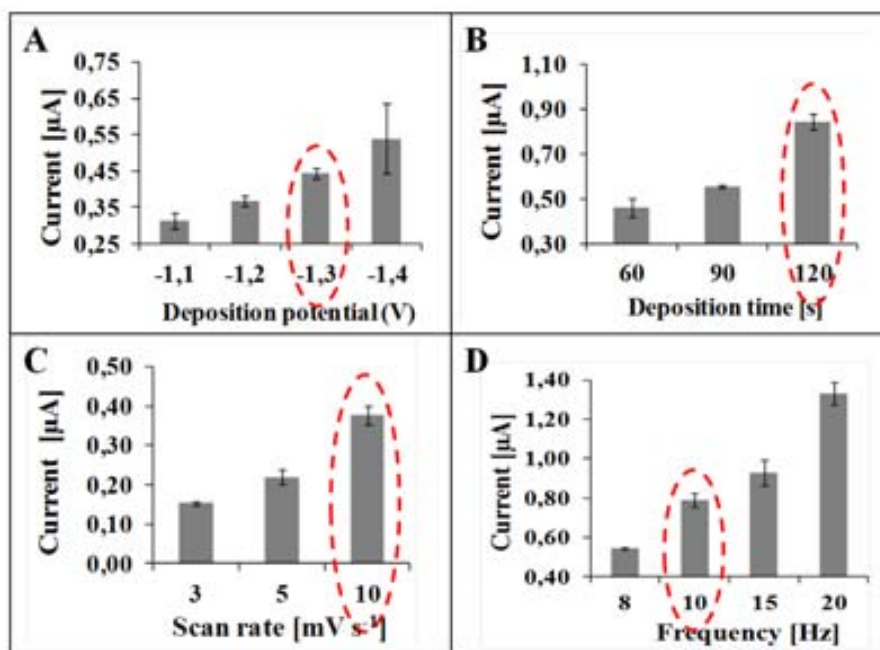


Figure 4.5. Optimization of electrochemical parameters for “in-chip” CdS QDs detection: (A) deposition potential, (B) deposition time, (C) scan rate and (D) frequency. Experimental conditions as described in the text.

Calibration curve and repeatability studies

The calibration curve for different CdS QDs concentrations in acetate buffer (0.2 M, pH 4.5) was obtained using the polycarbonate based platform achieving a linear range of detection between 50 and 8000 ng QDs/mL (see Figure 4.6A,B). The results show a well-defined stripping peak at -0.83 V in concordance with the Cd⁰ oxidation potential.

Three replicate determinations of each concentration were carried out with a maximum RDS of 6.5%.

Thanks to this device, we can achieve a sensitivity of 0.0009 µA (ng mL⁻¹)⁻¹ which is similar than the sensitivity obtained in static mode with commercial electrodes (with a

working electrode area 50 times bigger than the chip electrode) as it can be seen in Figure 4.6C.

The obtained range of response shows that this device shows promising potential for its integration in biosensing systems for future applications in immunosensors and DNA sensors using QDs as labels.

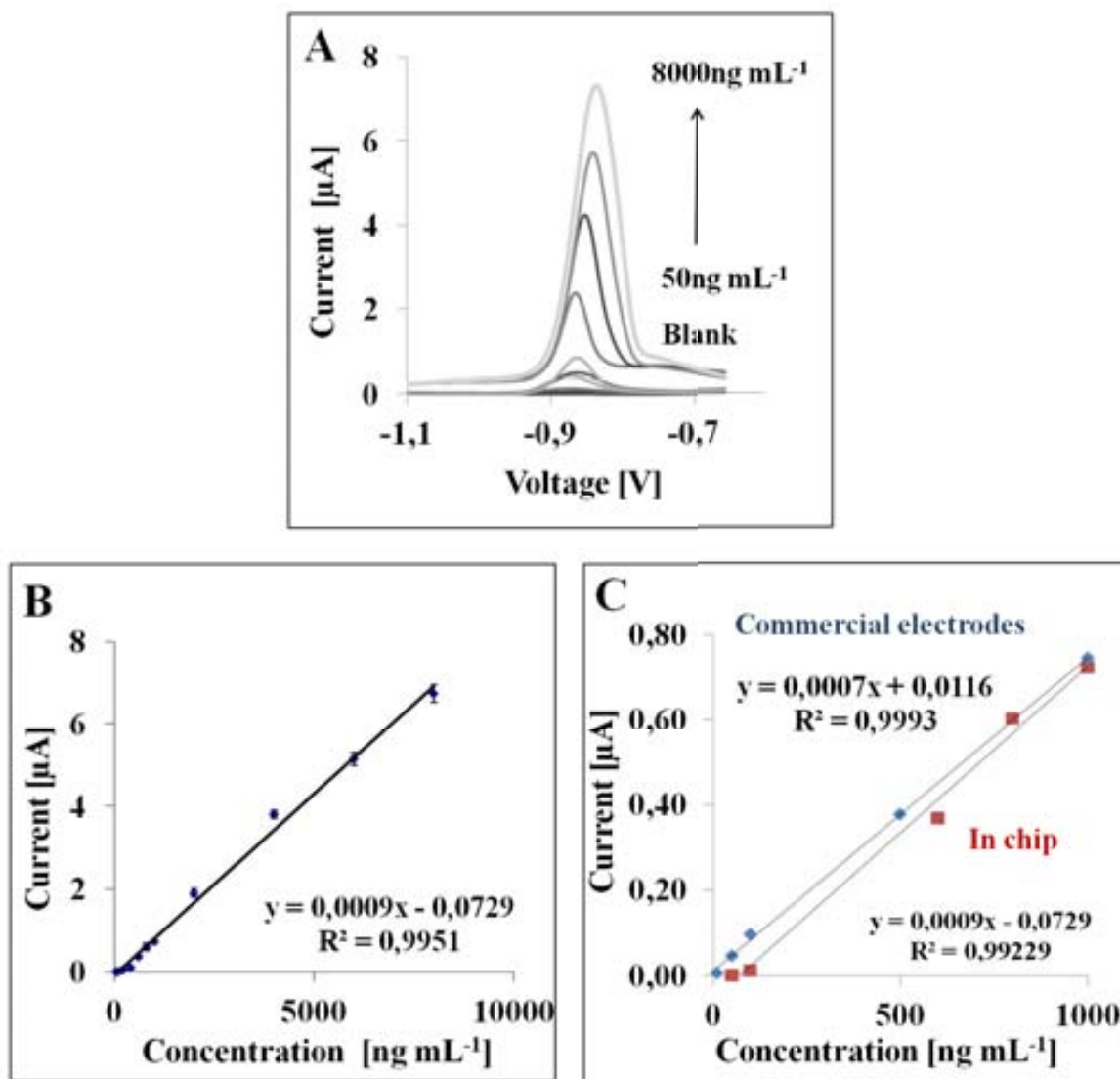


Figure 4.6. Calibration curve of CdS QDs electrochemical detection “in-chip” platform. (A) Typical voltammetry peak of CdS QDs re-oxidation in chip measurements with homemade carbon screen printed electrodes, (B) the linear calibration curve, and (C) comparison of calibration curves between batch measurements with commercial mercury based SPCEs and in chip measurements with homemade SPCEs. Blank and curves with increasing peaks from 50 to 8000 ng mL⁻¹ are shown.

The repeatability of the device was also studied using a second polycarbonate chip. The reproducibility and the sensitivity (results not shown) were in the same range as the first device.

The flow-through conditions allow the concentration of QDs to be always constant during the deposition step so the process is not limited by the diffusion. In addition, the peak current can be increased due to the continuous renewed solution during deposition time.

In concordance with the previous work related with QDs electrochemical detection, and due to the difficulties to functionalize the home-made CdS QDs because their small size (3 nm) and not biocompatible external layer, we decided to work with core-shell cadmium-selenide/zinc-sulfide (CdSe@ZnS) quantum dots modified with streptavidin. These QDs were obtained from Invitrogen, Spain. Electrochemical detection of these QDs as labeling carriers in an assay for apolipoprotein E (ApoE) detection has been evaluated.

4.3. On-chip magneto-immunoassay for Alzheimer's biomarker electrochemical detection by using Quantum Dots as labels.

4.3.1. Experimental Section

Reagents.

Real samples in plasma were provided by the research laboratory for Neurochemical Dementia Diagnostics, Department of Neurology, Ulm University, Germany. Human ApoE ELISA kit (HRP) was purchased from Mabtech (Nacka Strand, Sweden). Streptavidin-QD655 were obtained from Invitrogen (Spain). PBS, Tween 20, milk powder and bovine serum albumin (BSA) labeled with ALEXA 555 were acquired from Sigma Aldrich (Spain). PBS supplemented with 5 % (w/v) of milk powder and 0.005 % (v/v) of Tween 20 was prepared as blocking buffer. PBS supplemented with Tween 20 at 0.05 % (v/v) was used as washing buffer (PBST). PBS was employed as immunobuffer, except for QDs conjugation. In this case, commercial buffer Borate buffer, pH: 8.3, 0.05 % sodium azide) was used. Tosylactivated magnetic beads (2.8 μm of diameter) were also obtained from Sigma Aldrich (Spain) as well as the Human IgG, anti-Human IgG produced in goat (α -HIgG), and biotin anti-Human IgG (biotin α -HIgG) produced also in goat.

Characterization techniques.

The morphology of streptavidin-QD655 was checked through high resolution transmission electron microscope (TEM). A 2 μL drop of QD solution (12.5 nM in milli-Q water) was deposited onto a holey carbon layer copper grid and then air-dried. A Tecnai TEM (USA) operating at 200 kV was used to obtain the images for posterior analysis. Magneto-

immunoassay was also checked by MAGELLAN scanning electron microscopy (SEM), operating at 2 kV. A Leica TCS SP5 AO BS spectral confocal microscope (Leica Microsystems, Germany) was employed to evaluate the effect of blocking step into microfluidic channel.

Magneto-immunoassay in flow mode.

40 μg of tosylactivated magnetic particles (15 μL from stock solution) were washed 3 times with borate buffer and suspended in 135 μL of the same buffer. 15 μL of capture antibody at 0.5 mg mL^{-1} were added and the conjugation was achieved by gentle stirring of the suspension overnight at 700 rpm and 37°C. The unbound antibodies were eliminated by washing the carriers 3 times with PBST. 150 μL of PBS supplemented with Tween 20 at 0.05 % (v/v) and BSA at 5 % were added to the particles which were stirred during 2 h at 700 rpm and 25°C, washed 3 times with PBST and finally suspended in 150 μL of PBS.

The microchannel was first cleaned with PBST during 15 min with a flow rate of 10 $\mu\text{L min}^{-1}$, then treated by injecting the blocking buffer (see in reagents), at a flow rate of 5 $\mu\text{L min}^{-1}$ during 10 min and washed again with PBST during 10 min at 5 $\mu\text{L min}^{-1}$ to avoid unspecific absorption. The effect of the blocking step was evaluated by incubation of a BSA labeled with fluorophore (ALEXA 555) during 1 hr followed by washing step (see Figure 4.7).

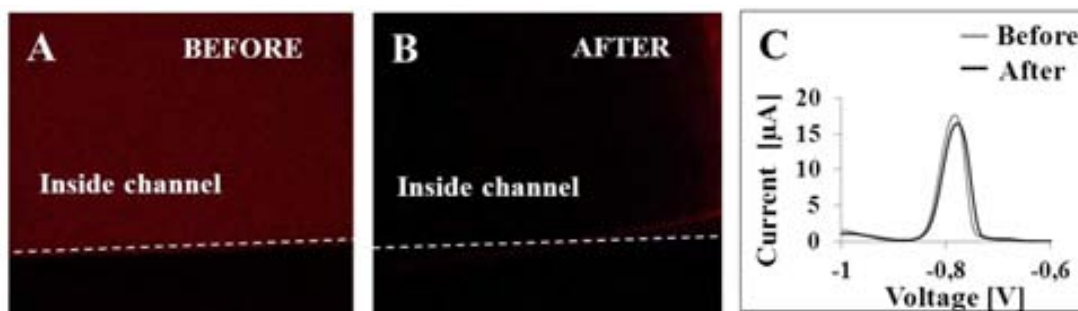


Figure 4.7. Effect of blocking step onto microfluidic channel as well as the screen printed electrode: (A) channel before blocking step (BSA with ALEXA 555 was incubated in PBS buffer during 1 hr. The image was taken after washing step using PBST) to see the unspecific absorption, (B) channel after blocking step (introduction of blocking buffer during 10min at flow rate of 5 $\mu\text{L min}^{-1}$, and (C) evaluation of screen printed electrode before and after blocking step by using a fix concentration of QDs in the measurement buffer .

The working electrode was then activated by cyclic voltammetry (10 cycles at potential range from -0.8 V to 0.8 V and scan rate of 10 mV sec^{-1} in PBS buffer). Magnetic beads already modified with antibodies were immobilized into the channel during 1 min at 5 $\mu\text{L min}^{-1}$, by using a neodymium magnet (1 mm of diameter, 3 mm of thickness) placed underneath the substrate, 1cm before the electrode. (Figure 4.8)

The target solution (ApoE) in PBS was flushed through the magnetic beads during 10 min at different concentrations [0, 25, 50, 100, and 200 ng mL^{-1}]. 15 μL of (biotinylated

antibody of 0.05 mg mL^{-1} in PBS) were then injected during 10 min. Streptavidin QD655 at 25 nM in borate buffer were introduced to complete the magneto immunocomplex. The incubation steps were performed at a flow rate of $5 \mu\text{L min}^{-1}$. Finally after the last washing step with PBST during 15 min at the same flow rate, the QDs were partially dissolved with acetate solution at pH 3 and detected electrochemically as described in the following paragraph (see Figure 4.9).

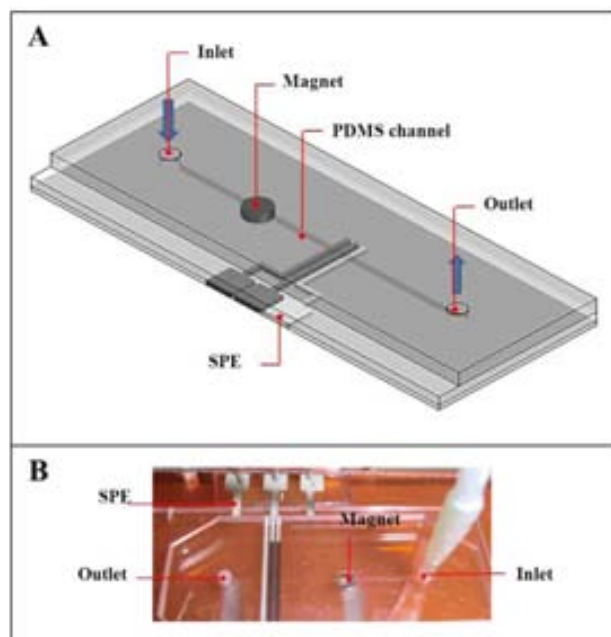


Figure 4.8. Schematic representation of electrochemical magnetoimmunosensing system for ApoE detection: (A) Components of the microfluidic platform with integrated screen-printed electrodes (SPCEs), and (B) the set-up used.

QDs electrochemical detection.

A 13.5 nm CdSe@ZnS QDs suspension was electrochemically detected using square wave anodic stripping voltammetry (SWASV) technique already reported by our group. The Cd^{2+} ions released from QDs were reduced to Cd^0 followed by their reoxidation to Cd^{2+} giving this way the electrochemical response to be used as analytical signal.

The CdSe@ZnS QDs concentrations (directly related to the biomarker concentration) were determined by SWASV. In order to get a maximum sensitivity, the electrochemical parameters (deposition time, conditioning potential, conditioning time and frequency) were optimized.

The limit of detection (LOD) of the respective calibration curve was calculated as the mean intensity (MI) of four chips (incubated with a blank-control measurement in PBST) plus three times the standard deviation of the blank measurement (without QDs).

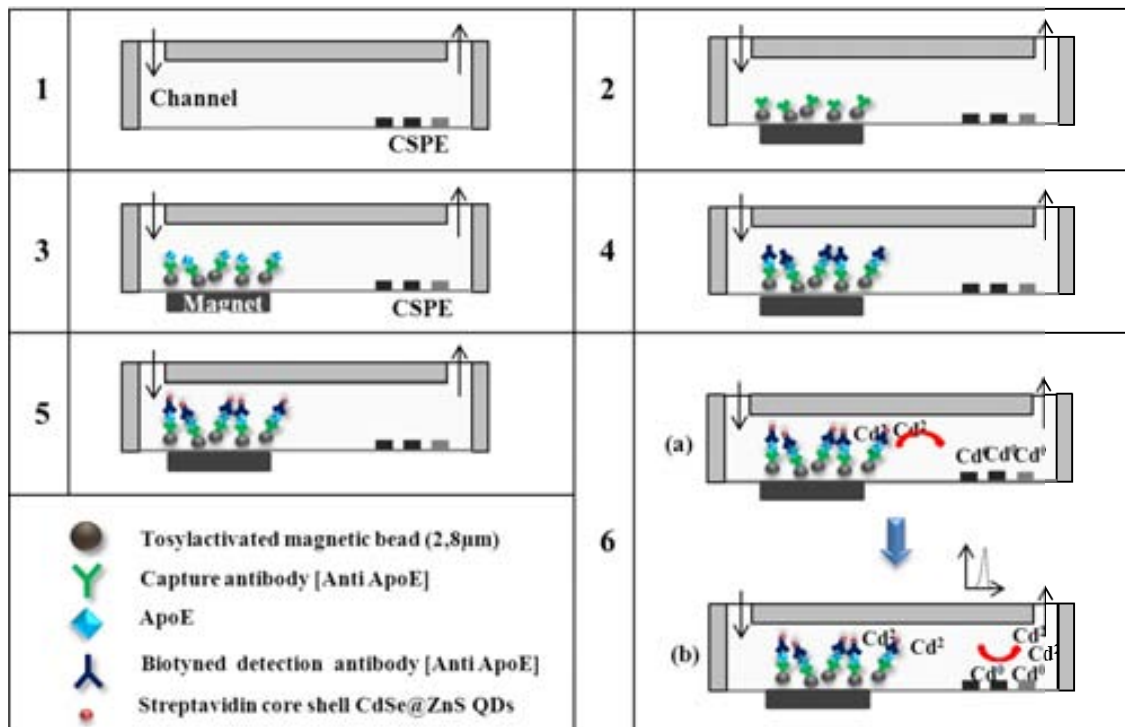


Figure 4.9. Schematic representation of electrochemical magneto-immunosensing for apolipoprotein-E (ApoE) detection. Microchannel blocking with milk powder in PBST and PBS (1), introduction of magnetic beads with the capture antibody previously conjugated (2), ApoE introduction at different concentrations (from 25 to 200 ng mL⁻¹) (3), biotinylated antibody introduction (4), QDs conjugation (5), and finally the electrochemical detection by using square wave voltammetry: deposition step, where the Cd²⁺ released from the QDs, is reduced to Cd⁰ (a) and measurement of re-oxidation of Cd during stripping the potential between -1.1 V to -0.15 V. Between each step PBST as washing agent was flowing.

4.3.2. Results and Discussion

Characterization of the QDs.

The size, shape, and crystallinity of the QD655 were characterized by TEM. The images revealed a very homogeneous and well-dispersed solution of the QD655, which did not show any aggregation. The studied nanocrystals display a rice-grain shape nanocrystals, in which crystalline planes can be appreciated.

The average size of the QD655 is 13.5 ± 1.91 nm. The magneto-immunocomplex was also characterized by SEM, with two relevant samples (casein- and ApoE biomarker at 100 ng mL⁻¹, Figure 4.10).

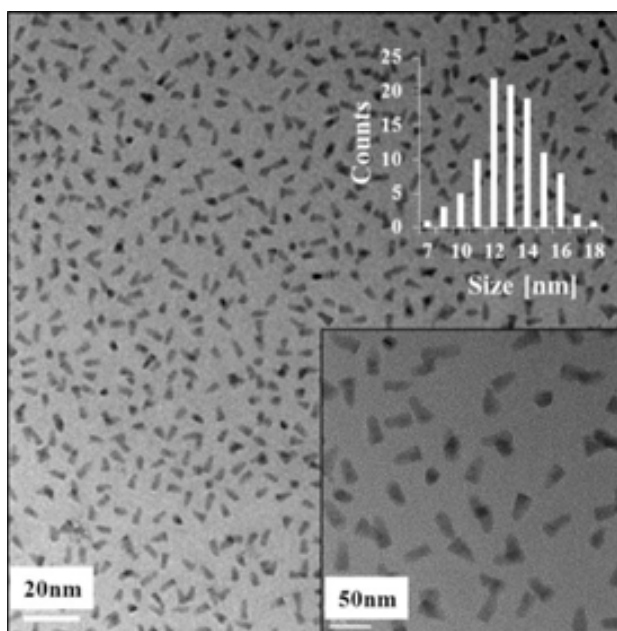


Figure 4.10. Characterization of the QD. TEM image of the studied quantum dots (QD655). Inset size distribution of the QD655 (average size: ca. 13.55 ± 1.9 nm) are also shown.

Electrochemical stripping parameters optimization.

The influence of the variation of the pH of the dissolving solution, taking into account the compromise between signal and electrode stability and the low resistance of PDMS and PC (microchannel materials) against acidic solutions upon the QDs a signal was studied (Figure 4.11). The selected pH was 2.5 dissolving solution, which was used for the electrochemical parameters optimization. Signal to noise ratio and the sensitivity were chosen as criteria.

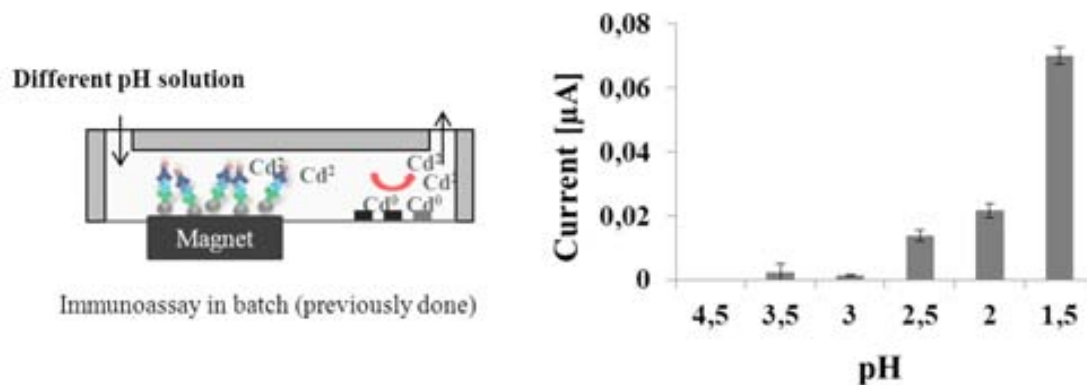


Figure 4.11. Effect of pH of the dissolving solution over QDs signal.

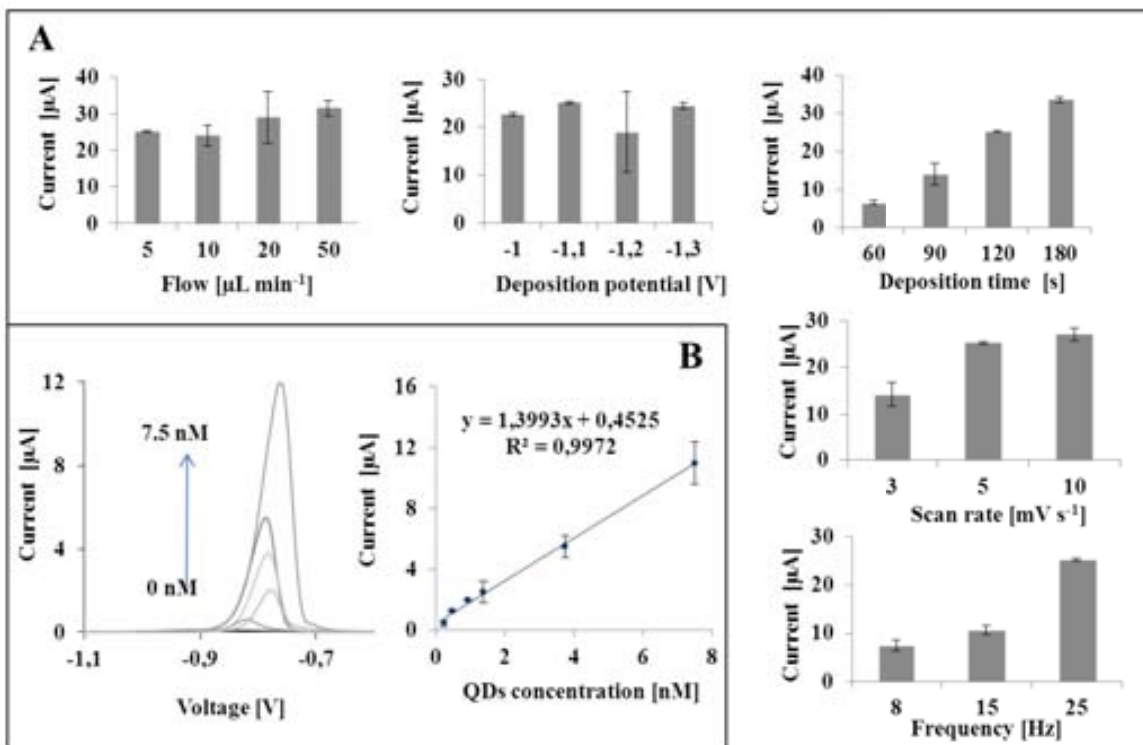


Figure 4.12. (A) Electrochemical parameters optimization and (B) typical response of QDs by square wave voltammetry, from 0 to 7,5 nM with its respective calibration curve. The optimal found conditions were: deposition voltage: -1.1 V; deposition time: 120 s, equilibrium time: 30 s; frequency: 25 Hz, and scan rate: 10 mV s⁻¹.

Evaluation of the microfluidic platform performance using QDs labels for a model protein detection (HIgG produced in goat), in order to optimize the conjugation parameters in flow were previously performed, in order to choose the lowest incubation time without losing efficiency. This study was performed following the same protocol previously described in experimental section. All incubation steps were performed by changing the flow rate from 5 to 50 μL min⁻¹. The more efficient conjugation step was produced between 5 and 10 μL min⁻¹, otherwise, the flow could drag the magnetic beads previously immobilized due to external magnet force limitation. Flow rate for conjugation was finally set at 5 μL min⁻¹ according also to electrochemical parameters optimization. Different incubation times such as 5, 10 and 15 min were also tested. An accepted / normal electrochemical signal was observed from 10 and 15 min without any significant difference, but for shorter times (ex. 5 min) irreproducible signals were observed. Finally, 10 min of incubation was selected for further experiments. Washing steps were done with different times at the same incubation flow and 10 min time interval to clean the channel from antibodies excess was found satisfactory. Figure 4.13.

Electrochemical detection was performed by dissolving QDs after the last washing step. Typical peak of ZnS@CdSe QDs at -0.85 V is shown in Figure 4.13. Calibration curve for

HIgG detection was also obtained, with a very good LOD (1.72 ng mL^{-1}) and a RSD of 17.3 %. The control was performed with a concentration of HIgG of 0 ng mL^{-1} .

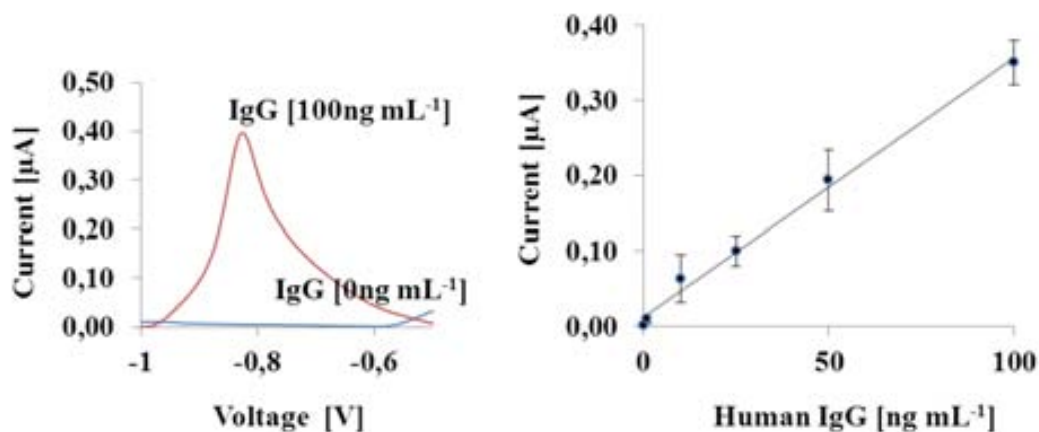


Figure 4.13. Performance of the human IgG-magnetoimmunoassay using QDs as electrochemical labels: Square wave voltammetry of QDs present in the magneto-immunocomplex ($-1,1 \text{ V}$ of deposition potential during 120 s, and stripping between $-1,1 \text{ V}$ to $-0,15 \text{ V}$ with scan rate of 5 mV s^{-1} , Frequency of 25 Hz and flow rate of $5 \mu\text{L min}^{-1}$), and calibration curve of human IgG with a LOD of 1.72 ng mL^{-1} . The error bars were obtained from parallel assays of four microfluidics chips.

Alzheimer biomarker (ApoE) detection.

Once the previous parameters were optimized, they were applied to the detection of ApoE biomarker in both standard and real samples. Each ApoE concentration was checked 4 times using different chips to obtain the error bars. Incubation steps and electrochemical detection was performed with the same conditions used for HIgG determination.

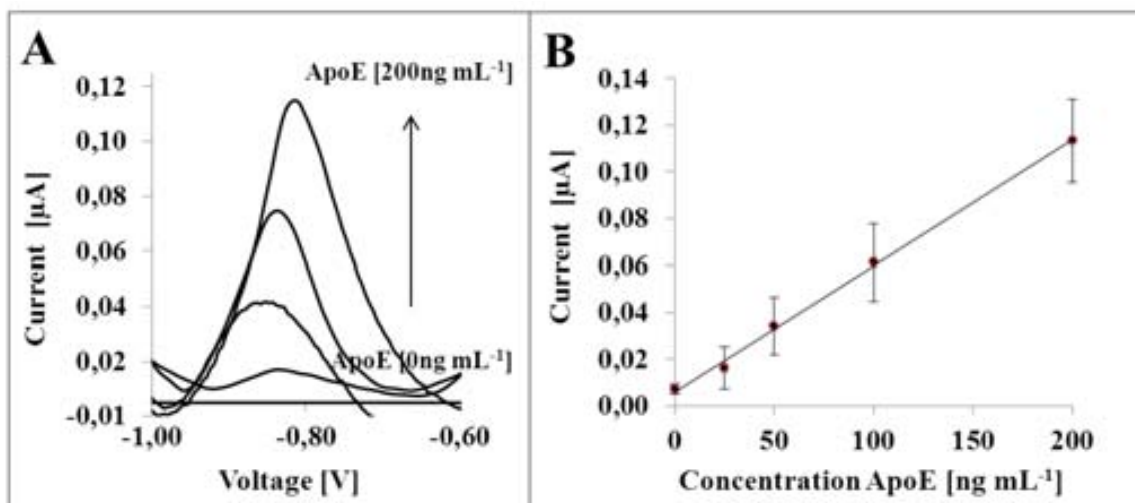


Figure 4.14. (A) Performance of the ApoE-magnetoimmunoassay using QDs as electrochemical labels: Square wave voltammetry of QDs present in the magneto-immunocomplex ($-1,1 \text{ V}$ of deposition potential during 120 s, and stripping between $-1,1 \text{ V}$ to $-0,15 \text{ V}$ with scan rate of 5 mV sec^{-1} , Frequency of 25 Hz and flow rate of $5 \mu\text{L min}^{-1}$) and (B) calibration curve of standard sample of ApoE.

QUANTUM DOTS AS ELECTROCHEMICAL REPORTERS IN LOCs

The calibration curve and repeatability studies for different ApoE concentrations in measurement buffer were obtained using a microfluidic platform achieving a LOD of 12.5 ng mL^{-1} in a linear range of detection between 0 and 200 ng mL^{-1} (see Figure 4.14). The results showed a well-defined stripping peak at -0.83 V in concordance with the Cd^0 oxidation potential.

Four replicates for each concentration were carried out. The obtained range of response demonstrates that this device shows promising potential for its integration in biosensing systems and immunosensors using QDs as labels. The reproducibility of the device was also studied using four different microfluidic chips. The reproducibility and the sensitivity are represented in the error bars in the calibration curve.

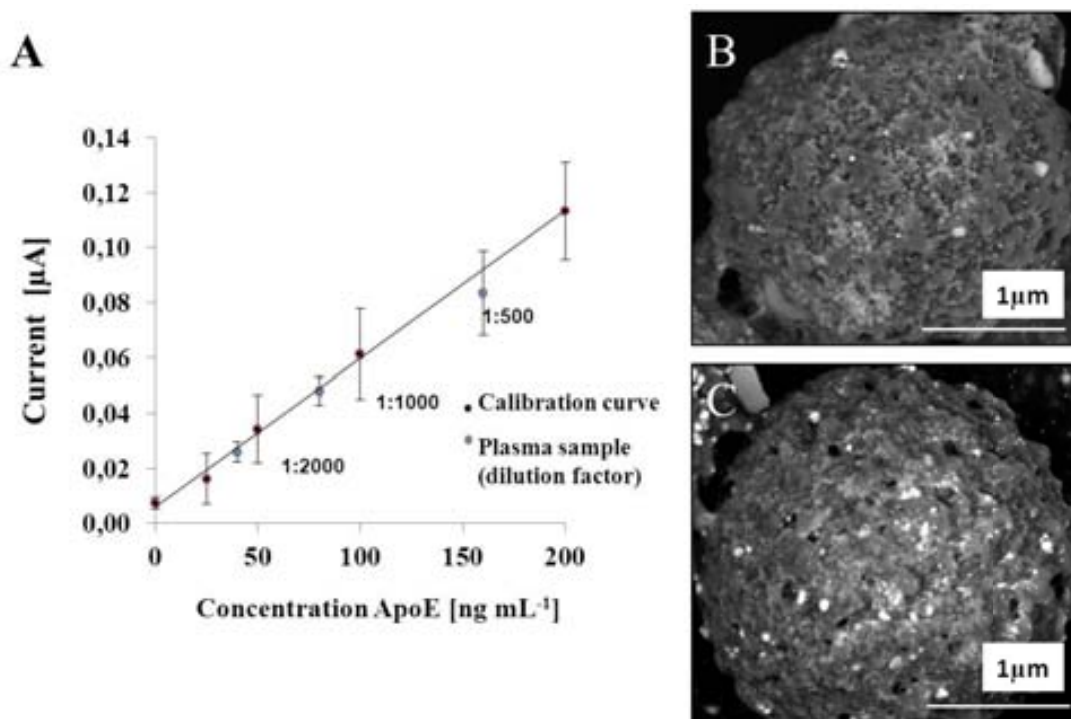


Figure 4.15. (A) Comparison between calibration curve of ApoE (red points) and ApoE in plasma samples (blue points). According to the electrochemical measurements, the original concentration of the inspected human plasma was $\sim 80 \pm 4,2 \text{ } \mu\text{g mL}^{-1}$. The error bars were obtained from parallel assays of fourth microfluidics chips. (B) SEM image of magnetoimmunoassay with control protein (casein at 100 ng mL^{-1}), and (C) SEM image of magnetoimmunoassay with ApoE protein of real sample (100 ng mL^{-1}).

Finally, human plasma samples were inspected in serial dilutions and assayed in a microfluidic platform as described in the experimental section (Figure 4.15A). As human plasma concentration values for ApoE typically range from $16 \text{ to } 169 \text{ } \mu\text{g mL}^{-1}$ ³³, very small volumes of plasma were diluted in a suitable volume of assay buffer before analysis. The concentration of ApoE in the assayed plasma was estimated by interpolating the current intensities of the ApoE electrochemical detection in human plasma into a

calibration curve, finding an original concentration of ApoE in the plasma sample of $\sim 80 \pm 4.6 \mu\text{g mL}^{-1}$. In Figure 4.15B few amounts of QDs unspecifically attached are observed but there is a significant difference with Figure 4.15C, where a high amount of QDs is observed, onto the surface of magnetic beads after the complete magnetoimmunoassay. This assay was performed as a negative control by incubation of casein instead of ApoE biomarker

These results are in concordance with the previous work performed in our group³⁴, but using microarrays strategy. (Figure 4.16).

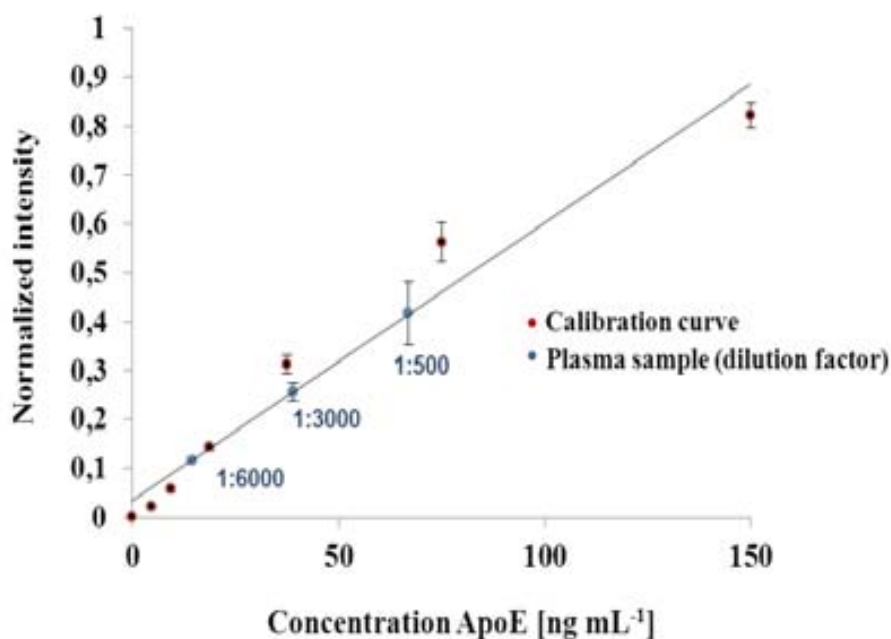


Figure 4.16. ApoE screening in human serum using the QD microarray. Small volumes ($1 \mu\text{L}$) of plasma were diluted in a suitable volume of assay buffer. The concentration of ApoE in the assayed plasma was estimated by interpolating the fluorescence intensities from the screen into a calibration curve. According to the QD microarray, the original concentration of the inspected human plasma was $\sim 80 \pm 8.2 \mu\text{g mL}^{-1}$. The error bars were obtained from parallel assays of ten spots. QD655, quantum dot 655nm of excitation wavelength.

4.4. Conclusions

The fabrication of a hybrid PDMS-PC microfluidic chip with integrated SPCE electrodes has been demonstrated. Screen printed carbon electrodes (SPCE) has been integrated as a SWASV detector and shown to be a simple alternative for easy to use, low cost and mass produced chips.

The electrochemical parameters of the in-chip CdS QDs detection such as scan rate, deposition potential, deposition time, frequency, and flow rate in order to obtain the best relation electrochemical response vs. noise using the developed microfluidic platform have been optimized.

The developed in-chip QDs detection in addition to the integration of other operations such as microreaction, pre-concentration, separation, and bioconjugation can open the way to the design of various biosensing platforms. These operations in addition to the high sensitivity of the detector will open the way to future applications of the developed device in diagnostics between other applications.

The presented lab-on-a-chip platform allows the characterization of electrochemical behavior of QDs as labels, as well as its application for ApoE biomarker detection with very good accuracy and LOD for standard and real samples. The use of polymeric substrates such as PC, widely used for lab-on-a-chip prototype fabrication show special interest for future mass production through injection molding or hot embossing processes.

In addition, the use of a microchannel with a magnetic retention zone, allowed the sample purification and preconcentration using magnetic beads as stationary support, providing good sensitivity and more controllable sample manipulation.

Detection systems for microfluidic immunoassays are usually bulky and expensive, therefore developing and integrating miniaturized, portable and cheap detection systems like screen printed electrodes with a micro-potentiostat make them suitable for low cost point of care devices.

Finally, very small volumes of human plasma were assayed with high sensitivity and acceptable precision and accuracy. This approach could be extended to a multiplexed detection of ApoE isoforms and other AD related biomarkers.

The technique was applied for the detection of ApoE in real sample with a good correlation of 99.8% of R^2 respect to the standard sample and the same slope showing identical sensitivity. The assay time was also reduced in a 33 % respect to the batch method.

4.5. Futures perspectives

Regarding the incorporation of QDs in microchannels as labels, many challenges remain to be addressed. Multidetected analyses could be addressed using QDs with different composition (CdSe, ZnS, CdS, etc.) as electrochemical labels. Microchannels design could be also improved in order to reduce incubation time and enhance the reaction stages, incorporating for example mixers. Other nanomaterials could be used for electrode surface modification in order to increase the sensitivity of the electrochemical measurement.

Electrochemistry also allows the miniaturization of the readout system, giving the possibility to produce a portable and accessible point-of-care device for real-world bioanalytical scenarios for applications in diagnostics, safety, security, and environmental monitoring.

4.6. References

¹S. Haeberle and R. Zengerle. *Microfluidic platforms for lab-on-a-chip applications*. Lab Chip. 2007, 7 (9), 1094-1110.

²R.P. Baldwin. *Recent advances in electrochemical detection in capillary electrophoresis*. Electrophoresis. 2000, 21, 4017-4028.

³A. M. Smith and S. Nie. *Next-generation quantum dots*. Nat. Biotech. 2009, 27, 732-733.

⁴M. Amelia, C. Lincheneau, S. Silvi, and A. Credi. *Electrochemical properties of CdSe and CdTe quantum dots*. Chem. Soc. Rev., 2012, 41, 5728-5743.

⁵A. Merkoçi, J. H. Marcolino-Junior, S. Marín, O. Fatibello-Filho, and S. Alegret. *Detection of cadmium sulphide nanoparticles by using screen - printed electrodes and a handheld device*. Nanotechnology. 2007, 18, 035502 1-6.

⁶N. Pamme. *Magnetism and microfluidics*. Lab Chip. 2006, 6, 24-38.

⁷R. Brookmeyer, S. Gray, and C. Kawas. *Projections of Alzheimer's disease in the United States and the public health impact of delaying disease onset*. Am. J. Public Health. 1998, 88(9), 1337-1342.

⁸M. C. Reza Mohamadi, Z. Svobodova, R. Verpillot, H. Esselmann, J. Wiltfang, M. Otto, M. Taverna, Z. Bilkova J-L. and Viovy. *Microchip Electrophoresis Profiling of A β Peptides in the Cerebrospinal Fluid of Patients with Alzheimer's Disease*. Anal. Chem. 2010, 82, 7611-7617.

⁹R. J. Clifford, D. Jr, W. Knopman, L. Jagust, P. M Shaw, M. S Aisen, R. W Weiner, and T. John Q, *Hypothetical model of dynamic biomarkers of the Alzheimer's pathological cascade*. Lancet Neurol. 2010, 9(1): 119-139.

¹⁰M. Takeda, R. Martínez, T. Kudo, T. Tanaka, M. Okochi, S. Tagami, T. Morihara, R. Hashimoto, and R. Cacabelos. *Apolipoprotein E and central nervous system disorders: reviews of clinical findings*. Psychiatry Clin. Neurosci. 2010, 64, 592–607.

¹¹J. Kim, J. M. Basak, and D. M. Holtzman. *The role of apolipoprotein E in Alzheimer's disease*. Neuron. 2009, 63, 287–303.

¹²A. Ambrosi, M. Guix, and A. Merkoçi. Magnetic and electrokinetic manipulations on a microchip device for bead-based immunosensing applications. Electrophoresis. 2011, 32 (8), 861-869.

¹³Y. Zhang, S. Ge, S. Wang, M. Yan, J. Yu, and X-Liu W. Song. *Magnetic beads-based electrochemiluminescence immunosensor for determination of cancer markers using quantum dot functionalized PtRu alloys as labels*. Analyst. 2012 , 137(9):2176-2182.

¹⁴ L. Fang, Z. Rui, Z. Kaihong, C. Huanchun, H. Yonggang. *Magnetic beads-based electrochemical immunosensor for detection of pseudorabies virus antibody in swine serum*. Talanta. 2011, 87, 302–330.

¹⁵ L. Kang-Yi, H. Lien-Yu, H. Tze-Bin, T. Yi-Che, L. Huan-Yao, and L. Gwo-Bin. *Rapid detection of influenza A virus infection utilizing an immunomagnetic bead-based microfluidic system*. Biosens. Bioelectron. 2011, 3900–3907.

¹⁶L. Yen-Heng, W. Shih-Hao, W. Min-Hsien, C-S. Tung-M., L. Ji-Dung, and C. Chiuan. *Integrating solid-state sensor and microfluidic devices for glucose, urea and creatinine detection based on enzyme-carrying alginate microbeads*. Biosens. Bioelectron. 2013, 328–335.

¹⁷B. Teste, A. Ali-Cherif, J-L. Viovy, and L. Malaquin. *A low cost and high throughput magnetic bead-based immuno-agglutination assay in confined droplets*. Lab Chip. 2013, 13, 2344-2349.

¹⁸J.H. Kang, S. Krause, H. Tobin, A. Mammoto, M. Kanapathipillai, and D.E. Ingber. *A combined micromagnetic-microfluidic device for rapid capture and culture of rare circulating tumor cells*. Lab Chip. 2012, 12, 2175-2181.

¹⁹ E. Zacco, MI. S. Alegret, R. Galve, and MP. Marco. *Electrochemical magnetoimmunosensing strategy for the detection of pesticides residues*. Anal Chem. 2006,15;78(6), 1780-1788.

-
- ²⁰L. Chun-Che, W. Jung-Hao, W. Hui-Wen, and L. Gwo-Bin. *Microfluidic Immunoassays*. J. Lab. Automat. 2010, 15, 253-274.
- ²¹ B.V. Chikkaveeraiah, A.A. Bhirde, N.Y. Morgan, H.S. Eden, and X. Chen. *Electrochemical immunosensors for detection of cancer protein biomarkers*. ACS Nano. 2012, 6, 6546–6561.
- 22 N. Godino, D. Snakenborg, J.P. Kutter, J. Emnéus, M.F. Hansen, X. Muñoz, and F. J. del Campo. *Construction and characterisation of a modular microfluidic system: coupling magnetic capture and electrochemical detection*. J. Microfluid Nanofluid. 2010, 8, 393–402.
- ²³K. Islam, Y-C. Jang, R. Chand, S. K. Jha, H-H. Lee, and Y-S Kim. *Microfluidic biosensor for β -Amyloid (1-42) detection using cyclic voltammetry*. J. Nanosci. Nanotechnol. 2011, 11, 5657-5662.
- ²⁴ V. Picot, M. Rossi, B. Alies, C. Hureau, P. Faller, and P. Joseph. *Microfluidics for Alzheimer's disease: screening and diffusion to study amyloid- β aggregation*. 16th International Conference on Miniaturized Systems for Chemistry and Life Sciences (Okinawa, Japan), 2012, 1030-1032.
- ²⁵ J.S. Lee, and C. Beum-Park. *Microfluidic dissociation and clearance of Alzheimer's β -amyloid aggregates*. Biomaterials. 2010, 31, 6789-6795.
- ²⁶M. Meier, J. Kennedy-Darling, S. Hoon Choi, E.M. Norstrom, S.S. Sisodia, and R.F. Ismagilov. *Plug-based microfluidics with defined surface chemistry to miniaturize and control aggregation of amyloidogenic peptides*. Angew Chem Int Ed Engl. 2009, 48(8), 1487–1489.
- ²⁷L. Tang and N. Yoon Lee. *A facile route for irreversible bonding of plastic-PDMS hybrid microdevices at room temperature*. Lab Chip. 2010, 10, 1274-1280.
- ²⁸Ch. Barglik-Chory, D. Buchold, M. Schmitt, W. Kiefer, C. Heske, C. Kumpf, O. Funchs, L. Weinhardt, A. Stahl, E. Umbach, M. Lentze, J. Gerts, and G. Müller. *Synthesis, structure and spectroscopic characterization of water-soluble CdS nanoparticles*. Chem. Phys. Let. 2003. 379, 443-451.
- ²⁹S. Marin and A. Merkoçi. *Direct electrochemical stripping detection of cystic fibrosis related DNA linked through cadmium sulphide quantum dots*. Nanotechnology. 2009, 20, 055101, 1-6.

³⁰R. G. Compton, AC. Fisher, RG. Wellington, PJ. Dobson, and PA. Leigh. *Hydrodynamic voltammetry with microelectrodes: channel microband electrodes; theory and experiment*. J. Phys. Chem. 1993, 97, 10410–10415.

³¹X. Illa, O. Ordeig, D. Snakenborg, A. Romano-Rodríguez, R. G. Compton, and JP. Kutter. *A cyclo olefin polymer microfluidic chip with integrated gold microelectrodes for aqueous and non-aqueous electrochemistry*. Lab Chip. 2010, 10, 1254–1261.

³²I. Palchetti, S. Majid, A. Kicela, G. Marraza, and M. Mascini. *Polymer-mercury coated screen printed sensors for electrochemical stripping analysis of heavy metals*. Int. J. Environ. Anal. Chem. 2003, 83, 701-711.

³³M. Vincent-Viry, F. Schiele, R. Gueguen, K. Bohnet, S. Visvikis, and G. Siest. *Biological variations and genetic reference values for apolipoprotein E serum concentrations: results from the STANISLAS cohort study*. Clin. Chem. 1998, 44, 957–965.

CHAPTER 5. NOVEL STRATEGIES TO OBTAIN ELECTROCHEMICAL LOCs WITH HIGHER SENSITIVITY.....	105
5.1. Introduction	107
5.2. Magnetic plug-based platform development	109
5.2.1. Experimental details	110
5.2.2. Results and discussion	113
5.3. Design and fabrication of a recycling flow micro-system.....	120
5.3.1. Experimental details.	120
5.3.2. Results and discussions.....	122
5.4. Enhanced detection sensitivity of quantum dots labelled protein by bismuth electrodeposition into microfluidic channel.	130
5.4.1. Experimental details	131
5.4.2. Results and discussions.....	133
5.5. Conclusions	139
5.6. Reference	140

CHAPTER 5

NOVEL STRATEGIES TO OBTAIN ELECTROCHEMICAL LOCs WITH HIGHER SENSITIVITY

Related Publications

M. Medina-Sánchez, S. Miserere, and A. Merkoçi. “Design and fabrication of a recycling flow micro-system for immunoassay based on quantum dots as electrochemical labels”. Technical communication. In preparation. (Annex 2).

In this Chapter, three different approaches to improve the electrochemical signal of Quantum dots (QDs) as labels in LOC immunoassays are discussed. The first one is the use of a microfluidic channel with integrated magnets to immobilize magnetic beads in a specific pattern, where the immunoassay is performed. This platform is reusable because magnetic beads can be easily cleaned once the magnets are removed and a flow-rate is applied. The second approach presented is the use of a home-made QDs recycling system. In this part, the QDs increasing signal is demonstrated by using an external peristaltic pump connected with a microfluidic chip forming a loop system. The flow containing QDs is recycled since in the first turn some of the metal ions and QDs themselves are not deposited onto the electrode, so when the solution is flowed during more turns, the probability to deposit the remaining residual ions and QDs is higher, increasing in this way the electrochemical signal. After this demonstration, the fabrication of a micro-peristaltic pump with integrated pneumatic valves is proposed. All the fabrication steps were optimized and the software for sequential control of the valves was developed. Finally, bismuth was used as it is a well-known material to agglomerate heavy metals. We take advantages of this property for improving the electrochemical signal of QDs, due to the cadmium content in that QDs core. Optimization of the bismuth concentration was done in order to achieve the highest signal. This detection was performed in batch as well as in microfluidic mode.

5.1. Introduction

Magnetic particles in microfluidics. Magnetic particles are widely used in biomedical and bioanalytical applications for capturing, transport and detection of biomolecules and cells¹ due to their high surface to volume ratio, versatility and ease of manipulation using an external magnetic field². Target molecules can be immobilized on their surface in order to inherit this molecule with the magnetic properties for a rapid separation from the surrounding liquid³, or to tailor the magnetic particle with a specific functionality to carry out different reactions and bindings with various purposes such as immunoassays⁴, DNA hybridization⁵ or mRNA isolation⁶.

Microfluidic platforms offer the possibility to control and manipulate these particles, providing with new opportunities for on-chip experiments and tackling the inherent problems of the batch methods such as the high consumption of time and reagents. In addition, the efficiency of separations is increased because the magnetic force on a particle is higher closer to the magnet surface⁷. Mirowski et al.⁸ for example developed a microfluidic chip with a patterned magnetic thin-film to create magnetic field gradients in order to trap magnetic particles. In this way, they could control and position the particles. Dutz et al.⁹ developed a microfluidic chip for the continuous size dependent fractionation of magnetic microspheres by a simple adjustment of the flow velocity, and Slovakova et

NOVEL STRATEGIES TO OBTAIN ELECTROCHEMICAL LOCs WITH HIGHER SENSITIVITY

al.¹⁰, also used grafted trypsin magnetic beads in a microchip for performing protein digestion. This system has the advantage of easy replacement, as the bead matrix is easily washed out and replaced. Reproducibility for digesting recombinant human growth hormone was also studied.

Analyte recycling and in-chip valves for such purpose. The electrochemical signal of the quantum dots (QDs) can also be increased without increasing the sample volume but by simply achieving the sample flow recycling. In a previous work, this fact was demonstrated by recycling a QDs containing sample through a close-loop system using a peristaltic micropump¹¹. However, further research is needed for the design of a microfluidic structure that allows the integration of such a function within a chip. With this purpose, pressure-activated valves fabricated by multilayer soft lithography are of particular interest. These valves are fabricated by routing dead-end channels in a layer over (“push down” mode) or below (“push-up” mode) the layer containing the flow channels, forming a thin membrane between them at their intersection. When the pressure in the control channel is increased, the membrane is deflected, stopping the liquid motion in the flow channel and creating in this way a pressure-activated valve¹². When the sample inside the flow channel must be in contact with the substrate (for example when the latter is modified) the “push-down” mode should be used¹³. Tan et al. for example, fabricated a polydimethylsiloxane (PDMS) control channel over a polymethylmethacrylate (PMMA) flow channel, integrating in this way the advantages of each polymer for the fabrication of a microfluidic chip with a better performance¹⁴. These kinds of valves were proposed by Unger et al.¹⁵, and as they mentioned, the shape of the flow channel must present a round cross section in order to close completely. This shape can be achieved by melting and reflowing the positive photoresist during the master fabrication¹⁶.

Enhancement by using bismuth modified electrodes. The use of micro / nanomaterials to modify electrodes is a well-known procedure in biosensing for functionalization and transducer modification. In this chapter we are also focused on the modification of screen printed electrodes (SPE) for improving the electrochemical signal of QDs. Different materials have been used for heavy metal detection, such as mercury¹⁷, bismuth (Bi)¹⁸, graphene¹⁹, etc. The high toxicity of mercury film electrodes, which have been widely applied for the determination of heavy metals by stripping voltammetry^{20,21}, makes necessary the search for more environmental-friendly materials with similar performance. One important alternative is the bismuth, which was used for the first time by Wang *et al.*²² as bismuth film electrode (BiFE) on glassy-carbon or carbon-fiber substrate for the detection of microgram per liter levels of cadmium, lead, thallium and zinc by stripping voltammetry. Apart from the low toxicity of BiFEs compared to mercury, they offer other advantages such as ability to form alloys with different metals, wide potential ranges and low sensitivity to dissolved oxygen. They have already been applied for the detection of several targets. Calvo-Quintana *et al.*²³, coupled Bi-modified electrodes to a small portable

instrument for the detection of lead at legal limits ($20 \mu\text{g Kg}^{-1}$) in a complex matrix such as milk. Caldeira *et al.*²⁶ applied Bi films for the determination of traces of Tl(I) separately and together with Zn(II) and Pb(II), with a limit of detection (LOD) of 2 nmol L^{-1} , showing that the sensitivity to Tl does not depend on the presence of other ions, and finally determining Tl in juice samples.

Among the differently fabricated electrodes, SPEs are advantageous^{24,25}. They present a planar configuration and consist of different layers of electrically conductive inks machine-printed on the substrate. They can be miniaturized and mass-produced, they are cost-effective, and the surface fouling problem is eliminated as they are employed only once, and then replaced by new ones from the same batch.

Bi can be deposited onto SPEs following different procedures, in different conditions and on different substrates depending on the target analyte or the aim of analysis²⁶. The fabrication can be done using “ex situ”, “in situ” and “bulk” approaches. In the “ex situ” method, the electrodes are immersed in a solution containing Bi^{3+} and a potential is applied to reduce it to Bi^0 for its deposition²⁷. In the *in situ* method, both Bi and the target analyte are electrochemically deposited on the electrodes, forming alloys followed by anodic stripping of metals from the electrode²⁸. The third option is based on the incorporation of bismuth oxide to the ink for the fabrication of the SPE, which is then reduced to metallic bismuth for the formation of a Bi layer²⁹.

In our group, a phenol detection system by immobilization of a mushroom tissue onto plain screen printed electrode (SPE) and multiwall carbon nanotube (MWCNT) modified SPE (SPE/MWCNT) via Bi deposition was performed. This sensor achieved a LOD for phenol of 0.48 mM and 1.17 mM for SPE/Bi/Tissue and SPE/MWCNT/Bi/Tissue respectively³⁰.

5.2. Magnetic plug-based platform development

Magnetic beads offer the advantage of simple and fast handling by using magnets. One of the most important characteristics of the superparamagnetic particles is its ability to self-assemble due to a magnetic field, when they are exposed to an uniform external magnetic field; the magnetic beads acquire a magnetic moment. The resulting dipole interactions cause an instantaneous self-organization of the magnetic beads in the direction of the magnetic field. In the following section, we present a microfluidic chip for magnetic beads assembling where the maximum intensity of magnetic field is produced into the microfluidic platform in order to produce a stable magnetic plug. These magnetic beads have been functionalized with an antibody to recognize the analyte and they were blocked to avoid unspecific absorption. Once, the magnetic plug is produced, the analyte is also

NOVEL STRATEGIES TO OBTAIN ELECTROCHEMICAL LOCs WITH HIGHER SENSITIVITY

conjugated with a secondary antibody, which is bonded with a tracer, in this case with QDs as electrochemical label. This conjugation steps were performed in flow-mode, achieving a LOD of 0.36 ng mL^{-1} for human immunoglobulin G (HIgG) detection, 4.7 times better than the already described platform in Chapter 4.

The microchannel device used strong magnets to create a magnetic field perpendicular to the flow with a strong gradient pointing through the center of the chip channel. This allows for the stable formation of a magnetic beads plug that serves as a matrix for protein immunoassay. This device represents an inexpensive way of fabricating a simple reusable reactor for immunoassays.

5.2.1. Experimental details

Reagents

Streptavidin–QD655, tosylactivated magnetic beads MyOne (1 μm of diameter), Human IgG, anti-Human IgG produced in goat (α -HIgG), and biotin anti-Human IgG (biotin α -HIgG) produced in goat were obtained from Invitrogen (Spain). Phosphate buffer saline (PBS), Tween 20, milk powder and bovine serum albumin (BSA) labeled with ALEXA 555 were acquired from Sigma Aldrich (Spain). PBS supplemented with 5 % (w/v) of milk powder and 0.005 % (v/v) of Tween 20 was prepared as blocking buffer for the channel wall treatment. PBS supplemented with 5 % (w/v) of bovine serum albumin (BSA) and 0.005 % (v/v) of Tween 20 was prepared as blocking buffer for avoiding unspecific absorption onto the magnetic beads. PBS supplemented with Tween 20 at 0.05 % (v/v) was used as washing buffer (PBST). PBS was employed as immunobuffer, except for QDs conjugation. In this case, commercial buffer Borate buffer, pH: 8.3, 0.05 % sodium azide) was used. Rare earth (neodymium iron boron, 1.72 T) permanent magnets were purchased in ChenYang, Germany. 250 μL HAMILTON glass syringes were used for fluid introduction into the microchannels.

Microfluidic platform design and fabrication

Microchannels were fabricated by rapid prototyping and PDMS technologies as described previously in Chapter 3. Briefly, a 4 inch silicon wafer was spin coated with a negative photoresist SU-8 and patterned by photolithography. PDMS was poured onto the resulted mold and cured at 65°C for 2 hours (Chapter 3). Channels of two different sizes were fabricated for two different chips: one of them was 100 μm width, 50 μm depth and 3 cm long, while the second one was 200 μm width, keeping the other dimensions identical to the first one (Figure 5.1).

The electrochemical detector consists of a set of three electrodes of 500 μm width separated by 500 μm with an approximate thickness of 4 μm . They were produced by screen printing technology (explained in Chapter 3). The fabrication process involved two steps. In a first step, the graphite layer (WE, CE) was printed onto a cyclic olefin copolymer sheet (COC) and cured at 120 $^{\circ}\text{C}$ for 40 min. The RE was obtained by printing a second layer of silver/silver chloride ink which was cured in the same conditions.

Finally, the PDMS channel and the COC substrate were assembled using a previously reported protocol³¹. The COC substrate was treated by air-plasma for 1 min and then immersed into a 2% (v/v) 3-aminopropyltriethoxysilane (APTES) (Sigma Aldrich) solution in water for 1 hour. The surface of the PDMS channel was also activated for 1 min by plasma, and put into contact with the COC sheet to achieve irreversible bonding (details in Chapter 3).

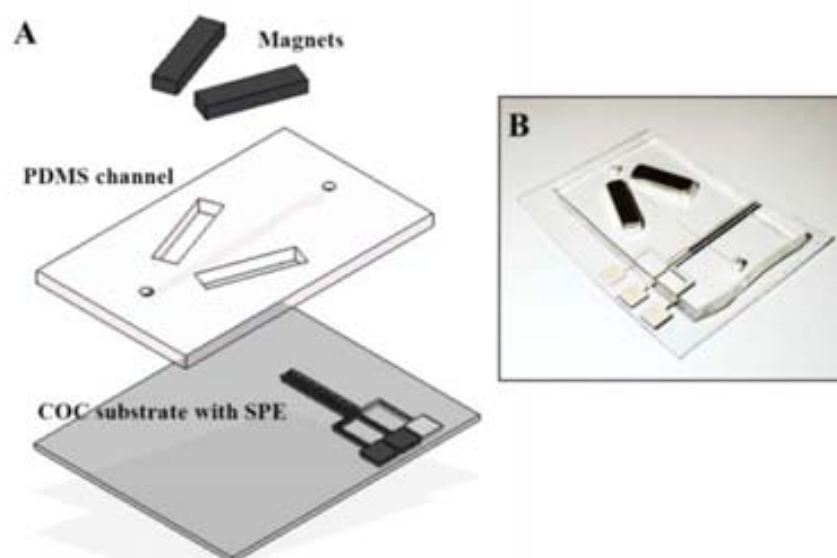


Figure 5.1. Schematic representation of electrochemical magneto-immunosensing system for HIgG detection: (A) Components of the microfluidic platform with integrated screen printed carbon electrodes (SPCEs) and permanent magnets and (B) picture of the microfluidic chip.

Magnetic plug formation

Rare earth (neodymium iron boron, 1.72 T) permanent magnets were inserted into the PDMS block with an optimal angle respect to the channel. The magnets have dimensions of 4x4x15 mm with polarization in the length of the magnet. The optimization of the plug was achieved changing different parameters: channel diameter, separation between magnets (2 and 3 mm), angle respect to the channel (20, 30 and 45 degrees), and flow rate (from 2.5 to 20 $\mu\text{L min}^{-1}$), all of them maintaining the magnetic beads concentration fixed (5 μg). In addition, this optimization was performed with the already modified magnetic beads since their organization into the microchannel differs from the unmodified beads.

NOVEL STRATEGIES TO OBTAIN ELECTROCHEMICAL LOCs WITH HIGHER SENSITIVITY

Magneto-immunoassay in flow mode

40 μg of tosylactivated magnetic particles (15 μL from stock solution) were washed 3 times with borate buffer and suspended in 135 μL of the same buffer. 15 μL of capture antibody at 0.5 mg mL^{-1} were added and the conjugation was achieved by gentle stirring of the suspension overnight at 700 rpm and 37°C. The unbound antibodies were eliminated by washing the carriers 3 times with PBST. 150 μL of PBS supplemented with Tween 20 at 0.05 % (v/v) and BSA at 5 % were added to the particles which were stirred during 2 h at 700 rpm and 25°C, washed 3 times with PBST and finally suspended in 150 μL of PBS.

The microchannel was treated with the blocking buffer (described in the Reagents part). This solution was flowed for 10 min at 5 $\mu\text{L min}^{-1}$. After the blocking step, PBST was introduced again during 10 min at the same flow rate in order to clean the excess of the blocking solution.

The working electrode was then activated by cyclic voltammetry (10 cycles at a potential range from -0.8V to 0.8V and a scan rate of 100 mV sec^{-1} in PBS buffer). Magnetic beads already modified with antibodies were then immobilized into the channel with the optimized volume and flow-rate (20 μL at 5 $\mu\text{L min}^{-1}$).

Once the magnetic plug was produced, the target solution (HIgG) in PBS was flushed at 0.55 $\mu\text{L min}^{-1}$ through the magnetic beads during 20 min at different concentrations [0, 12.5, 25, 50, and 100 ng mL^{-1}]. Then, the channel was washed again with PBST during 10 min at flow rate of 5 $\mu\text{L min}^{-1}$.

15 μL of Anti-Human IgG (gamma-chain specific)-biotin in 135 μL of PBS was introduced into the channel at 0.55 $\mu\text{L min}^{-1}$ for 20 min. Then, 2 μL of QD 655 ITK Streptavidin (2 μM from stock solution) were suspended in 148 μL of QD incubation buffer (50 mM borate pH8.3, 0.05 % sodium azide) and introduced at the same flow rate for 20 min, to complete the immunocomplex. Between each step, PBST for 10 min at 5 $\mu\text{L min}^{-1}$ was introduced for excess removing.

Finally after the last washing step, the QDs were partially dissolved with acetate solution at pH 2.5 and detected electrochemically as described in the following paragraph. This solution was introduced at a low flow rate of 0.05 $\mu\text{L min}^{-1}$, for 600 s in order to partially dissolve all the QDs and obtain the best electrochemical response.

QDs electrochemical detection

For the electrochemical measurements a computer-controlled Autolab PGSTAT-12 (302N-High performance) (potentiostat / galvanostat) with general-purposes software operating system (GPES version 4.9.007, from Eco Chemie B.V., Utrecht, The Netherlands) was used.

The CdSe@ZnS QDs concentrations (directly related to the analyte concentration) were determined by SWASV. In order to get a maximum sensitivity, the electrochemical parameters (deposition time, conditioning potential, conditioning time and frequency) were optimized in Chapter 4.

The LOD of the respective calibration curve was calculated as the mean intensity (MI) of four chips (incubated with a blank-control measurement (PBST)) plus three times the standard deviation of the blank measurement.

5.2.2. Results and discussion

Magnetic plug optimization

In this part we discuss the assembling of magnetic beads due to the magnetic field lines. One alternative, previously reported¹⁰ is to simply insert the two magnets in a repulsive conformation, creating a magnetic field in parallel direction respect to the flow; and the other option consists of the use of a magnetic field perpendicular to the flow (attractive conformation). We demonstrate the stable formation of the magnetic plug by using the last magnet positioning alternative.

Formation of the perpendicular-like plug

When the transversal magnetic field is created by the two permanent magnets, the magnetic beads are organized like cluster in chain-like columns through the channel. In contrast, when this magnetic field is longitudinal, the cluster parallel to the channel is formed (Figure 5.2). Different magnet positions were tested by changing the shape of the channels and the orientation and separation of the magnets and confirmed by using simulation software (COMSOL Multiphysics 3.4). The plug optimization were performed for two diameter channels (100 and 200 μm), obtaining the optimal conditions, when the conformation is in an attractive way, with the polarization making an angle of 20° respect to the microchannel, and the separation between the magnets is 2 mm.

NOVEL STRATEGIES TO OBTAIN ELECTROCHEMICAL LOCs WITH HIGHER SENSITIVITY

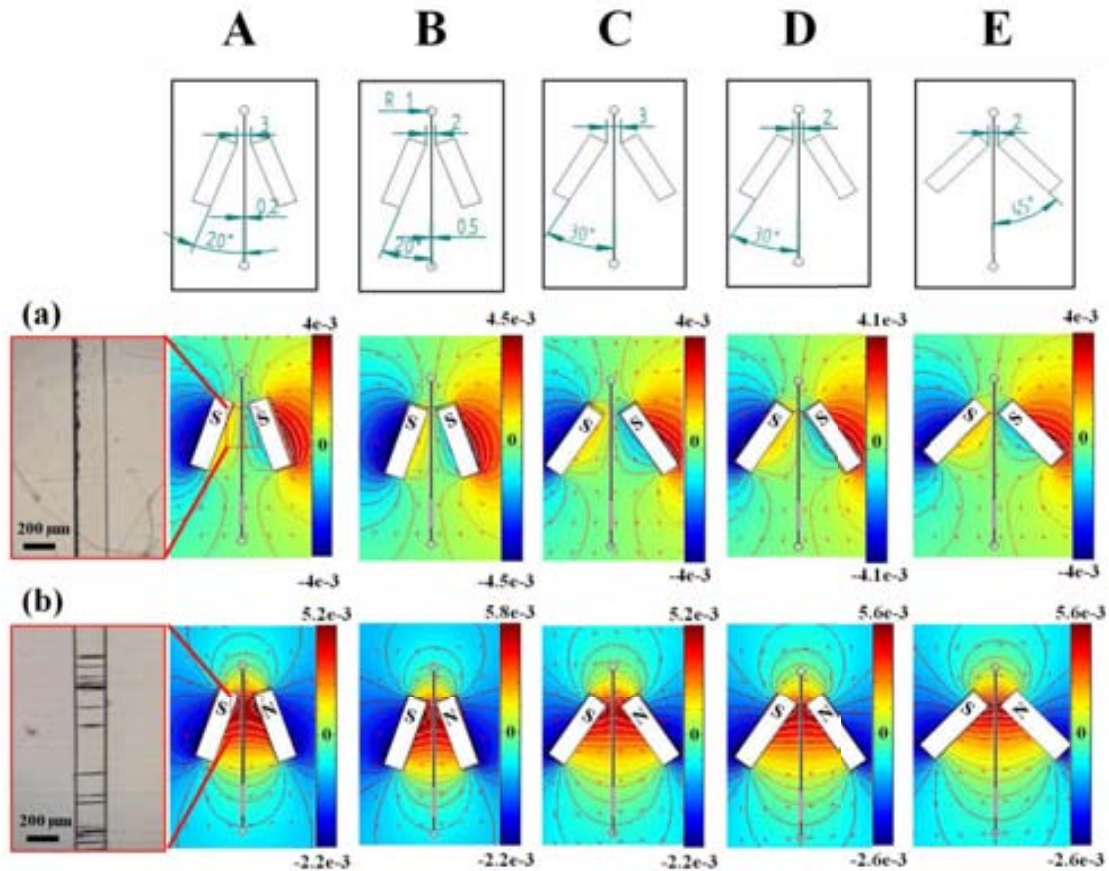


Figure 5.2. Different magnet positioning (A) 20° with separation of 3 mm, (B) 20° with separation of 2 mm, (C) 30° with separation of 3 mm, (D) 30° with separation of 2 mm and (E) 45° with separation of 2 mm. (a) Represents south-south and (b) south-north conformation with their respective optical microscopy images, which show the magnetic beads organization into the microchannel due to the magnetic field lines.

In Figure 5.2 we can clearly see that the magnetic field lines (represented by the arrows) follow the flow direction. The color scale represents the point of highest magnetic field with the red color as well as the lower magnetic field with blue color. Indeed, the force that a paramagnetic bead experiences under a non-homogeneous field is proportional to the gradient of the magnetic energy: $F = V\Delta x \nabla E_m$, where V and Δx are the volume and the magnetic susceptibility of the particle relative to that of the suspending medium, respectively. As a result, the columns accumulate around the red zone (high magnetic field). This zone also defines the length of the plug yet that a sufficient amount of beads is injected. According with the same Figure 5.2 B,b, which the magnets are in a attractive conformation shows the higher magnetic potential at $5.8 \text{ e-}3 \text{ W b m}^{-1}$ that ensured more stability for the magnetic beads into the channel. Also the active distance (higher magnetic potential) is longer than the other configuration, allowing the immobilization of a higher amount of MBs ($\sim 5\mu\text{g}$). It means that if there are more MBs, more analyte can be captured and labeled.

Flow-rate optimization

Once the optimal configuration was obtained, flow-rate test was performed by using two different channel diameters (100 and 200 μm) with a depth of 50 μm . These measurements were realized with a syringe pump, changing the injection volume and the flow-rate. In Figure 5.3A the setup used for the microscopy quantification is shown. The microfluidic chip is located in an inverted optical microscopy. The inlet of the chip is connected to the HARVARD Apparatus syringe pump, which allows the control of the flow rate and the injected volume according with the kind of syringe.

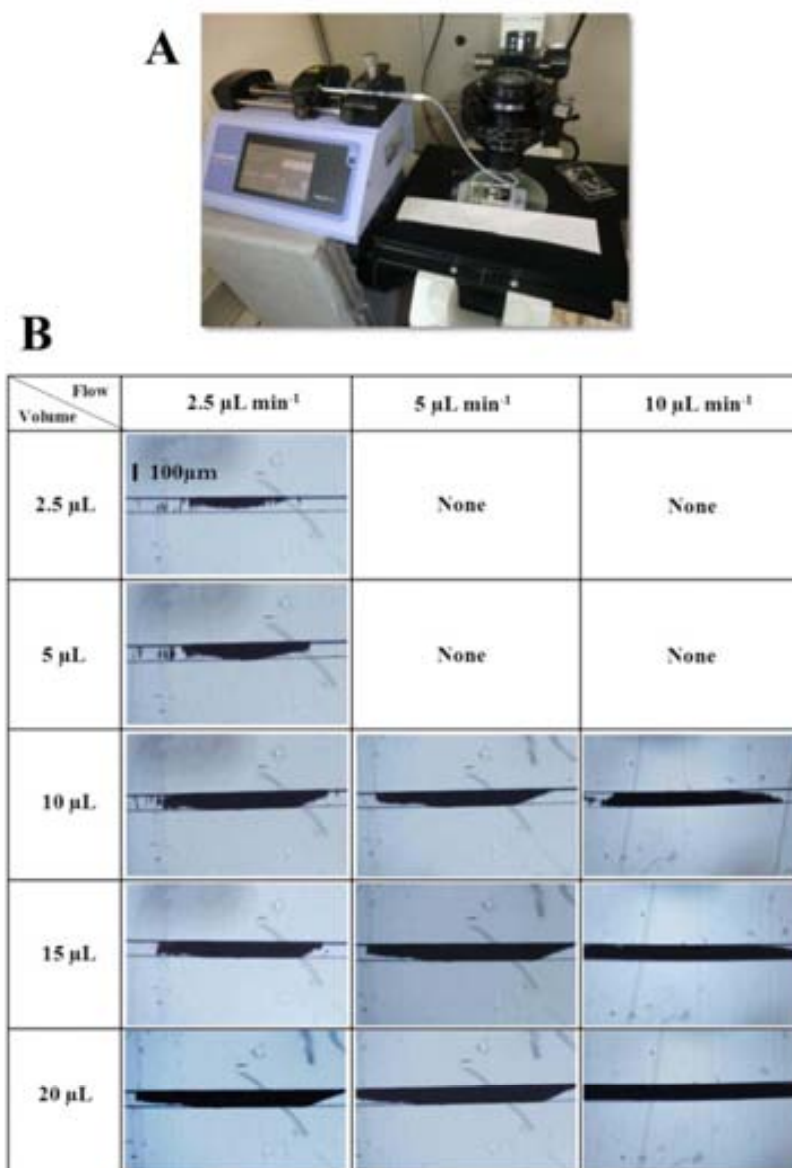


Figure 5.3. Flow-rate optimization. (A) Picture of the set-up located in an inverted microscope with the syringe pump to control the flow-rate, and (B) Tests done by changing the magnetic beads volume at a fixed amount of 5 μg and flow rate into a channel of 100 μm of diameter and attractive conformation between the two magnets.

NOVEL STRATEGIES TO OBTAIN ELECTROCHEMICAL LOCs WITH HIGHER SENSITIVITY

In Figure 5.3B the different combinations between flow rate and injected volume performed in order to obtain the optimal conditions for the plug formation are shown. For the range between 2.5 and 5 μL of injected volume and 5 and 10 $\mu\text{L min}^{-1}$ flow-rates, the plug was not correctly formed, probably because these two flows are high enough for allowing the magnetic beads immobilization into the channel of 100 μm of diameter, although for the higher volumes, the plug was produced, perhaps due to the magnetic beads amount. However these are not the ideal conditions, because most of the introduced magnetic beads are removed due to the flow; thereby, the optimal experimental parameters for this channel features were: 10 μL of MB volume at 2.5 $\mu\text{L min}^{-1}$. These parameters were also chosen considering the time of plug formation as well as the reasonable amount of magnetic beads to avoid channel clogging.

The previous optimization was also done for microchannels with 200 μm of diameter. In this case, due to the diameter, the flow rate is less critical than the previous one, thereby we can produce the plug with a wide range of possibilities. In this work the optimal volume was 20 μL at flow-rate of 5 $\mu\text{L min}^{-1}$. See Figure 5.4.

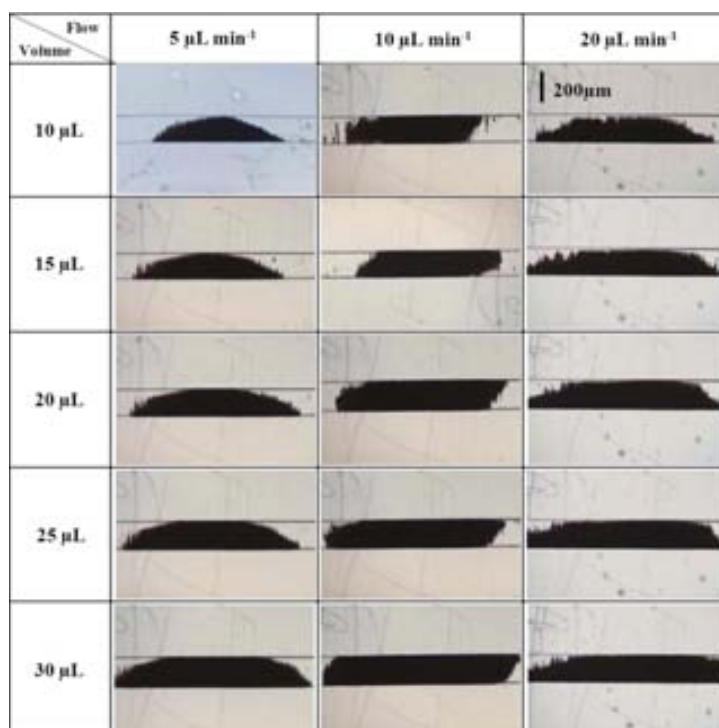


Figure 5.4. Flow-rate optimization changing the magnetic beads volume at a fixed concentration of 5 μg and flow rate into a channel of 200 μm of diameter and attractive conformation between the two magnets.

Finally a simple test to know the stability of the plug was performed. Once the magnetic plug was established, the flow rate was increased from 10 to 150 $\mu\text{L min}^{-1}$ increasing 10 $\mu\text{L min}^{-1}$ each time. In Figure 5.5, it is possible to observe that at 100 $\mu\text{L min}^{-1}$ in a channel of 200 μm diameter, the plug begins to collapse, however it also demonstrates that the

attractive conformation between magnets ensure a strong magnetic plug. This is important for different reasons: i) for the stability while the incubation steps are performed, as well as the washing steps, and ii) because the exchange between syringes in each conjugation step produce a backflow that in the repulsive conformation of the magnets, is enough to remove all the magnetic beads.



Figure 5.5. Magnetic plug stability when the flow rate is increased up to $200 \mu\text{L min}^{-1}$.

Immunoassay performance

Once the magnetic plug was optimized, we chose the $200 \mu\text{m}$ wide channel because for the $100 \mu\text{m}$ wide one, the magnetic plug was not stable under pressure and the flow-rates must be high to produce the plug in a short time. In addition, a 20° inclination of the magnets respect to the channel, separation of 2 mm and flow rate of $5 \mu\text{L min}^{-1}$ were found as the optimal parameters. To confirm that, the evaluation of the microfluidic platform using QDs labels was performed for a model protein detection (HIgG produced in goat).

This study was performed with the same protocol previously described in the experimental section. All incubation steps were performed by changing the flow rate from 0.05 to $5 \mu\text{L min}^{-1}$. The most efficient conjugation step was produced between 0.5 and $1 \mu\text{L min}^{-1}$, otherwise, the higher flow could reduce the probability of binding. Flow rate for conjugation was finally set at $0.5 \mu\text{L min}^{-1}$. Different times of incubation such as 5 , 10 and 15 min were also tested. A proper electrochemical signal was observed properly for 15 min . Finally, the time of 10 min was chosen for incubation steps. Washing steps were done for different times at $5 \mu\text{L min}^{-1}$. 10 min were enough to clean the channel from antibodies excess. The final device is shown in Figure 5.6A, as well as the location of the SPCE at the end of the channel. The electrode is located in a wider zone of $500 \mu\text{m}$ wide, due to the electrode width (also $500 \mu\text{m}$) to assure the correct flow and avoid liquid leakages.

NOVEL STRATEGIES TO OBTAIN ELECTROCHEMICAL LOCs WITH HIGHER SENSITIVITY

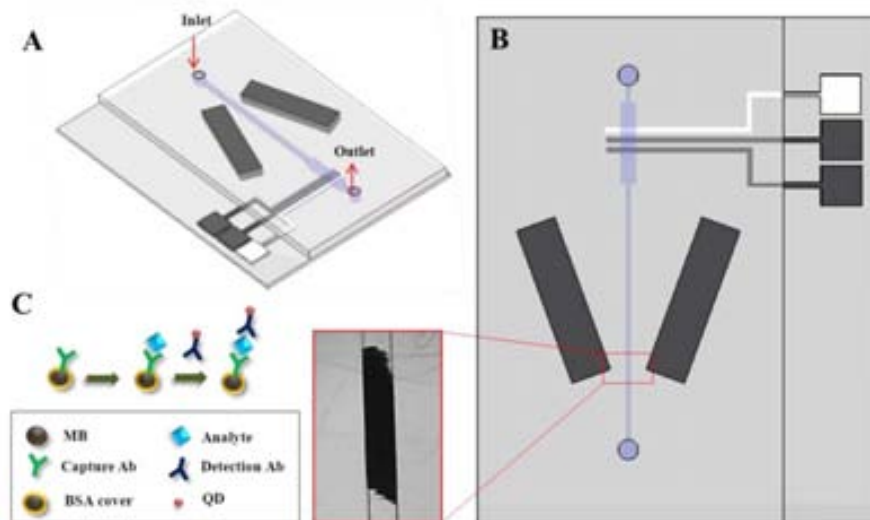


Figure 5.6. Complete magnetic plug device (A) schematic draw of the system, (B) the location of SPCE in the microfluidic channel and (C) steps of magnetic beads immobilization and conjugation with the analyte and secondary antibody labeled with QDs.

Electrochemical detection of QDs

Once the previous parameters were optimized, they were applied to the detection of a model protein (Human Immunoglobulin IgG). Each HIgG concentration was checked 3 times using different chips to obtain the error bars. On the other hand, the influence of the pH variation of the dissolving solution was also studied. The selected pH for the dissolving solution was 2.5, which was used for the electrochemical parameters optimization (Chapter 3). Signal to noise ratio and sensitivity were chosen as criteria. The optimal conditions were: deposition voltage: -1.1 V, deposition time: 600 s, equilibrium time: 30 s; frequency: 25 Hz, and scan rate: 10 mV s^{-1} .

The calibration curve and repeatability studies for different HIgG concentrations in measurement buffer were obtained using a microfluidic platform achieving a LOD of 0.36 ng mL^{-1} in a linear detection range between 1 and 100 ng mL^{-1} (see Figure 5.7). The results showed a well-defined stripping peak at 0.83 V in concordance with the Cd^0 oxidation potential.

Three replicates for each concentration were carried out. The obtained range of response demonstrates that this device shows promising potential for its integration in biosensing systems and immunosensors using QDs as labels. The reproducibility of the device was also studied using four different microfluidic chips. The reproducibility is represented in the error bars and the sensitivity by the slope in the calibration curve. The quantified data are shown in Table 5.1.

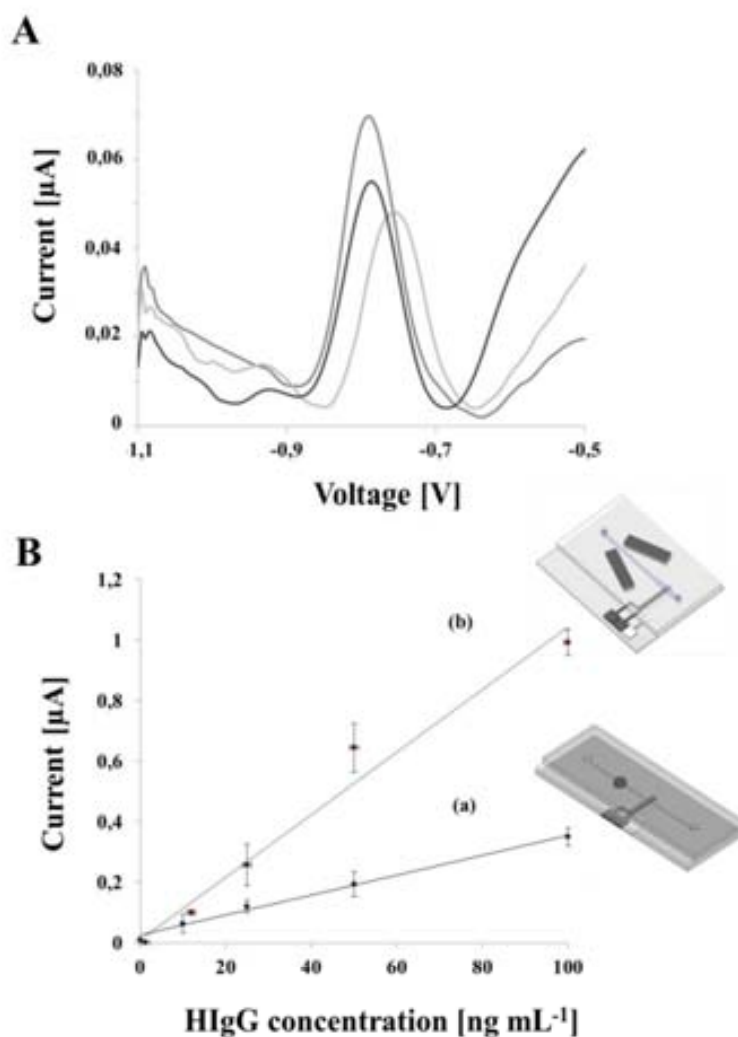


Figure 5.7. (A) Typical response of QDs detection by using square wave voltammetry, and (B) Comparison between two different magnetic separation platforms for immunoassay performance.

Table 5.1. Comparison between two different magnetic separation platforms as was showed in Figure 5.7.

	LOD [ng mL^{-1}]	Sensibility [$\mu\text{A}(\text{ng mL}^{-1})^{-1}$]	R^2
(a)	1.72	0.0033	0.99
(b)	0.36	0.0105	0.97

5.3. Design and fabrication of a recycling flow micro-system

5.3.1. Experimental details.

Reagents

AZ9260 positive photoresist and its developer were purchased in Microchemicals, Germany. Polyethylene naphthalate (PEN) and polyethylene terephthalate (PET) were purchased in Corning, USA.

3 nm CdS-QDs were synthesized by arrested precipitation using water-dispersed cadmium chloride and hexamethyldisilathiane (HMST) as sulfide precursor³². The procedure for CdS QDs detection has been previously described in Chapter 4.

Simple microfluidic channel and screen printed electrodes fabrication

Microchips were fabricated by rapid prototyping and PDMS technologies as described previously (Section 5.2). The electrochemical detector consists of a set of three electrodes of 500 μm width separated by 500 μm with an approximate thickness of 4 μm . Finally, the PDMS channel and the PC substrate were assembled using a previously reported protocol.

Electrochemical analysis by using an external peristaltic pump

For the electrochemical measurements a computer-controlled Autolab PGSTAT-12 (302 N-High performance) (potentiostat / galvanostat) with general-purposes software operating system (GPES version 4.9.007, from Eco Chemie B.V., Utrecht, The Netherlands) was used. The microfluidic channel with the integrated SPCE was connected to the Autolab PGSTAT-12 with a specially adapted electrical edge connector. The flow-through system consists of a peristaltic pump (PERIMAX 12, USA) used for pumping the measuring solutions to the microfluidic device. Once the microchannels were filled with the solution, as well as the tube, it was located in the peristaltic pump, whose inlet and outlet were respectively connected to the both tube ends.

Micro-peristaltic pump fabrication

The fabrication process consists in three layers. The first layer is related to the control channel (valves). This layer was fabricated by spin coating of a silicon wafer with a negative photoresist (SU-8 from Microchem) and patterned by photolithography. The designs of the photomask were done by using computer assisted design (CAD) software, with different features (valves with different dimensions, number of valves and separation between them) and printed in a flexible substrate (PET or PEN). After the master fabrication, PDMS was poured onto it in a proportion 10:1 with its catalyzer, and cured at 65°C for 2 hours. Figure 5.8a.

The second layer is the microchannel fabrication. As it was explained in the Introduction of this chapter, the microchannel layer maybe is the most important one. The channel should be thin (flexible layer) and it should have a rounded shape to avoid dead volumes and ensure proper closure of the valve. The master of the channel was fabricated by two different approaches: the first one was by micromechanization of an aluminum block, and the other one by photolithography method. In the last one, a positive photoresist (AZ9260) was deposited by spin coating with a thickness of around $45\ \mu\text{m}$ (1000 rpm for 30 s). After the deposition, the photoresist was cured at 110°C onto a hotplate, for 3 min. Once the photoresist solvents were evaporated, the photoresist was exposed with a UV aligner for 50 s, and it was finally developed with its respective developer (water developer proportion was 4:3) and cleaned with deionized water. Until this step, the channel profile is square-shaped; however when the already developed master is exposed with a temperature (150°C) superior than the transition temperature (for AZ9260 photoresist is between 120 and 130°C) during 5 s the channel begins to deform taking a parabolic shape. This change is observed by using a Dektak-150 mechanical profilometer (VEECO, USA). (see Figure 5.8b). PDMS was poured onto the master with the same elastomer: catalyzer proportion (10:1) mentioned before by using spin coater (400 rpm, 50 s) and cured onto the hotplate at 100°C for 30 min.

The third layer is the substrate, where the SPCE is printed. In this work the used materials were glass and polycarbonate (PC). In addition the SPCE was printed onto these substrates, especially onto PC due to the better ink adhesion. Figure 5.8c.

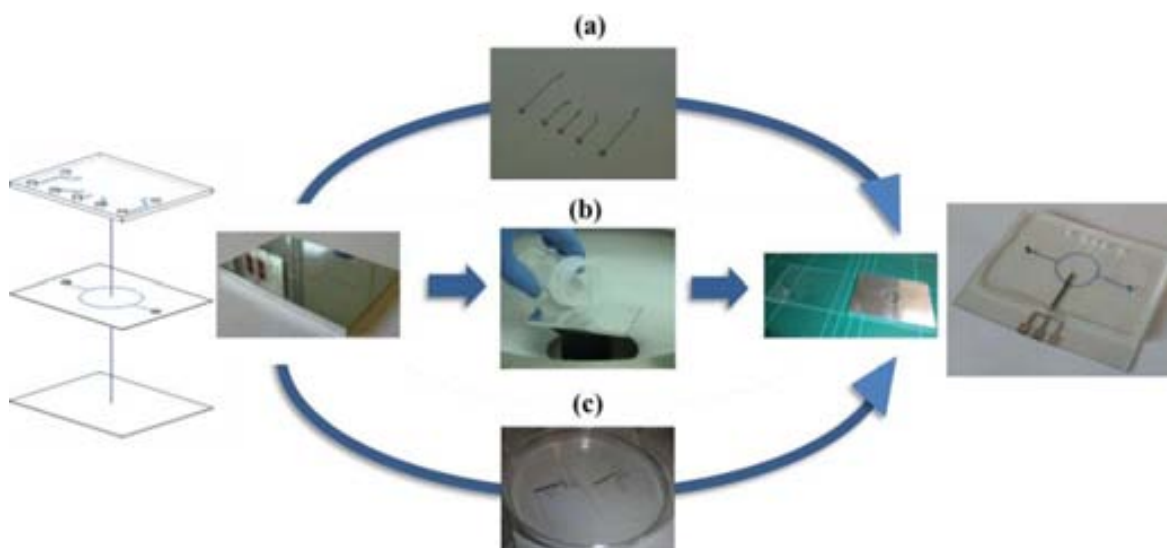


Figure 5.8. Micro-recycling system: (a) Valves, (b) microchannel, and (c) substrate layers. Layers fabrication process and the finished device in the right side of the Figure.

Finally, the assembly of the three layers was performed in two steps: (i) Valves layer with microchannel layer was bonded by using air plasma (described in the previous section), and

NOVEL STRATEGIES TO OBTAIN ELECTROCHEMICAL LOCs WITH HIGHER SENSITIVITY

(ii) the substrate was activated with air plasma and immersed into APTES solution at 2% v/v in MilliQ water, for 30 min. Then, it was washed with Milli-Q water. In parallel, the PDMS channel layer, already bonded with the valves layer, is activated with plasma (channel side exposed). In the end, both faces are put in contact to achieve an irreversible bonding.

Valves characterization

An inverted microscope Olympus IX71 was used in order to observe the operation of the valves, changing the air pressure into the valve channels. A solution of trypan blue (Sigma Aldrich, Spain) was introduced into the channel (blue color) to properly see when the valves state change from close to open mode and vice versa.

CdS and CdSe@ZnS QDs electrochemical detection

The CdS QDs concentrations were determined by SWASV. The optimal electrochemical parameters have been mentioned in Chapter 4.

5.3.2. Results and discussions

External peristaltic pump

A flow-through recycling system based in a close-loop system by using a peristaltic micropump (Figure 5.9A) is designed and studied with the aim of improving the electrochemical signal, decreasing the LOD and reducing the sample volume used in each measurement. The flow recycling mode was applied after filling the electrochemical flow cell with 25 μL of a sample of CdS QDs (500 ng mL^{-1}) in acetate buffer.

Maintaining the same electrochemical parameters for CdS QDs (Chapter 4) (e.g. deposition time, 120 s; deposition potential, -1.3 V; flow rate, $50 \mu\text{L min}^{-1}$), an increase of around 6 times of the cadmium stripping peak was achieved with the flow recycling mode (2 turns) in comparison to the normal in-chip flow-through mode without the need of increasing the deposition time. Such recycling mode reported earlier for trace metals detection using SWASV technique was found to be an efficient way for ions detection³³. Figure 5.9B shows the voltammetry responses corresponding to three consecutive measurements of a CdS QDs suspension (500 ng mL^{-1} in acetate buffer) using the flow-recycling system (one single turn for each measurement). An increase of the stripping peak was observed measurement after measurement which might be due to the QDs accumulation onto the surface of the WE after each measurement and the impossibility of cleaning during the duration of the applied conditioning time. For that reason the conditioning time was increased from 60 s to 150 s ($V_{\text{cond}} = -0.15 \text{ V}$) in order to achieve a better cleaning of the electrode surface prior to the deposition step. Figure 5.9C shows the voltammetry stripping responses of three consecutive measurements using the new conditioning parameters.

A good reproducibility was obtained between the three consecutive measurements (RSD 9.8%) showing that a higher conditioning time at -0.15 V allows a complete re-oxidation of the Cd^0 accumulated onto the WE surface and consequently giving reproducible peak after each measurement.

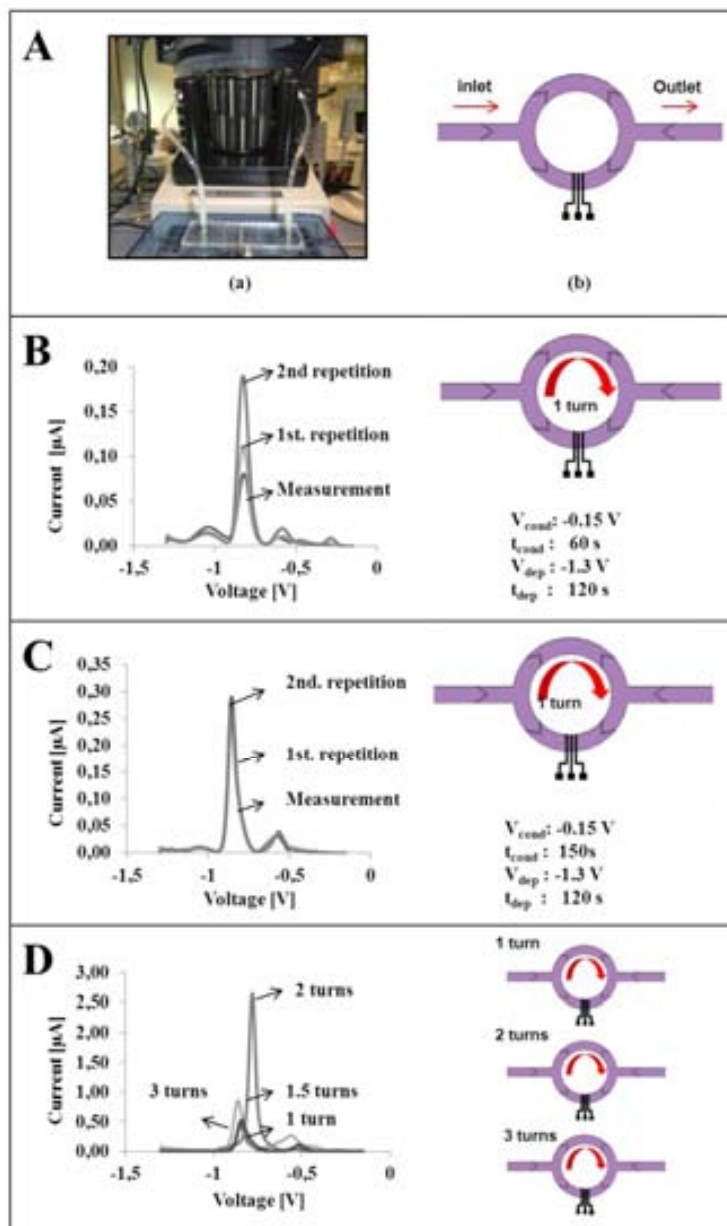


Figure 5.9 (A) Recycling platform set-up picture (a) and schematic (b). (B) Voltammetry responses of three consecutive measurements of CdS QDs (500 ng mL^{-1}) using in flow-recycling mode with a conditioning time of 60 s. (C) Voltammetry responses of three consecutive measurements of CdS QDs (500 ng mL^{-1}) using in flow-recycling mode with a conditioning time of 150 s. (D) Voltammetry responses of CdS QDs (500 ng mL^{-1}) using different flow rates corresponding to 1 single turn ($50 \text{ } \mu\text{L min}^{-1}$), 1.5 turns ($75 \text{ } \mu\text{L min}^{-1}$), 2 turns ($100 \text{ } \mu\text{L min}^{-1}$) and 3 turns ($125 \text{ } \mu\text{L min}^{-1}$).

NOVEL STRATEGIES TO OBTAIN ELECTROCHEMICAL LOCs WITH HIGHER SENSITIVITY

After achieving good reproducibility between measurements, the flow rate of the recirculation process was studied in order to evaluate the effect of the number of turns during which the sample passes through the WE toward the response of the chip. The initial flow rate used for the reproducibility study ($50 \mu\text{L min}^{-1}$) represents one single turn of the sample through the electrode. Other flow rates to obtain 1.5, 2 and 3 turns of the sample through the system were tested (75 , 100 , and $125 \mu\text{L min}^{-1}$, respectively) (see Figure 5.9D).

The results show a correlation between the intensity of the peak current and the flow rate when working between $50 \mu\text{L min}^{-1}$ and $100 \mu\text{L min}^{-1}$. However, the use of higher flow rates ($125 \mu\text{L min}^{-1}$) provokes a decrease on the electrochemical response which might be caused by the short time that QDs have to be in contact with the WE owing the high rate of the flow that do not allow their efficient reduction and further detection.

Once demonstrated the increasing of QDs signal by recycling the sample, the fabrication of a peristaltic pump into microfluidic channel is proposed. It allows the fluid recirculation through the channel, reducing in this way the dead volumes (tubes) and the time of measurement, set-up miniaturization, etc.

Micro-peristaltic pump

Design and fabrication

In Figure 5.10A the circular channel with its dimensions of 3.5 cm diameter (the circular trajectory), $500 \mu\text{m}$ width and $45 \mu\text{m}$ thickness. In Figure 5.10B-F, valves with different dimensions and separations are also presented. This separation distance is related with the displaced volume into the microchannel, as well as the flow continuity. This is assured when there are more than three valves, avoiding backflows when the valves state change.

Another important factor is the dimension of the valve (equivalent to the air volume needed for the valve filling), because it is also related with the switching speed. When the channel thickness is increased, the air volume to fill it is also increased, thus filling time to close the channel is greater. In this work, the volume was tailored with the valve dimensions between 0.5 and 2 mm wide and a fixed thickness of the $50 \mu\text{m}$ and separations also between 0.5 and 2 mm between them.

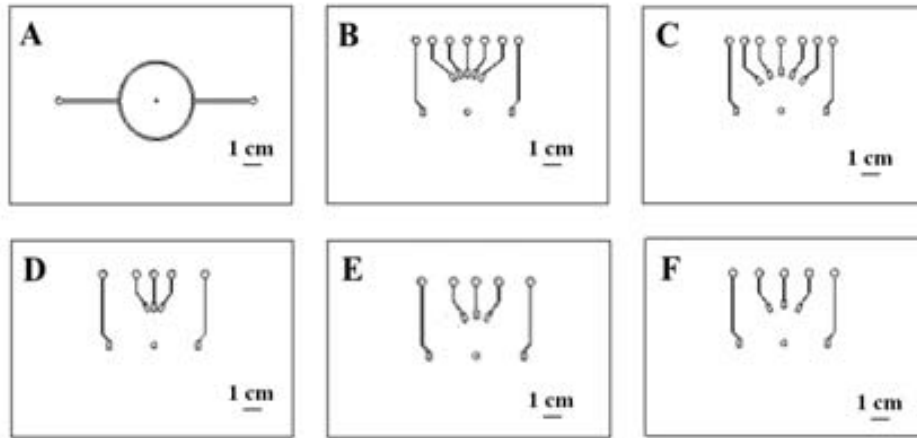


Figure 5.10. Micro-recycling system: (A) Circular channel with 500 μm width and 45 μm of thickness, valves layer (B-C) five valves (1X2 mm) with 0.5 and 1 mm of separation between them, (D-F) three valves with 0.5, 1 and 2 mm of separation between them.

Regarding the channel layer, two fabrication processes were performed: micromechanization of a aluminum block (fabricated at Curie Institute, Paris, France) and photolithography. AZ9260 positive photoresist was chosen for this second process due to its viscosity, given the possibility to achieve a thickness around 45 μm by deposition of three consecutive layers. After the master fabrication, it was treated with heat at 150 $^{\circ}\text{C}$ in order to modify the profile shape (Figure 5.11a,b). In Figure 5.11b it is possible to observe a deformation of the photoresist due to the increasing of the photoresist transition temperature; although a trend to coffee ring formation is observable maybe due to the relation between channel diameter and thickness.

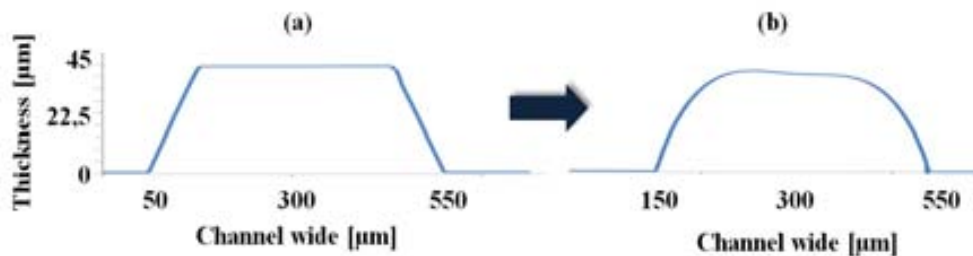


Figure 5.11. Channel profile by using positive photoresist AZ9260, (a) before the deformation, and (b) after deformation produced for the transition temperature increasing.

Flow rate control and sequences

Once defined the optimal size of micro-valves (2 mm width) as well as their separation distance (1 mm), homemade software was developed in order to control the valves in

NOVEL STRATEGIES TO OBTAIN ELECTROCHEMICAL LOCs WITH HIGHER SENSITIVITY

sequential mode (three or five valves). Two different programming languages and environments were used for the control system; the first one was LABVIEW 2012, which is characterized for its graphical programming and user friendly interface. It requires the use of a computer. The other programming platform is Arduino, an open-source electronic prototyping platform based on flexible, easy-to-use hardware and software simpler than the previous one. In addition, Arduino's board provides autonomy to the system and possibility to be miniaturized by using an external battery and simpler electronics.

Different sequences were tested according to the system operation mode (recycling or mixing). In Figure 5.12, the graphical interface for three kinds of programs is shown. In Figure 5.12A, general software is proposed for the first valve testing, it is possible to choose eight different valves in on-off or in pulsatile control. It means that it is possible to activate the desired number of valves for each application, and to define the commutation time; in this way the selected valves are sequentially activated. In addition, in Figure 5.12B the interface for the recycling flow microsystem is shown. It offers manual and automatic control. In the manual control, each valve should be manually activated and the commutation time should be defined. With automatic control, the user needs just to define the starting time for each step and the number of cycles needed for the measurement. Finally the program executes all the steps in automatic mode. The respective codes are presented in Annex 3.

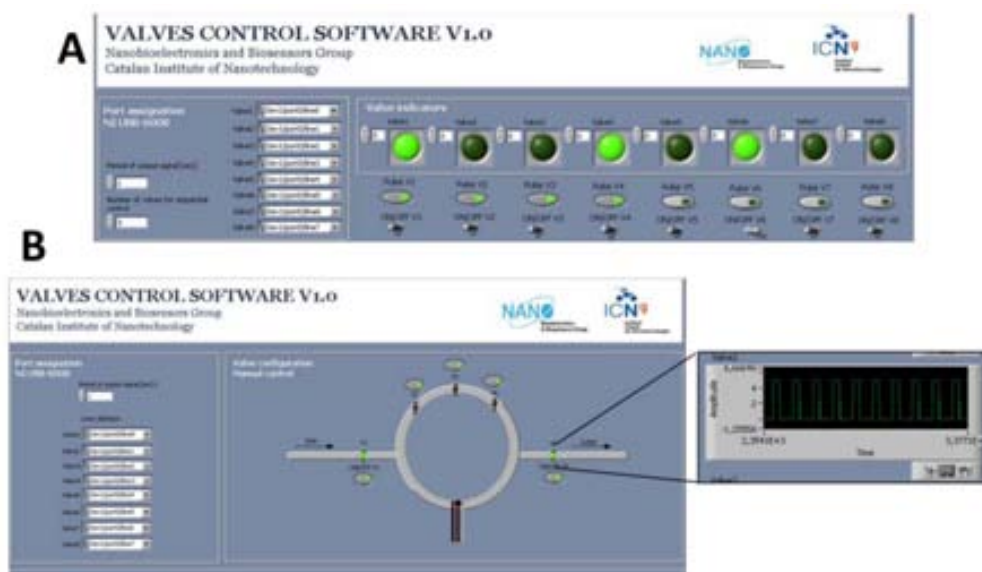


Figure 5.12. Graphical interface of the valve control software. (A) General purpose software for valve testing, and (B) Graphical interface for the recycling flow microsystem.

The order through which the valves are activated is an important parameter because an appropriate sequence defines the flow behavior into the channel. For example, for

recycling, is essential to avoid backflows into the channel (See Figure 5.13A). In this case the continuous flow around the channel in the clockwise direction was demonstrated; otherwise for mixing purposes the flow would have turbulence behavior produced by the sequence shown in Figure 5.13B like alternative movement changing the direction in each control step. With this behavior we take the advantages of “semi-turbulent flow” for mixing performing, breaking the laminar flow when the flow direction is suddenly changed.

Another interesting possibility is the use of more than three valves, providing with a higher control of the flow. In our case, the channel is circular, and when the solution is in the opposite side respect to the valves position, the flow resistance is higher and sometimes the flow is turned back phenomena that can be avoided with the use of more valves (i.e. 5 valves).

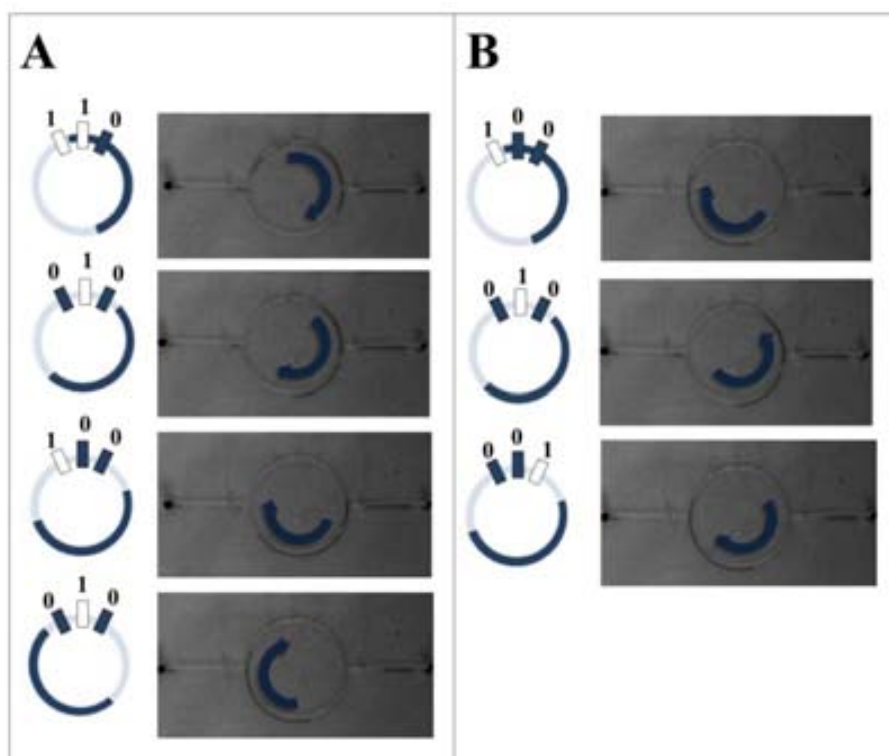


Figure 5.13. Two different sequences for the micro-pump. (A) For recycling process – continuous flow around the entire channel with laminar regime, and (B) For mixing process – alternative flow producing turbulence when the flow is changed suddenly.

Hardware

The scheme of the electronic system is shown in Figure 5.14. It is composed of an energy source which consists in a voltage transformer (the alternating signal is transformed from 110 V to 24 V). This alternating current is rectified and filtered to obtain a direct current.

NOVEL STRATEGIES TO OBTAIN ELECTROCHEMICAL LOCs WITH HIGHER SENSITIVITY

Once a DC signal is obtained, it is regulated by using LM7405 component, getting 5 volts output. This voltage is suitable for logical components and also for the LABVIEW control hardware. The used Labview platform was NI 6008, with 24 digital I/O and 12 analogic I/O. Since the actuation of the valves requires on-off operation and sequential activation, 8 digital outlets were used for the electro-valves actuation. These electro-valves LHD A0523112H 5 V DC 30 PSI (from The Lee Company, USA) need 5 V to be energized. Finally, an additional circuit was needed to isolate the control board from the power zone to avoid eddy currents that could destroy the control board. The current was also increased by using TIP 110 power transistors in cutoff and saturation region for the proper electro-valve operation. The electro-valve is an electromechanically operated valve and it is controlled by an electric current through a solenoid: in the case of a two-port valve the air flow is switched on or off; in the case of a three-port valve, the air outflow is switched between the two outlet ports.

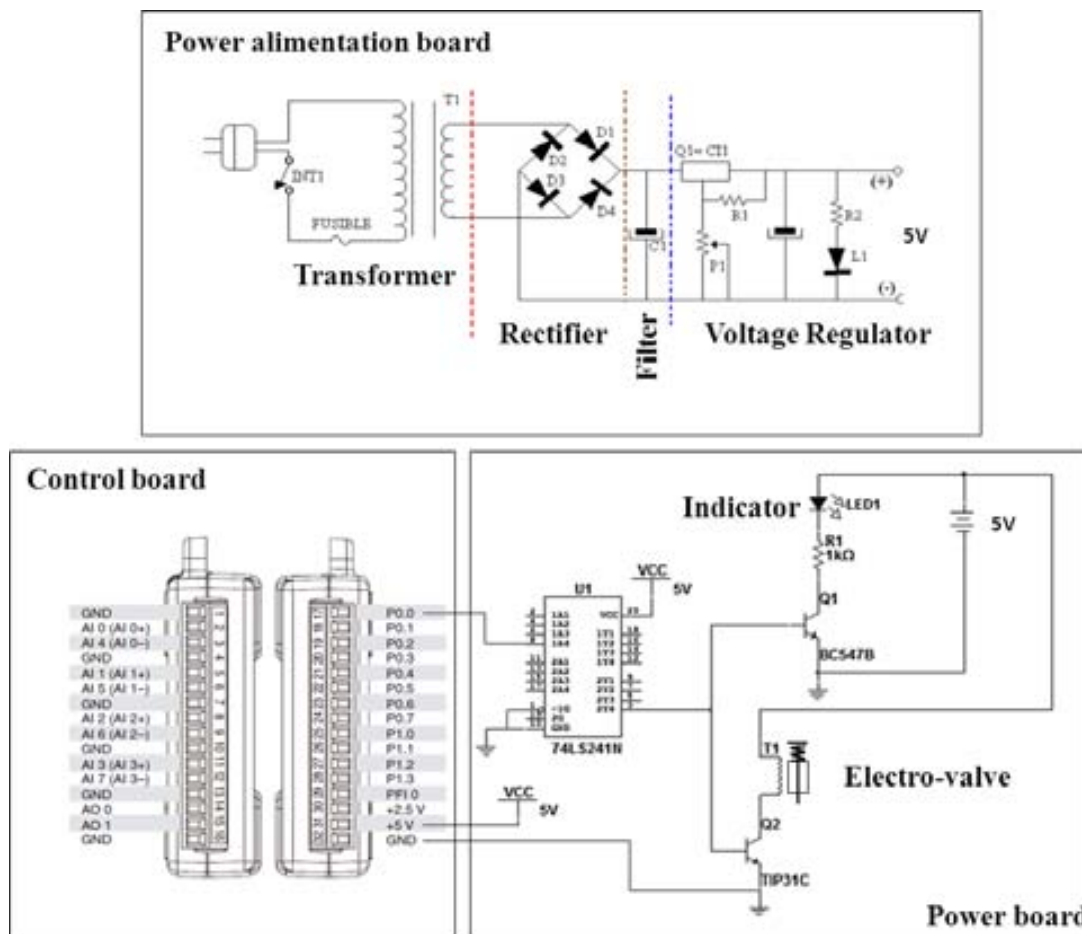


Figure 5.14. Hardware circuit design. The system is composed by three parts: the power supply, the control and power (conditioning) boards. The power supply and power conditioning board were supplied by Curie Institute under the NADINE European Project collaboration.

Valve pressure optimization

After having assembled the chip, the control system was connected (Figure 5.15). The air outlet from the Laboratory air lines was used as a control flow, which was managed by the mentioned electro-valves. Air outlet has an installed barometer, which can display the line pressure. In this way, the air pressure was increased from 0.5 to 2.5 bars, observing the deformation of the thin layer of the channel due to the air introduced into the control layer, thus, depending of the flexibility of the channel layer the pressure range can change. In our case, the optimal pressure was defined in 2 bars. After 2 bars the chip began to be pulled off. It is important to note that when the pressure limit is achieved for the fabrication limitations, it is possible to reduce the channel thickness or change the proportion between PDMS and catalyzer in order to increase its elasticity.

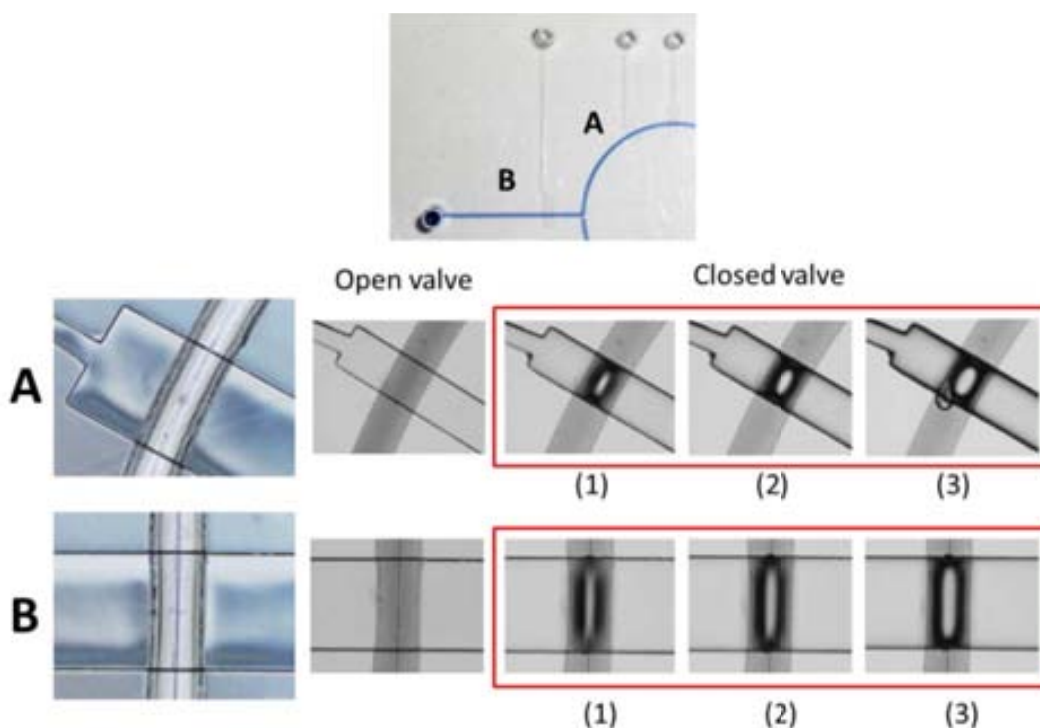


Figure 5.15. Air pressure calibration for valve closing: (A) Curved valve, and (B) Normal valve. 1-2-3 corresponded to the variation of air pressure in 0.5, 1 and 2 bars respectively.

Immunoassay detection perspectives

In Figure 5.16 a schematic system where the microperistaltic pump could be integrated is shown. Since the electrochemical signal of QDs was increased by recycling the same volume of sample, future work is being continued by using two alternatives. The first one is the integration of a micromixer to perform the immunoassay for a model protein detection and then to perform the detection in the recycling chip by introducing the sample into the

NOVEL STRATEGIES TO OBTAIN ELECTROCHEMICAL LOCs WITH HIGHER SENSITIVITY

channel and close the inlet and outlet valves in order to move the same volume sample inside the entire circular channel. The second possibility is to use the circular channel as a mixer; incubator and detector chip by tailoring the valve sequence actuation.

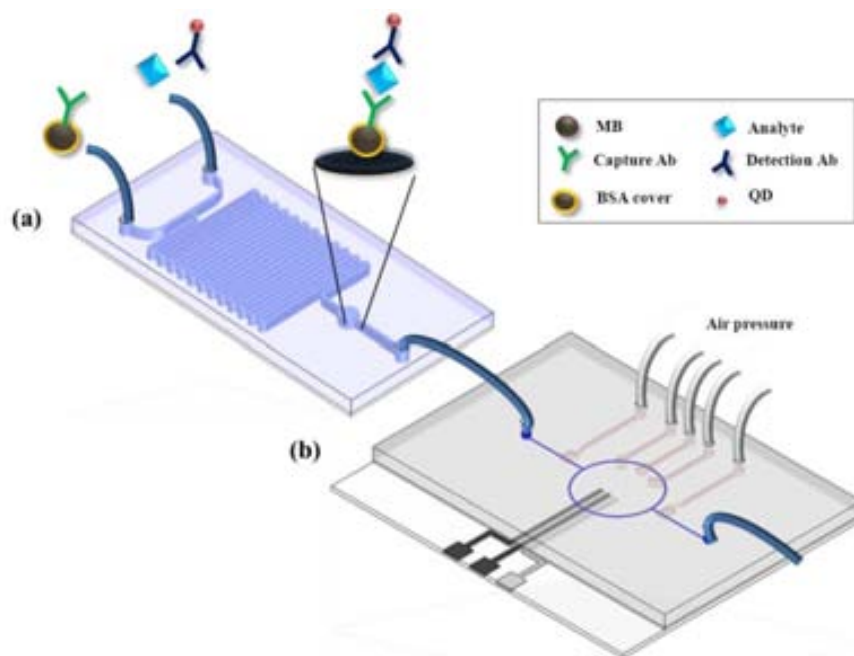


Figure 5.16. Schematic of a Lab-on-a-chip platform including the recycling chip for protein detection by using QDs as labels.

5.4. Enhanced detection sensitivity of quantum dots labeled protein by bismuth electrodeposition into microfluidic channel.

In this section we describe a disposable electrochemical immunoassay into a microfluidic platform by using QDs as labels and their enhanced detection using bismuth as an alternative mercury-free electrochemical stripping electrode. The immunoassay was performed by using a micromixer with a separation zone, where the magnet was located in order to capture the magnetic beads (MBs) used as the support for the immunoassay performance. A SPE was also integrated in a second microchannel (detection channel). The QDs signal was determined by highly sensitive stripping voltammetry of the dissolved metallic component (cadmium in the case of QDs). This system coupled to a portable electrochemical analyzer is a promising approach for the development of point of care devices for protein detection. Different parameters (i.e. bismuth deposition, flow rate, incubation times, mixers geometry, etc.), for achieving sensitive and reproducible system were optimized. The first optimization was performed by using only QDs by batch and chip measurements. Human IgG was used as a model protein for this proof of concept device.

In the last years, our group has described the use of mercury-coated SPEs for the monitoring of heavy metals in seawater²³. Despite the very good performance obtained in terms of LOD our focus is now on the mercury-free SPCE. Carbon-based SPEs make use of the large available surface area and porosity of the working electrode area so as to exhibit an attractive electro-analytical performance with well-separated stripping signals for each metal²⁴

5.4.1. Experimental details

Reagents

Bismuth (III) nitrate pentahydrate, reagent grade, 98%, was from Aldrich. The reagents used for immunoassay performance are the same as those described in the section 5.2.

Microfluidic platform design and fabrication

The channel fabrication procedure is the same as the one explained in previous sections. The geometry of the channel changes because it consists in the use of a micromixer, where the antibodies, sample and labels are mixed and conjugated in order to reduce incubation time and volumes. Different mixer configurations were designed. The mixing was optimized by using different flow rates and confirmed by simulation (Comsol Multiphysics 3.4). (See Annex 4).

Characterization

Scanning electron microscope (SEM) analyses were performed by using an EVO (Carl Zeiss NTS GmbH, Germany). Bare and Bismuth modified SPCE were analyzed both in drop and flow configurations.

QDs electrochemical detection by using Bi

Both measurements, in batch and in-chip, were tested in order to compare the sensitivity of the systems. Commercial CdSe@ZnS QD655 (10 μ L at 5 nM of concentration) were first partially dissolved by using HCl 1M for 2 min (adding 50 μ L). After the dissolving, 200 μ L of acetate buffer (pH 4.5) was added to the solution. For the comparison between samples with and without bismuth, 40 μ L of bismuth (at different concentrations) and PBS was added respectively. The first experiment consisted in the optimization of the bismuth concentration for both platforms. The electrochemical parameters were optimized in the previous Chapter. Since the cadmium reduction potential (-1.1 V) is also suitable for the bismuth electrodeposition. The sample containing bismuth was introduced in the same solution, ensuring the simultaneous reduction of the cadmium (II) and bismuth (III) (within 120 s).

NOVEL STRATEGIES TO OBTAIN ELECTROCHEMICAL LOCs WITH HIGHER SENSITIVITY

Immunoassay performance by using Bi

This protocol is the same as the one described in the section 5.2. Briefly, 40 μg of tosylactivated magnetic particles (15 μL from stock solution) were washed 3 times with borate buffer and suspended in 135 μL of the same buffer. These MBs were functionalized with capture antibody by electrostatics by using a borate buffer pH 8.5 overnight under agitation (700 rpm, 37°C). The conjugated MBs were washed with PBST three times in order to remove the antibody excess, followed by a blocking step using PBS supplemented with Tween 20 at 0.05 % (v/v) and BSA at 5 % for 2 hours under agitation conditions (700 rpm, 25°C). The blocked MBs were washed again with PBST three times by using the magnetic separator. Then, the microchannel was blocked by using PBS supplemented with Tween 20 at 0.05 % (v/v) and milk powder at 5 %. This solution was flowed during 10 min at 5 $\mu\text{L min}^{-1}$. After the blocking step, PBST was introduced for 10 min more at the same flow rate in order to clean the excess of the blocking solution.

The working electrode was then activated by cyclic voltammetry (10 cycles at a potential range from -0.8 V to 0.8 V and a scan rate of 100 mV s^{-1} in PBS buffer). Magnetic beads already modified with antibodies were then immobilized into the mixer by location of a permanent magnet behind the mixer outlet, with the optimized volume and flow-rate (2 m at 5 $\mu\text{L min}^{-1}$).

7.5 μL of QD 655 ITK Streptavidin (2 μM from stock solution) were suspended in 492.5 μL of QD incubation buffer (50 mM borate pH 8.3, 0.05% sodium azide), as well as 45 μL of Anti-Human IgG (gamma-chain specific)-biotin. They were mixed and incubated for 30 min (750 rpm 25°C) in batch. Then the excess of antibody was removed by filtering using eppendorf filters and centrifuged at 15000 rpm for 5 min.

A mixer (500 μm diameter and 50 μm thickness) with two inlets was fabricated and used for immunoassay performance. In one of the inlets, a syringe containing the analyte (Human IgG) is located while in the second inlet, the QDs already functionalized with detection antibody were located. Both of them were introduced at the same time with a flow-rate of 2.5 $\mu\text{L min}^{-1}$ during 15 min. After the mixing and incubation, the channel was washed with PBST at flow-rate of 2.5 $\mu\text{L min}^{-1}$ for 15 min. After that, a dissolving solution (HCl 1M) was introduced from the outlet in order to dissolve the QDs (labels in the immunoassay). This procedure was performed at flow-rate of 5 $\mu\text{L min}^{-1}$ for 3.5 min (the time needed to fill the entire channel at this flow-rate). The dissolving solution was remained in static mode for 3 min. Finally, the mixer was connected to the measurement chip (a simple channel with integrated screen printed electrode), then, acetate buffer (pH. 4.5) was introduced from the two inlets with a flow rate of 5 $\mu\text{L min}^{-1}$ and the electrochemical measurement was performed using the following parameters (without conditional potential because for each measurement, a new chip was used, so it was no necessary to reoxidize the cadmium deposited onto the electrode after the measurement):.

The deposition potential was defined in -1.1 V (as the optimized one in the previous Chapter), although in this case, the deposition time was fixed in 400 s because it is the needed time to flow all the solution across the channel to assure all sample deposition. The stripping measurement was done from -1.1 V to -0.15 V with a step potential of 5 mV sec^{-1} and amplitude of 0.3 V. This measurement was done with only acetate buffer as well as with acetate buffer containing bismuth (with the optimal concentration).

5.4.2. Results and discussions

Bismuth concentration optimization

The modification of the SPCEs was done by a simple electrodeposition of bismuth which was previously mixed with the sample containing QDs. Figure 5.17 shows the typical peaks corresponding to the cadmium present in the QDs core at -0.85 V and the bismuth peak, which appear at -0.25 V.

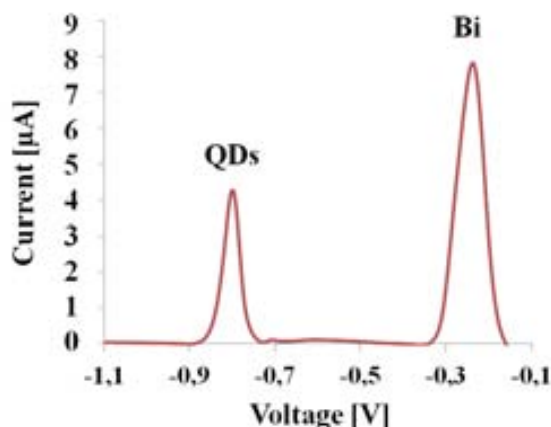


Figure 5.17. Typical peaks corresponding to the QDs and Bismuth in chip measurements. Deposition time of 120 s at -1.1 V and stripping between -1.1 to -0.1 V.

This optimization was performed in batch (a drop of a sample onto SPE) and on chip format. In Figure 5.18A, the QDs signal is shown for different bismuth concentrations, in drop format. The continuous lines show how the peak is increased until the addition of $50 \mu\text{g mL}^{-1}$ of bismuth, while the dotted lines represent the system inhibition after $50 \mu\text{g mL}^{-1}$ bismuth concentrations. In Figure 5.18B, the same results are shown for in chip measurements. In the microchannel system, the inhibition is achieved with less bismuth concentration compared to the drop format. This is related with the electrodeposition produced in flow and with the electrode size, because the continuous flow produces a homogeneous bismuth layer and the amount of deposited bismuth is higher in flow mode due to the bismuth renovation.

NOVEL STRATEGIES TO OBTAIN ELECTROCHEMICAL LOCs WITH HIGHER SENSITIVITY

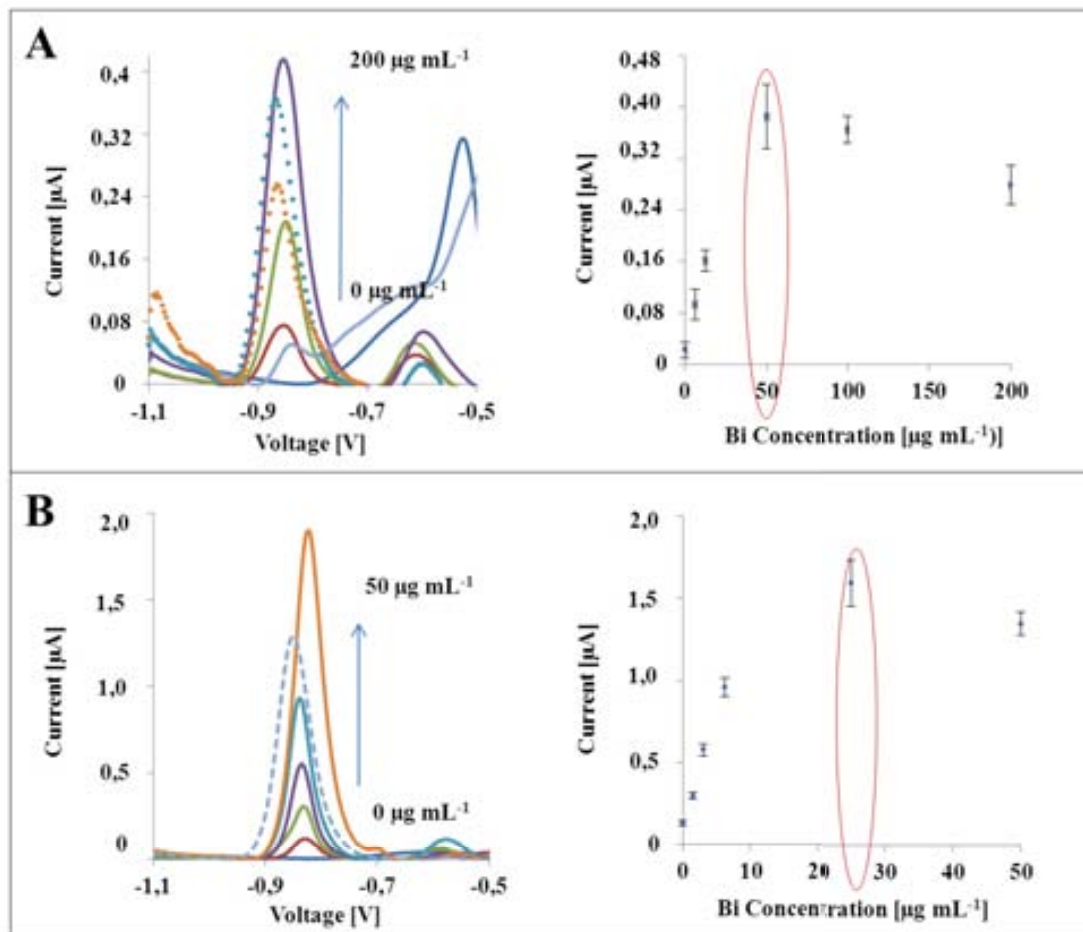


Figure 5.18. Bismuth concentration optimization in (A) drop and (B) formats. The Figure show the typical peak of QDs at -0.85 V and its increasing due to the Bismuth addition at different concentrations.

SEM characterization

The modification of the SPCE electrodes after the deposition of bismuth in flow mode and static mode has been evaluated by scanning electron microscopy. Using this methodology, homogeneous distribution of the Bi on the electrodes surface can be observed when the deposition is in flow mode due to the continuous renovation of the solution located onto the electrode and the diffusion phenomena that occurs faster than in static mode.

In Figure 5.19A, the SEM image of bare surface of screen printed carbon electrode is shown. A uniform binding of carbon onto polyester substrate was observed, as a result of the printing process. Instead of that in Figure 5.19B the bismuth formation is observed when the bismuth electrodeposition is performed in static mode by drop casting of the solution containing $50 \mu\text{g mL}^{-1}$ bismuth. In the case of the bismuth electrodeposition in flow mode, a more homogenous thin layer is observed onto the working electrode as it is shown in Figure 5.19C, with a thickness around 400 nm as is observable in Figure 5.19D.

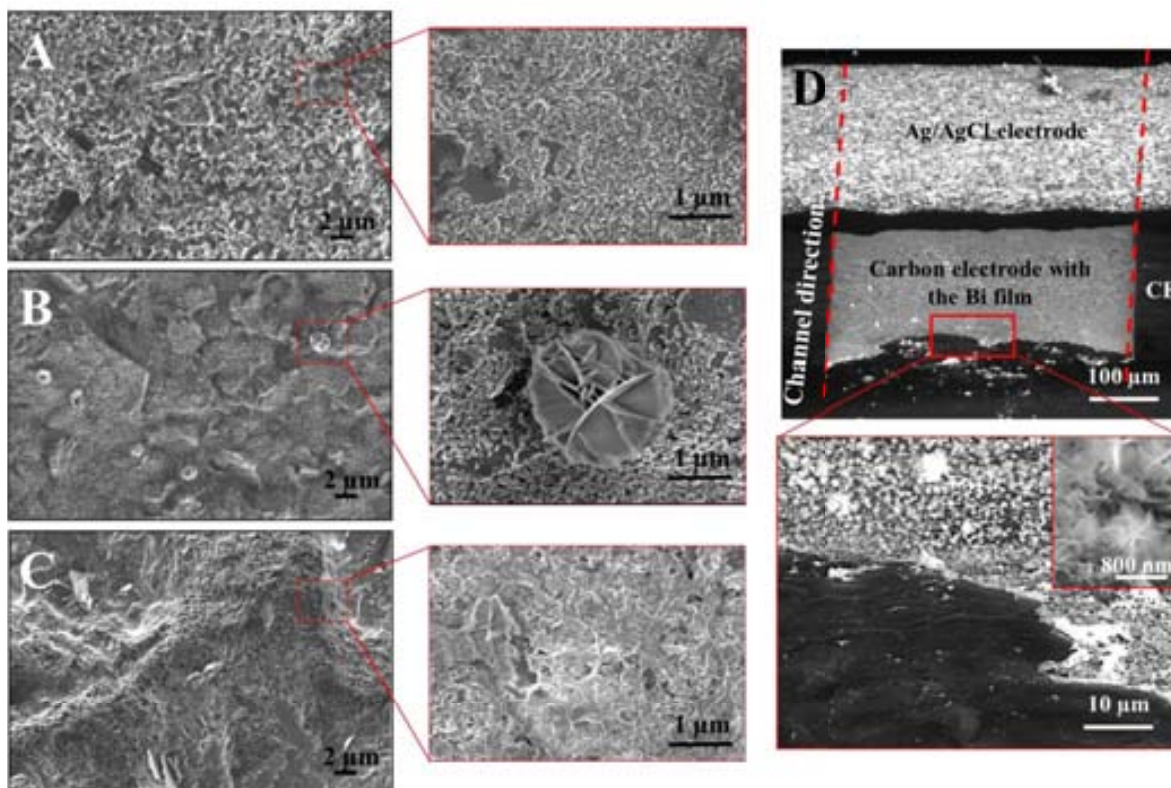


Figure 5.19. Bismuth electrodeposition onto screen printed electrode (SE). (A) Bare SPCE, (B) Electrodeposited bismuth in static mode, (C) Thin layer of Bismuth onto the SPE when the bismuth is deposited in flow mode, and (D) SEM image at 70° of the Bismuth layer deposited in flow mode.

Comparison between drop and in-chip measurements

Figure 5.20A,B shows the comparison between QDs calibration in bare-SPE and QDs sample containing bismuth respectively. In Figure 5.20C, the respective calibration curves are also showed. The same Figure also shows the SPCE response integrated into a microchannel system.

In batch measurements, the use of bismuth increases around 1.2 folds the electrochemical signal, with a sensitivity of $7 \times 10^{-6} \text{ A nM}^{-1}$ and R^2 of 0.997, while in chip format the increase is 5.5 fold with a sensitivity of $5 \times 10^{-6} \text{ A nM}^{-1}$ and R^2 of 0.915. If the current is expressed in current density because the drop measurement was performed using an electrode with a working area of 7.06 mm^2 , while the electrode integrated into the microchannel had a working area of 0.25 mm^2 the results are much better. If we compare the chip with the batch measurements, the achieved sensitivity is 100 fold better in flow than in batch mode. This means that the chip format helped to improve the sensitivity because the sample is permanently flowed onto the working electrode being the total

NOVEL STRATEGIES TO OBTAIN ELECTROCHEMICAL LOCs WITH HIGHER SENSITIVITY

volume even smaller (50 μL at 50 $\mu\text{g mL}^{-1}$ for batch measurements and 10 μL 25 $\mu\text{g mL}^{-1}$ for microchannel measurement)

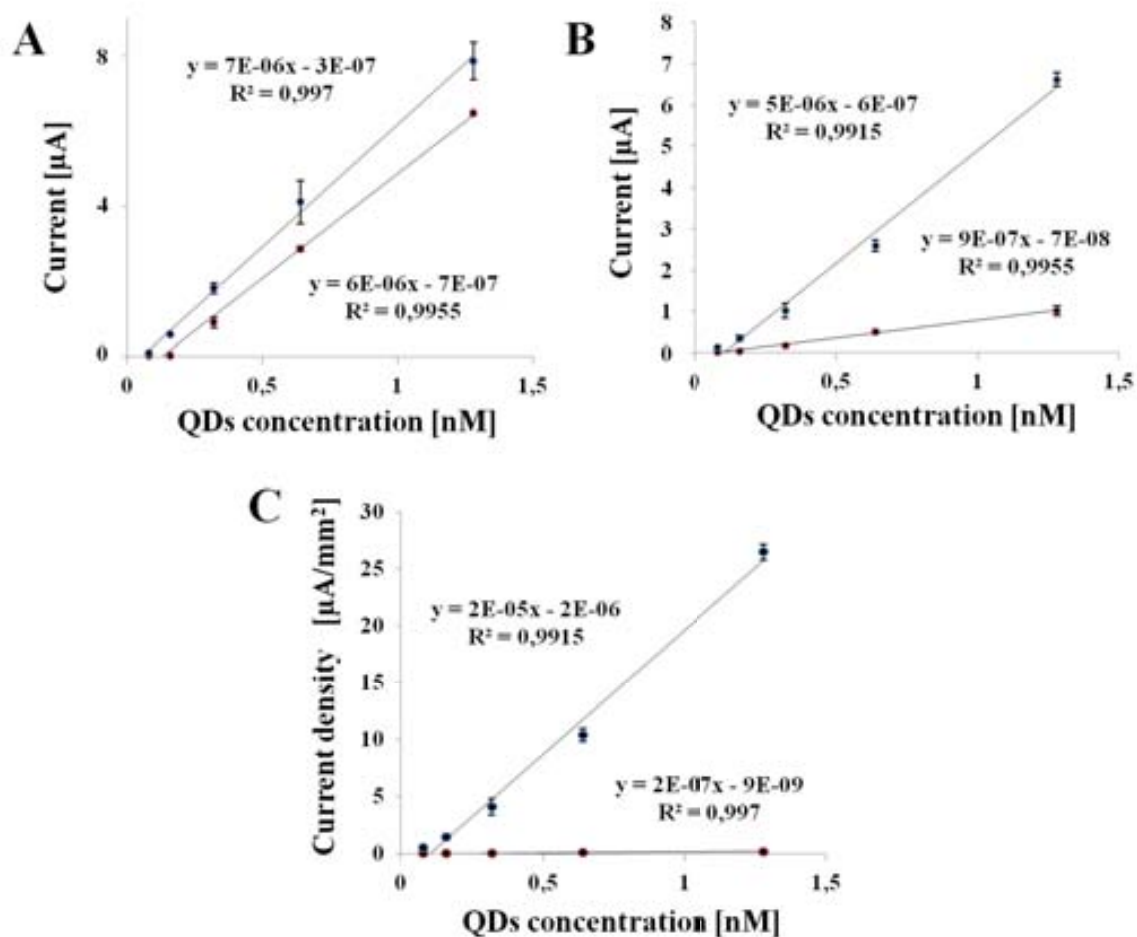


Figure 5.20. Calibration curves corresponding to (A) drop measurements, (B) In chip measurement. Both of them with and without bismuth (the higher slope for the curve related with the sample containing bismuth), and (C) The comparison between drop and chip formats.

Application in a simple immunoassay

In order to demonstrate the use of bismuth as strategy to improve the detection of QDs as labels in a magneto-immunoassay, a micromixer was integrated with a detection channel. First behind the micromixer, at the end of the channel, a neodymium magnet was located in the circular zone (see Figure 5.21) in order to immobilize the previously modified magnetic beads (details in the Section 5.2).

The conjugation parameters in flow were also optimized, in order to choose the shortest incubation time without losing efficiency. This study was performed following the same protocol previously described in Section 5.2. All incubation steps were performed by changing the flow rate from 1 to 5 $\mu\text{L min}^{-1}$. The most efficient conjugation was obtained

for flow rate up to $5 \mu\text{L min}^{-1}$, otherwise, the higher flow could reduce the probability of binding event to occur as desired inside the micromixer. Different incubation time intervals such as 5, 10, and 15 min were also tested. A proper electrochemical signal was observed at 15 min time interval due to the fact that the first 5 minutes were necessary to fill the entire micromixer at this flow rate, being necessary 10 min more to perform the binding between the immobilized magnetic beads and the detection antibody labeled with QDs. The effect of washing time at $5 \mu\text{L min}^{-1}$ flow rate was also studied finding the 10 minutes interval as enough to clean the channel from antibodies excess.

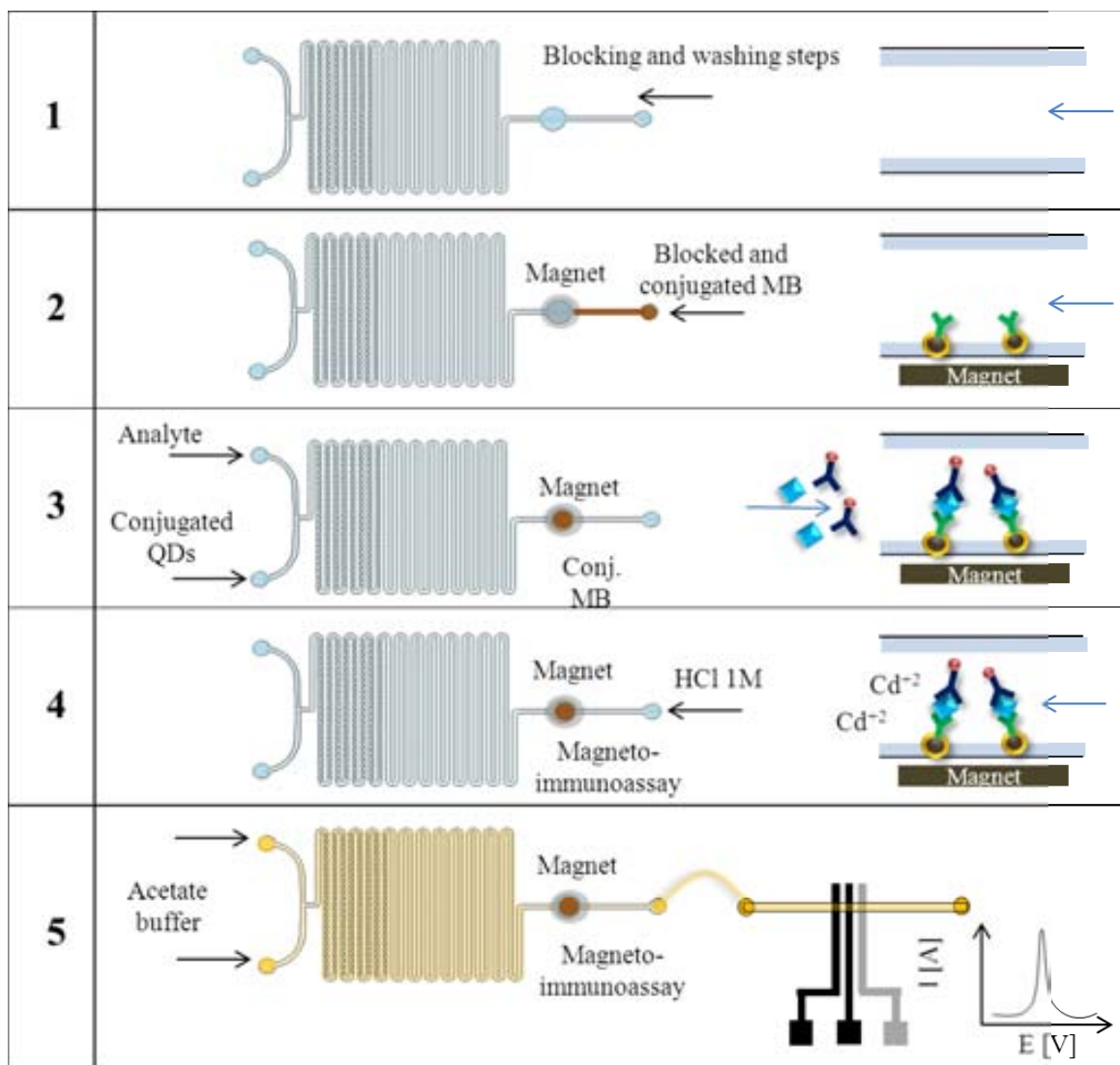


Figure 5.21. Schematic of the steps to perform the immunoassay including the detection. 1) the introduction of blocking step, 2) the immobilization of magnetic beads already modified with the capture antibody and blocking, 3) the conjugation step of the model protein and detection antibody already modified with QDs. Between each step a washing step is performed by using PBST. After the last washing step, in 4) HCl 1M is introduced from the outlet to dissolve the external layer of the QDs and liberate the Cd ions from the QDs core to be detected in step 5) After the introduction of acetate buffer.

NOVEL STRATEGIES TO OBTAIN ELECTROCHEMICAL LOCs WITH HIGHER SENSITIVITY

In Figure 5.21 all the needed steps for the immunoassay performance and detection are represented. The process is divided in 5 steps. 1) Channel is blocked with PBS supplemented with 0.5% of milk powder and 0.05% of Tween, then it was washed with PBST; 2) The magnetic beads functionalized with the capture antibody and blocked are located into the channel, introducing the solution from the outlet as it is shown in the same Figure, for 2 min at flow rate of $5 \mu\text{L min}^{-1}$; 3) the analyte (HIgG as model protein) and the detection antibody labelled with QDs at the same time with the same flow rate ($5 \mu\text{L min}^{-1}$) are introduced. After 15 min of incubation (20 min for the channel filling and 10min for immobilization onto the magnet, the channel was cleaned with PBST in order to remove the excess of protein and QDs; 4) After that, an acidic solution (HCl 1M) is introduced from the outlet to dissolve the external layer of the QDs and also to liberate the Cd ions from the QDs core. This process was performed during 5 min. After that in step 5) acetate buffer is introduced from the two inlets to drag all the Cd ions to the detection zone. This acetate buffer was also mixed with bismuth at $25 \mu\text{g mL}^{-1}$ (optimized concentration) for sensitivity increasing.

Electrochemical measurements of a model protein

SWASV was again used for QDs detection used as labels and as such related with the protein concentration. The measurements were carried out in 0.1 M acetate buffer (pH 4.5) after the partial dissolving by using 1M HCl. As it was mentioned before, the reduction potential was -1.1 V. The duration of the measurement was 400 s. In order to confirm the advantages of the use of bismuth in the improvement of immunoassay performance, a magneto-immunoassay with three different concentrations of analyte (0, 50 and 100 ng mL^{-1}) was performed into the micromixer. After the cleaning and dissolving steps, the measurements were performed in acetate buffer in presence or absence of bismuth (see results in Figure 5.22). It can be observed that the sensitivity in the case of immunocomplex (labelled with QDs) is lower than in the case of QDs alone due to the fact that the biological sample inhibits the electrochemical signal and affects the electrode performance along the time; however the increasing of the signal for the measurement with the presence of bismuth was around 3 times with a RSD of 13.2 %.

The increase of the sensitivity for an immunoassay based on QDs as electrochemical labels was demonstrated as a proof of concept with the performance of a complete magneto-immunoassay for human IgG determination (optimized protocol in the previous sections) into a microfluidic system, by addition of bismuth in the acetate buffer at the last step. It is an easy and promising strategy to reduce the LOD with a simple addition in the measurement buffer without the addition of more steps in a magneto-immunoassay.

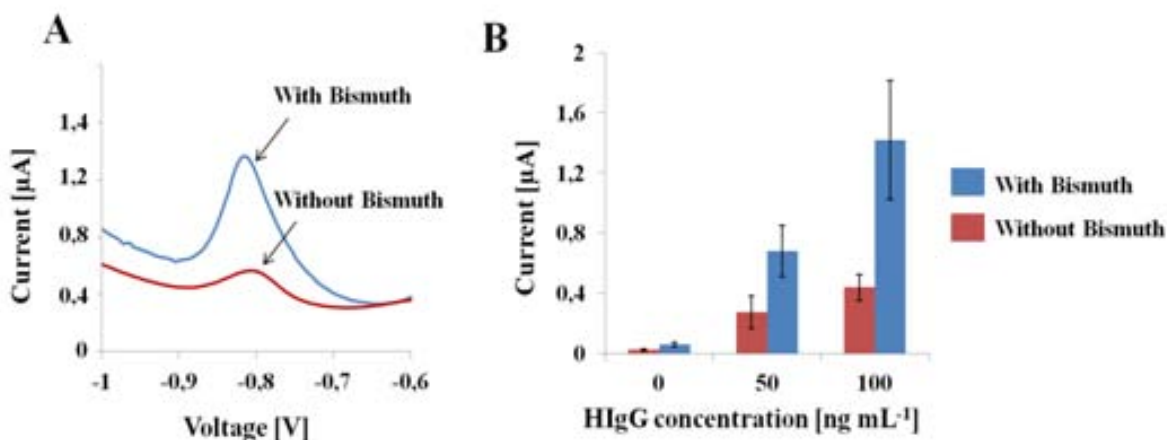


Figure 5.22. Electrochemical response of QDs used as labels in a magnetoimmunoassay for HIgG determination. (A) Effect of the bismuth presence in the electrochemical measurement for an immunoassay with a fixed concentration of HIgG (50 ng mL^{-1}), and (B) Comparison between three different concentrations of HIgG.

5.5. Conclusions

The magnetic separation platform showed excellent properties to be used for many applications (i.e. sample purification and manipulation, preconcentration, etc.). It was possible to demonstrate its operation by the detection of a model protein and it was also compared with the platform explained in Chapter 3, which uses a single magnet behind the channel.

For the magnetic plug, it was also demonstrated that the most stable immobilization of magnetic beads was achieved in the attractive conformation of the magnets, being stable up to $200 \mu\text{L min}^{-1}$. For this platform, it was necessary to increase the measurement time due to the small dimensions of the channel, since it was necessary to reduce the flow-rate down to $0.05 \mu\text{L min}^{-1}$, to ensure the total QDs dissolving.

In addition, the magnetic beads were changed for this approach, due to the size and time needed for the plug formation, since, large particles ($2.8 \mu\text{m}$) precipitated more easily than the small ones ($1 \mu\text{m}$).

In addition to the single on-chip flow through measurements, the design of a recirculation system with the aim of achieving lower LODs using reduced sample volumes was proposed as a proof-of-concept. The use of an external peristaltic pump adapted to a simple microfluidic channel demonstrated that the QDs electrochemical signal increases 5.5 fold

NOVEL STRATEGIES TO OBTAIN ELECTROCHEMICAL LOCs WITH HIGHER SENSITIVITY

when the flow is recycled twice. A micro-peristaltic pump with integrated pneumatic valves was also proposed in order to miniaturize and integrate the system. It consisted in a “push-down” valve configuration. All the fabrication steps were optimized for future applications.

A microfluidic device based on enhancement via bismuth for protein detection achieving very low LOD (3.5 ng mL^{-1}) as well as an increase in the sensitivity up to 100 fold respects to the batch format is successfully developed. The device takes advantage of the speed and low cost of the conventional immunoassay technologies. Under optimal conditions, the device was capable of detecting three times less concentration than the conventional system, in 6.6 min by using the sample containing the bismuth solution at the optimized concentration.

The exposed devices coupled with a portable electrochemical analyzer are promising for in-field quantitative testing for disease-related protein biomarkers. The developed device thus provides a rapid and quantitative tool for protein detection. Further tests are necessary to evaluate the applicability in real clinical samples.

5.6. Reference

¹R. Afshar, Y. Moser, T. Lehnert, M.A.M. Gijs. *Magnetic particle dosing and size separation in a microfluidic channel*. *Sensor. Actuat. B-Chem.*, 2011, 154, 73-80.

²M.D. Tarn, S.A. Peyman, D. Robert, A. Iles, C. Wilhelm, N. Pamme. *The importance of particle type selection and temperature control for on-chip free-flow magnetophoresis*. *J. Magn. Mater.* 2009, 321, 4114-4122.

³N.Z. Danckwardt, M. Franzreb, A.E. Guber, V. Saile. *Pump-free transport of magnetic particles in microfluidic channels*. *J. Magn. Mater.* 2011, 323, 2776-2781.

⁴H.T. Kuo, J.Z. Yeh, C.M. Jiang, M.C. Wu. *Magnetic particle-linked anti hCG β antibody for immunoassay of human chorionic gonadotropin (hCG), potential application to early pregnancy diagnosis*. *J. Immunol. Methods*. 2012, 381, 32-40.

⁵O.A. Loaiza, E. Jubete, E. Ochoteco, G. Cabañero, H. Grande, J. Rodríguez. *Gold coated ferric oxide nanoparticles based disposable magnetic genosensors for the detection of DNA hybridization processes*. *Biosens. Bioelectron.* 2011, 26(5), 2194-2200.

-
- ⁶D. Huska, J. Hubalek, V. Adam, D. Vajtr, A. Horna, L. Trnkova. *Automated nucleic acids isolation using paramagnetic microparticles coupled with electrochemical detection*. *Talanta*. 2009, 79(2), 402-411.
- ⁷N. Pamme, A. Manz. *On-chip free-flow magnetophoresis: continuous flow separation of magnetic particles and agglomerates*. *Anal. Chem.* 76, 2004, 7250-7256.
- ⁸E. Mirowski, J. Moreland, S.E. Russek, M.J. Donhaue. *Integrated microfluidic isolation platform for magnetic particle manipulation in biological systems*. *Appl. Phys. Lett.* 2004, 84, 1786-1789.
- ⁹S. Dutz, M.E. Hayden, A. Schaap, B. Stoeber, U.O. Häfeli. *A microfluidic spiral for size-dependent fractionation of magnetic microspheres*. *J. Magn. Magn. Mater.* 2012, 324, 3791-3798.
- ¹⁰ M. Slovakova, N. Minc, Z. Bilkova, C. Smadja, W. Faigle, C. Futterer, M. Taverna, and J-L. Viovy, *Use of self assembled magnetic beads for on-chip protein digestion*, *Lab Chip*. 2005, 5, 935–942.
- ¹¹ M. Medina-Sánchez, S. Miserere, S. Marín, G. Aragay, A. Merkoçi. *On-chip electrochemical detection of CdS quantum dots using normal and multiple recycling flow through modes*. *Lab Chip*. 2012, 12, 2000-2005.
- ¹² P.M. Fordyce, C.A. Díaz-Botia, J.L. DeRisi, R. Gomez-Sjoberg. *Systematic characterization of feature dimensions and closing pressures for microfluidic valves produced via photoresist reflow*. *Lab Chip*. 2012, 12, 4287-4295.
- ¹³S. J. Maerkl and S. R. Quake. *A Systems approach to measuring the binding energy landscapes of transcription factors*. *Science*. 2007, 315, 233–237.
- ¹⁴H.Y. Tan, W.K. Loke, N.T. Nguyen. *A reliable method for bonding polydimethylsiloxane (PDMS) to polymethylmethacrylate (PMMA) and its application in micropumps*. *Sensor. Actuat. B*. 2010, 151, 133-139.
- ¹⁵ M. A. Unger, H. P. Chou, T. Thorsen, A. Scherer and S. R. Quake. *Monolithic microfabricated valves and pumps by multilayer soft lithography*. *Science*. 2000, 288, 113-116.

¹⁶M.H. Wu, G.M. Whitesides. *Fabrication of two-dimensional arrays of microlenses and their applications in photolithography*. J. Micromech. Microeng. 2002, 12, 747-758.

¹⁷I. Bontidean, C. Berggren, G. Johansson, E. Csoregi, B. Mattiasson, JR. Lloyd, KJ. Jakeman, and NL. Brown. *Detection of heavy metal ions at femtomolar levels using protein-based biosensor*. Anal. Chem. 1998, 70(19), 4162-4169.

¹⁸V. Rechacek, I. Hotovy, M. Vois, and F. Miks, *Bismuth film electrodes for heavy metals determination*. Microyst. Technol. 2008, 14, 491-498.

¹⁹Z. Wang, and E. Liu. *Graphene ultrathin film electrode for detection of lead ions in acetate buffer solution*. Talanta. 2013, 103, 47-55.

²⁰I. Palchetti, A. Cagnini, M. Mascini, A.P.F. Turner. *Characterisation of screen-printed electrodes for detection of heavy metals*. Microchim. Acta. 1999, 131, 65–73.

²¹I. Palchetti, M. Mascini, M. Minunni, A.R. Bilia, F.F. Vincieri. *Disposable electrochemical sensor for rapid determination of heavy metals in herbal drugs*. J. Pharm. Biomed. Anal., 2003, 32, 251-256.

²²J. Wang, J. Lu, S.B. Hocevar, P.A.M. Farias, B. Ogorevc. *Bismuth-coated carbon electrodes for anodic stripping voltammetry*. Anal. Chem. 2000, 72(14), 3218, 3222.

²³J. Calvo-Quintana, F. Arduini, A. Amine, F. Punzo, G. Li-Destri, C. Bianchini, D. Zane, A. Curulli, G. Palleschi, D. Moscone. *Part I: A comparative study of bismuth-modified screen-printed electrodes for lead detection*. Anal. Chim. Acta. 2011, 707, 171-177.

²⁴N. Serrano, A. Alberich, J.M. Díaz-Cruz, C. Ariño, M. Esteban. *Coating methods, modifiers and applications of bismuth screen-printed electrodes*. Trends Anal. Chem. 2013, 46, 15-29.

²⁵J. Dedík, M. Janovcová, H. Dejmková, J. Barek, K. Pecková. *Utilization of unmodified screen-printed carbon electrodes in electroanalysis of organic compounds (an overview)*. Sensing in Electroanalysis, UNESCO Laboratory of Environmental Chemistry, Czech Republic, 2011, 6, 129-138.

²⁶A. Caldeira, C. Gouveia-Caridade, R. Pauliukaite, C.M.A. Brett. *Application of square wave anodic stripping voltammetry for determination of traces of Ti(II) at carbon electrodes in situ modified with Bi films*. Electroanalysis. 2011, 23(6), 1301-1305.

-
- ²⁷ L. Lin, N.S. Lawrence, S. Thongngamdee, J. Wang, Y. Lin. *Catalytic adsorptive stripping determination of trace chromium (VI) at the bismuth film electrode*. *Talanta*. 2005, 65, 144-148.
- ²⁸ Z. Nie, C.A. Nijhuis, J. Gong, X. Chen, A. Kumachev, A.W. Martínez, M. Narovlyansky, G.M. Whitesides. *Electrochemical sensing in paper-based microfluidic devices*. *Lab Chip*. 2010, 10(4), 477-483.
- ²⁹ R.O. Kadara, N. Jenkinson, C.E. Banks. *Disposable bismuth oxide screen printed electrodes for the high throughput screening of heavy metals*. *Electroanalysis*. 2009, 21(22), 2410-2414.
- ³⁰ A. Merkoçi, U. Anik, S. Çevik, M. Çubukçu, and M. Guix. *Bismuth film combined with screen-printed electrode as biosensing platform for phenol detection*. *Electroanalysis*. 2010, 22, 1429-1436.
- ³¹ L. Tang and N. Yoon Lee. *A facile route for irreversible bonding of plastic-PDMS hybrid microdevices at room temperature*. *Lab Chip*. 2010, 10, 1274-1280.
- ³² Ch. Barglik-Chory, D. Buchold, M. Schmitt, W. Kiefer, C. Heske, C. Kumpf, O. Funchs, L. Weinhardt, A. Stahl, E. Umbach, M. Lentze, J. Gerts, and G. Müller. *Synthesis, structure and spectroscopic characterization of water-soluble CdS nanoparticles*. *Chem. Phys. Lett*. 2003. 379, 443-451.
- ³³ S. Armalis and G. Johansson. *On-line trace metal determination by pre-concentration on immobilized 8-quinolinol with flow recycling anodic stripping voltammetry*. *Anal. Chim. Acta*. 1997, 339, 155-159.

DIAMOND BASED PLATFORMS.....	147
6.1. Introduction	149
6.2. Experimental details	150
6.2.1. Reagents.....	150
6.2.2. Apparatus.....	150
6.2.3. Preparation of BDD electrode.....	151
6.2.4. Microfluidic channel fabrication and BDD electrode integration	151
6.2.5. Platinum nanoparticles electro-deposition onto BDD electrode.....	152
6.2.6. Atrazine derivatization.....	152
6.2.7. Biosensor variables optimization.....	152
6.2.8. ELISA magneto-immunoassay for atrazine detection	152
6.2.9. On-chip ELISA magneto-immunoassay for Atrazine detection.....	153
6.3. Results and discussions	155
6.3.1. Morphological characterization of BDD electrode.....	155
6.3.2. Optimization of experimental variables of the biosensor for atrazine detection based on ELISA immunoassay.....	156
6.3.3. Electrochemical magneto-immunosensing strategy	157
6.3.4. Implementation of the ELISA magnetic immunoassay for atrazine detection by using a microfluidic chip with BDD Pt-NPs electrode as detection platform.....	159
6.3.5. Implementation of the complete ELISA magnetic immunoassay for atrazine detection by using a micromixer coupled to the BDD Pt-NPs based detection platform.....	161
6.4. Conclusions	162
6.5. References	164

CHAPTER 6

DIAMOND BASED PLATFORMS

Related Publications

M. Medina-Sánchez, C. Mayorga-Martínez, Y. Honda, T. Watanabe, T. A. Ivandinni, Y. Einaga and A. Merkoçi. “On-chip sensitive electrochemical analysis of pesticides by magneto-immunoassay strategy with boron-doped diamond electrode modified with platinum nanoparticles”. *In preparation* (2013). (Annex 2).

This chapter shows an alternative microfluidic platform for biosensing applications based on diamond electrode. On-chip electrochemical analysis of atrazine based on magneto-immunoassay using boron-doped diamond (BDD) electrode, modified with platinum nanoparticles (Pt-NPs) is achieved. The detection system is based on a competitive immunoassay using free atrazine and atrazine conjugated with horseradish peroxidase (HRP) as enzymatic label and magnetic microparticles as preconcentration platform. In-chip electrochemical detection of up to 5 μL of the conjugate was performed using chronoamperometry technique, achieving a detection limit of 0.1 pM. This method will be with great interest for automatic control systems used in environment monitoring between other applications.

6.1. Introduction

Atrazine and its degradation products are members of the family of triazine herbicides which represent the most commonly toxic agents found in groundwater. Moreover, atrazine was found to be a persistent environmental contaminant due to its polarity. This herbicide was extensively used for selective control of annual grasses and broad leaved weeds^{1,2} and it has been recognized for its effect on the reproductive system as mutagenic toxic.³

Several methods for pesticide determination have been reported, but most of them require sample pretreatment, purification procedures, large volumes of reagents, expensive equipment and prepared personnel, being the conventional methodologies expensive and wasteful. For this reason, the development of portable quantification devices and particularly of simple microfluidics systems is becoming of great interest due to low volume consumption, easy transducer integration, possibility to be miniaturized for in-situ measurements and good cost-efficiency relation.⁴

Immunosensing technologies in general and particularly those based on labeling strategies due to their specificity and sensitivity are showing to be interesting for pesticides detection. The integration of immunoassay strategy with microfluidic platforms constitutes a potential alternative for high sensitivity devices, with fast response, low volume consumption and simple instrumentation compared with the classic methods.⁵

In addition, nanomaterials (NMs) application in sensors and biosensors have been very useful for transducers modification, improving in this way the electrochemical (amperometric, impedimetric, potentiometric), optical (light absorbance, dispersion, fluorescence) and other mixed signals (i.e. electrochemiluminescence and nanomechanics) based measurements.^{6,7,8} Of special interest is the application of NMs in lab-on-a-chip (LOC) systems^{9,10} including the use of magnetic beads as capture / preconcentration

DIAMOND BASED PLATFORMS

platform to improve the enzymatic¹¹ or immunological¹² reactions thanks to their surface area, faster assay kinetics and easy washing steps due to their easy magnetic manipulation using external magnets.

In this work we take now advantages of on-chip magnetic bead manipulation and couple it with the advantages of boron doped diamond (BDD) modified with Pt nanoparticles (BDD-Pt-NPs) that shows high electrical conductivity, wide potential window and low background current. Such on-chip coupling of a BDD Pt-NPs detector offers robust, stable and very low limits of detection (LOD) including excellent signal / noise relation for immunosensing of pesticides. In particular the use of Pt-NPs offer to BDD catalytic properties with interest for enzymatic reactions^{13,14}. Furthermore, the BDD electrode shows low organic contaminant adsorption characteristic that in combination with flow systems provides with a clean surface and more repeatability between measurements.¹⁵

The BDD Pt-NPs LOC is found here as a very effective system for chronoamperometric detection of atrazine in an electrochemical ELISA magneto-immunoassay format. The developed set-up is based on a hybrid material polydimethylsiloxane-polyester (PDMS-PE) compatible with mass production being offered as an excellent tool for monitoring of specific pesticides beside other monitoring applications.

6.2. Experimental details

6.2.1. Reagents

Atrazine magneto-ELISA kit was purchased from Abraxis (Pennsylvania, USA). For the atrazine derivatization: standard atrazine ((2-chloro-4-(ethylamino)-6-isopropylamino-s-triazine), 3-mercaptopropanoic acid, KOH, absolute ethanol, sodium bicarbonate (NaHCO₃), and chloroform, were utilized (all of them obtained from WAKO, Japan). Potassium tetrachloroplatinate (K₂PtCl₄), phosphate buffered saline (PBS), 3-aminopropyltriethoxylane (APTES) were obtained from Sigma Aldrich, Spain. The screen-printed inks (graphite ink (Electrodag 423SS) and Ag/AgCl ink (Electrodag 6037SS)) were purchased from Acheson Industries, USA. Diamond powder and negative photoresist were purchased from Kemet corp., UK and SU-8 from Microchem (Newton, MA, USA).

6.2.2. Apparatus

Electrochemical measurements were performed with an Autolab (Echo Chemie, The Netherlands), two syringe pumps (standard infusion only pump 11 Elite) from Harvard apparatus (USA) were used for injected the conjugated stock solution and buffer PBS respectively. Scanning electron microscope (SEM) analysis was performed by using a

MAGELLAN SEM (USA). Raman spectroscopy (Renishaw System 2000, UK) was used for evaluated the BDD film formation. SPCE were fabricated by screen-printing technology using a screen-printing machine (DEK 248, UK). Polycrystalline boron-doped diamond thin films were grown on Si (111) substrates using a 2.45 GHz microwave plasma chemical vapor deposition (CVD) system equipped with a 6 kW microwave plasma CVD reactor (Model AX6500 CORNES Technologies Corp., Japan).

6.2.3. Preparation of BDD electrode

Details of the preparation of BDD films are described elsewhere.^[16] In order to enhance the diamond nucleation density, the silicon substrates were pretreated by abrading with diamond powder ($\sim 1 \mu\text{m}$ of diameter), and were then ultrasonically cleaned in distilled water and isopropyl alcohol. The film was grown at a pressure of 80 torr with a total gas flow of 500 sccm. A hydrogen / methane / trimethylboron gas mixture was used, with methane-to-hydrogen ratio of 4% and carbon-to-boron ratio of 1%. The deposition time was 4 h, giving a film thickness of approximately $2 \mu\text{m}$.

6.2.4. Microfluidic channel fabrication and BDD electrode integration

Microfluidic channels were fabricated by rapid prototyping and PDMS technologies as previously described.¹⁷ Briefly, a 4-inch silicon wafer was spin coated with a negative photoresist and patterned by photolithography by using a flexible mask. PDMS was poured onto the resulting mold and cured at $65 \text{ }^\circ\text{C}$ for 2 h. The channels were 3.5 mm wide, $100 \mu\text{m}$ depth and 1 cm long. Two reservoirs were punched at the inlet and the outlet of the channel.

The electrochemical detector consists in a set of three electrodes: counter electrode (graphite) and reference electrodes (Ag/AgCl) fabricated by screen-printing technology using a screen-printing machine (DEK 248) and previously fabricated BDD electrode was used as working electrode (WE). Screen-printed electrodes are based on the sequential deposition of a graphite ink and Ag/AgCl ink. After the deposition of each layer, a drying process is performed followed by keeping the polyester sheet substrate at 120°C for 45 min (graphite) and 30 min (Ag/AgCl).

After this, the PDMS channel and polyester sheet (PE) substrate were assembled using a previously reported protocol;¹⁸ polyester substrate was treated by air-plasma for 1 min and then immersed into a 2% (v/v) APTES solution in water for 1 h in order to functionalize the surface with amino groups. The surface of the PDMS channel was also activated for 1 min by plasma, and put into contact with the PE sheet to achieve irreversible bonding. Once the first bonding was done, the integration of BDD wafer as working electrode was attached

DIAMOND BASED PLATFORMS

using double-sided adhesive tape. Previously, the PE was drilled in the middle of counter and reference electrode with a diameter of 3 mm.

6.2.5. Platinum nanoparticles electro-deposition onto BDD electrode

Platinum nanoparticles (Pt-NPs) growth was achieved by electrodeposition of 25 mM K_2PtCl_4 solution in phosphate buffer pH 7.0 applying -0.75 V for 100 s onto the BDD working electrode once it was integrated into the microfluidic channel. This potential corresponds to platinum reduction peak onto BDD working electrode evaluated previously using cyclic voltammogram. The electrodeposition was performed in static flow.

6.2.6. Atrazine derivatization

The synthesis of the carboxylic acid atrazine derivative, 3-{4-(ethylamino)-6-[(1-methylethyl)amino]-1,3,5-triazin-2-yl} propanoic acid, required for conjugation of atrazine to HRP, was carried out according to Smyth et al.¹⁹ A solution of 5.4 mmol 3-mercaptopropanoic acid, 10.8 mmol 85% (w/v) KOH and 10 ml absolute ethanol was added to a stirred homogeneous mixture of 5.01 mmol atrazine and 100 ml absolute ethanol. The mixture was refluxed under nitrogen for 5 h until a white solid remained, which was then taken up in 25 ml of 5% (w/v) $NaHCO_3$. This solution was washed with 3×10 ml chloroform and acidified to pH 2 with 6 M HCl. The white solid was collected, washed with milli-Q water and dried. Additional product was obtained through evaporation and crystallization of the residue from methanol.

6.2.7. Biosensor variables optimization

In order to evaluate the effect of BDD electrode modified with Pt-NPs in the HRP response in presence of H_2O_2 , cyclic voltammograms were carried out at the potential range of -1 to 1 V vs. Ag/AgCl. Amperometric detection was performed applying -0.25 V DC potential vs. Ag/AgCl in 0.1 M phosphate buffer (PBS) at pH 7.0 with 0.1 M KCl. The measurement time for three conjugated injections was 50 s. All electrochemical experiments were performed at room temperature.

6.2.8. ELISA magneto-immunoassay for atrazine detection

The Atrazine kit that applies the principles of enzyme linked immunosorbent assay (ELISA) to the determination of atrazine and related triazines was used. 200 μ L of home-made derivatized atrazine at different concentrations, including the control sample (PBST) was introduced into different eppendorfs, followed by the addition of 200 μ L of the atrazine-HRP conjugate in each one, which were mixed with the atrazine antibody coupled to paramagnetic particles (400 μ L), and incubated for 30 min at room temperature. After

the incubation, the conjugates were washed three times with PBST by using a magnetic separator and suspended in 300 μL PBS (Figure 6.1).

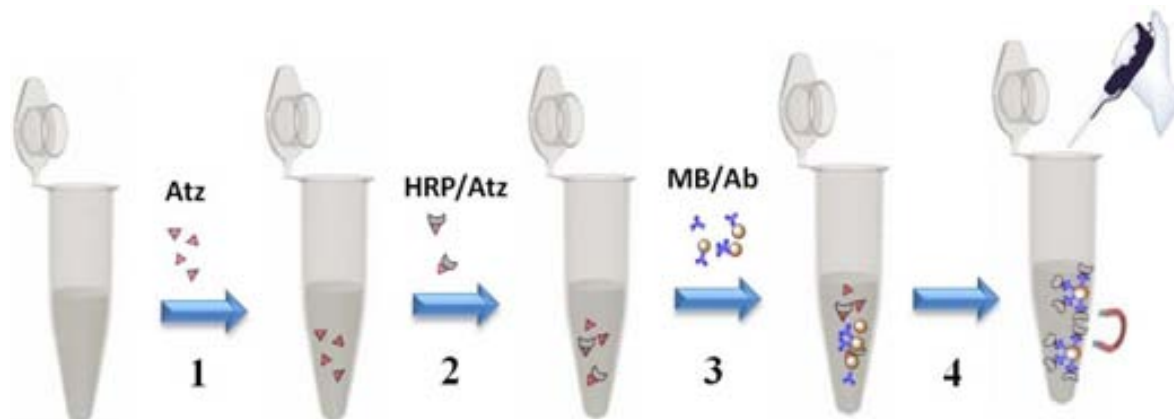


Figure 6.1. Schematic representation of incubation steps to obtain the complete magneto-immunoassay for atrazine detection: 1) Addition of free atrazine at different concentrations, 2) Addition of atrazine labeled with HRP, 3) Conjugation with Ab-MB for 30 min, and 4) excess removing (before measurement this sample was mixed with hydrogen peroxide).

For colorimetric measurement, 3,3',5,5' - tetramethylbenzidine (TMB) containing hydrogen peroxide (10 mL / 2 μL at 10 M) was added to each eppendorf (300 μL) and incubated for 20 min at room temperature. Finally, stopping solution (300 μL of sulfuric acid) was introduced into each tube, changing the color of the initial TMB from blue to yellow. This color intensity variation depends on atrazine concentration and is it possible to be quantified by a spectrophotometer at 450 nm within 15 min after the addition of stopping solution. The concentration of atrazine is calculated on the basis of a standard calibration curve (atrazine concentration vs. absorbance at 450 nm).

6.2.9. On-chip ELISA magneto-immunoassay for Atrazine detection

Two different experiments were performed on chip for atrazine detection. The first one was performed for electrochemical measurements in flow system (Figure 6.2). Hydrogen peroxide (8 mM) was added to each eppendorf (300 μL) and incubated during 20 min at room temperature. After the incubation, the sample (5 μL) was introduced into the microfluidic channel followed by the buffer solution (PBS) to be measured by amperometry at -0.25 V DC, potential previously optimized.

DIAMOND BASED PLATFORMS

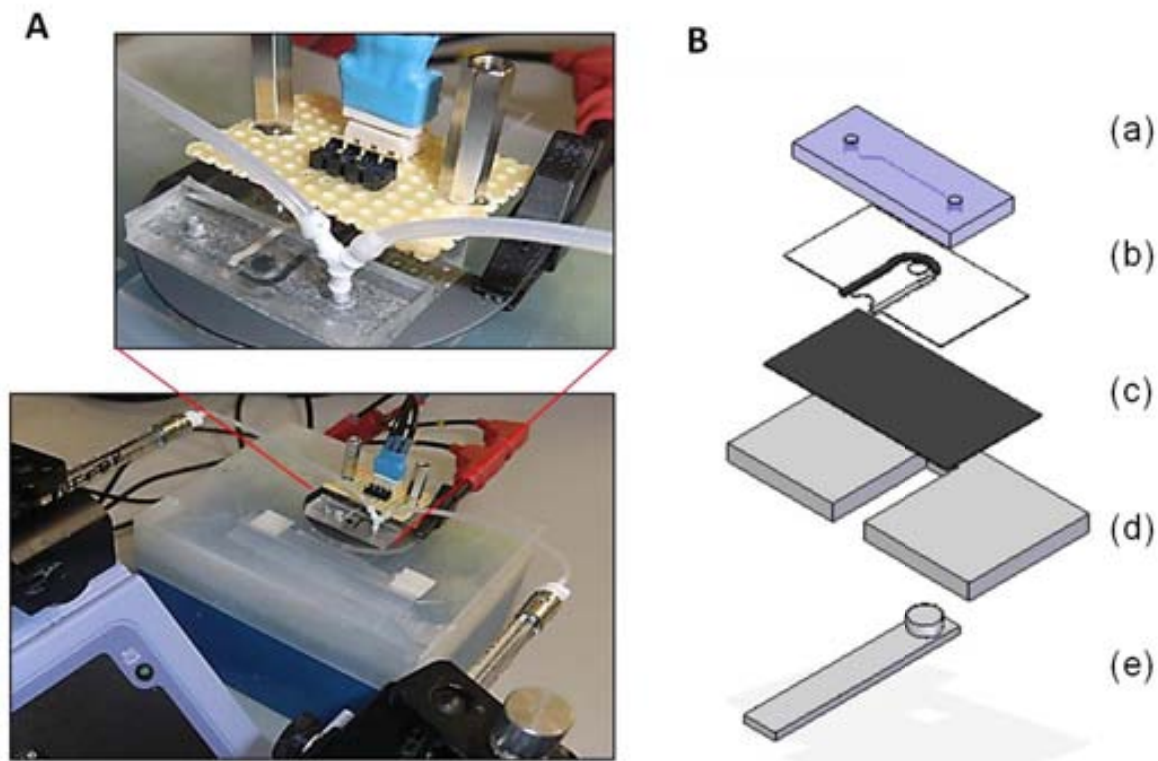


Figure 6.2. Schematic representation of electrochemical magnetoimmunosensing system for atrazine detection. (A) BDD-PtNP electrode integrated with microfluidic channel, and (B) Components of the hybrid BDD Pt-NPs-SPCE into microfluidic channel: (a) PDMS microchannel, (b) screen printed electrodes onto polyester substrate (RE and CE), (c) BDD electrode, (d) Magnetic support, and (e) permanent magnet.

Between (c) and (d) a double side adhesive tape was attached to join both parts.

In the second experiment, the conjugation and the detection were performed into the chip. In this case a mixer chip was used before the detection one. First the magnetic beads already modified with anti-atrazine were introduced in an eppendorf (600 μ L) and separated with a magnetic separator in order to preconcentrate them twice (by suspension in 300 μ L of PBS). Then 150 μ L of free atrazine at different concentrations (0, 0.09, 0.9, 2.25 and 4.5 nM) and 150 μ L of atrazine labeled with HRP were mixed in the same eppendorf. The next step was to introduce these two solutions, in each mixer inlet and incubate them for 20 min at a flow rate of 5 μ L min^{-1} . Before the incubation the mixer is connected to the detection microchannel based on BDD Pt-NPs electrodes with a magnet located behind the working electrode. In this way, the conjugate is trapped onto the working electrode (See Figure 6.3A). After the incubation step, the mixer is isolated from the detection chip, and the washing buffer is introduced into the detection chip in order to remove the excess of sample at a flow rate of 50 μ L min^{-1} . Finally, consecutive injections of 5 μ L of 8mM hydrogen peroxide in PBS were introduced by using two syringe pumps (Figure 6.3B).

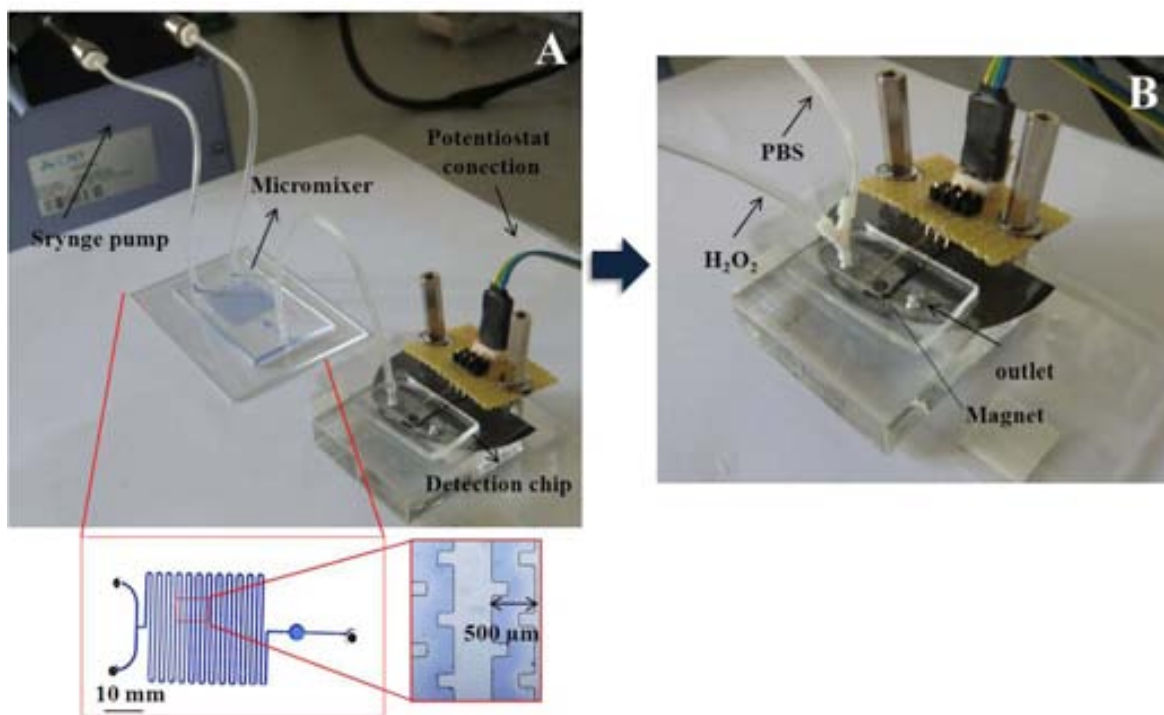


Figure 6.3. Set-up pictures (A) Micromixer for the atrazine magnetoimmunoassay coupled to the detection chip in order to immobilize the magneto-immunoassay onto the working electrode, and (B) the detection chip based on boron doped diamond electrode modified with Pt-NPs.

6.3. Results and discussions

6.3.1. Morphological characterization of BDD electrode

The morphological characterization of bare boron-doped diamond (BDD) and Pt-NPs modified BDD (BDD-Pt-NPs) electrodes was performed using scanning electron microscopy (SEM). Figure 6.4A shows a typical SEM image of a polycrystalline BDD electrode. The BDD films were also confirmed by Raman spectroscopic measurement (Figure 6.4B) showing typical spectra with a peak at 1333 cm^{-1} related to sp^3 carbon bonds. A couple of peaks observed at ~ 500 and 1200 cm^{-1} confirmed the existence of boron doping in the diamond structure.²⁰ No peak was observed at $\sim 1600\text{ cm}^{-1}$, which is generally attributed to “nondiamond” carbon, indicating that the BDD thin films were of fine quality. Homogeneous and well-dispersed Pt-NPs at the BDD surface were observed (Figure 6.4C). Highly regular Pt-NPs with uniform average diameter of around 800 nm (Figure 6.4D) can be measured.

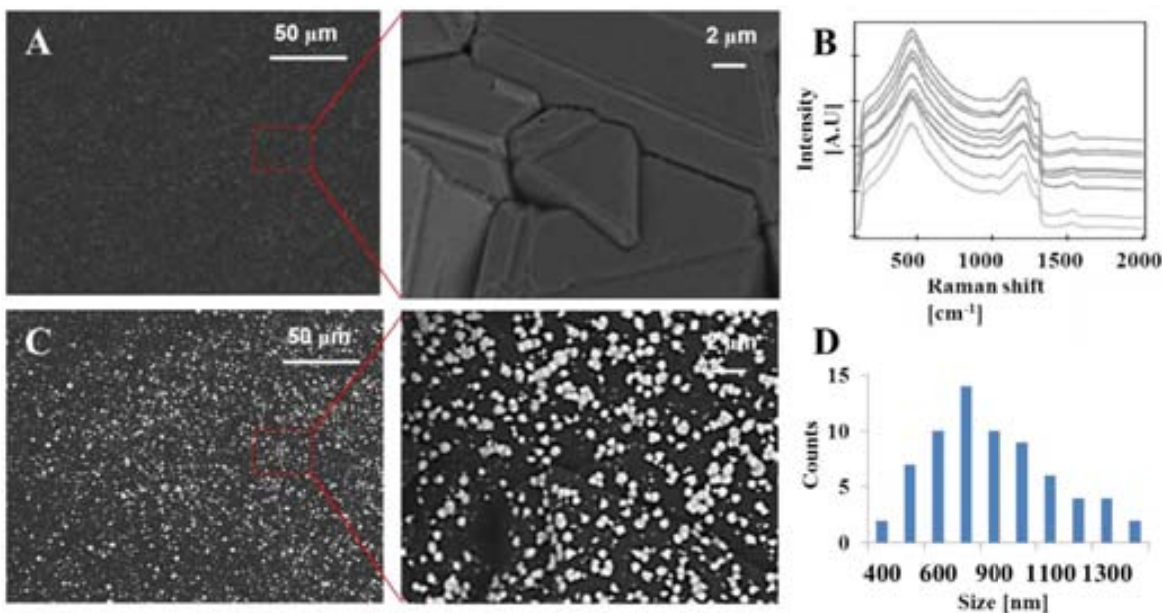


Figure 6.4. SEM images of (A) BDD surface without modification, (B) Typical Raman spectroscopy of boron-diamond electrode, (C) BDD modified with platinum nanoparticles (Pt-NPs) produced by electrodeposition of potassium tetrachloroplatinate (K_2PtCl_4) in PBS 0.1 M pH 7.0, at 25 mM. Inset (D) shows the Pt-NPs size distribution.

6.3.2. Optimization of experimental variables of the biosensor for atrazine detection based on ELISA immunoassay.

Figure 6.5A shows CVs of three different system: BDD without Pt-NPs (a), BDD Pt-NPs in presence of 8 mM hydrogen peroxide (b), and BDD Pt-NPs in presence of MBs conjugated with atrazine-HRP (without free atrazine), in presence of hydrogen peroxide 8 mM (c). The reduction peak for the MBs conjugated with atrazine-HRP appears at 250 mV when the electrode surface is modified with Pt-NPs; in contrast, no signal is observed using the bare electrode, which demonstrates that Pt-NPs are an essential component of the biosensor. Finally a simple measurement by injection of HRP at different concentrations with 0.5 mM H_2O_2 into microfluidic platform, and detection by amperometry was performed to confirm the operation potential in flow mode. When the HRP concentration increases the reduction peak magnitude increases (Figure 6.5B).

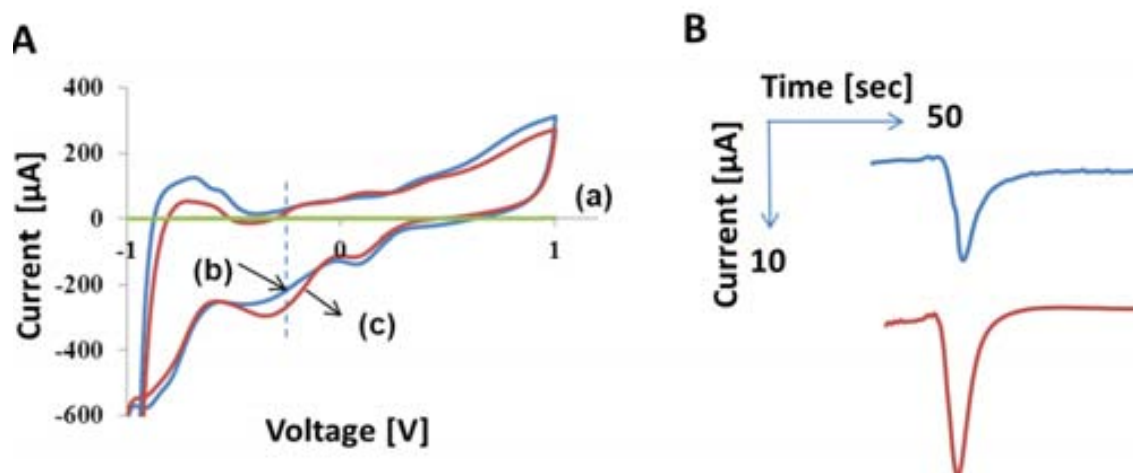


Figure 6.5. (A) Cyclic voltammogram for: (a) MBs conjugated with HRP in presence of H_2O_2 8 mM detection with BBD bare electrode, (b) H_2O_2 8 mM detection with BBD Pt-NPs electrode and (c) MBs conjugated with HRP in presence of H_2O_2 8 mM detection with BBD Pt-NPs electrode (b), and (B) Amperometry (with a fixed voltage of 250 mV) of HRP at (a) 25 nM and (b) 50 nM, in presence of the same concentration of hydrogen peroxide (0.5 mM).

6.3.3. Electrochemical magneto-immunosensing strategy

ELISA magneto immunoassay for atrazine detection is based on the competitive assay between the free atrazine and the Atrazine-HRP conjugate, for binding to a limiting number of antibody sites (against atrazine) coated onto magnetic beads. Following the protocol explained in the experimental section, electrochemical measurements were performed in order to characterize the magneto-immunoassay for atrazine detection. For this electrochemical experiment, cyclic voltammetry was used as electrochemical technique, observing a reduction peak at -250 mV with a slight shift to more negative potentials. When the atrazine concentration increases the reduction peak decreases (Figure 6.6A). From these results, we confirmed that the catalytic current was mainly due to the direct electron transfer from the HRP molecules. Since platinum nanoparticles allow efficient electron tunneling, they can also assist the electron transfer between the redox protein and the BDD electrode surface (see Figure 6.6B). In this case the catalytic current is inversely related to the atrazine concentration.

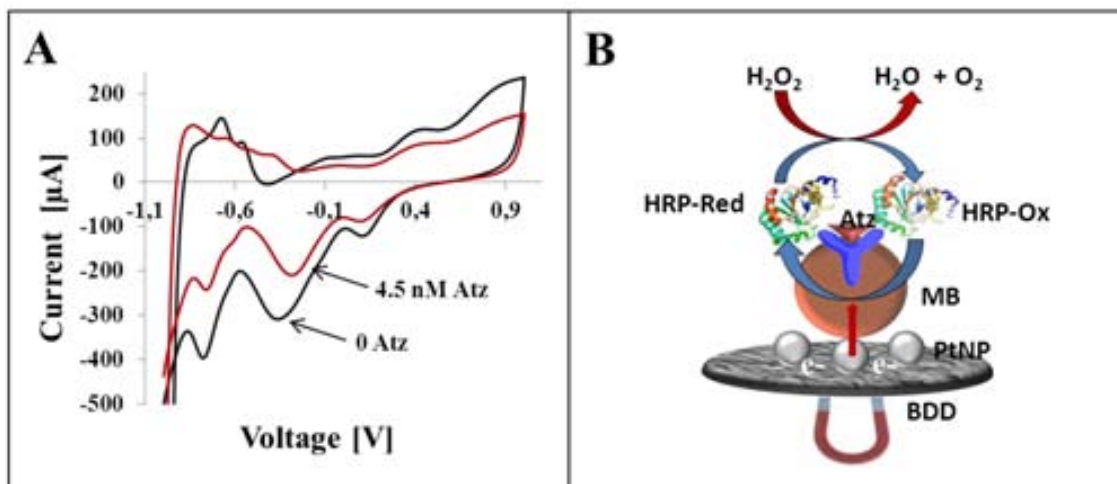


Figure 6.6. (A) Voltammogram of atrazine detection by using competitive magneto immunoassay in presence of H_2O_2 (8 mM) with and without 4.5 nM of atrazine. (B) Mechanism of atrazine electrochemical detection by magnetoimmunoassay using HRP as enzymatic label.

The calibration curve was obtained for the atrazine range between 0 to 45 nM in drop measurement format confirming again the behavior of the system (Figure 6.7A). The atrazine conjugation and the detection were performed also in batch mode to confirm the system operation. In this case the conjugate was prepared as was explained in the experimental section. The range of the checked atrazine concentrations was between 0.0045 and 45 nM. The already cleaned magneto-immunoassay after the conjugation was immobilized onto the working electrode by a magnet located behind the electrode. Then PBS with hydrogen peroxide 8 mM was dropped onto the electrode in order to perform the electrochemical measurement. Typical reduction peaks are shown in the range between -1 to 0 V.

The absorbance measurements (Figure 6.7B) using the atrazine kit were performed in order to compare both methods (electrochemical and colorimetric). It is observed that the absorbance decreases when the atrazine concentration increases which means that for higher amounts of free atrazine, less binding sites will be available in the antibody for the HRP-labeled atrazine. A LOD of 7.2 pM for optical measurements was obtained, similar to the LOD with electrochemical ones.

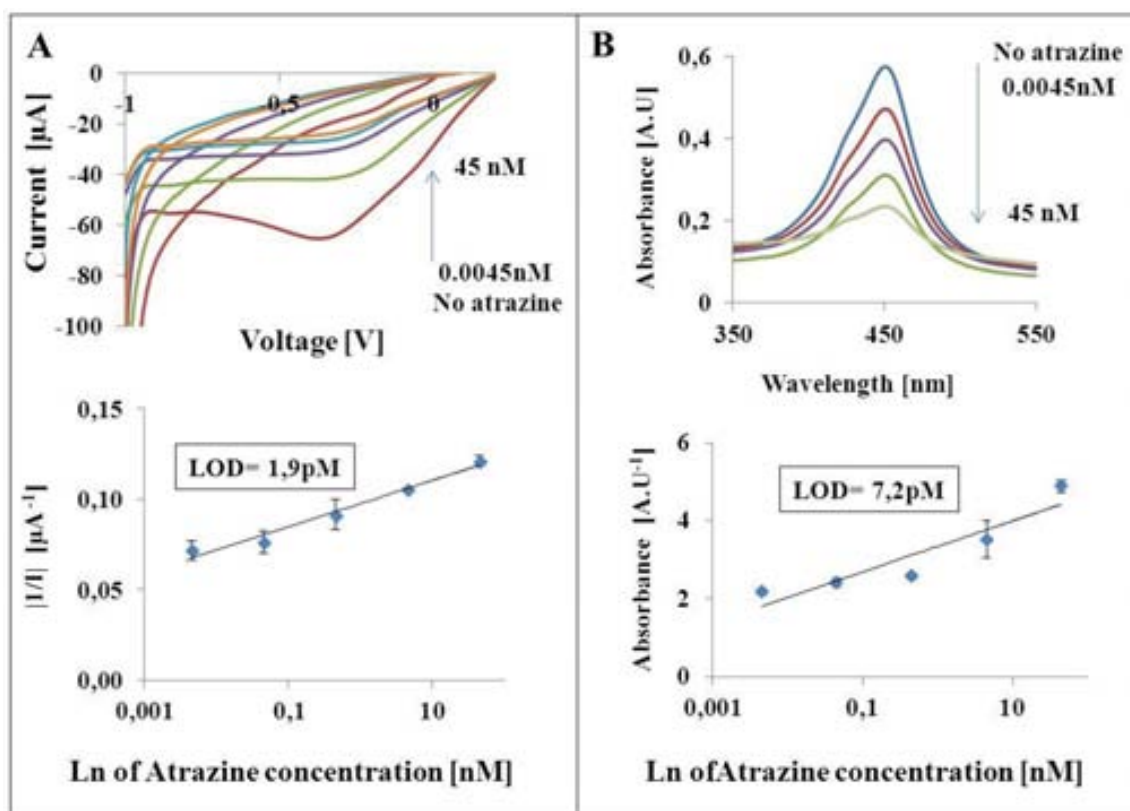


Figure 6.7. Atrazine detection using ELISA kit for atrazine detection. (A) Voltammogram of atrazine detection by using competitive magneto immunoassay in presence of H_2O_2 (8 mM) with previous reaction time of 20 min, the calibration curve from 0 to 45 nM of atrazine is also shown, and (B) Absorbance measurements by addition of TMB at the end of the conjugation step and its calibration curve. Volumes of sample for electrochemical and optical detection were 50 μL and 1 mL respectively.

6.3.4. Implementation of the ELISA magnetic immunoassay for atrazine detection by using a microfluidic chip with BDD Pt-NPs electrode as detection platform.

A simple and cheap microfluidic platform with hybrid screen-printed electrodes and BDD working electrode modified with Pt-NPs was fabricated and used for on-chip measurements. The system and the corresponding integration steps are shown in Figure 6.8 and set-up details explained in the experimental Section.

Once obtained the optimal parameters, ELISA magneto immunoassay for on-line atrazine detection was performed. On-chip measurements were done using -250 mV DC working potential; flow rate 50 $\mu\text{L min}^{-1}$ and injection volume of 5 μL . Well defined current vs. time peaks for different atrazine concentrations (from 4.5 pM to 45 nM) were observed (see Figure 6.8A).

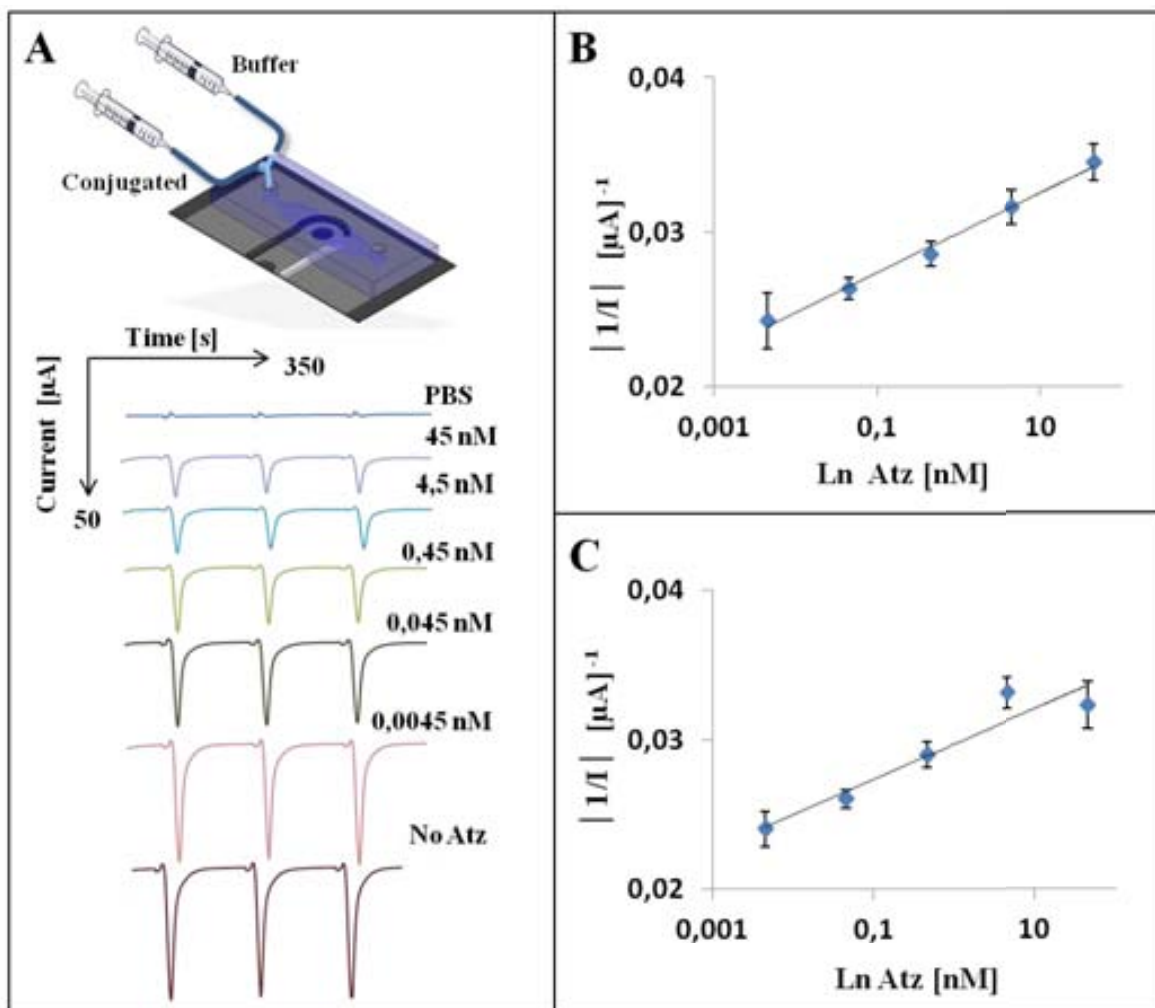


Figure 6.8. (A) Amperometry measurements performed at -0.25 V vs. Ag/AgCl reference electrode. Measurements done using microfluidic platform. Typical amperometric measurements for $5 \mu\text{l}$ of conjugated injection (three times repetitions), at different concentrations of atrazine from 0 to 45 nM, (B) calibration curve with error bars corresponding to repeatability of measurement at the same chip, and (C) calibration curve of atrazine detection with error bars corresponding to reproducibility between three different chips and conjugations.

The biosensors showed a rapid and sensitive electrocatalytic response, reaching steady-state current within 50 s after each sample addition step. To evaluate the repeatability and the reproducibility of this system, three different experiments were performed. The first one corresponds to a calibration curve for the microfluidic chip and the same ELISA magneto-immunoassay (see Figure 6.8B) showing good repeatability (RSD 3.73%), with a linear response range from 4.5 pM to 45 nM and $r^2=0.9928$. A second experiment was performed so as to evaluate the reproducibility of this system. Figure 6.8 C shows the repetition measurements by using three different chips, and different ELISA magneto-immunoassays in the same concentration range of atrazine resulting in a $r^2=0.91$ and a LOD of 4.5 pM

(1 pg mL^{-1}) of atrazine (RSD 4.46%). Environment Protection Agency (EPA) has set the limit of atrazine of drinking water in 3 ng mL^{-1} and 20 ng mL^{-1} for food.²¹

6.3.5. Implementation of the complete ELISA magnetic immunoassay for atrazine detection by using a micromixer coupled to the BDD Pt-NPs based detection platform.

An alternative micromixer to perform the conjugation steps for atrazine detection in flow mode reducing sample volume, assay times, and equipment requirements is shown in Figure 6.9. The micromixer fabrication was previously optimized (See Annex 5). After the mixing and incubation step, the sample is immobilized onto the working electrode in the detection chip based on BDD Pt-NPs electrode where a magnet is placed behind it. After the sample preconcentration, the buffer and $5\text{ }\mu\text{L}$ hydrogen peroxide were injected.

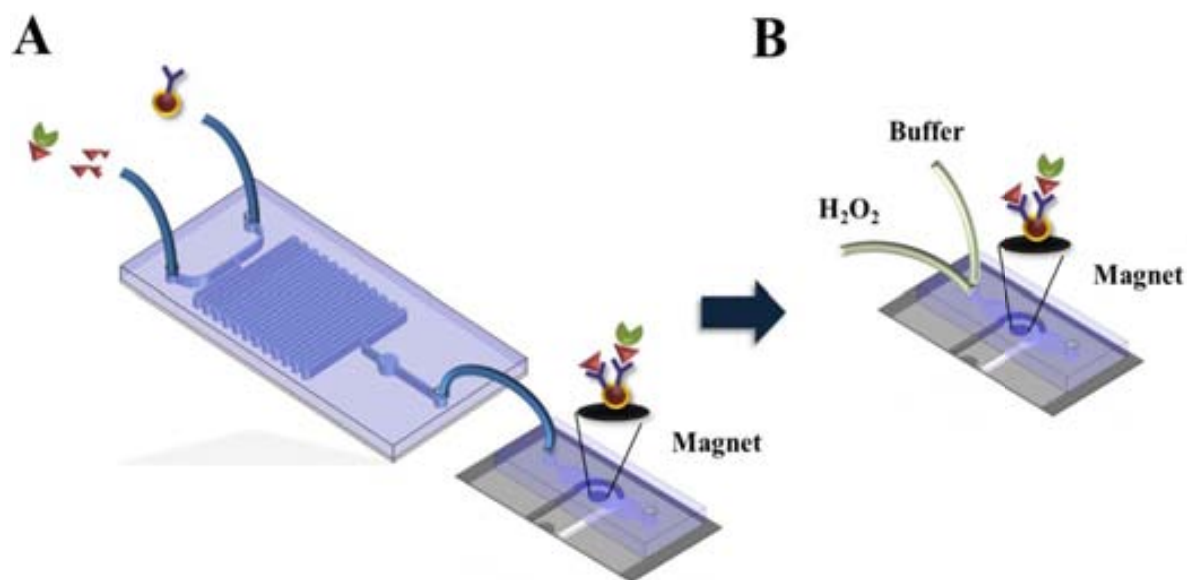


Figure 6.9. (A) Micromixer for the atrazine magnetoimmunoassay, and (B) the detection chip based on boron doped diamond electrode modified with Pt-NPs.

The complete microsystem showed a rapid and sensitive electrocatalytic response related to atrazine detection. To evaluate the repeatability and the reproducibility of this system, three measurements were performed (Figure 6.10A). The first one corresponds to the calibration curve for the microfluidic chip and the same ELISA magneto-immunoassay (see Figure 6.10B) showing good repeatability (RSD 4.2%), with a linear response range between 0.9 nM and 4.5 nM and $r^2=0.9683$. For this system the achieved LOD was 3.5 pM . The LOD is in the same range as the one achieved by the previous system when all the incubations steps were performed in batch mode.

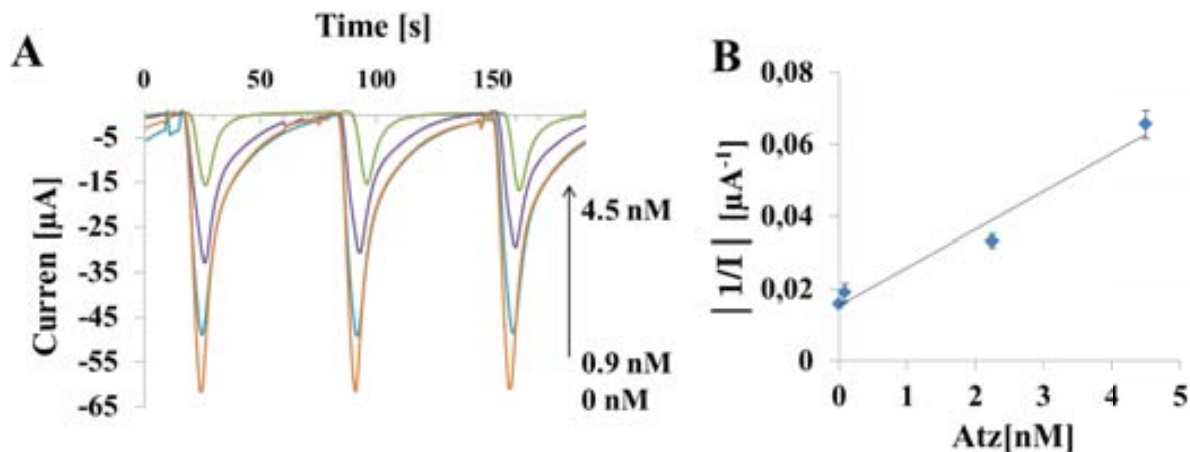


Figure 6.10. (A) Peaks related with the atrazine concentration after the conjugation into the micromixer and (B) the corresponding calibration curve.

6.4. Conclusions

The well-known electrochemical properties of BDD electrodes modified with platinum nanoparticles (Pt-NP) (to render it catalytic to the direct electron transfer from the HRP molecules) are demonstrated for the first time with even higher efficiency in a microfluidic platform than in batch. This new LOC system with a simple in-chip integrated BDD electrode is used to increase the sensitivity for atrazine pesticide detection showing clear advantages in comparison to other measuring formats such as in drop / batch ones that require a volume sample of at least 10 times bigger and that show lower sensitivity. This fluidic microsystem platform with the integrated BDD electrode is easy to be fabricated, disposable and amenable to mass production. Very sensitive amperometric detection allowed atrazine determination at very low concentration (0.1 pM). The developed system uses a very low DC potential, decreasing in this way the effect of interferences. In addition, the use of a magneto-immunoassay assures specific detection. By using the microfluidic platform, a reduction of the LOD in comparison to the ELISA format (72-fold) and drop measurements (20-fold) and LODs 10 times lower than those reported in the literature (see Table 1) have been achieved. Finally, the lower reagent consumption, inherent to the miniaturization and the versatility represent the main advantages of the developed device which could be used in the future in automatic control systems with interest for environment monitoring among other applications.

Table 6.1. Comparison between similar systems for atrazine detection founded in the literature.

Detection Method	Transducer	LOD	Immunoassay format	REF.
Optical detection	Nanocantilever (Beam deflection)	1 pg mL ⁻¹	Immunoassay – label free	[22]
Admittometric Electrochemical Determination	Multi walled carbon nanotube /Au NPs and ionic liquid on glassy carbon electrode surface	20 pM	Immunoassay with enzymatic label	[23]
Thermometric biosensor	Thermistor	0.4µg mL ⁻¹	Immunoassay with enzymatic label	[24]
Cyclic voltammetry	Glassy carbon	27 pM	Magnetic immunoassay with enzymatic label	[25]
Pulse amperometry	Gold electrodes made by photolithography	0.45 nM	Direct detection	[26]
Quartz crystal microbalance	Dual-electrode pattern was screen printed onto 10 MHz quartz discs with gold paste	0.33mg mL ⁻¹	By replica antibody (plastic molding of immunoassay)	[27]
Amperometry	BDD Pt-NPs electrode integrated into microfluidic platform	0.1 pM (0.45pg mL ⁻¹)	Magnetic immunoassay with enzymatic label	This work

6.5. References

-
- ¹F. Hernandez, C. Hidalgo, J. V. Sancho, and F. J. Lopez. *Coupled-column liquid chromatography applied to the trace-level determination of triazine herbicides and some of their metabolites in water samples*. *Anal. Chem.*, 1998, 70, 3322-3328.
- ²S. K. Papiernik, R. F. Spalding. Atrazine, Deethylatrazine, and Deisopropylatrazine Persistence Measured in Groundwater in Situ under Low-Oxygen Conditions. *J. Agric. Food Chem.*, 1998, 46, 749-754.
- ³S.E. George, R.W. Chadwick, M.J. Kohan, J.C. Allison, S.H. Warren, R.W. Williams. Atrazine treatment potentiates excretion of mutagenic urine in 2,6-dinitrotoluene-treated Fischer 344 rats. *Environ. Mol. Mutagen.*, 1995, 26(2), 178-184.
- ⁴R.P. Baldwin. *Recent advances in electrochemical detection in capillary electrophoresis*. *Electrophoresis*, 2000, 21, 4017-4028.
- ⁵N. Maleki, G. Absalan, A. Safavi, E. Farjami. *Ultra trace adsorptive stripping voltammetric determination of atrazine in soil and water using mercury film electrode*. *Anal. Chim. Acta*, 2007, 581, 37-41.
- ⁶A. Merkoçi. *Nanoparticles-based strategies for DNA, protein and cell sensors*. *Biosens. Bioelectron.*, 2010, 26, 1164-1177.
- ⁷G. Aragay, J. Pons, and A. Merkoçi. *Recent trends in macro-, micro-, and nanomaterial-based tools and strategies for heavy-metal detection*. *Chemical Reviews*, 2011, 111 (5), 3433-3458.
- ⁸G. Aragay, F. Pino, and A. Merkoçi. *Nanomaterials for Sensing and Destroying Pesticides*. *Chemical Reviews*, 2012, 112 (10), 5317-5338.
- ⁹A. Merkoçi, and J. P. Kutter. *Analytical miniaturization and nanotechnologies*. *Lab Chip*, 2012, 12, 1915-1916.
- ¹⁰M. Medina-Sánchez, S. Miserere, A. Merkoçi. *Nanomaterials and lab-on-a-chip technologies*. *Lab Chip*, 2012, 12, 1932-1943.

-
- ¹¹ X. Llopis, M. Pumera, S. Alegret, A. Merkoçi. *Lab-on-a-chip for ultrasensitive detection of carbofuran by enzymatic inhibition with replacement of enzyme using magnetic beads*. *Lab Chip*, 2009, 9, 213-218.
- ¹² A. Ambrosi, M. Guix, A. Merkoçi. *Magnetic and electrokinetic manipulations on a microchip device for bead-based immunosensing applications*. *Electrophoresis*, 2011, 32 (8), 861-869.
- ¹³ Y. Zou, C. Xiang, L. X. Sun, and F. Xu. *Glucose biosensor based on electrodeposition of platinum nanoparticles onto carbon nanotubes and immobilizing enzyme with chitosan-SiO₂ sol-gel*. *Biosens. Bioelectron.*, 2008, 23, 1010-1016.
- ¹⁴ S. Min-Jung, K. Jong-Hoon, L. Seung-Koo, L. Dae-Soon, H. Sung Woo, and W. Dongmok. *Analytical Characteristics of Electrochemical Biosensor Using Pt-Dispersed Graphene on Boron Doped Diamond Electrode*. *Electroanal.*, 2011, 23, 10, 2408-2414.
- ¹⁵ S. Fierro, M. Yoshikawa, O. Nagano, K. Yoshimi, H. Saya, and Y. Einaga. *In vivo assessment of cancerous tumors using boron doped diamond microelectrode*. *Sci. Rep.* 2012, 2, 901.
- ¹⁶ A. Suzuki, T. A. Ivandini, K. Yoshimi, A. Fujishima, G. Oyama, T. Nakazato, N. Hattori, S. Kitazawa, and Y. Einaga. *Fabrication, characterization, and application of boron-doped diamond microelectrodes for in vivo dopamine detection*. *Anal. Chem.*, 2007, 79, 8608-8615.
- ¹⁷ Y. Xia and G. M. Whiteside. *Soft lithography*. *Annu. Rev. Mater. Sci.*, 1998, 28, 153-184.
- ¹⁸ L. Tang and N. Yoon Lee. *A facile route for irreversible bonding of plastic-PDMS hybrid microdevices at room temperature*. *Lab Chip*, 2010, 10, 1274-1280.
- ¹⁹ K. Grennan, G. Strachan, A. J. Porter, A. J. Killard, and M. R. Smyth. *Atrazine analysis using an amperometric immunosensor based on single-chain antibody fragments and regeneration-free multi-calibrant measurement*. *Anal. Chim. Acta* 500, 2003, 287-298.
- ²⁰ Y. Einaga. *Diamond electrodes for electrochemical analysis*. *J. Appl. Electrochem.*, 2010, 40, 1807-1816.
- ²¹ US Environmental Protection Agency, National survey of pesticides in drinking water wells, phase II report, EPA 570/9-91-020, National Technical Information Service, Springfield, VA, 2011.

²²Raman Suri, J. Kaur, S. Gandhi and G. S Shekhawat, *Label-free ultra-sensitive detection of atrazine based on nanomechanics* Nanotechnology, 2008, 19, 235502-235508.

²³ P. Norouzi, B. Larijani, M. R. Ganjali, and F. Faridbod, *Admittometric Electrochemical Determination of Atrazine by Nano-composite immune-biosensor using FFT-Square wave Voltammetry*. Int. J. Electrochem. Sci., 2012, 7, 10414 – 10426.

²⁴ E. Zacco, M. I. Pividori, and S. Alegret, *Electrochemical magnetoimmunosensing strategy for the detection of pesticides residues*. Anal. Chem., 2006, 78, 1780-1788.

²⁵ Z. Qie, B. Ning, M. Liu, J. Bai, Y Peng, N. Song, Z. Lv, Y. Wang, S. Sun, X. Su, Y. Zhang, and Z. Gao, *Fast detection of atrazine in corn using thermometric biosensors*. Analyst, 2013, 138(17), 5151-5156.

²⁶ I. Kamrul, K. J. Sandeep, C. Rohit, H. Dawoon, and K. Yong-Sang, *Fast detection of triazine herbicides on a microfluidic chip using capillary electrophoresis pulse amperometric detection* Microelectronic Engineering, 2012, 97, 391–395.

²⁷ R. Schirhagl, U. Latif and F. L. Dickert, *Atrazine detection based on antibody replicas*. J. Mater. Chem., 2011, 21, 14594.

CHAPTER 7. INK-JET BASED BIOSENSING PLATFORM	169
7.1. Introduction	171
7.1.1. Principle of operation.....	172
7.2. Experimental Section.....	174
7.2.1. Reagents.....	174
7.2.2. Instruments.....	174
7.2.3. Dielectric layer optimization	174
7.2.4. OTFTs Fabrication.....	175
7.2.5. MMAcoMAA functionalization and label-free immunoassay	176
7.3. Results and Discusssion	177
7.3.1. BioOTFT fabrication	177
7.3.2. Dielectric layer optimization	179
7.3.3. SEM Characterization of the different TFT layers	182
7.3.4. Electrical characterization of OTFT	183
7.3.5. MMA Functionalization	184
7.3.6. Label free immunoassay	186
7.4. Conclusions	190
7.5. References	191

CHAPTER 7**INK-JET BASED BIOSENSING PLATFORM***Related Publications*

M. Medina-Sánchez, E. Ramon, A. Alcalde-Aragonés, S. Miserere, C. Martínez-domingo, J. Carrabina, and A. Merkoçi. “Ink-jet printed field effect transistor for biosensing applications”. MICROTAS proceedings, Japan (2012). (Annex 1).

C. Martínez-Domingo, M. Medina-Sánchez, A. Alcalde-Aragonés, J. Carrabina, H. L. Gomes, A. Merkoçi and E. Ramon. “Material characterization and electrochemical performance for inkjet printed organic ISFET-based biosensor”. In preparation (2013). (Annex 2).

M. Medina-Sánchez, E. Ramon, A. Alcalde-Aragonés, S. Miserere, C. Martínez-domingo, J. Carrabina, and A. Merkoçi. “Double gate inkjet Bio-OTFT transistor for label-free protein detection”. In preparation (2013). (Annex 2).

In this chapter we report a flexible organic double gate Bio-Organic-Thin-Film Transistor (Bio-OTFT) developed mainly by inkjet technology onto a flexible substrate. This kind of organic transducers has important advantages for biosensors in terms of fabrication cost and biocompatibility. To demonstrate the applicability of this device in the biological field, we have functionalized it with a capture antibody which detects a model protein without any label. The device fabrication, considering the structure, materials optimization, electrical characteristics, and functionalities are also discussed.

7.1. Introduction

Organic Electronics (OE) is a branch of materials science; it gives thin and flexible devices being an environmental friendly technology. OE differs from the traditional electronics as it uses organic charge transfer complexes instead of inorganic conductors and semiconductors. OE allows the production of a wide range of low cost electrical components. It is a rapidly expanding area because of their wide range of applications, including intelligent textiles, antennas, electronics, and sensors¹. One of the most important structures made by this technology is the thin film field effect transistor (TFT), which is a powerful single element in semiconductor manufacture and the base for a great number of electronic devices: memories², photovoltaic³, logic gates⁴, sensors⁵, etc.; however some new challenges, such as the high operating voltage requirement, material stability and lifetime are appearing.

The Organic Thin Film Transistors (OTFTs) development in the last decade has also been an interesting research field in biosensing applications that is achieved by replacing the gate by an electrolyte and a reference electrode⁶. By functionalizing OTFT with biological materials, a Bio-OTFT can be obtained⁷. The main advantage of TFT based biosensor is the possibility to get an all-integrated, portable and low cost system, compatible with the “single-use sensor” concept. In addition, these devices are generally fabricated by photolithography methods that require expensive masks and clean room facilities. To overcome these issues an inkjet based TFT for biosensing applications is proposed.

In general the Bio-Field-effect-transistors (BioFETs) to be used as biomedical devices require specific interactions between biological molecules used as receptors and the analyte contained in the sample fluid. Up to date the fabrication of such biosensors has involved the assembly of many parts making them expensive and non-reproducible. Recently, the production of BioFETs has moved to fabrication and production processes with high throughput and integration level. Indeed traditional silicon-based semiconductor electronics tend to be replaced by organic, hybrid and flexible printed electronic methodologies. Among examples of biosensors fabricated with these new technologies is the development of electrochemical biosensor based on gold electrodes by inkjet printing onto polyimide

(PI) substrate, for detection of a cancer biomarker such as interleukin-6 (IL-6) in serum⁸. Organic field effect transistors are also used for glucose detection. A simple poly(3,4-ethylene dioxythiophene)/poly(styrene sulfonic acid) based transistor was used for glucose detection through a mechanism that involves sensing of hydrogen peroxide⁹.

Regarding the deposition of organic materials¹⁰ several technologies such as inkjet-printing¹¹ screen-printing¹², micro contact-printing¹³, gravure and flexography¹⁴ beside lithography's such as scanning probe¹⁵, photo and e-beam and laser printing have been extensively studied. Between them, inkjet printing has become one of the most promising techniques capable of manufacturing devices by using small volumes of ink, in a rapid and additive procedure, achieving high pattern precision and resolution with greater reproducibility. Inkjet printing technology is very well suited for research, being a mask-less technology oriented to rapid prototyping for production¹⁶. It is a good alternative for depositing a wide range of materials which could have different functionalities (electrical, chemical, optical, biological, etc.). The materials can be soluble liquids, dispersions of small particles or nanoparticles, melts or blends. Some types of functional molecules, such as conductive and semiconductive polymers or large biomolecules cannot be deposited by the conventional vacuum deposition techniques, and need to be deposited by using a solution based technique.

In the biosensing field, there are two main strategies for protein analysis, label-based¹⁷ and label free immunoassays^{18,19,20}. The label-based method requires molecules like fluorescent dyes²¹, radioisotopes²², quantum dots²³, etc., to detect protein concentration in an indirect way. On the other hand, label-free techniques measure the inherent property of the primary transducing signal itself (mass, conductivity, dielectric characteristics). Here, we present the development a flexible transducer prototype for label-free protein detection. The device was tested by using a model protein (Human immunoglobulin G (HIgG)), as a proof of concept.

The detection of the mentioned model protein is based on the use of specific antibodies immobilized onto the transducer surface of a FET (specifically onto the dielectric material). The detection of proteins in a point-of-care application will allow an early diagnosis achieving prompt treatments of patients²⁴.

7.1.1. Operation principle

BioOTFT or BioFET is based on the electrolyte–insulator–semiconductor field-effect transistor (EISFET) that ensures the electrical detection of the biomolecular interactions by their capacitive coupling with the organic semiconductor. A scheme of this device with its respective layers is shown in Figure 7.1A. It consists in two integrated conventional FET

structures that include source, drain and two gates (Figure 7.1Aa,b). However, in this device, the top gate contact is replaced by an electrolytic solution (phosphate buffer saline, PBS), an antibody-protein conjugate and a reference electrode. The amount of accumulated charge on the dielectric gate in the BioFET can result in an increase (or decrease) of the source-drain current. This would create variations in the transistor responses (I-V curves) that are proportional to the amount of the introduced charge. If the change of the electrical charge is related to the interaction between biological molecules, then it can be used to monitor this process effectively and with very high sensitivity.

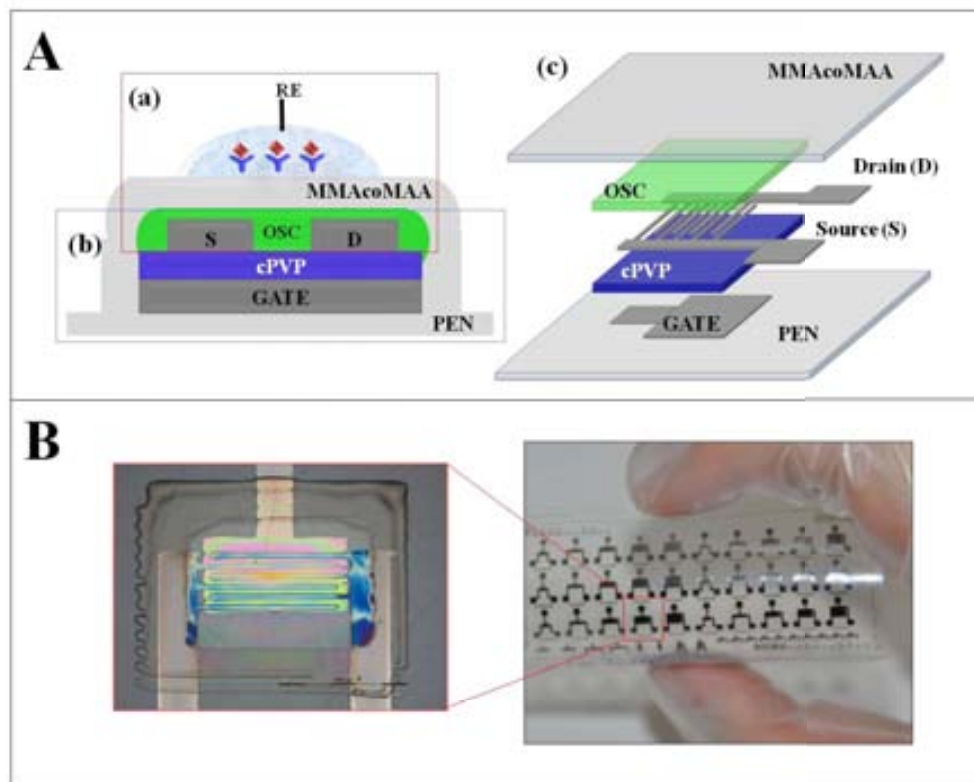


Figure 7.1. (A) Scheme of the double gate OTFT (a) BioFET (top OTFT), (b) bottom OTFT and (c) double gate OTFT layers. and (B) Device pictures. The OTF channel dimensions used were; $W/L = 20.000 \mu\text{m} / 40 \mu\text{m}$ and $W/L = 40.000 \mu\text{m} / 40 \mu\text{m}$. Where W is the channel width and L the channel length. Materials shown are: OSC: organic semiconductor; MMAcoMAA: Methylmetacrylate copolymer; PEN: polyethylenephthalate; cPVP: cross linked poly-4-vinylphenol; and RE: reference electrode.

The developed structure has two main advantages; the first one is the possibility to be miniaturized for future complex circuit applications. In addition, for biosensing purposes, the bottom OTFT was used as performance checking device, in order to ensure that the organic semiconductor is working properly. In some cases, the double gate is suitable for the current control. Finally, it can also be useful as a fix parameter for biosensor response normalization, due to the high device variability. A picture of the printed sheet is also shown in figure 7.1B.

7.2. Experimental Section

7.2.1. Reagents

The BioFET layers were deposited by using different inks: For the gate, drain and source contacts, 20 % weight silver nanoparticle solution (EMD5603) from Sunchemical Inc., Spain, was used. Cross-linked poly-4-vinylphenol (PVP) $\overline{M}_w = 25000$, and Metil metacrylate copolymer (MMAcoMAA 8.5 EL9) purchased in Sigma Aldrich and MicroChem, Spain, respectively, were used as dielectric materials. The active channel was fabricated using an amorphous polymer p-type semiconductor (FS 0027) provided by FlexInk Inc., Spain, propylene glycol monomethyl ether acetate (PGMEA) and poly(melamine-co-formaldehyde) methylated (pMFM sol. 84% in 1-butanol) were purchased in Aldrich, Spain. 0.2 μm Whatman filter was from Millipore, Spain, and finally, the substrate was a flexible PEN substrate obtained from Dupont Teijin Teonex Q65FA, Japan.

Acid orange II dye, microparticles based on polystyrene (1 μm diameter, in aqueous solution, 10 % solids and density of 1.05 g cm^3), bovine serum albumin (BSA) labeled with ALEXA 555 fluorophore, 3-Aminopropyl)triethoxysilane (APTES), casein, capture antibody (Anti-human IgG produced in goat) and Human IgG (analyte), ethyl(dimethylaminopropyl) carbodiimide (EDC), and N-Hydroxysuccinimide (NHS) were purchased in Sigma Aldrich, Spain.

7.2.2. Instruments

Fujifilm Dimatix DMP2831 desktop printer, USA was used as a printing setup. It uses one user-fillable piezo-based inkjet print cartridge with 16 nozzles, able to jet 1 pL or 10 pL drops of a wide range of fluids with a variable jetting resolution. The drop-on-demand printing was undertaken in a class 10000 cleanroom laboratory environment. The printer includes an alignment system to avoid layer misalignment when sample is moved for curing processes or cartridge change. Electrical measurements were performed using a semiconductor analyzer B1500A Agilent and Agilent E4980A LCR meter, Spain.

7.2.3. Dielectric layer optimization

In order to choose a biocompatible material and at the same time to keep dielectric characteristics that do not affect the TFT working function, different dielectrics were tested by using a simple structure based on capacitance measurements. It consists in a first conductive layer, a dielectric (NOA 68, polyester resin, PMMA, CYTOP, PVP, and MMAcoMAA) deposited by spincoating, and finally, a drop of 2 μL of electrolyte (acetate buffer with pH 4.0, and PBS with 7.4) that was placed onto the dielectric and contacted

with an external reference electrode (Pt wire 0.2 mm of diameter) to perform different electrical measurements such as I-V curves and parallel capacitance (C_p) and resistance (R_p) at 1 KHz. The main goal of these measurements was to study the leakage current through dielectric.

Additionally, scanning electron microscope (SEM) analysis was performed by using a MAGELLAN SEM (USA) to characterize each layer and know the real thickness and morphological details.

7.2.4. OTFTs Fabrication

A complete double gate OTFT (see Figure 7.2) with silver nanoparticle bottom gate, source and drain electrodes, a polymeric organic semiconductor and two dielectric layers was fabricated. One of these layers is deposited between the bottom gate and source-drain contacts and it is based on cPVP. The second one is based on MMAcoMAA 8.5 EL9 (chosen materials after the optimization) and it was deposited after the semiconductive layer. Finally, the Pt electrode was used as a reference, which is in contact with the electrolyte. Briefly, the fabrication steps are explained as follow:

Prior to the printing, the PEN foil was cleaned with ethanol during few seconds. Then the cleaned foil was dried with nitrogen in order to remove remaining particles from the substrate. First, the bottom gate was deposited by inkjet on the PEN substrate using a silver nanoparticle solution with an average height of about 450 nm and sintered at 130°C during 30 min in a convection oven (Figure 7.2A).

To prepare cPVP, PVP was dissolved in PGMEA at room temperature in a concentration of 55 mg mL⁻¹. Then the crosslinker, pMFM, was added to the PVP solution with a concentration of 15.4 mg mL⁻¹ suspended in PGMEA. The solution was stirred for 30 min and then diluted 1:1 in PGMEA to obtain the appropriate physical properties required to be ink-jetted. The cPVP solution was filtered, deposited by inkjet printing and baked at 200 °C for 20 min yielding 300 nm cross-linked PVP. (Figure 7.2B).

The next step was to deposit the drain-source electrodes by inkjet. Silver can be printed onto cPVP without any surface pre-treatment. The printing conditions and post-printing procedure were the same that the bottom gate process (Figure 7.2C). The active channel was fabricated using an amorphous polymer as p-type semiconductor already mentioned in the Reagents part. This material was deposited by inkjet method after a necessary treatment with O₂ (60 %) Plasma (25 W) for 30 s, and cured on a hot plate for 15 min at 120 °C (Figure 7.2D). On the other hand, dielectric ink MMAcoMAA, based on 9 wt% methyl methacrylate, 8.5 wt% methacrylic acid and ethyl lactate as solvent was deposited onto the

INKJET BASED BIOSENSING PLATFORM

semiconductive layer. The polymeric solution was spincoated onto the substrate and baked at 150 °C for 90 s on a hot plate (Figure 7.2 E). The thickness of the MMAcoMAA dielectric layer was optimized and characterized by scanning Electron Microscopy (SEM). The dielectric breakdown and the semiconductor dielectric interface were characterized by electrical measurements.

For operation in aqueous media for bio-chemical sensing experiments, a solution of 0.1 M freshly prepared phosphate buffered saline (PBS - Aldrich) solution at pH 7.4 was used as electrolyte and incubation buffer. Regarding pH evaluation tests, pH 7.4 and pH 4 (acetate buffer with adjusted pH by using HCl 1M) were tested to evaluate the device performance at two different pH, and in this way to detect proteins with different isoelectric points for future applications.

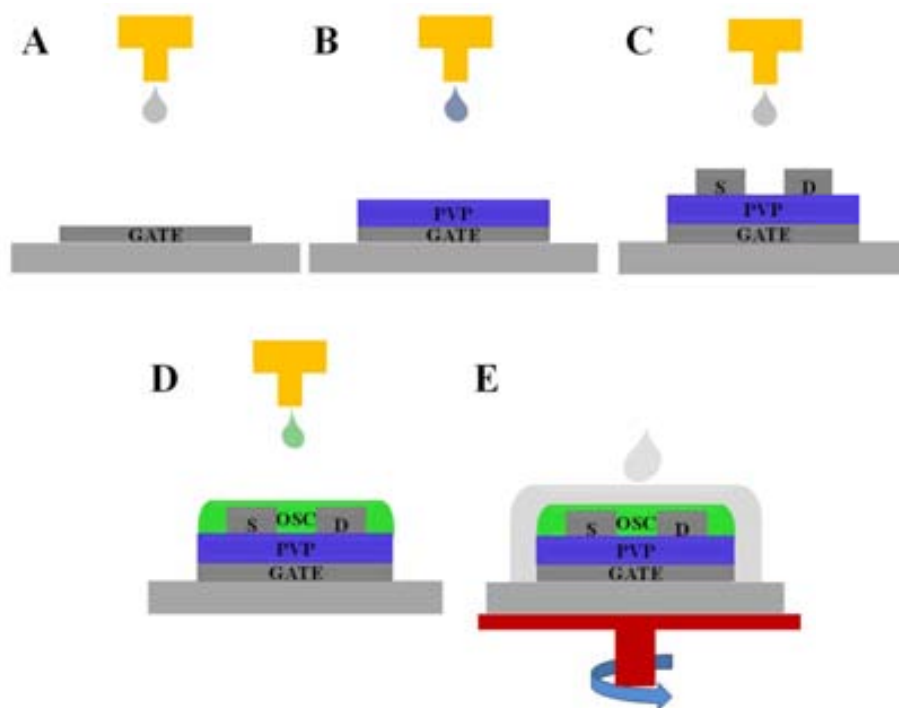


Figure 7.2. Fabrication steps (A) bottom gate based on silver ink deposited by inkjet, (B) dielectric based on cPVP deposited by inkjet, (C) silver source-drain contacts deposited by inkjet, (D) semiconductor channel deposited by inkjet, and (E) MMAcoMAA dielectric deposited by spin coating.

7.2.5. MMAcoMAA functionalization and label-free immunoassay

MMAcoMAA functionalization for protein immobilization was performed. It consists in plasma oxidation of the MMAcoMAA layer followed by an incubation using 3-aminopropyltriethoxysilane (APTES). Different concentrations of amino-groups were compared and characterized by a colorimetric method for quantification of amine groups by

using acid orange II dye. This method consist in the immersion of the substrate with the APTES modified MMAcoMAA within water with pH 3 (setted by HCl 1M), and containing acid orange II (AO). After shaking overnight at least for 12 h at room temperature, samples were washed twice with the acidic water. In order to dissolve the adsorbed AO, they were shaken for 15 min at room temperature in water with pH 12, set by NaOH. The AO concentration (which is similar to the amine concentration of the surfaces) of the solution was colorimetrically determined with an optical spectrometer at 485 nm²⁵. This functionalization was also confirmed by different methods such as polystyrene microparticles immobilization, contact angle and AFM studies.

Once the optimal parameters for producing amino groups onto the MMAcoMAA surface were obtained, 15 µL of anti-human IgG produced in goat (0.5 mg mL⁻¹) were put in contact to covalently bind them with the amino groups through EDC chemistry by the addition of EDC-NHS in PBST (135 µL at a concentration of 5 mg mL⁻¹ each one) for 30 min at room temperature. Then, the already modified surface was blocked with PBS supplemented with 5% (w/v) casein and 0.005% (v/v) Tween 20 for other 30 min. Among the previous incubations, a washing step was performed by using PBS supplemented with Tween 20 at 0.05% (v/v) (PBST). Finally, the analyte (Human IgG) incubation was performed during 30 min and washed with PBST to remove the analyte excess. All of the incubation steps were done by drop casting onto the APTES modified MMAcoMAA surface.

7.3. Results and Discussion

7.3.1. BioOTFT fabrication

Printing parameters can be tailored in order to define the optimal morphologies even the intrinsic constraints of the materials. To explain this relation it is necessary to take into consideration all the variables that affect the transfer characteristic in the saturation regime.

$$I_{DS} = \mu \cdot C_i \cdot \frac{w}{L} \cdot \frac{(V_G - V_\tau)^2}{2}$$

where, I_{DS} is the drain-source current (amperes), μ is the field effect mobility (cm²/(V.s)), C_i is the capacitance per unit area of the insulating layer (F/cm²), w is the channel width of the transistor (µm), L is the channel length of the transistor from source to drain in the direction of the current flow (µm), V_G is the gate voltage and V_τ is the threshold voltage (V), is the V_G corresponding to the opening of the conduction channel. Thus the most important parameters are related with the dimensions of the device including the thickness of each layer.

INKJET BASED BIOSENSING PLATFORM

In inkjet printing processes it is well known that the relative distribution of the material across the printed geometry can be controlled by temperature and drop-on-demand delays changing the cartridge or plate temperature as well as the frequency and voltage of nozzles activation (inkjet machine parameters). Other important parameters can be changed to achieve better features: the drop spacing, the viscosity, ink concentration, surface tension, and waveform of piezoelectric printhead (related with the dispensed volume and its velocity to drop it) to obtain a good bead expelling without ink spreading. Drop spacing is the distance between two consecutively printed drops and it is scaled by the wetting diameter of the drop on the substrate; the jetting frequency is inversely proportional to the delay period of the consecutive expelled beads; drop lattice is related with the pixel lattice in the designed pattern, which could be adjusted geometrically depending of the ink deposited per area unit, and the platen temperature related with the solvent evaporation rate which can affect the ink spreading and coffee ring effect²⁶.

Parameters as dots size (depending of the cartridge capacity 1 pL or 10 pL) between 20 and 40 μm , the resolution (100 to 5080 dpi), accuracy (10 μm), maximum cartridge volume of 1.5 mL, cartridge temperature up to 70°C, holder maximum temperature of 60°C and maximum substrate size of 210x315 mm are already defined for the inkjet machine specifications and they were modified to obtain the most accurate and well-defined features. The used inkjet machine consists of a piezoelectric transducer for the drop ejection that is actuated by a voltage pulse; the frequency of this pulse is in the range from 1 to 20 kHz for the commercial printing machine. This ejection is controlled by a waveform which is defined in the inkjet machine software. This waveform is divided into four segments with properties like duration, level and slew rate. The applied voltage is related with the volume pumped by each nozzle (the correct voltage depends of the ink viscosity) and the slew rate is related with the velocity of this ejection. These parameters directly affect the drop formation.

The ink viscosity is usually adjustable by modifying the solvent or the material concentration in the fluid. Although low viscosity fluids are desirable for jetting purposes, the high viscosity guarantees the reduced droplet spreading when the fluid lands on the substrate. The control of this parameter is critical since the droplet condition strongly influences the film uniformity. Therefore, a good ejecting quality is usually characterized by small ejecting drop volume variation among the generated droplets, no wetting of nozzle plate during ejection, uniform droplet velocity from droplet to droplet, absence of satellite droplets, straight droplet trajectory along the nozzle/substrate direction and long term ejecting stability, including during the on / off cycles.

After setting-up the inkjet machine parameters the substrate selection was done. The commonly used materials are glass, plastics such as PET due to its low cost, or PEN for its low surface roughness, but a wide variety of materials can be used. However, the interaction between the deposited ink and the substrate surface is very important in the

deposition printing optimization, as well as the drying process which is controlled by the “coffee-ring” effect²⁷, which describes the propensity of the solute to flow out towards the droplet edge through a capillary flow during drying. This occurs due to the maximum of the evaporation rate (Figure 7.3).

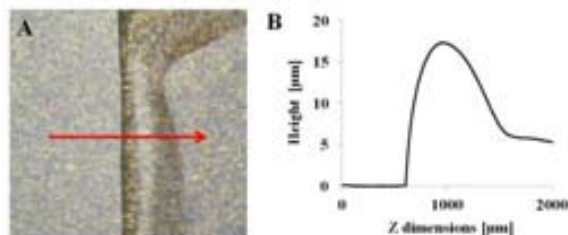


Figure 7.3. Coffee ring effect (A) picture of a printed structure, and (B) edge profile.

7.3.2. Dielectric layer optimization

A simple test was firstly done for the dielectric material pre-selection, taking into account the compatibility with the biomolecules and keeping dielectric characteristics that do not affect the FET working function. In Figure 7.4A a Metal-Insulator-Electrolyte (MIE) scheme of the testing structure for dielectric characterization is showed. For this purpose, materials such as NOA 68, polyester resin, and PMMA were deposited onto silver contact and put in contact with the electrolyte. After the voltage application (0 to -20 V) the material surface characteristics were observed by optical microscopy as well as by current measurements. The previous materials were discarded due to the presence of many pinholes when the potential was applied, opening a bias between the reference electrode and the silver contact (See Figure 7.4, B,C and D).

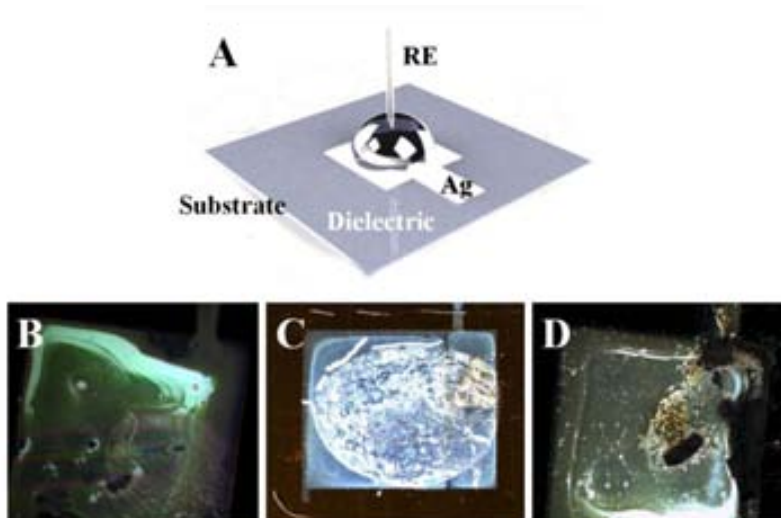


Figure 7.4. (A) Metal-Insulator-Electrolyte (MIE) scheme of the testing structure for dielectric characterization; Pictures of the tested structures during dielectric characterization studies performed after the voltage application and contact with the electrolyte, (B) NOA68, (C) polyester resin, and (D) PMMA.

INKJET BASED BIOSENSING PLATFORM

Other tested materials were CYTOP, MMA-coMAA and cPVP formulated for inkjet printing. These materials show better performance than the previous ones because the presence of pinholes was not easily detected by optical inspection. For this reason different electrical measurements (capacitance, resistance and current at -30V) were performed in order to have a better understanding of the electrical behavior and restriction limits of these dielectric materials.

Figure 7.5A,B shows the I-V dielectric for MIE structure when a sweep voltage is applied in the electrolyte and the image of the dielectric breakdown for cPVP dielectric. As it can be observed, soft breakdowns occur reaching a high current density losing totally its dielectric properties. Although the goal of this section is to study the dielectric reliability, more measurements are needed.

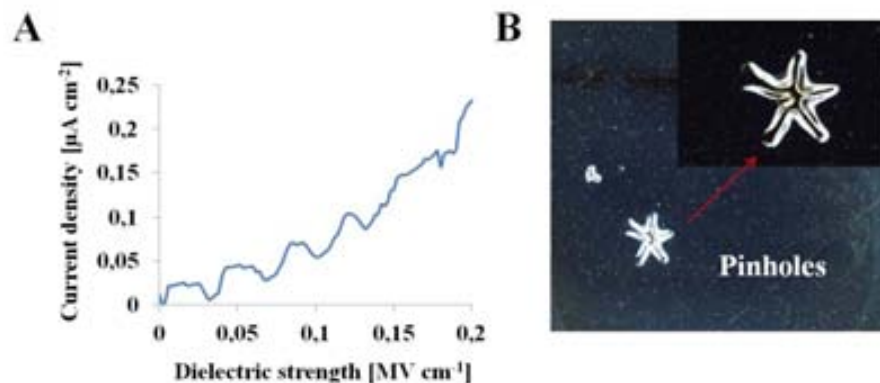


Figure 7.5. (A) Curve which represents the change of the current between the two capacitance contacts when a voltage range is applied between -20 and 20 V (corresponding to the dielectric strength multiplied by the dielectric thickness (1 μm) in order to evaluate the dielectric rupture for cPVP dielectric, and (B) picture of the pinholes, which appear when a voltage is applied in the cPVP.

A comparison between the current leakages produced when the mentioned materials are tailored is studied using pH 4 and 7.4 as electrolyte. Figure 7.6A,B shows the capacitance, resistance and current for each dielectric. As can be observed, CYTOP presents the best performance in terms of leakage current for both pH (4, and 7.4) (from 500 nm of thickness), however, cPVP (1 μm) does not support the electrolyte and therefore the leakage current reaches up to 0.6 μA but, compared with the others presents a good capacitance. The same behavior was observed for the MMA-coMAA with a minimal thickness of 2 μm. However the cPVP is not useful as the gate of the BioFET for the reasons as we mentioned before, cPVP has good printability and good properties as insulator concerning the OTFT. For these reasons cPVP was used for bottom dielectric gate and MMA-coMAA for top dielectric gate.

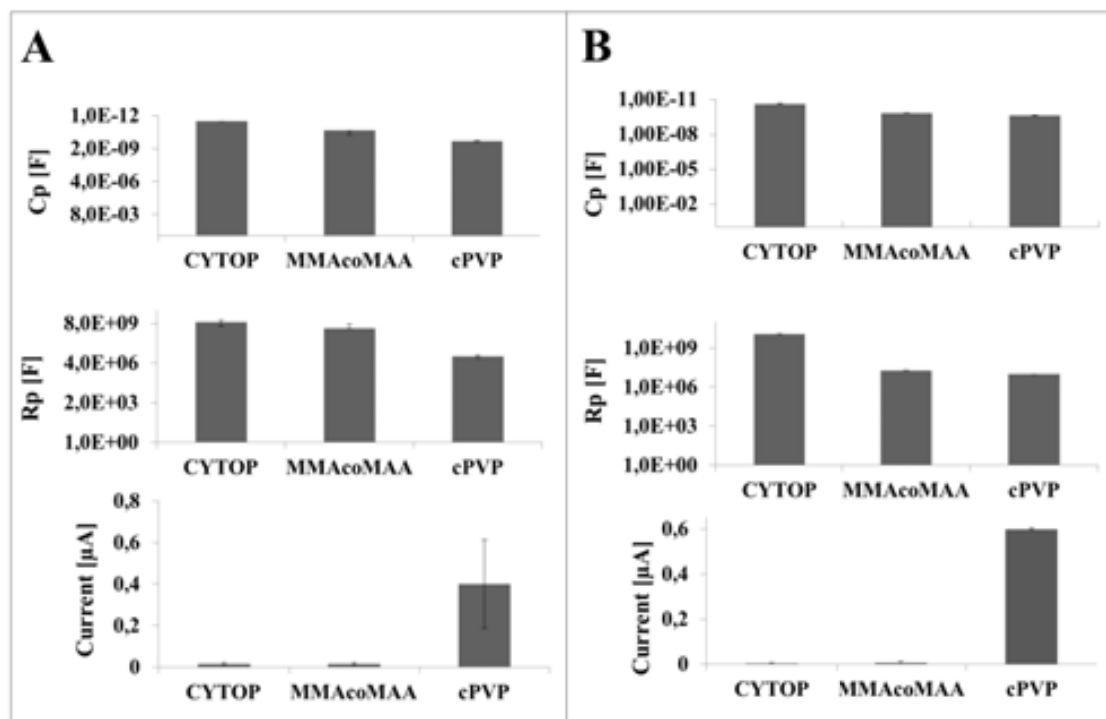


Figure 7.6. Electrical characterization of different dielectrics: Interface resistance, capacitance and current density at -30 V measurements at 1 KHz for (A) electrolyte with pH 4.0 and (B) electrolyte with pH 7.4.

For most of biosensing applications, the top of the gate insulator film should be in contact with an aqueous solution. It is well known that silver nanoparticles present electrocatalytic activity in aqueous media²⁸ so it is crucial to analyze the resistance of the top dielectric layer in such an aggressive medium. Since one of the main advantages of OE is the possibility of massive production, the dielectric materials to test must be cheap and easily obtainable besides being biocompatible.

Finally, as dielectric material for the top gate, MMAcoMAA 8.5 EL9 copolymer was used as interface between semiconductor and electrolyte. This material was chosen after the study of different dielectrics, due to the fact that, although it has never been used as dielectric in OE, this family of compounds forms the basis of many positive resists having high resolution powers and good adhesion to metallic and semiconducting supports, as well as good resistance to solvents and reagents, however an additional optimization was needed to achieve the proper MMAcoMAA layer thickness. Current-voltage (I-V) measurements were performed by applying a bias voltage on top of the BioOTFT by using KCl 0.1 M as electrolyte. The current density for different MMAcoMAA thickness and layer is shown in Figure 7.7. Concerning these results, the thickness of 2 μ m and one layer of dielectric was the option chosen for the BioFET fabrication since it presents the lowest current density.

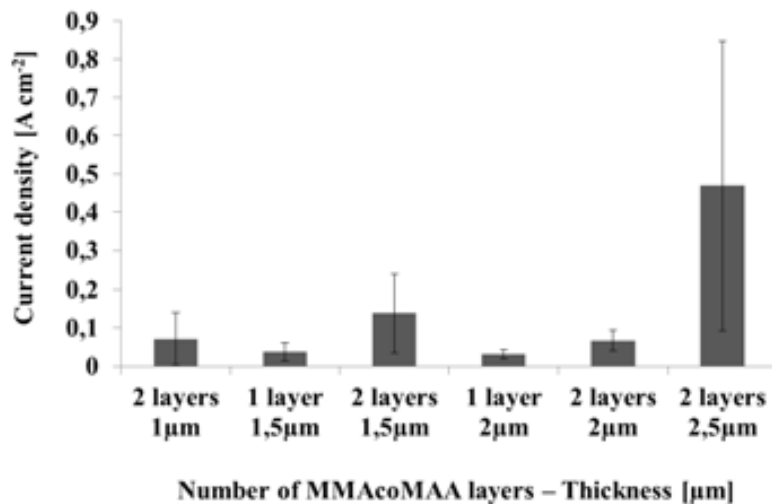


Figure 7.7. Electrical characterization of different MMAcoMAA thickness: current density measurements at - 30 V and 1 KHz.

7.3.3. SEM Characterization of the different TFT layers

The morphological characterization of each BioFET layer was performed using scanning electron microscopy (SEM) and optical microscopy. Figure 7.8 shows an optical image for the BioFET layers top view and SEM image of their respective cross section to measure the real thickness of each layer. (a) Lower gate based on silver nanoparticle ink with a thickness around 1 μm, (b) cPVP dielectric. In this image it is possible to observe the formation of the coffee ring effect; however cPVP layer is homogenous and has a similar thickness such as the silver layer, (c) source and drain contacts, printed also with silver nanoparticle ink with less thickness than the first silver layer, due to the wettability of the cPVP, (d) the p-type semiconductive ink which has around 300 nm and finally (e) the MMAcoMAA layer with 2 μm thickness. In the same Figure, a SEM image of the whole layers is also shown after a precise cutting by using Focus Ion Beam facility (the cutting dimensions were 200 μm x 10 μm x 8 μm with an extra polishing process to obtain a good quality image of the complete BioFET cross section.

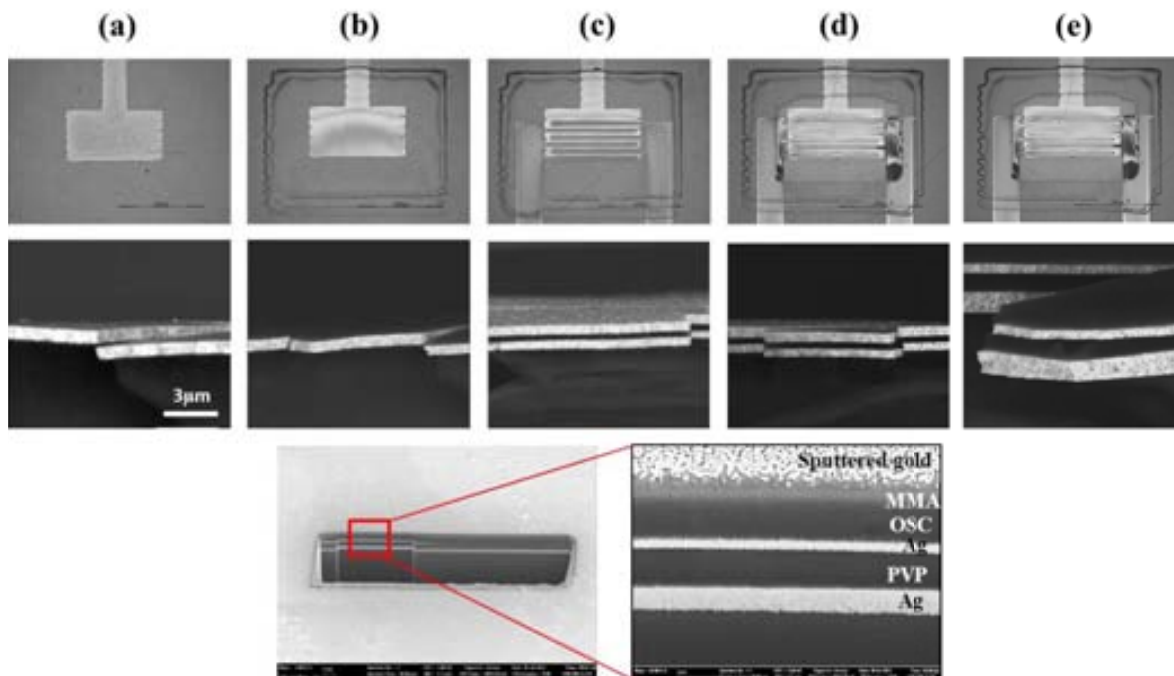


Figure 7.8. SEM Images of BioFET layers: (A) Bottom gate, (B) cPVP as first dielectric layer, (C) Source and drain contacts, (D) p-type semiconductor material, and (E) MMAcoMAA second dielectric layer. (1) represents the top view of each layer and (2) its 3D view.

7.3.4. Electrical characterization of OTFT

In the OTFT, the control of the electrons or holes from source to drain depends as it was mentioned before from the size and shape of the channel, being also affected by the applied gate voltage. In n-channel depletion-mode device, the applied voltage between gate and source (negative) produces a depletion region where the channel is decreased in size. If this depletion closes totally the channel, the resistance from source and drain becomes large and the TFT is turned off. Instead of that, if the gate to source voltage is positive, the increase of the channel size allows the electron flow and the TFT are turned on. In an n-channel, the conductive channel does not exist within the transistor, and a positive gate-to-source voltage is necessary so as to produce it. The positive voltage attracts free-floating electrons toward the gate forming a conductive channel. These electrons should be enough to counter the dopant ions, forming a free region of mobile carriers called a depletion region. This voltage change is called threshold²⁹.

Organic FETs use to work in the accumulation mode differently from the inorganic devices that operate in the inversion mode. The conduction mainly occurs in the on-state, due to the layer of charge carriers which are formed in the semiconductor within few angstroms from the insulator/semiconductor interface, and after the application of a suitable V_g . Thereby,

OTFTs operate through the creation and elimination of a sheet of charge carriers at the gate dielectric/semiconductor interface. Figure 7.9A,B shows the transfer and the output plot for the TFT without electrolyte (lower TFT). For this technology, V_{TH} is around 0 and -3V, and the mobility is $2.5 \times 10^{-4} \text{ cm}^2/(\text{V}\cdot\text{s})$.

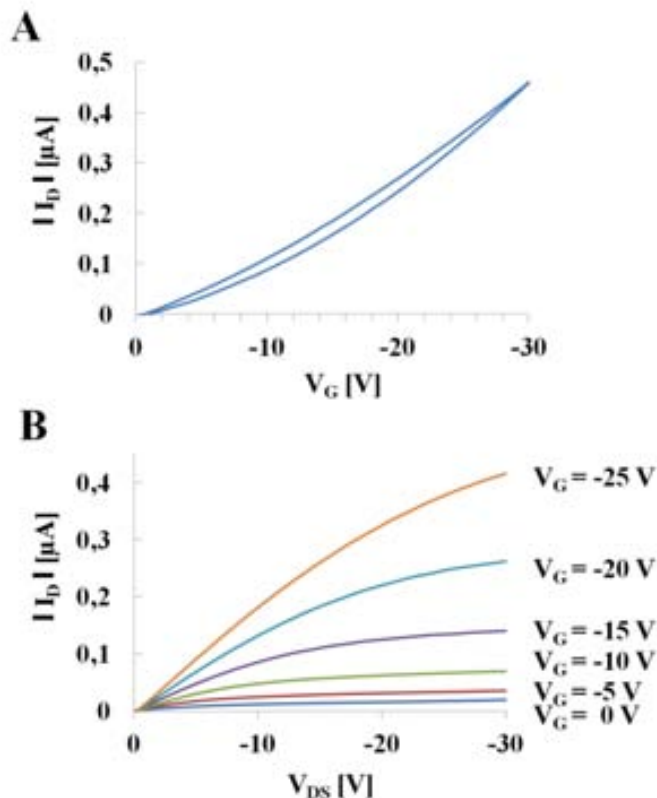


Figure 7.9. Transfer curves for the FS027 semiconductor at room temperature. (A) OTFT curve in the saturation mode ($V_{DS}=-30\text{V}$), and (B) OTFT output plot.

7.3.5. MMA Functionalization

1% of APTES was chosen as a suitable concentration that does not affect the physical properties of the material, obtaining a density of $0.18 \mu\text{M}\cdot\text{cm}^2$ amine groups (Figure 7.10A) as determined by the colorimetric quantification with acid orange II dye.

Fluorescence characterization of the BSA-ALEXA 555 by using epifluorescence microscope confirmed the selective adhesion of the analyte onto the device (Figure 7.10B). In this experiment, the BSA-ALEXA 555 was dropped onto the MMAcoMAA with and without amino-groups during two hours, and then the MMAcoMAA was cleaned with PBST and observed by fluorescence measurements.

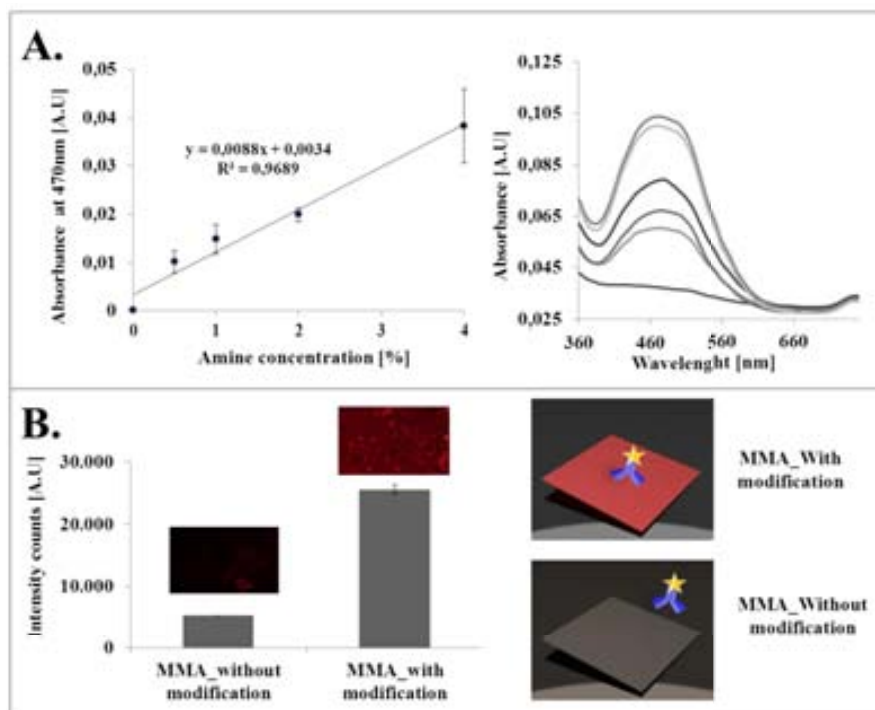


Figure 7.10. (A) Absorbance measurements to quantify the aminosilanes onto MMAcoMAA surface, with its respective calibration curve, and (B) Fluorescence measurements carried out after the immobilization of a protein labeled with fluorophore ALEXA555, with and without aminosilanes modification.

Another simple test was the immobilization of polystyrene microparticles after the functionalization with amino-groups, by a simple dropping and incubation for 15 min and then after the washing step with PBST. The polystyrene particles still remained when the surfaces were functionalized; otherwise they were totally removed with PBST (Figure 7.11).

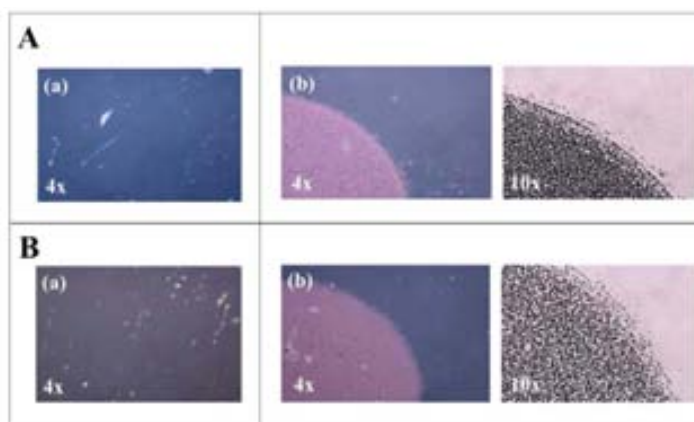


Figure 7.11. MMAcoMAA surface before and after amino-groups functionalization when the polystyrene microparticles are incubated and washed (A) for thickness around 750 nm, and (B) thickness of 1500 nm.

INKJET BASED BIOSENSING PLATFORM

In Figure 7.12A the change of contact angle is shown. First, a decrease from 74° to 13° was observed due to the appearance of more hydrophilic functional groups after the plasma treatment. Then when the APTES is bound onto the surface, the contact angle increases again, reaching different values (from 46° to 75°) that depend on the APTES concentration (0.1, 1, 2, 4 %). Additional studies were performed by using contact angle measurements as well as Atomic Force Microscopy (AFM).

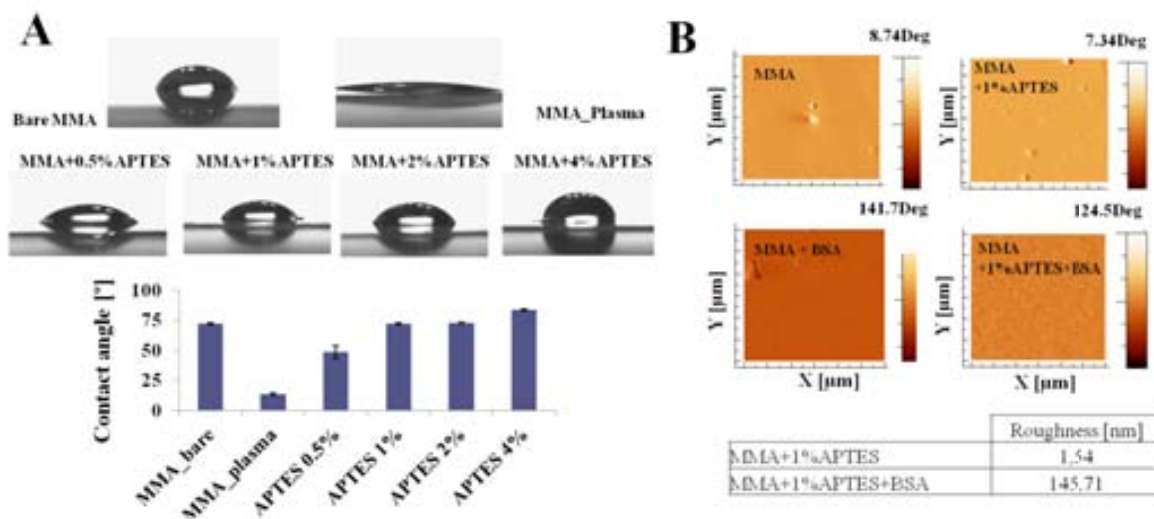


Figure 7.12. MMA surface functionalization. (A) Contact angle measurements, and (B) AFM Images.

Finally a simple inspection by atomic force microscopy was performed comparing the phase angle of different surfaces (bare MMAcoMAA, MMAcoMAA with 1% of APTES), MMAcoMAA with and without APTES functionalization, when the BSA is incubated. This angle phase shows a difference of the composition in each case, being more significantly different when the BSA is placed onto the MMA surface. However a protein such as the BSA is easily attached nonspecifically to almost any surface without a previous APTES functionalization. (Figure 7.12B).

7.3.6. Label free immunoassay

MIE platform

To evaluate the detection of the immobilized protein BSA ($1\mu\text{g mL}^{-1}$), two kinds of capacitive structures were fabricated. The MIE structures are based on buffer electrolyte PBS / MMAcoMAA dielectric functionalized / FS027 semiconductor with and without BSA protein onto the dielectric surface. The capacitance-voltage (C-V) measurements were performed at 1 kHz frequency at room temperature. This technique allows determining the response of surface states, surface accumulation and layer thickness beside others³⁰. Figure 7.13A shows the C-V characteristics of electrolyte-insulator-semiconductor for the case of

(a) aminated structure and (b) structure with immobilized BSA protein. The capacitances depend on bias voltage and have two regions of accumulation-depletion indicating the modulation of the carriers. The capacitance remains constant under forward bias; although above the threshold it gradually increases to reach the maximum peak value. This phenomenon is explained by short-circuited parallel capacitance and it is based on the RC model circuit. As shown in Figure 7.13A, a significant difference of peak heights of capacitance for (a) and (b) is observed. The capacitance ranges from 100 nF to 280 nF with low variability for different devices shown in Figure 7.13B. Confocal images are shown in Figure 7.13C with (a) 1% APTES functionalization and (b) with immobilized protein structures.

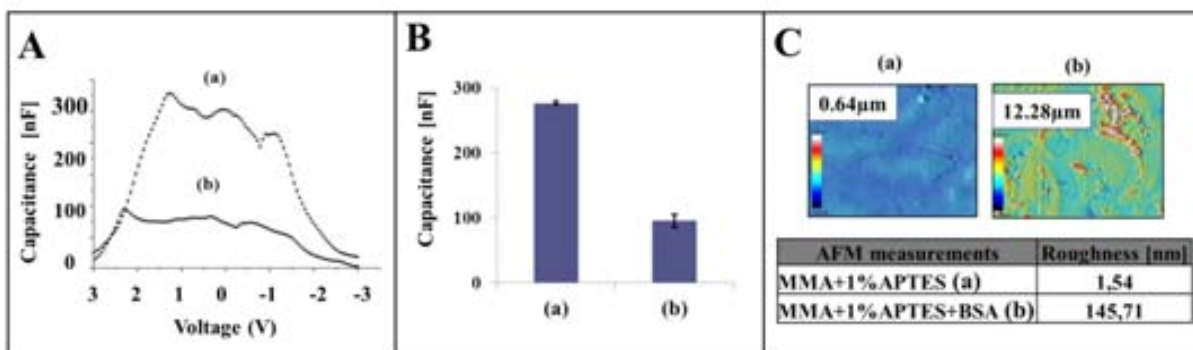


Figure 7.13. Electrical measurements. (A) Capacitance-voltage with electrolyte (PBS) onto dielectric-semiconductive-conductive structure functionalized with 1% APTES (a) and functionalized with immobilized protein BSA (1 μg/mL) (b); (B) Capacitance measurements for three different devices, and (C) confocal images with 1% APTES functionalization and with immobilized protein.

BioFET platform

Figure 7.14A,B shows the electrical measurements for the double gate-BioFET. In Figure 7.14a the electrical response of the lower TFT can be observed when the gate voltage is applied to the bottom gate. It is possible to observe that the hysteresis is not so high; this means that the system is reversible. In Figure 7.14b is shown this response when a drop of the electrolyte is placed onto the MMAcO/MAA remaining the connection like in Figure 7.14a. In this case, we assume that the electrolyte introduces a pronounced hysteresis, an increase of off-current and a decrease of I_{ON}/I_{OFF} ratio changing the semiconductor properties, in Figure 7.14c the signal is observed when the upper TFT is connected, meaning that the electrolyte is contacted with the reference electrode as gate. This gate allows holes to flow through or blocks their passage by creating or eliminating a channel between the source and drain. As it can be observed, when the BioFET works in configuration (c) a decrease of current occurs caused by the difference of dielectric thickness, constant permittivity of the MMAcO/MAA among others. Figure 7.14 C shows the repeatability of the transfer curve of the BioFET.

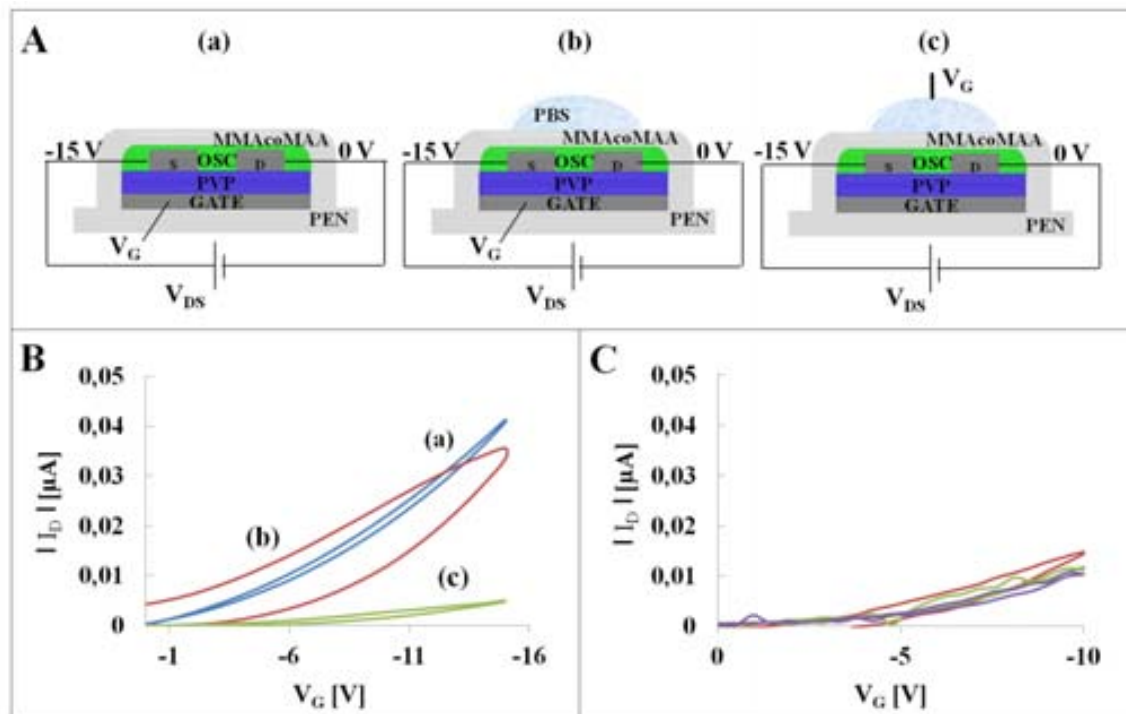


Figure 7.14. (A) I-V OTFT measurements using different configurations: (a) bottom gate, (b) bottom gate with the electrolyte placed onto the MMAcoMAA, and (c) top gate with the electrolyte placed onto the MMAcoMAA and a connected Pt reference electrode (BioFET), (B) corresponding I-V, and (C) repeatability of the BioFET configuration.

Once studied the behavior of the BioFET when an electrolyte is introduced onto the gate, a study of the different functionalization steps was performed in order to monitorize the current change in each step (Figure 7.15 A). In Figure 7.15B different transfer curves are shown starting from: the BioFET after the amino-groups functionalization (Figure 7.14a); a decrease in the current is observed due to the addition of the capture antibody (Figure 7.14b), any significant difference is produced when the free spaces are blocked with the blocking buffer (PBS supplemented with casein and tween) due to the excess of immobilized antibody (Figure 7.14 c) and finally, when the analyte is incubated and the excess is removed, and a significant change in current occurs due to the detection of the conjugation concentration of 100 ng mL^{-1} of HIgG is immobilized (Figure 7.14d).

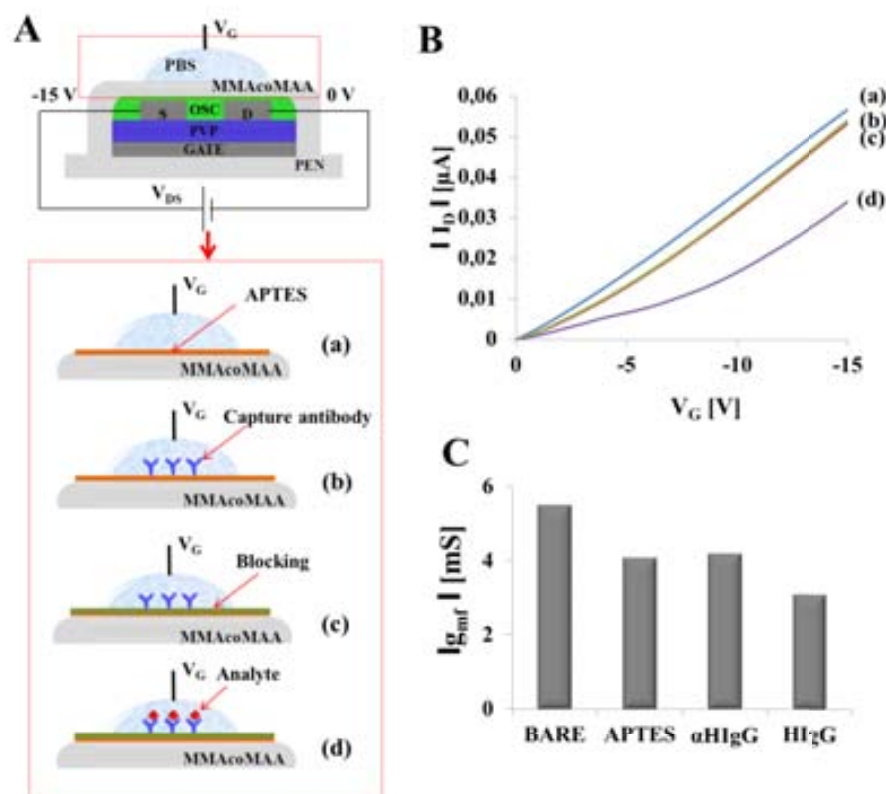


Figure 7.15. (A) Scheme of each step of functionalization, (B) electrical measurement with the MMacoMMA BioFET gate after each conjugation step. (a) APTES functionalization, (b) capture antibody immobilization, (c) blocking with BSA, and (d) analyte conjugation, and (C) Calculated transconductance (transistor gain) for each functionalization step.

The main characteristics of the detection capacity of a BioFET device is its inherent sensitivity to surface charge or surface potential, which can be quantified by the transistor gain. The gain performance of the BioFET in solution can be quantified by replacing the gate voltage by V_{ref} in the traditional transistor gain definition, yielding: $g_{mf} = dI_{DS}/dV_{ref}$.

Figure 7.15C shows the change in the BioFET transconductance, which quantifies the drain current variation with a gate-source voltage variation while keeping the drain-source voltage constant. Taking into account the decrease in capacitance in the MIE structure when BSA protein is deposited, the reduction in g_{mf} can be attributed to changes in effective capacitance due to the addition of organic layers such as APTES, and so onto the BioFET³¹.

7.4. Conclusions

An all integrated and functional BioFET by using organic materials mostly deposited by inkjet technology and spin-coating was designed and fabricated. Characterizations of the deposited layers by using SEM and profilometry were performed. Dielectric rupture evaluation at different thicknesses (one and two layers of MMAcoMAA dielectric layer) was also performed. MMAcoMAA surface functionalization (with interest for future biological applications) study through colorimetric assay to determine the quantity of amine groups onto FET surface, fluorescence measurements and AFM images to confirm the selective adhesion of proteins onto BioFET surface were also carried out. Detection of the immobilized protein BSA was performed by means of C-V measurement. Moreover, we present the repeatability with different devices. Finally, confocal and interferometry images were undertaken to assess the roughness of functionalized and immobilized protein structures.

Morphological and electrical characterizations for all materials used to fabricate the OTFTs are also shown. Both cPVP (for bottom OTFT) and MMAcoMAA (for top BioFET) were validated as good insulators for the range of used voltages.

Good electrical performance was obtained for both dielectrics, but some difficulties arise due to the presence of pinholes in the dielectric modifying the electrical properties (devices using MMAcoMAA dielectric) or reducing yield. Although the mobility obtained for the semiconductors is in the state of the art, the electrical performance for the OTFT was not as expected. This leads to keep improving the materials and processes.

The effects under the channel gain were studied by the calculus of the scope of the different functionalization steps. It is affected by the organic layers due to their dielectric nature which changes the effective capacitance of the system, resulting in reduction of the gain following the formation of each of the organic layers of the device. These results showed the effects of the organic layers on the performance of OTFT device.

Finally, the developed device is promising and may open a wide range of possibilities but overall it provides an important starting point with the gained experience in inkjet technology and material's handling for the development of new projects.

7.5. References

-
- ¹ B. A. Ridley, B. Nivi, and J.M. Jacobson. *All-organic field effect transistors fabricated by printing*. Science. 1999, 286, 746-749.
- ² T. Sekitani, T. Yokota, U. Zschieschang, H. Klauk, S. Bauer, K. Takeuchi, M. Takamiya, T. Sakurai, and T. Someya. *Organic nonvolatile memory transistors for flexible sensor arrays*, Science. 2009, 326, 1516-1519.
- ³ A. Facchetti. *Pi-Conjugated polymers for organic electronics and photovoltaic cell applications*. Chem. Mater. 2011, 23(3), 733-758.
- ⁴ D. Gentili, P. Sonar, F. Liscio, T. Cramer, L. Ferlauto, F. Leonardi, S. Milita, A. Dobabalapur, and M. Cavallini. *Logic-gate devices based on printed polymer semiconducting nanostripes*. Nano Letters. 2013, 13(8), 3643-3647.
- ⁵ A. N. Sokolov, M. E. Roberts, and Z. Bao. *Fabrication of low-cost electronic biosensors*. Mater. Today. 2009, 12(9), 12-20.
- ⁶ C. R. Newman, C. D. Frisbie, D. A. da Silva Filh, J. L. Brédas, P. C. Ewbank, and K. R. Mann, *Introduction to Organic Thin Film Transistors and Design of n-Channel Organic Semiconductors*, Chem. Mater. 2004, 16 (23), 4436-4451.
- ⁷ M. J. Schöning and A. Poghossian, Recent advances in biologically sensitive field-effect transistors (BioFETs), Analyst. 2002, 127, 1137-1151.
- ⁸ G. C. Jensen, C. E. Krause, G. A. Sotzingab and J. F. Rusling. *Inkjet-printed gold nanoparticle electrochemical arrays on plastic. Application to immunodetection of a cancer biomarker protein*, Phys. Chem. Chem. Phys. 2011, 13, 4888-4894.
- ⁹ N. Y. Shim, D. A. Bernardis, D. J. Macaya, J. A. DeFranco, M. Nikolou, R. M. Owens, and G. G. Malliara, *All-Plastic Electrochemical Transistor for Glucose Sensing Using a Ferrocene Mediator*, Sensors. 2009, 9(12), 9896-9902.
- ¹⁰ Y. Wen, Y. Liu, Y. Guo, G. Yu, and W. Hu, *Experimental Techniques for the Fabrication and Characterization of Organic Thin Films for Field-Effect Transistors*, Chem. Reviews. 2011, 111(5), 3358-3406.
- ¹¹ M. C. Dang, T. M. D. Dang and E. Fribourg-Blanc. *Inkjet printing technology and conductive inks synthesis for microfabrication techniques*, Adv. Nat. Sci.: Nanosci. Nanotechnol. 2003, 4, 015009-015016.

- ¹²M. Tudorache and C.Bala, *Biosensors based on screen-printing technology, and their applications in environmental and food analysis*, Anal. Bioanal. Chem. 2007, 388, 565–578.
- ¹³S. A. Ruiz and C. S. Chen, *Microcontact printing: A tool to pattern*, OFT Matter. 2007, 3, 1–11.
- ¹⁴X Liu, J. T Guthrie, *A review of flexographic printing plate development*, Surface Coatings International Part B: Coatings Trans. 2003, 86(2), 91-99.
- ¹⁵W-K Lee, and P. E. Sheehan, *Scanning Probe Lithography of Polymers: Tailoring Morphology and Functionality at the Nanometer Scale*, Scanning. 2008, 30, 172–183.
- ¹⁶M. Singh, H. M. Haverinen, P. Dhagat, and G. E. Jabbour, *Inkjet printing-process and its applications*, Adv. Mater. 2010, 22, 673-685.
- ¹⁷A. P. F. Turner. *Biosensors: sense and sensibility*. Chem. Soc. Rev. 2013, 42, 3184-3196.
- ¹⁸H. Jeong, N. Erdene, J.H. Park, D.H. Jeong, and S.K. Lee. *Real-time label-free immunoassay of interferon-gamma and prostate-specific antigen using a fiber-optic localized surface Plasmon resonance sensor*. Biosens. Bioelectron. 2013, 346-351.
- ¹⁹R. Li, H. Yu, Y. Li, R. Feng, X. Li, H. Li, Q. Wei, and B. Du. *Ultrasensitive label-free immunoassay for diethylstilbestrol based on Au nanoparticles on mesoporous silica and amino-functionalized graphene*. Anal. Methods, 2013, Advance Article. DOI: 10.1039/C3AY41186A.
- ²⁰T. Li, E-J. Jo, and M-G. Kim, *A label-free fluorescence immunoassay system for the sensitive detection of the mycotoxin, ochratoxin A*. Chem. Commun. 2012, 48, 2304-2306.
- ²¹R.D. Nargessi, B. Shine, and L. Landon, *Immunoassay for serum C-reactive protein employing fluorophore-labelled reactants*. J. Immuno. Methods. 1984, 71, 17-24.
- ²²H.V. Aboul-Enei, RI. Stefan, S. Litescu, and GL. Radu. *Biosensors for the enantioselective analysis of the thyroid hormones (+)-3,3',5-triiodo-L.thyrononine (T3) and (+)-3,3',5,5'-tetraiodo-L-thyrononine (T4)*. J. Immunoassay Immunochem. 2002, 23(2), 181-190.

-
- ²³ J. Li, and J-J. Zhu. *Quantum dots for fluorescent biosensing and bio-imaging applications*. *Analyst*. 2013, 138, 2506-2515.
- ²⁴ A.K. Yetisen, M. S. Akram and C. R. Low. *Paper-based microfluidic point-of-care diagnostic devices*. *Lab Chip*. 2013, 13, 2210-2251.
- ²⁵ Uchida E, Uyama Y, Ikada Y. *Sorption of low molecular-weight anions into thin polycation layers grafted onto a film*. *Langmuir*. 1993, 9, 1121–1124.
- ²⁶ E. Ramon, C. Martínez-Domingo, A. Alcalde-Aragones and J. Carrabina. *Inkjet geometric design and compensation rules generation and characterization*. NIP: International Conference on Digital Printing Technologies (Quebec, September, 2012).
- ²⁷ R.D. Deegan, O. Bakajin, T.F. Dupont, G. Huber, R. Nagel, T.A. Witten, “*Capillary flow as the cause of ring stains from dried liquid drops*”, *Nature*. 1997, 389, 827-829.
- ²⁸ Z-J. Jiang, C-Y. Liu, and L-W. Sun. *Catalytic properties of silver nanoparticles supported on silica spheres*. *J. Phys. Chem.* 2005, 109(5), 1730-1735.
- ²⁹ Y. Guo, G. Yu, and Y. Liu. *Functional organic field-effect transistors*. *Adv. Mater.* 2010, 22, 4427-4447.
- ³⁰ A. Tataroglu, and S. Altindal. *Characterization of current-voltage (I-V) and capacitance-voltage-frequency (C-V-f) features of Al/SiO₂/p-Si (MIS) Schottky diodes*, *Microelectron. Eng.* 83, 582 (2006).
- ³¹ B. Khamaisi, O. Vaknin, O. Shaya, and N. Ashkenasy. *Electrical performance of silicon-on-insulator field-effect transistors with multiple top-gate organic layers in electrolyte solution*. *Acs. Nano*. 2010, 8, 4601-4608.

CHAPTER 8

CONCLUDING REMARKS

The study of the integration of various kinds of transducers (based on carbon, boron doped diamond, conductive polymers between others) into hybrid PDMS microfluidic platforms fabricated with different substrates (Glass, COC, polyester, MMAcoMAA, and polycarbonate) and their successful use in different biosensing applications (Alzheimer related biomarker, model protein or pesticide detection) have been y achieved.

Considering the objectives previously described in Chapter 2, along with the obtained results presented from Chapter 3 to Chapter 7, the following specific conclusions on this PhD thesis can be given for each chapter:

8.1. Fabrication methodologies

Microfluidic platforms, electrode fabrication and integration procedures were optimized. Most of them were focused on the use of home-made SPE because they are produced faster, offer the possibility to be mass produced with a low cost, and can be easily integrated within the microfluidic device. The fabrication of a hybrid PDMS-thermoplastic microfluidic chip with integrated SPE electrodes was demonstrated. SPEs were integrated as SWASV detector and shown to be a simple alternative for easy to use, low cost and mass produced chips. The use of the soft-lithography and PDMS replica for rapid prototyping of microfluidic devices offers several advantages over conventional photolithography and micromachining in silicon or glass that have previously been used to create masters for molding polymeric microfluidic systems: i) transparencies take less time to be produced (hours compared to weeks) and are substantially less expensive (20 EURO vs. 500-1000 EURO); ii) the development of photoresist to create a relief on silicon is easier and more flexible in the types of patterns that can be produced than the etching needed in micromachining of silicon.

8.2. Quantum Dots as electrochemical reporters in lab-on-a-chip devices

The electrochemical parameters for the on-chip homemade CdS QDs detection, such as scan rate, deposition potential, deposition time, frequency and flow rate, in order to obtain the best relation electrochemical response vs. noise were optimized using the developed microfluidic platform. This allowed the characterization of electrochemical behavior of commercial QDs as labels, as well as its application in ApoE biomarker detection with a very good accuracy and LOD for standard and real samples. The use of polymeric substrates such as thermoplastics widely used for lab-on-a-chip prototype fabrication showed to be of special interest for future mass production through injection molding or hot embossing processes. In addition, the use of a microchannel with a magnetic retention zone, allowed the sample purification and preconcentration using magnetic beads as stationary

CONCLUDING REMARKS

support, providing good sensitivity and controllable sample manipulation. Moreover, very small volumes of human plasma were assayed with high sensitivity and acceptable precision and accuracy. This approach could be extended to a multiplexed detection of ApoE isoforms and other AD related biomarkers. The technique applied for the ApoE detection in real sample was achieved with a very good correlation ($R^2 = 99.8\%$) respect to the standard sample and identical sensitivity. The assay time was also reduced by 33 % compared to the batch method. This development, in addition to the integration of other operations such as microreaction, pre-concentration, separation, and bioconjugation, can open the way to the design of various biosensing platforms.

8.3. Novel strategies to obtain electrochemical LOCs with higher sensitivity

Different strategies to improve the sensitivity of the LOCs were evaluated, starting from the improvement of the magnetic separation zone, in order to increase the capture efficiency of the analyte. It was possible to demonstrate its operation by the detection of a model protein (HIgG) and it was also compared to the single magnet platform. COC polymer was chosen as substrate for the fabrication of this LOC due to its optical and mechanical properties. Since it does not present self-fluorescence, it was possible to monitor the immobilization of QDs through fluorescence inspection. In addition, it is more resistive to aggressive solvents such as acids, acetone, DMF, etc. It was demonstrated that the most stable immobilization of magnetic beads was achieved in the attractive conformation of the magnets for microchannels of 100 and 200 μm width and 50 μm depth, being stable up to 200 $\mu\text{L min}^{-1}$. Due to the small dimensions of the channels and the necessity to reduce the flow rate down to 0.05 $\mu\text{L min}^{-1}$, it was necessary to increase the measurement time to ensure the partial dissolution of the QDs as well as their Cd ions reduction onto the working electrode. Smaller magnetic beads (1 instead of 2.8 μm) were used to minimize their precipitation.

A recirculation system was designed and fabricated in order to deposit the free Cd ions and the rest of QDs which were not deposited in the first turn, achieving lower LOD using reduced volumes of sample. The use of an external peristaltic pump adapted to a simple microfluidic channel demonstrated that the QDs electrochemical signal increase 5.5 fold when the flow is recycled twice. A micro-peristaltic pump with integrated pneumatic valves was also proposed, which consisted in a “push-down” valve configuration. In this way, the development of a micropump integrated in the measurement channel was achieved.

Finally, Bismuth was used as an easy-to-perform alternative to increase the sensitivity of the QDs detection. A microfluidic device for protein detection (HIgG) was developed, achieving a very low LOD as well as a 100 fold higher sensitivity compared to the drop

format. The device takes the advantage of the speed and low cost of the conventional immunoassay technologies.

The exposed devices coupled with a portable electrochemical analyzer shows great promise for in-field quantitative testing for disease-related protein biomarkers. The developed devices thus provide rapid, clinically accurate, and quantitative tools for protein detection.

8.4. Boron-doped diamond based platforms

The well-known electrochemical properties of BDD electrodes modified with platinum nanoparticles (Pt-NPs) in order to render its catalytic activity to the direct electron transfer from the HRP molecules are demonstrated for the first time with even higher efficiency integrated in a microfluidic platform. This new and simple platform was used to increase the sensitivity for atrazine pesticide detection in 10 times less volume than drop/batch methods, decreasing the obtained LOD by amperometric detection to 0.1 pM, which is 72, 20 and 10 fold lower compared to ELISA format, drop format and other methods reported in the literature, respectively. It is easy to fabricate, disposable and amenable to mass production. It uses a very low DC potential, decreasing in this way the effect of interferences. In addition, the use of a magneto-immunoassay ensures specific detection. All these advantages could be used in automatic control systems with interest for environment monitoring among other applications.

8.5. Ink-jet based biosensing platform

An all integrated and functional BioFET by using organic materials mostly deposited by inkjet technology and spin-coating was designed and fabricated. Characterizations of the deposited layers by using SEM and profilometry were performed. Dielectric rupture evaluation at different thicknesses (one and two layers of MMAcoMAA dielectric layer) was also performed. MMAcoMAA surface functionalization (with interest for biological applications) study through colorimetric assay to determine the quantity of amine groups onto FET surface, fluorescence measurements and AFM images to confirm the selective adhesion of proteins onto BioFET surface were also carried out. Detection of the immobilized protein BSA was performed by means of C-V measurement. Moreover, we present the repeatability with different devices. In addition, confocal and interferometry images were undertaken to assess the roughness of functionalized and immobilized protein structures.

The effects under the channel gain were studied by the calculus of the scope of the different functionalization steps. It is affected by the organic layers due to their dielectric nature which changes the effective capacitance of the system, resulting in reduction of the gain

CONCLUDING REMARKS

following the formation of each of the organic layers of the device. These results showed the effects of the organic layers on the performance of OTFT device

Finally, a brief graphical summary of the different developed platforms for various analytes including the achieved detection limits is shown in Table 8.1.



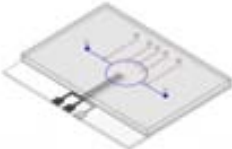


Microfluidic platform	Analyte	LOD [ng mL^{-1}]
	- QD 655 - HIgG - ApoE	0.5 1.72 12.5
	HIgG	0.36
	CdS QDs	External pump (~2)
	-QD 655 -HIgG	0.1 3.5
	Atz	0.001 (4.5 pM)

Table 8.1. Summary of the different microfluidic platforms designed and studied along the Thesis.

ANNEXES

ANNEX 1

ANNEX 1

CHAPTER 8

New Trends in DNA Sensors for Environmental Applications: Nanomaterials, Miniaturization, and Lab-on-a-Chip Technology

ALFREDO DE LA ESCOSURA-MUÑIZ,^{1,2} MARIANA MEDINA¹ AND ARBEN MERKOÇI^{1,3}

¹ Nanobioelectronics & Biosensors Group, Institut Català de Nanotecnologia, Bellaterra, Barcelona, Spain

² Aragon Institute of Nanoscience, Universidad de Zaragoza, Zaragoza, Spain;

³ ICREA, Barcelona, Spain

Abstract

The purpose of this chapter is to review the latest trends in the use of nanomaterials (nanoparticles, quantum dots, nanotubes, *etc.*) as well as miniaturization and lab-on-a-chip technologies for nucleic acid based biosensing systems with interest for environmental applications. Although most of the principles of nanomaterial-based sensors have been addressed earlier, in this chapter we aim to focus on the DNA and nanomaterial-based systems that are of interest for environmental applications. In addition to nanomaterials the chapter will also consider lab-on-a-chip systems involving DNA as a novel trend in environmental monitoring. Due to the lack of relevant reports in the literature on specific DNA-based systems, other analytes will be also discussed for some of the detection modes reviewed here, keeping in mind future

Nucleic Acid Biosensors for Environmental Pollution Monitoring

Edited by Ilaria Palchetti and Marco Mascini

© Royal Society of Chemistry 2011

Published by the Royal Society of Chemistry, www.rsc.org

extension of these methods as possible alternatives for DNA-based environmental monitoring.

8.1 Introduction

The permanent interest in monitoring pollutants in water, air, or elsewhere that may present risks to human health and the ecosystem suggests the development of diverse analytical techniques that may allow fast and cost-efficient detection methods.

The aim of this chapter is to summarize the latest trends in the use of nanomaterials (nanoparticles, quantum dots, nanotubes, *etc.*) as well as miniaturization and “lab-on-a-chip” technologies for nucleic acid (NA)-based biosensing systems with interest for environmental applications.

The emergence of nanoparticles (NPs) as an alternative to other labels (fluorescent dyes, enzymes, *etc.*) for DNA detection has been previously reviewed by our group.¹ In addition to NPs, other materials such as carbon nanotubes (CNT) have been also reviewed for their general applications in sensors² and analytical methods³ in general, with some examples of DNA detection systems. Although most of the principles of the nanomaterial-based sensors have been addressed previously, in this chapter we aim to focus on DNA and nanomaterial-based systems that are of interest for environmental applications.

In addition to nanomaterials, the chapter will also consider lab-on-a-chip systems involving DNA as a novel trend for environmental monitoring. Electrochemically based lab-on-a-chip devices were reviewed earlier by our group,⁴ but here we focus on some applications related to the current use and future applications of these systems for environmental monitoring. Because of the lack of reports on specific DNA-based systems for some of the detection modes under review, other analytes will be also discussed keeping in mind future extension of these methods as DNA-based environmental monitoring possibilities.

8.2 Nanomaterial-based Sensors for DNA Detection

The discovery and study of nanomaterials has enabled the development of ultrasensitive optical and electrochemical biosensors, because of their large surface area, favorable optical and electronic properties, and electrocatalytic activity as well as good biocompatibility due to their nanometer size and specific physicochemical characteristics. The resulting sensors have been applied in areas of food quality, clinical analysis, and environmental control.

Different detection approaches for pathogen-related DNA are reviewed in this section. In most cases, the analysis of environmental pollution using nanomaterial-based biosensors consists of the detection of DNA related to environmental pathogens, using single-stranded (ss) DNA as a bioreceptor and

final optical or electrochemical transducing. Nanomaterials can be used to modify the surface of the transducer, improving the performance of the sensor, or as optical or electroactive labels for the sensitive detection of pollutants.

8.2.1 Optical Sensors

8.2.1.1 Nanoparticles as Optical Labels

The intrinsic optical properties (UV-visible light absorption and auto-fluorescence properties) of NPs (NPs) and also their ability to change optical properties of sensor surfaces (*i.e.*, in surface plasmon resonance and devices based on light scattering) have been applied for their detection when used as labels in DNA hybridization assays.

It is well known, for example, that the NP plasmon band shifts when gold NPs (AuNPs) are aggregated, owing to a decrease in the interparticle distance. The absorbance maximum shifts from 520 nm to 580 nm (red to blue) when the aggregation takes place, and this phenomenon can be monitored for biosensing purposes. For example, an AuNP suspension previously modified with a ssDNA probe has been hybridized with a target DNA (complementary at its two ends with ssDNA), thus giving rise to the aggregation of NPs with the consequent change in color (Figure 8.1). This principle was pioneered by Mirkin's group and applied to the detection of DNA characteristic of anthrax, a biological warfare agent.⁵

Silica NPs (SiNPs), doped with either magnetic materials or dyes, have also been widely exploited for the collection, purification and detection of DNA/RNA.⁶ The bioconjugation of SiNPs with DNA/RNA molecules can provide unique biofunctions. These NPs tend to exhibit very high luminescence and photostability, within a broad size range from 5 to 400 nm. Furthermore, dye-doped SiNPs have been extensively used in bioimaging and biochemical analysis because of advantages such as signal enhancement, photostability, and surface modification availability for the immobilization of biomolecules.⁷ For example, SiNPs were doped with an europium ternary complex by the reverse microemulsion method⁸ and used as fluorescence labels for the detection of *Escherichia coli* in water samples, resulting in an effective tool for environmental monitoring of pathogen DNA.

Core-shell NPs such as magnetic/luminescent $\text{Fe}_3\text{O}_4/\text{Eu}:\text{Gd}_2\text{O}_3$ synthesized by spray pyrolysis were used by Son *et al.*⁹ both as platforms for the hybridization reactions and as fluorescence labels. The DNA hybridization sensor they developed has the capability of distinguish perfectly matching targets from two-base pair mismatching, allowing the discrimination of different bacterial species. These results opened the way to the quantification of specific bacteria based on the 16 S ribosomal DNA (rDNA) gene sequence in environmental samples. Moreover, core-shell NPs are highly versatile because they can be synthesized in many colors with a variety of phosphorescent lanthanide ions (*e.g.*, europium, terbium, samarium), allowing a multiplex detection of a number of targets via optical encoding.

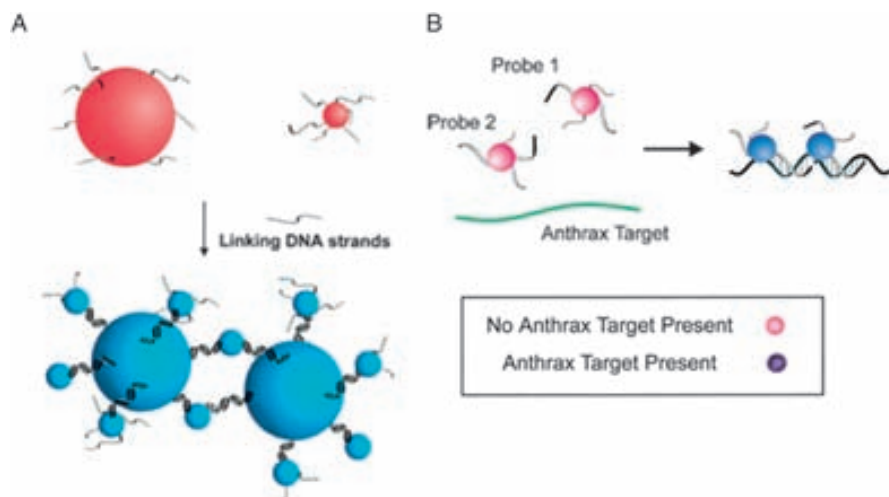


Figure 8.1 (A) General scheme of the principle of the DNA detection based on the change in the absorption spectra due to the AuNPs aggregation. (B) Application for the detection of an anthrax PCR product. Adapted from ref. 5, with permission.

The autofluorescence properties of inorganic semiconductor nanocrystal CdSe/ZnS core-shell NPs were applied by Vora *et al.* in DNA microarrays for the sensitive detection of pathogenic organisms from environmental matrices, allowing the detection of 10^3 polymerase chain reaction (PCR) copies of *Vibrio cholera*.¹⁰ In the same work, the resonance light scattering properties of AuNPs were also used for the detection of a few copies of the PCR product.

Other optical properties of NPs that have been utilized for DNA hybridization detection and are promising for their further application in environmental monitoring are the ability of AuNPs to act as quenchers of the fluorescence of other markers,¹¹ and the ability of AuNPs to change the scattering properties of a surface where they are attached through the hybridization reaction.¹²

8.2.1.2 Nanomaterials as Modifiers of Optical Transducers

In addition to their use as optical labels, NPs can be used as modifiers of the optical transducer surface, improving the performance of the optical sensor. A NP-modified surface for the optical detection of DNA has been reported by Endo *et al.*¹³ It consisted of a gold-capped NP layer substrate immobilized with peptide nucleic acids (PNAs) for the development of a localized surface plasmon resonance (LSPR)-based label-free optical biosensor (Figure 8.2). The NP layer was formed on the gold-deposited glass substrate by the surface-modified SiNPs using a silane-coupling reagent. The PNAs recognize the DNA sequence of interest and the PNA–DNA hybridization produces a change in the LSPR

signal that allows detection both of target oligonucleotides and of PCR-amplified real samples. This detection mode may be applied in the future for the environmental control of pathogens.

In addition to NPs, one-dimensional (1D) nanostructures (including nanowires, nanotubes, nanobelts, and nanorods) have also received significant research attention over the past years, due to their intriguing properties and promising applications.¹⁴ In particular, porous structures of these 1D nanomaterials, owing to their intrinsic pore structures and high surface-to-volume ratio, have been the focus of recent studies, which further broaden the potential applications in catalysis, bioengineering, environmental protection, sensors, and other areas. Their advantageous properties have also been applied for use as modifiers of optical transducers. For example, layered-lanthanum crystalline nanowires (NWs) with hierarchical pores were synthesized via a hydrothermal route by Wang *et al.*¹⁵ and luminescence properties were achieved by doping nanowires with Eu^{3+} . By combining the merits of hierarchical porous nanowires and layered hydroxides, these products have shown a unique bioengineering application of capture and rapidly release of short DNA fragments in dilute solution. Environmental engineering applications resulting from the remarkable capability of these products to remove an organic dye (Congo red, a common azo dye in the textile industry) from wastewater have been reviewed.

8.2.2 Electrochemical Sensors

Electrochemical biosensors based on immobilized DNA combine detection sensitivity with a high specificity for biomolecules. This reduces the consumption of DNA and gives rise to the development of modern methods of analysis of chemicals affecting DNA, including toxic substances with environmental and biological effects.^{16,17} Various electrochemical DNA systems for environmental analysis have been developed.

8.2.2.1 Nanoparticles as Electroactive Labels

The excellent electroactivity of metallic NPs, together with their easy bioconjugation, has given rise to their extensive use as labels in DNA sensors in recent years. Several electrochemical routes (voltammetric, potentiometric, conductometric, impedimetric, and scanning electrochemical microscopy methods) have been exploited for the sensitive detection of these NPs tags in bioassays.¹⁸ Although in most cases these electrochemical DNA biosensors have not yet been used for environmental monitoring, the established methodologies may open the way for very sensitive, simple, and cost-efficient sensors for future applications.

NP-based amplification schemes have improved the sensitivity of bioelectronic assays by several orders of magnitude. In 2001, the groups of Wang¹⁹ and Limoges²⁰ both pioneered the use of AuNP tags for electronic detection of DNA hybridization. This protocol relies on capturing the NPs to the

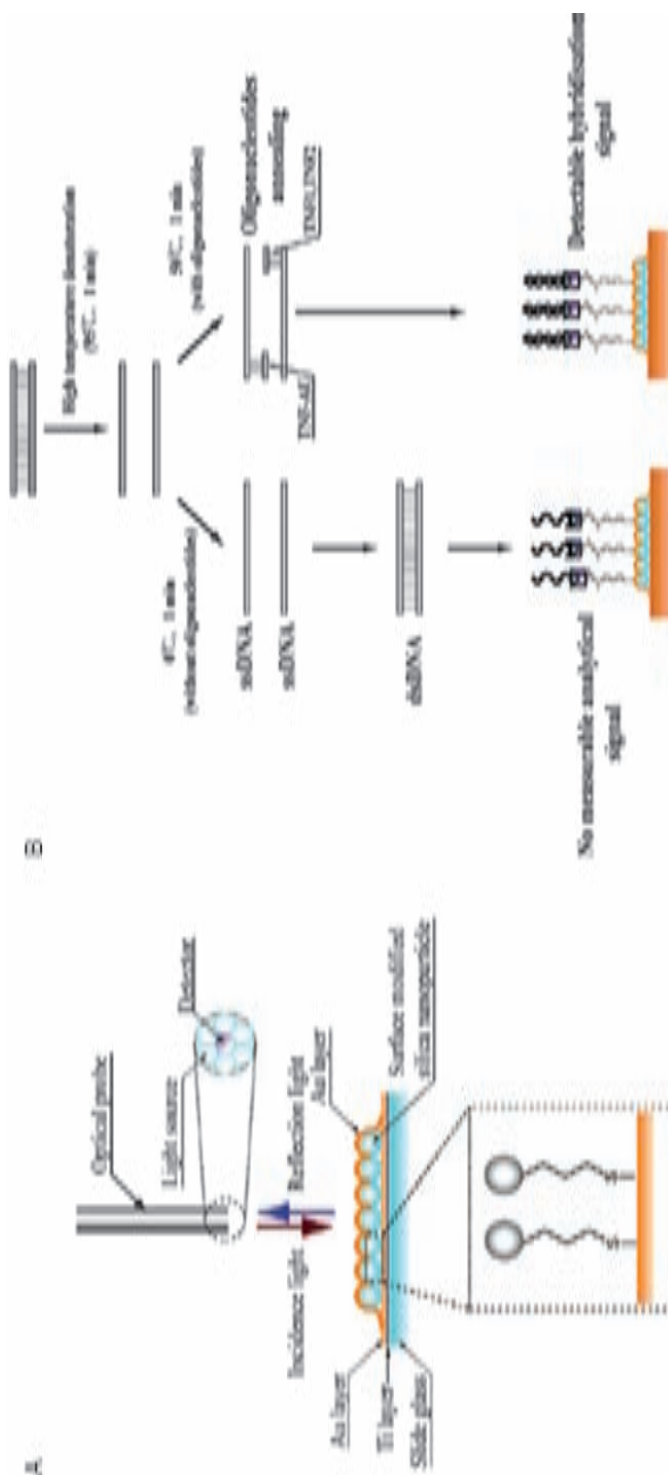


Figure 8.2 (A) Experimental setup and construction of LSPR-based optical biosensor. (B) Label-free detection of PCR-amplified samples using LSPR-based optical biosensor. Adapted from ref. 13, with permission.

hybridized target, followed by highly sensitive anode-stripping electrochemical measurement of the metal tracer.

Commonly, coupling the biorecognition element to the surface of magnetic beads effectively minimizes nonspecific binding. The hybridization of probe-coated magnetic beads with metal-tagged targets results in three-dimensional network structures of magnetic beads, cross-linked together through DNA and AuNPs. Such a magnetic-bead/DNA/metal-label assembly packing onto the electrode leads to direct contact between the metal label and the surface, and enables electrochemical measurements without dissolving the metal tag.^{21–23} Electronic DNA hybridization assays have been extended to other metal NP tracers, including AgNPs,²⁴ CdS QDs,²⁵ and Fe₂O₃/Au core-shell NPs,²⁶ opening the way to analysis for environmental control.

Furthermore, the well-known catalytic properties of AuNPs on the reduction of silver ions have been applied by Lee *et al.*²⁷ for the sensitive detection of ssDNA in sandwich assays on ITO electrodes, offering a protocol that has great potential for simple, reproducible, highly selective, and sensitive DNA detection on fully integrated microdevices in environmental monitoring applications.

Other strategies based on the use of inorganic nanocrystals offering an electrodiverse population of electrical tags as needed for designing electronic coding have been reported (Figure 8.3). Three encoding NPs (ZnS, CdS, and PbS) have been used in this way to differentiate the signals of three ssDNA target strands in connection with a sandwich hybridization assay and stripping voltammetry of the corresponding metals.²⁸

Finally, we can also highlight a variation in the use of NPs as direct electroactive labels, which consists in their use as carriers of a large quantity of other labels with electrochemical properties, achieving an improvement in the sensitivity of the assays. For example, a simple, sensitive electrochemical DNA biosensor based on *in situ* DNA amplification with AgNPs as carrier of horseradish peroxidase (HRP) electroactive labels has been designed by Fu *et al.*²⁹ Other nanomaterials such as CNTs have also been used as carriers. For example, the use of CNTs as carriers for several thousand enzyme tags has been reported, allowing the detection of DNA down to 1.3 zmol,^{30–32} with future potential for environmental monitoring.

8.2.2.2 Nanomaterials as Modifiers of Electrotransducers

The presence of NPs on the electrotransducer surface promotes electron transfer, improving the electrochemical responses while using potentiometric and conductimetric techniques. Furthermore, some NPs provide a congenial microenvironment, similar to that of redox proteins in a native system, for retaining their bioactivity, giving the molecules more freedom in orientation. For these reasons, attempts to develop DNA hybridization assays using nanostructured surfaces have been reported in the last few years. The introduction of NPs into the transducing platform is achieved by their adsorption onto conventional electrode surfaces in various forms, including composites.

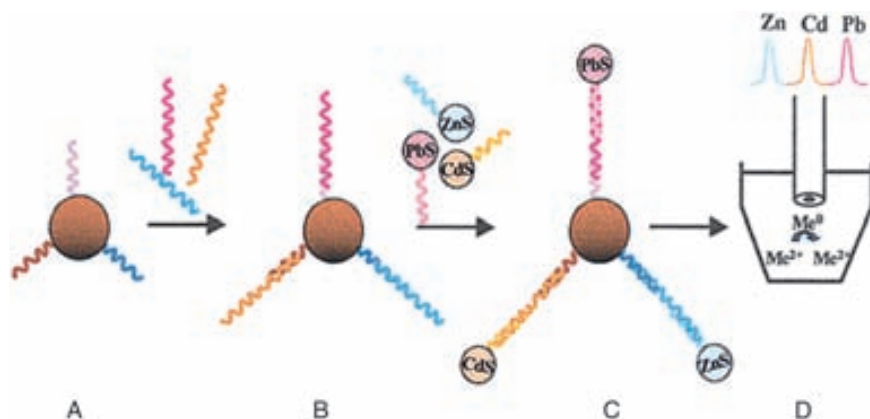


Figure 8.3 Multitarget electrical DNA detection protocol based on different inorganic colloid nanocrystal tracers. (A) Introduction of probe-modified magnetic beads. (B) Hybridization with the DNA targets. (C) Second hybridization with the QD-labeled probes. (D) Dissolution of QDs and electrochemical detection. From ref. 28, with permission.

Regarding NP application for DNA detection of environmental interest, Feng *et al.*³³ constructed AuNP/polyaniline nanotube membranes on a glassy carbon electrode (Au/nanoPAN/GCE) for sensing DNA. The properties of the Au/nanoPAN/GCE and the characteristics of the immobilization and hybridization of DNA were studied by cyclic voltammetry (CV), differential pulse voltammetry (DPV), and electrochemical impedance spectroscopy (EIS). The synergistic effect of the two nanomaterials, AuNP and nanoPAN, dramatically enhanced the sensitivity for DNA hybridization recognition, achieving a detection limit of $3.1 \times 10^{-13} \text{ mol L}^{-1}$ of a specific DNA sequence of the phosphinothricin acetyltransferase gene.

Other nanomaterials used as modifiers of electrotransducers are 1D NWs. They have been used for bridging two closely spaced electrodes for label-free DNA detection. A p-type silicon nanowire, functionalized with PNA probes, was shown to be extremely useful for real-time, label-free, conductimetric monitoring of the hybridization event.³⁴ This technique relies on the binding of the negatively charged DNA target, which leads to an increase in conductance, reflecting the increased surface charge.

Hybrid techniques (mechanic/electric), such as microgravimetric methods based on piezoelectric quartz crystal (PQC) sensing, are also very sensitive methods for the detection of DNA hybridization. Compared to electrochemical and optical methods, the PQC biosensor provides a label-free detection method using a simple and portable equipment set-up, hence having the potential for direct detection of environmental pathogens. A practical approach to enhance the sensitivity of PQC biosensors consists of incorporating NPs onto biosensing layers in order to increase the amount of active recognition molecules at the surface of the PQC biosensor and facilitate the capture of the DNA analyte.

In this way, a highly sensitive PQC DNA biosensor was fabricated by photodepositing silver NPs (AgNPs) modified with neutravidin molecules on TiO_2 -coated PQC electrodes.³⁵ The immobilization of biotinylated probe DNA strands is greatly improved by the NPs, making it possible to achieve a limit of detection of 0.4 ng of PCR products related to *E. coli* in 1 L of drinking-water.

8.3 DNA and Nanomaterial-based Sensing Platforms

The structure of DNA is very sensitive to the influence of environmental pollutants (*e.g.*, heavy metals, polychlorinated biphenyls, or polyaromatic compounds). These substances are characterized by a great affinity to DNA, causing mutagenesis and carcinogenesis. Based on these characteristics it is very attractive to use DNA-containing systems (*e.g.*, DNA-based biosensors) to perform genotoxic assays, or for rapid testing of pollutants for mutagenic and carcinogenic activity. Furthermore, some heavy metals have the ability to coordinate with DNA bases, allowing their capture by DNA probes and later detection.

8.3.1 Optical Detection Methods

The coordination-based interaction between Hg^{2+} and bisthymine has recently attracted significant interest.³⁶ In detail, T-T mismatches in DNA duplexes selectively and strongly capture Hg^{2+} (binding constant higher than A-T), and the metal-mediated T-Hg-T forms stable DNA duplexes. This principle can be applied to selectively bind Hg^{2+} , which can be detected later following different strategies where NPs can be used as labels or as enhancers of the analytical signal.

An example of this approach has recently been reported by Wang *et al.*³⁷ They designed a visual and fluorescent sensor for Hg^{2+} in aqueous solution, based on the Hg^{2+} -induced conformational change of a T-rich ssDNA and the difference in electrostatic affinity between ssDNA and dsDNA with AuNPs (Figure 8.4). The dye-tagged ssDNA containing T-T mismatched sequences was chosen as Hg^{2+} acceptor. At high ionic strength, introduction of the ssDNA to a colloidal solution of the aggregates of AuNPs results in a color change of the solution, from blue-gray to red, and the fluorescence quenching of the dye. Binding of Hg^{2+} by the ssDNA induces the double-stranded structure formation. This dsDNA formation reduces the capability to stabilize bare NPs against salt-induced aggregation, the color of the solution remaining blue-gray, but the fluorescence signal enhancement compared to that without Hg^{2+} achieved a detection limit of 40 nM. Furthermore, both the color and fluorescence changes of the system were extremely specific for Hg^{2+} even in the presence of high concentrations of other heavy metal and transition metal ions, which meet the selective requirements for environmental applications.

The same principle has recently been applied by Liu *et al.* for Hg^{2+} detection at 1.0 nM levels in water samples³⁸ by measuring the enhanced light-scattering

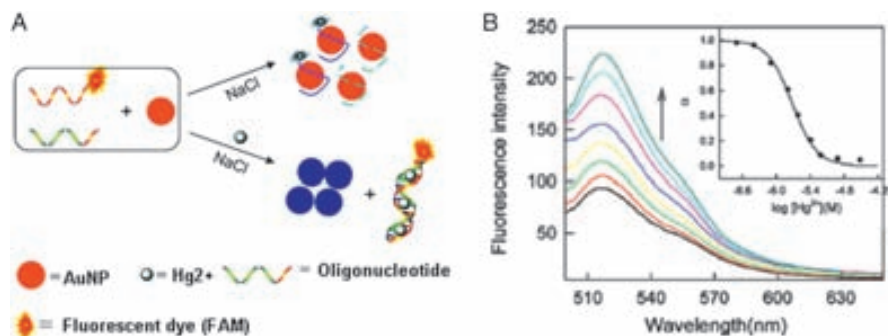


Figure 8.4 (A) Schematic description of colorimetric and fluorescent sensing of Hg²⁺ based on the modification-free AuNPs. (B) Changes in the fluorescence emission spectra of the dye-DNA modified AuNPs in the Tris-HCl buffer (0.1 M NaCl) upon addition of different concentrations of Hg²⁺. Excitation wavelength was 480 nm. Inset: Response (R) parameter as a function of logarithm of Hg²⁺ concentration (M) at pH 7.4. From ref. 37, with permission.

plasmon resonance signals resulted from Hg²⁺-DNA complex-induced aggregation of AuNPs.

DNAzymes (DNA-based biocatalysts capable of performing chemical transformations) have also been used for heavy metal detection, taking advantage of NP properties. In this way, Wei *et al.*³⁹ reported a simple, sensitive, and label-free DNAzyme-based sensor for Pb²⁺ detection using unmodified AuNPs. The technique is based on the fact that unfolded ssDNA can be adsorbed on the citrate-protected AuNPs while dsDNA cannot. Using this method the substrate cleavage by the DNAzyme in the presence of Pb²⁺ can be monitored by color change of AuNPs. Pb²⁺ detection was realized with a detection limit of 500 nM. A similar approach was reported by Lu's group⁴⁰ for the detection of 100 nM Pb²⁺.

In addition to heavy metals, other pollutants have also been optically detected using this kind of DNAzyme biosensor. For example, colorimetric uranium sensors based on uranyl (UO₂²⁺)-specific DNAzyme and AuNPs have been developed and demonstrated using both labelled and label-free methods for the sensitive detection of this ion, the most soluble and bioavailable form of uranium (Figure 8.5).⁴¹

In the labelled method, a uranyl-specific DNAzyme is attached to the AuNPs, forming purple aggregates. The presence of the uranyl ion induces disassembly of the DNAzyme-functionalized AuNP aggregates, resulting in red individual AuNPs and giving rise to a "turn-on" sensor that can detect 50 nM of uranyl. On the other hand, the label-free method utilizes the different adsorption properties of ssDNA and dsDNA on AuNPs, which affects the stability of AuNPs in the presence of NaCl. The presence of uranyl results in cleavage of substrate by DNAzyme, releasing ssDNA that can be adsorbed on AuNPs and protects them from aggregation. Taking advantage of this

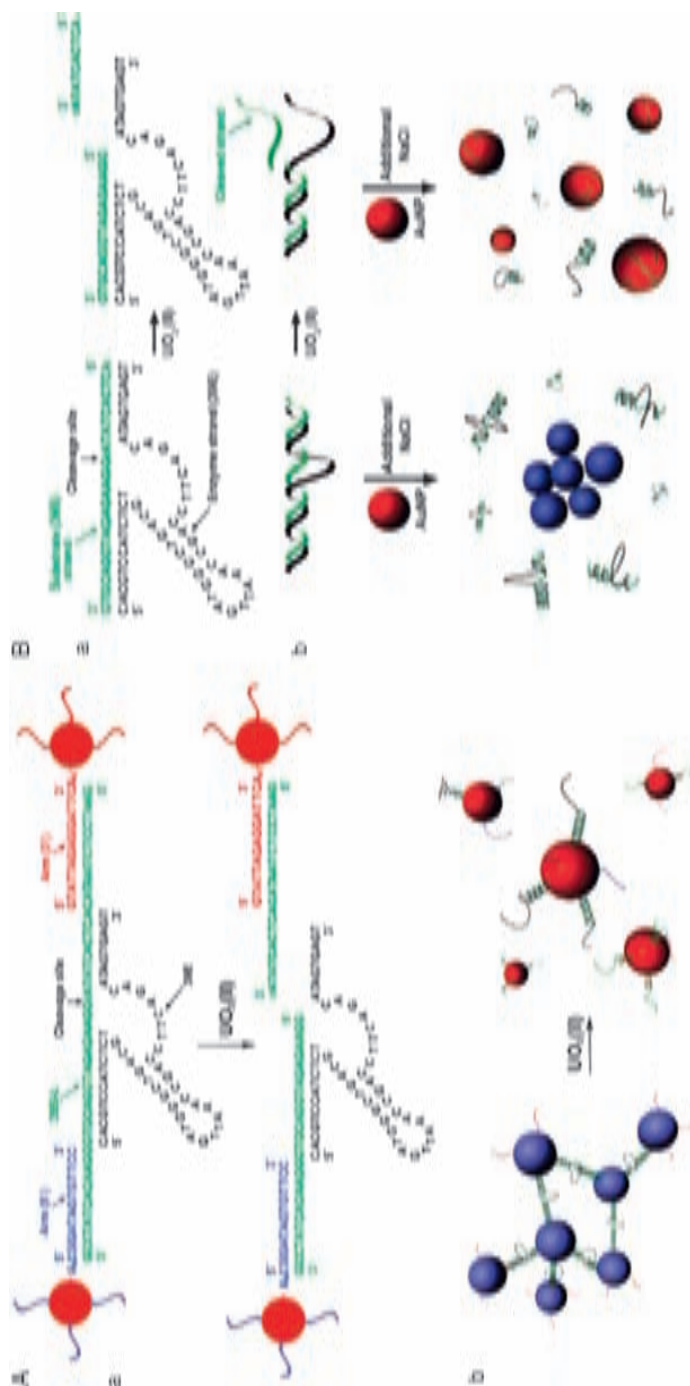


Figure 8.5 (A) (a) Scheme of labelled colorimetric sensor based on AuNP disassembly in the absence and presence of UO_2^{2+} . In the presence of UO_2^{2+} , the length of the weakest complementary part in the aggregates becomes shorter due to UO_2^{2+} -induced substrate cleavage. The substrate cleavage can decrease the melting temperature of AuNP aggregates. (b) As UO_2^{2+} is introduced into AuNP aggregates and the temperature is controlled above the melting temperature of UO_2^{2+} -treated aggregates, AuNP disassembles. (B) (a) Design and sequence of the label-free sensor (complex). After UO_2^{2+} -induced cleavage, 10 mer ssDNA is released which adsorbs on AuNP surface. (b) AuNP reaction in addition of UO_2^{2+} treated/untreated complex and additional NaCl. AuNPs aggregate in the absence of UO_2^{2+} but remain dispersed in its presence. From ref. 41, with permission.

phenomenon, a “turn-off” sensor was developed with a detection limit of 1 nM. Moreover, both sensors showed excellent selectivity over other metal ions.

Aptasensors represent another kind of DNA-based biosensors that has been applied for environmental monitoring. Aptamers are single-stranded DNA or RNA ligands that can be selected for different targets, starting from a huge library of molecules containing randomly created sequences. DNAzymes can only perform chemical modifications on NAs, whereas aptamers can bind a broad range of molecules. A combination of the two has generated a new class of functional NAs known as allosteric DNAzymes or *aptazymes*,⁴² the characteristics of which can be improved using nanomaterials. For example, an adenosine-dependent aptazyme built on the basis of the Pb^{2+} -specific DNAzyme previously described was used to assemble AuNPs.⁴³ In the presence of adenosine, the substrate is cleaved and the assembly inhibited. Several aptazymes (activated RNAzymes) have been shown to have metal-ion-dependent activities,⁴⁴ with further environmental monitoring interest.

8.3.2 Electrochemical Detection Methods

The previously explained strong interaction between Hg^{2+} and bisthymine has also been investigated using electrochemical sensors. Zhu *et al.*⁴⁵ recently reported a sensor for the highly sensitive detection of Hg^{2+} in aqueous solutions, using a T-rich, mercury-specific oligonucleotide (MSO) probe and AuNP-based signal amplification (Figure 8.6). The MSO probe contains seven T bases at both ends and a “mute” spacer in the middle, which, in the presence of Hg^{2+} , forms a hairpin structure via the Hg^{2+} -mediated coordination of T- Hg^{2+} -T base pairs. A thiolated MSO probe is immobilized on gold electrodes to capture free Hg^{2+} in aqueous media, and the MSO-bound Hg^{2+} can be electrochemically reduced to Hg^+ , which provides a readout signal for quantitative detection of Hg^{2+} . This direct immobilization strategy leads to a detection limit of 1 μM . This sensitivity is improved by using MSO probe-modified AuNPs to amplify the electrochemical signals. AuNPs are comodified with the MSO probe and a linking probe that is complementary to a capture DNA probe immobilized on gold electrodes, giving an amplification factor of more than three orders of magnitude. This leads to a limit of detection of 0.5 nM (100 ppt) with an excellent selectivity over a spectrum of interference metal ions.

Zheng *et al.*⁴⁶ have reported a CNT-based DNA biosensor for the sensitive monitoring of phenolic pollutants. The biosensor was constructed by immobilizing DNA on a GCE modified with multiwall carbon nanotubes (MWNTs) dispersed in Nafion (DNA/MWNTs/GCE). The DNA-modified electrode exhibited two well-defined oxidation peaks corresponding to the guanine (G) and adenine (A) residues of DNA, respectively. Phenol, *m*-cresol, and catechol showed noticeable inhibition towards the response of the electrode due to their interactions with DNA. These findings were used to design biosensors with linear response to these phenolic pollutants, obtaining detection limits of 16 μM , 1.2 μM , and 0.52 μM for phenol, *m*-cresol, and catechol respectively.

telomeric i-motif sequence. This DNA is modified with a redox-active dye, methylene blue (MB), and attached to gold electrodes. In the absence of target, the immobilized 26-mer DNA remains unfolded in the buffer, observing a faradaic current due to the attached MB tag. In the presence of the i-motif cDNA, the faradaic current decreases, indicating the formation of telomeric DNA duplex, which prevents the MB tag approaching the electrode surface, allowing the detection of 0.2 ppm of SWNTs (Figure 8.7). Furthermore, the decrease in the signal strongly depends on the type of CNT, making possible the discrimination between SWNTs and MWNTs. This methodology seems to provide new insights into how to design a biosensor for CNT detection.

8.4 Nanoprobe- and Nanochannel-based Sensing

The use of CNTs as a probe in scanning probe microscopy has become an interesting alternative for real applications with industrial interest. The unique mechanical buckling properties of the CNT seem to diminish the imaging force exerted on the sample, thus making CNT scanning probes ideal for imaging soft materials, including samples in liquid environments. Stevens *et al.*⁴⁸ demonstrated the instability of CNT scanning probes when submerged in aqueous solution and introduced a novel approach to resolve this chemical incompatibility by coating the CNT probe with ethylenediamine, thus rendering the CNT probe less hydrophobic and showing the liquid imaging capability of treated CNT probes. This set-up allows the imaging of DNA molecules in aqueous solutions, opening the way to further environmental applications.

The use of synthetic nanopores/nanochannels for biosensing also shows promise. In natural ion channels the ionic current flows through and is altered when a molecule binds to a specific region of the channel. This principle is currently being applied for biosensing purposes, by using biological (α -hemolysin protein) or synthetic (alumina or silicon nitride membranes) biomimetic nanopores and nanochannels, simulating this natural behavior. Nanoporous materials also show a dramatic increase in surface/volume ratio that enhances

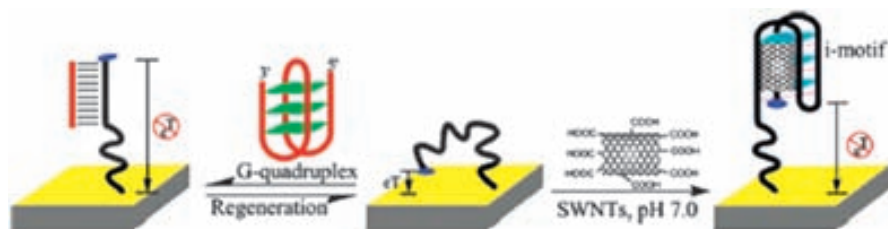


Figure 8.7 Schematic of the i-motif telomeric DNA-based electrochemical sensor for the detection of SWNTs. The sensor is based on a conformation change of an electrode-bound, methylene blue-modified human telomeric C-rich sequence. The plain and dashed lines show the hydrogen bonding formed by the C·C+ hemiprotonated base pair of the “building blocks” for i-motif formation on right panel. From ref. 47, with permission.

the signals corresponding to interaction between solutes and surfaces, including biomolecular reactions. In the case of DNA hybridization detection, the sensing principle is based in the fact that if a ssDNA is immobilized inside the channel, hybridization with the specific target produces a change in the ionic current through the channel that can be measured and related to the DNA concentration.⁴⁹ Based on these principles, nanopore/nanochannel arrays and single nanopores seem to present promising new features for the development of DNA sensors with potential for environmental monitoring.

8.5 Lab-on-a-chip Systems

The current trend in the development of biosensing systems is towards the miniaturization of the whole analytical chain, from sampling to the detection of analytes. The advantages of miniaturized systems in general, and of microfluidic-based biosensors in particular, include reduction of the amount of sample and reagents, detection facility, minimal handling of hazardous materials, and multiple and parallel sample detection capability. All of these characteristics make the process of environmental pollution and toxicity monitoring more efficient and cheaper.

Micro total analysis systems (μ TAS) and lab-on-a-chip (LOC) platforms have been available for several years and shown to be an interesting field of research and applications. Their size characteristics and production facilities allow the handling of extremely small quantities of fluids (picoliters), representing a promising option to improve the detection limit and sensitivity of NA-based biosensors.

Some approaches have been proposed for on-chip amplification and analysis of NAs. These devices can be used to detect DNA or RNA in various kinds of samples, thanks to their selectivity and wide range of physical, chemical, and biological activity.⁵⁰

Some lab-on-a-chip designs, their constituent materials and fabrication processes, control systems, and interfaces with nanoscale/nanomaterial based biosensors for future environmental monitoring possibilities are summarized in the following sections.

8.5.1 Fabrication Technologies

8.5.1.1 Micromanufacturing Techniques

Microtechnology originated in the 1960s, when academics and researchers were interested in developing chips containing many transistors in a small area, which remarkably improved performance and functionality, as well as decreasing costs and the volumes necessary for analysis, giving rise to what was known as the computer science revolution.⁵¹ The term *microelectromechanical system* (MEMS) was coined in the 1980s to describe the new mechanical systems on a chip, such as microelectrical resonators and motors, among others. MEMS processing is generally divided into surface mechanized processes and processes

that generate more complex 3D geometries. MEMS technology has generated many products in areas like the automotive industry, printing, electronics and computer science, among others.⁵² MEMS applications are of special interest for biosensing applications. Several micromanufacturing techniques, as described below, have been developed and applied for chip fabrication.

- *Photolithography*. This technique consists of transferring a pattern from a photomask to the surface of a silicon wafer in crystalline form. This wafer is then used as a substrate. It is possible to use other substrates, such as glass, polymers, sapphire and metals, among others.⁵³ 3D structures fabricated using this process have potential applications in MEMS sensors/actuators, optical devices, and microfluidics.⁵⁴
- *Soft lithography* is related to the manufacturing techniques of microstructures, using elastomers, molds, and conformable photomasks. It is called “soft” because elastomeric materials are used, especially poly(dimethylsiloxane) (PDMS). This technique is generally used to build devices at the micro- and nanometer scale. Processes include impression by micro contact, molding by replica, molding by micro transference, and micromolding in capillaries.⁵⁵
- *Micromachining* is an important manufacturing technology. It is based on the use of a cutting tool to obtain predefined material geometries.⁵⁶ Although the sizes obtained with micromachining are not as small as those obtained using lithography, this technique allows the fabrication of platforms for integration with smaller devices. Other processes used to fabricate microfluidic systems are X-ray lithography,⁵⁷ high-precision molding, hot embossing,⁵⁸ microinjection molding,⁵⁹ and roll-to-roll embossing.⁶⁰ This technology has great potential, thanks to the facility of designing complex 3D structures in a great variety of materials, such as metals, polymers, glass, and ceramics.
- Finally, *microerosion processes* use poly(dimethylsiloxane) (PDMS) and flexopolymer as masking materials for the 3D microstructuring of glass, using powder blasting technology. Such elastomeric masks provide a promising alternative to metallic contact masks for the definition of microstructures⁶¹ and laser micromachining.⁶²

Ink-printing technology was initially used for computer science and decorative objects. Now it is widely used to print on different surfaces, such as aluminum, glass, plastic, and paper, using special inks for different purposes like graphite inks, silver, CNT inks, and polymer inks, among others. It allows printing geometries with certain degrees of thickness and roughness to create 3D structures, without the use of masks.⁶³

8.5.1.2 Sample Treatment and Transport

The study of microfluids is an interdisciplinary field, where sciences like physics, chemistry, engineering, and biotechnology converge. Microfluidics

analyzes the behavior of fluids at the microscopic scale, which differs considerably from their macroscopic behavior; specifically, characteristic such as surface tension and energy dissipation change considerably. In microchannels (diameter 10–500 nm), the Reynolds number is extremely low; this is why the flow is always laminar and diffusion phenomena take place in fluid mixtures.⁶⁴

Microfluidics is related to systems and methods that manipulate fluids on the micron scale. Aspects that must be considered include (1) dimensions of the components; (2) geometry (length, cross-sectional section of the channels, and properties of the surface); (3) characteristics of the surface; (4) characteristics of the fluid (density, viscosity, electrical and thermal conductivity, diffusion coefficients, surface tension, among others), and (5) ambient temperature.

Microfluidic design depends on the application. In cases of special operational requirements such as bioanalytical reactions or biological sample treatment, the design of microfluidic geometries plays an important role. Sample transport and processing can be performed in different ways, such as: (1) electrophoresis^{65,66}; (2) dielectrophoresis;⁶⁷ (3) acoustic and magnetic stimuli;⁶⁸ (4) pneumatic injection;⁶⁹ (5) pressure difference between inlet and outlet, among others. Various detection systems (optical, magnetic, acoustic, electrochemical) have been reported.

8.5.1.3 Integration with Nanoscale Biosensing

DNA-based biosensors and molecular technologies such as the PCR for detection of pathogens are slowly replacing culture-based detection methods, because their higher sensitivity and selectivity and lower times of analysis than culture-based methods. Scientists are overcoming this limitation by miniaturizing molecular assays into a microsystems format. Microfluidics is the most useful technology for the development of miniaturized devices that transport, mix, and control reactive fluid volumes in the micron range.⁷⁰

The use of electronics principles to make the interface between bionanosensors with the microsize platform is continuously increasing because of its potential for easy integration. Microfluidic-based electrochemical sensors, using CNTs and paramagnetic microparticles,⁷¹ NWs,⁷² NW and CNT transistors,⁷³ and field-effect transistor (FET) sensors⁷⁴ have been reported in recent years.

Finally, problems such as nonspecific absorption of the sample in the biosensors and total integration of systems are being widely studied.⁷⁵ New challenges in detection systems, such as the use of new materials or some other modified materials to allow the integration of micro- and nanoscale devices, are being proposed.

8.5.2 Operation

8.5.2.1 Detection Methods

Various microsystems with defined areas for the capture and detection of target pathogen RNA and DNA sequences in materials such as PDMS,⁷⁶ poly(methyl

methacrylate) (PMMA),⁷⁷ and glass, using different kinds of geometries, mass production facilities, and detection techniques, have been developed.

- In *electrochemical detection*, the use of a microchannel with gold microelectrodes integrated to detect DNA fragments through amperometric method has been reported.⁷⁸
- *Optical detection*. In most cases, fluorescence dyes are coupled to specific target probes and used as labels. For example, using superparamagnetic beads and dye liposomes it was possible to detect the hybridization of dengue virus RNA using fluorescence microscopy.⁷⁹ Nucleic acids were also extracted for DNA and RNA analysis, using microfluidic platforms following the PCR principles.⁸⁰
- *Electrochemiluminescent sensing*. The luminol-based reaction has applications in the fields of enzymatic biosensors, immunosensors, DNA sensors, and biochips (Figure 8.8). In this kind of detection, luminescent transitions of excited molecules or atoms to a state of lower energy are characterized by electromagnetic radiations dissipated as photons in the ultraviolet, visible, or near infrared (radiation related with energy involved during the excitation step).⁸¹
- *Chromatography*. The microfluidic concept can be combined with lateral flow principles. One example of this is a lateral flow microarray as platform for DNA detection using the hybridization-mediated target with interest for anthrax detection (Figure 8.8, D).⁸²

8.5.2.2 Applications

NA biosensors using the concepts described above have been used to detect DNA/RNA fragments. Lab-on-a-chip platforms for toxin detection based on electrochemical transducing have been reported.⁸³ For example, a voltammetric DNA hybridization biosensor to detect single mismatches in ssDNA with application in toxicity studies and DNA damage caused by various compounds has been reported by Nowicka *et al.*⁸⁴ A microfluidic platform applied to DNA detection in environmental problems, based on PCR and a microfluidic architecture that compartmentalizes a sample into 1000 nanoliter-sized portions by centrifugation, was reported by Sundberg *et al.*⁷⁰ The platform has a rapid thermocycler with real-time fluorescence detection, achieving PCR cycle times of 33 s and 94% PCR efficiency. A 300-bp plasmid DNA product was amplified within the disk and analyzed in 50 min.

A PDMS microchip for capillary electrophoresis separation of DNA fragments and final amperometric detection has been reported by Joo *et al.*⁷⁸ The capillary is filled with 5% polyacrylamide gel, and separation of DNA fragments of different molecular weight is achieved by application of a high voltage potential across sample and waste reservoirs made at the capillary ends. The amperometric detection system involves in-channel gold microelectrodes to analyze oxidation peak for adenine residues in DNA chain, making it possible

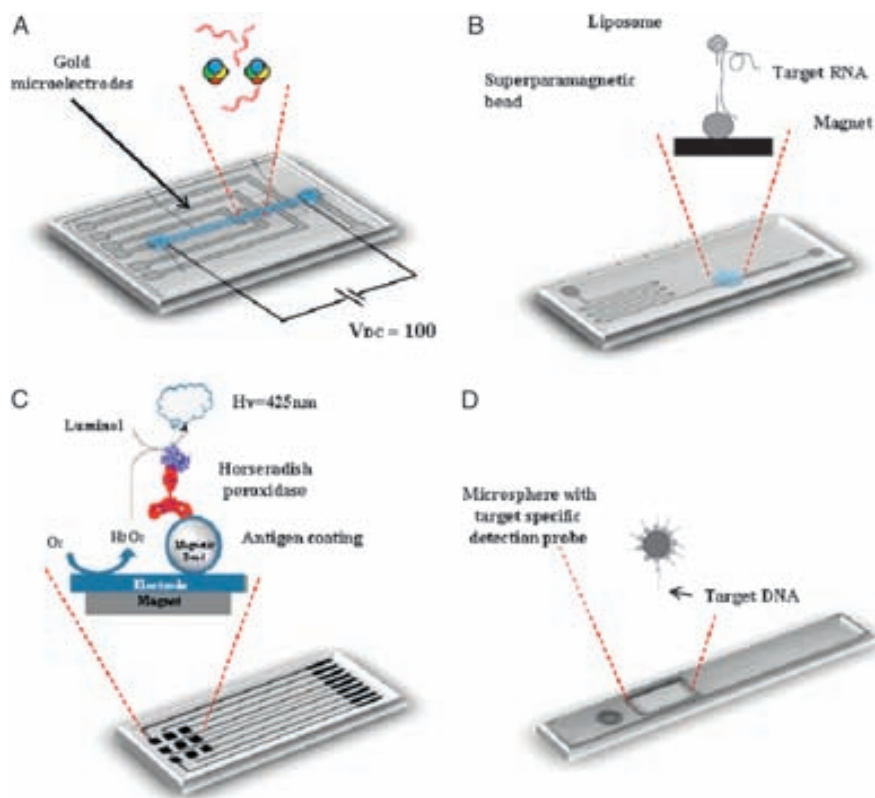


Figure 8.8 Example of acid nucleic detection in chips. (A) Schematic diagram of a capillary electrophoresis–amperometric detection (CE–AD) microchip. Adapted from ref. 78, with permission. (B) A DNA reporter probe is coupled to a liposome while a capture probe is coupled to a magnetic bead. When target RNA is present, the hybridization occurs. The liposome–RNA–bead complex is subsequently immobilized on a permanent magnet in the capture zone of the device. Adapted from 79 and 80, with permission. (C) In-chip electrochemiluminescent detection of glucose, lactate, or choline. Adapted from ref. 81, with permission. (D) Lateral flow device. A compact plastic housing was designed to carry conjugate release pad and a lateral flow membrane (LFM). Adapted from ref. 82, with permission.

to resolve ss and dsDNA fragments with further environmental control of pathogens.

A microfluidic system for the extraction of NAs for further DNA and RNA analysis has been developed by Wing *et al.*⁸⁰ DNA is extracted in a multistep process by isolating and lysing white blood cells, and viral RNA is extracted directly from the submicron-sized viruses in the blood. In both cases an integrated system consisting of a mixer, valves, filters, and binders in silicon/glass microchips is used. The purity of the extracted DNA is finally demonstrated by PCR.

Lateral flow detection of DNA or RNA amplification reaction products provides a simple and cheaper method of NA detection. Indeed, a lateral flow platform may offer many significant advantages for employing NA assays. Darren *et al.*⁸² have reported a nitrocellulose-patterning method that enables microarray feature density to attain lateral flow compatible with different substrates, making it possible to detect up to 250 fmol of target DNA using a low cost and widely available flatbed scanner, with similar sensitivity to that reported for fluorescence and chemiluminiscence detection.

Microfluidic devices have also been used for the detection of heavy metal pollutants. For example, the Pb²⁺-specific DNAzyme discussed in previous sections was also tested in a microfluidic device, and was able to detect less than 1 nL of DNA.⁸⁵ The voltage-controlled microfluidic device was capable of detecting Pb²⁺ concentrations at levels of 11 nM.⁸⁶ Quantitative measurements of Pb²⁺ in complex samples showed this sensor to be selective and suitable to be used for the analysis of lead pollution in groundwater or drinking-water.

The previously mentioned strong interaction between Hg²⁺ and bisthymine has also been applied in ionic metal detection, using capillary electrophoresis to monitor this interaction.⁸⁷ Using a dsDNA chelating fluorescence dye as marker and a polithymine oligonucleotide as probe, highly selective and sensitive detection of Hg²⁺ (0.6 ppb) in pond water and in batteries is achieved after fluorescence detection.

Zhihong *et al.*⁸⁸ described the fabrication and performance of a paper-based electrochemical sensing device capable of quantifying the concentration of different analytes in aqueous solutions, including biological fluids such as urine, serum, and blood. These authors obtained measurements of heavy metal ions with higher sensitivity and limit of detection of around 1 ppb using stripping voltammetry. Following a similar methodology, Zoua *et al.*⁸⁹ presented a heavy metal ion sensor for *in situ* environmental monitoring. The detection and quantification of Pb(II) and Cd(II) was performed by anodic stripping voltammetry, achieving detection limits of 8 ppb and 9.3 ppb for Pb²⁺ and Cd²⁺ respectively. This heavy metal detection system may be applied in future be linked to DNA detection modes, so as to increase the selectivity and sensitivity of heavy metal measurements.

8.6 Conclusions

DNA and nanomaterial-based sensors are proving to be interesting alternative devices for environmental applications. Nanomaterials are integrated in various ways in both electrochemical and optical detection devices. Of the various kinds of nanomaterials available, NPs such as gold NPs and quantum dots are the most reported for their use as labels, including multilabelling technologies. These applications have shown clear advantages over existing technologies. Stability, cost-efficiency, and overall multiplexing analysis seem to be the most important advantages in relation to their application in DNA-based sensors for environmental monitoring uses. Carbon nanomaterials—nanotubes, nanowires, and nanochannels—have also emerged as interesting materials to

improve the performance of DNA sensors. They can lead to significant improvements in both electrochemical and optical properties, thus improving the sensitivity and detection limit for pollutant detection.

Miniaturized systems and lab-on-a-chip devices are also focusing on environmental monitoring applications. Their linkage to DNA systems is still not satisfactory, because of problems related to real sample analysis. Nevertheless, their application as screening tools preliminary to laboratory testing may open the way to the fast and in-field environmental control of specific analytes.

Although in some of DNA-related biosensing systems described in this chapter have not yet been used for environmental monitoring, their established and interesting methodologies may open the way for future applications of sensitive, simple, and cost-effective sensors of interest in this field.

Despite the achievements in the field of nanomaterials and lab-on-a-chip systems for DNA-based environmental control, some inherent problems need to be better addressed before the real advantages of these materials and technologies can be fully exploited. The complex fabrication and measuring techniques currently required are not suited to mass production, and user-friendly technologies need to be developed in to bring these devices to end-users interested in environmental monitoring.

Acknowledgments

MEC (Madrid) for the projects MAT2008-03079/NAN, CSD2006-00012 “NANOBIOMED” (Consolider-Ingenio 2010) and Juan de la Cierva scholarship (A. de la Escosura) is acknowledged.

References

1. A. Merkoçi, M. Aldavert, S. Marín and S. Alegret, *Trends Anal. Chem.*, 2005, **24**, 341.
2. A. Merkoçi, M. Pumera, X. Llopis, B. Perez, M. del Valle and S. Alegret, *Trends Anal. Chem.*, 2005, **24**, 826.
3. A. Merkoçi, *Microchim. Acta*, 2006, **152**, 157.
4. M. Pumera, A. Merkoçi and S. Alegret, *Trends Anal. Chem.*, 2006, **25**, 219.
5. C. A. Mirkin, *Inorg. Chem.*, 2000, **39**(11), 2258.
6. L. Hilliard, X. Zhao and W. Tan, *Anal. Chim. Acta*, 2002, **470**, 51.
7. D. Knopp, D. Tang and R. Niessner, *Anal. Chim. Acta*, 2009, **647**, 14.
8. P. Z. Qin, C. G. Niu, G. M. Zeng, M. Ruan, L. Tang and J. L. Gong, *Talanta*, 2009, **80**, 991.
9. A. Son, D. Dosev, M. Nichkov, Z. Ma, I. M. Kennedy, K. M. Scow and K. R. Hristov, *Anal. Biochem.*, 2007, **370**, 186.
10. G. J. Vora, C. E. Meador, G. P. Anderson and C. R. Taitt, *Mol. Cell. Probes*, 2008, **22**, 294.
11. D. J. Maxwell, J. R. Taylor and S. Nie, *J. Am. Chem. Soc.*, 2002, **124**, 9606.
12. L. A. Lyon, M. D. Musick and M. J. Natan, *Anal. Chem.*, 1998, **70**, 5177.

13. T. Endo, K. Kerman, N. Nagatani, Y. Takamura and E. Tamiya, *Anal. Chem.*, 2005, **77**, 6976.
14. A. I. Hochbaum, R. K. Chen, R. D. Delgado, W. J. Liang, E. C. Garnett, M. Najarian, A. Majumdar and P. D. Yang, *Nature*, 2008, **451**, 163.
15. P. P. Wang, B. Bai, S. Hu, J. Zhuang and X. Wang, *J. Am. Chem. Soc.*, 2009, **131**, 16953.
16. F. Lucarelli, S. Tombelli, M. Minunni, G. Marrazza and M. Mascini, *Anal. Chim. Acta*, 2008, **609**, 139.
17. S. S. Babkina and N. A. Ulakhovich, *Anal. Chem.*, 2005, **77**, 5678.
18. A. de la Escosura-Muñiz, A. Ambrosi and A. Merkoçi, *Trends Anal. Chem.*, 2008, **27**, 568.
19. J. Wang, D. Xu, A. N. Kawde and R. Polsky, *Anal. Chem.*, 2001, **73**, 5576.
20. L. Authier, C. Grossiord and P. Brossier, *Anal. Chem.*, 2001, **73**, 4450.
21. J. Wang, D. Xu and R. Polsky, *J. Am. Chem. Soc.*, 2002, **124**, 4208.
22. M. T. Castañeda, A. Merkoçi, M. Pumera and S. Alegret, *Biosens. Bioelectron.*, 2007, **22**, 1961.
23. M. Pumera, M. T. Castañeda, M. I. Pividori, R. Eritja, A. Merkoçi and S. Alegret, *Langmuir*, 2005, **21**, 9625.
24. H. Cai, Y. Xu, N. Zhu, P. He and Y. Fang, *Analyst*, 2002, **127**, 803.
25. S. Marín and A. Merkoçi, *Nanotechnology*, 2009, **20**, 055101.
26. J. Wang, G. Liu and A. Merkoçi, *Anal. Chim. Acta*, 2003, **482**, 149.
27. T. M. H. Lee, H. Cai and I. M. Hsing, *Analyst*, 2005, **130**, 364.
28. J. Wang, G. Liu and A. Merkoçi, *J. Am. Chem. Soc.*, 2003, **125**, 3214.
29. X. H. Fu, *Bioprocess Biosyst. Eng*, 2008, **31**, 69.
30. J. Wang, A. N. Kawde and M. Musameh, *Analyst*, 2003, **128**, 912.
31. J. Li, H. T. Ng, A. Cassell, W. Fan, H. Chen, Q. Ye, J. Koehne, J. Han and M. Meyyappan, *Nano Lett.*, 2003, **3**, 597.
32. J. E. Koehne, H. Chen, A. M. Cassell, Q. Ye, J. Han, M. Meyyappan and J. Li, *Clin. Chem.*, 2004, **50**, 1886.
33. Y. Feng, T. Yang, W. Zhang, C. Jiang and K. Jiao, *Anal. Chim. Acta*, 2008, **616**, 144.
34. J. I. Hahm and C. M. Lieber, *Nano Lett.*, 2004, **4**, 51.
35. H. Sun, T. S. Choy, D. R. Zhu, W. C. Yam and Y. S. Fung, *Biosens. Bioelectron.*, 2009, **24**, 1405.
36. G. H. Clever, C. Kaul and T. Carell, *Angew. Chem. Int. Ed.*, 2007, **46**, 6226.
37. H. Wang, Y. Wang, J. Jin and R. Yang, *Anal. Chem.*, 2008, **80**, 9021.
38. Z. D. Liu, Y. F. Li, J. Ling and C. Zhihuang, *Environ. Sci. Technol.*, 2009, **43**, 5022.
39. H. Wei, B. Li, J. Li, S. Dong and E. Wang, *Nanotechnology*, 2008, **19**, 095501.
40. J. Liu and Y. Lu, *J. Am. Chem. Soc.*, 2003, **125**, 6642.
41. J. H. Lee, Z. Wang, J. Liu and Y. Lu, *J. Am. Chem. Soc.*, 2008, **130**, 14217.
42. Y. Lu and J. Liu, *Curr. Opin. Biotechnol.*, 2006, **17**, 580.
43. J. Liu and Y. Lu, *Anal. Chem.*, 2004, **76**, 1627.
44. S. Seetharaman, M. Zivartis, N. Sudarsan and R. R. Breaker, *Nat. Biotechnol.*, 2001, **19**, 336.

45. Z. Zhu, Y. Su, J. Li, D. Li, J. Zhang, S. Song, Y. Zhao, G. Li and C. Fan, *Anal. Chem.*, 2009, **81**, 7660.
46. Y. Zheng, C. Yang, W. Pu and J. Zhang, *Microchim. Acta*, 2009, **166**, 21.
47. Y. Peng, X. Wang, Y. Xiao, L. Feng, C. Zhao, J. Ren and X. Qu, *J. Am. Chem. Soc.*, 2009, **131**, 13813.
48. R. M. Stevens, C. V. Nguyen and M. Meyyappan, *IEEE Transactions on Nanobioscience*, 2004, **3**.
49. I. Vlassioup, P. Takmakov and S. Smirnov, *Langmuir*, 2005, **21**, 4776.
50. I. Palchetti and M. Mascini, *Analyst*, 2008, **133**(7), 825.
51. S. E. Lyschevski, *Nano and Microelectromechanical Systems: Fundamentals of Nano and Microengineering*, CRC Press, Boca Raton, FL, 2001, p. 76.
52. S. Achiche, F. Fan and F. Bolognini, *IEEE International Symposium on Industrial Electronics*, Vigo, Spain, 2007, 2150.
53. H. J. Levinson, *Principles of Lithography*, SPIE, Bellingham, WA, 2005, **7**.
54. J. Yeom and M. A. Shannon, *Adv. Funct. Mat.*, 2010, **20**, 289.
55. J. A. Rogers and R. G. Nuzzo, *Mater. Today*, 2005, 50.
56. L. Alting, F. Kumura, H. N. Hansen and G. Bissacco, *CIRP Ann. Manuf. Technol.*, 2003, **52**(2), 635.
57. S. Mongpraneet, A. Wisitsora, R. Phatthanakun, N. Chomnawang and A. Tuantranont, *Am. Vacuum Soc.*, 2009, **27**(3), 1299.
58. J. Greener, W. Li, J. Ren, D. Voicu, V. Pakhareenko, T. Tang and E. Humacheva, *Lab on a Chip*, 2010, **10**, 522.
59. D. S. Kim, S. H. Lee, C. H. Ahn, J. Y. Lee and T. H. Know, *Lab on a Chip*, 2008, **6**, 794.
60. L. P. Yeo, S. H. Ng, Z. Wang and N. F. Rooij, *Microelectro. Eng.*, 2009, **86**, 933.
61. A. Sayah, V. K. Parashar, A. Pawlowski and M. A. M. Gijs, *Sens. Actuators, A*, 2009, **125**, 84.
62. P. P. Shiu, G. K. Knopf and M. Ostojic, *Microsyst. Technol.*, 2010, **16**, 477.
63. S. Roy, *J. Phys. Appl. Phys.*, 2007, **40**, 413.
64. H. A. Stone and S. Kim, *AIChE J.*, 2001, **47**, 1250.
65. D. Wu, J. Qin and B. Lin, *J. Chromatogr.*, 2008, **1184**, 542.
66. D. Siddhartha, D. Tamal and C. Suman, *Sens. Actuators, B*, 2006, **114**(2), 957.
67. F. Grom, J. Kentsch, T. Müller, T. Schnelle and M. Stelzle, *Electrophoresis*, 2006, **27**, 1386.
68. J. D. Adams, P. Thévoz, H. Bruus and T. Soh, *Appl. Phys. Lett.*, 2009, **95**, 254103.
69. W. Zhang, S. Lin, C. Wang, J. Hu, C. Li, Z. Zhuang, Y. Zhou, R. A. Mathies and C. J. Yang, *Lab on a Chip*, 2009, **9**, 3088.
70. S. O. Sundaberg, C. T. Wittwer, C. Gao and B. K. Gale, *Anal. Chem.*, 2010, **82**, 1546.
71. V. Adam, D. Huska, J. Hubalek and R. Kizek, *Microfluid. Nanofluid.*, 2010, **8**, 329.
72. A. Agarwal, K. Buddharaju, I. K. Lao, N. Singh, N. Balasubramanian and D. L. Kwong, *Sens. Actuators, A*, 2008, **145**, 207.

73. M. Lee, K. Y. Baik, M. Noah, Y. K. Kwon, J. Lee and S. Hong, *Lab on a Chip*, 2009, **9**, 2267.
74. D. Kim, J. Park, J. Shin, P. Kim, G. Lim and S. Shoji, *Sensors and Actuators B*, 2006, **117**, 488.
75. H. Ogi, Y. Fukunishi, H. Nagai, K. Okomoto, M. Hirao and M. Nishiyamo, *Biosens. Bioelectron.*, 2009, **24**, 3148.
76. S. Kwakye and A. Baeumner, *Anal. Bioanal. Chem.*, 2003, **376**, 1067.
77. S. R. Nugen, P. J. Asiello, J. T. Connelly and A. J. Baeumner, *Biosens. Bioelectron.*, 2009, **24**, 2428.
78. G. S. Joo, S. K. Jha and Y. S. Kim, *Curr. Appl. Phys.*, 2009, **9**, 222.
79. C. Zhang and D. Xing, *Nucleic Acids Res.*, 2007, **35**, 4223.
80. W. C. Hui, L. Yobas, V. D. Samper, C. K. Heng, S. Liw, H. Ji, Y. Chen, J. Cong, J. Li and T. M. Lim, *Sens. Actuators, A*, 2007, **133**, 335.
81. C. A. Marquette and L. J. Blum, *Anal. Bioanal. Chem.*, 2008, **390**, 155.
82. D. J. Carter and R. B. Cary, *Nucleic Acid Res.*, 2007, **1**(11), 1.
83. I. Palchetti and M. Mascini, *Anal. Bioanal. Chem.*, 2008, **391**, 455.
84. A. M. Nowicka, A. Kowalczyk, Z. Stojek and M. Hepel, *Biophys. Chem.*, 2010, **146**, 42.
85. K. A. Shaikh, K. S. Ryu, E. D. Goluch, J. Nam, J. Liu, C. S. Thaxton, T. N. Chiesl, A. E. Barron, Y. Lu and C. A. Mirkin, *Proc. Natl. Acad. Sci. U. S. A.*, 2005, **102**, 9745.
86. I. H. Chang, J. Tulock, J. Liu, W. S. Kim, D. Cannon, J. R. Y. Lu, P. W. Bohn, J. Sweedler and D. Crokek, *Environ. Sci. Technol.*, 2005, **39**, 3756.
87. C. Chiang, C. Huang, C. Liu and H. Chang, *Anal. Chem.*, 2008, **80**, 3716.
88. Z. Nie, C. A. Nijhuis, J. Gong, X. Chen, A. Kumachev, A. Martinez, M. Narovlyasky and G. M. Whitesides, *Lab on a Chip*, 2010, **10**, 477.
89. Z. Zoua, A. Jangb, E. MacKnighta, P. Wua, J. Doa and P. L. Sens, *Actuators, B*, 2008, **134**, 18.

Micro- and Nanomaterials Based Detection Systems Applied in Lab-on-a-Chip Technology

Mariana Medina¹ and Arben Merkoçi^{1,2}

¹*Nanobioelectronics and Biosensors Group, Institut Català de Nanotecnologia, Bellaterra, Barcelona, Spain*

²*ICREA, Barcelona, Spain*

18.1 Micro- and Nanotechnology in Green Analytical Chemistry

Green Analytical Chemistry is an approach to the synthesis, processing and use of chemicals that reduce risks to humans and environment [1]. These approaches include new processes as well as new tools to minimize the effect of the pollution agents in the human health and nature. One of the main trends to achieve this goal during the design and fabrication of (bio)analytical systems is the introduction of miniaturized methods that can be disposable, cheap, with reusable materials, and that allow a reducing of the use of reagents and materials. That is the case of the lab-on-a-chip (LOC) or microfluidic platforms, where their features are in concordance with the green chemistry philosophy, therefore, the use of this technology allows preventing waste generation, by facilitating the safe use of solvents and other materials, and the optimal use of energy, making chemistry in general, and particularly bioanalytical processes, more sustainable.

Simple and miniaturized micro/nanofluidic platforms are especially interesting due to their advantages, like the use of reduced sample volume, low cost, portability and the possibility of being integrated into conventional analytical techniques. They represent promising alternative tools for point-of-care diagnostics and drug delivery between other applications.

The objective of this chapter is to present the latest trends in the use of nanomaterials (i.e. nanoparticles, quantum dots, nanotubes etc.) in combination with miniaturization and lab-on-a-chip technologies for several analytical chemistry applications of devices that can integrate multiple laboratory functions (separation,

identification and quantification of the chemical and biological analytes) on a single chip able to handle very small sample fluid volumes.

Although LOC technology already represents an established research field the efforts of scientists and engineers are facing a continuous growth toward the synergy of this technology with nanotechnology and material science in general; particularly nanomaterials. The development of novel sensors and biosensors based on nanomaterials and nanostructures – called also nanobiosensors – is opening the way to cost-effective devices that would be the perfect candidates to be integrated into LOC systems. The recent trends in the development of nanomaterials-based biosensors, followed by the LOC technology and the applications of the resulting synergic systems in diagnostics as well as other industries will be shown in the next sections.

18.2 Nanomaterials-based (bio)sensors

Nanotechnology is an emerging field, parallel to many knowledge areas where limits are established from 1 to 100 nm. Different applications can be distinguished such as: nanobiotechnology; nanomedicine; nanomaterials; nanoelectronics; and nanosensors/nanodevices, nanotechnological instrumentation and nanometrology [2].

The application of nanomaterials in the development of sensors and biosensors represents one of the main focuses of the current nanotechnology. The interesting optical and electrical properties are making nanomaterials new building blocks for the design of various kinds of sensing and biosensing devices with improved performance as well as cost-efficient in comparison to conventional materials.

In order to quantify and analyse changing the operation of nanosensors is necessary to use transducers that convert the chemical/biological recognition events to electrical/optical/piezoelectrical signals. Several kinds of nanomaterials such as nanoparticles, nanotubes and other nanostructured materials are being used to design various transducing platforms that lead to interesting nano(bio)sensing systems or nano(bio)sensors.

Transducing platforms based on optical detections such as light absorption and scattering induced by nanoparticles used as labels have proved to be very interesting and have been extended not only to DNA [3] and protein [4] analysis fields but also to other fields (i.e. heavy metal detection [5]). Surface plasmon resonance enhancement by using nanoparticles is also an interesting optical transducing alternative that is bringing advantages to this technique in terms of sensitivity. Between the different optical techniques, those related to fluorescence measurements, including its quench monitoring while using nanoparticles as tracers of biomolecules, are very interesting not only for the shown sensitivity but the possibility to achieve multidetection through multiplexing alternatives [6].

Other kinds of transducers are the *electrochemical transducers* with two classes of biosensors; the biocatalytic devices and the affinity sensors [7]. These transducers can be based on voltammetric/amperometric measurements during which a potential is applied in the working electrode versus a reference electrode and the current related to redox reactions occurring at the working electrode is measured. Amperometric detection is commonly used with biocatalytic and affinity sensors because of its simplicity and low detection limit. Transducers based on potentiometric measurements are related with the determination of the potential difference between either an indicator or a reference electrode or two reference electrodes separated by a perm-selective membrane, when there is no significant current flowing between them. Most common are ion-selective electrodes (ISEs) based on thin films or selective membranes as recognition elements for pH, F⁻, I⁻, CN⁻, Na⁺, K⁺, Ca²⁺ and so on. or even gases (i.e. CO₂, NH₃) [8]. Impedance measurements - during which resistive and capacitive properties of materials, while excited with a small amplitude sinusoidal ac typically of 2–10 mV - are also being used. On other hand, the frequency is varied over a wide range to obtain the impedance spectrum. The impedance based methods are very useful in affinity biosensors [9]; *Conductimetry*,

is another technique that measures the change of the conductivity, commonly used in applications such as environmental monitoring and clinical analysis.

Field effect transistors represent other interesting transducer ISFETs (ion sensitive field effect transistors) or FETs with open gates, with the purpose of using the sum of external gate tension with its own electroactive potential or ionic solution (sample to detect and quantify) have been studied. Most of the reported devices using FET based detectors are fabricated by using conventional photolithography process [10,11,12].

An important transducer used in mass sensors as cantilever, is the *piezoelectric based transducer*. The piezoelectric effect is related to a linear electromechanical interaction between the mechanical and electrical state in crystalline materials. This process is reversible, and is used to transform the variation in the deflection in a micro/nanocantilever where the response toward an analyte reacting with a biorecognizer is measured. These kinds of measurements can also take the advantages of surface acoustic wave detection by means of an interdigitated transducer [13].

Some of the most reported optical and electrochemical nano(bio)systems/nano(bio)sensors based on the various transducing mechanisms already mentioned in this section will be shown and discussed in the following part. The operation of these devices will be discussed in relation also to various kinds of nanomaterials (i.e. nanoparticles) due to their particularities in advantages that these bring in terms of detection performance as well as the variability of assays/detection systems.

18.2.1 Optical nano(bio)sensors

The intrinsic optical properties (UV-Vis light absorption and auto-fluorescence properties) of nanoparticles (NPs) in addition to their ability to change optical properties of sensor surfaces (i.e. in surface plasmon resonance and scattering light based devices) have been approached for their sensible detection in many analytical applications (i.e. detection of DNA, proteins, cells, heavy metals etc.). Various kinds of nanoparticles and other nanomaterials (i.e. nanotubes) are being used in the fabrication of optical sensors.

Core-shell nanoparticles such as magnetic/luminescent $\text{Fe}_3\text{O}_4/\text{Eu:Gd}_2\text{O}_3$ synthesized by spray pyrolysis were used by Son *et al.* as both platforms for the hybridization reactions and as fluorescence labels. The developed DNA hybridization sensor is capable of perfectly distinguishing of matching targets from two-base pair mismatching, allowing the discrimination of different bacterial species [14] (Figure 18.1a).

Some nanostructures are and optimally active have great interest for their potential applications thanks to their optical properties; these are the nanoshells [15]. They consist of small silica spheres covered by a thin gold layer of approximately 100 nm in diameter. Besides their composition, two fundamental factors exist for the optical response of nanoshell: its geometric structure and its dimensions. Modifying these two parameters makes it possible to control the wavelength of the emitted light when the particle scatters the light or when it absorbs radiation and consequently temperature increases. These structures have provided hopeful results in experiments carried out in animal weaves for diagnosis and treatment in cancer patients [16].

Also, simple *gold nanoparticles* (AuNPs) are a promising approach for the cancer cells detection. The University of San Francisco showed that by conjugating gold nanoparticles with specific antibodies, it is possible to detect cancer cells and further remove them by applying ordinary light using a simple optical microscope [17].

It is well known, for example, that the NP plasmon band shifts when AuNPs are aggregated, due to a decrease in the interparticles' distance. The maximum of absorbance shifts from 520nm to 580nm (red to blue colour) when the aggregation takes place and the monitoring of this phenomenon can be used for biosensing purposes. For example, AuNPs suspension previously modified with ssDNA probe has been hybridized with a DNA target (complementary in its two ends with ssDNA) producing NPs aggregation with the consequent change in colour in this way. This principle was pioneered by Mirkin's group and applied for the detection of DNA characteristic of anthrax, a biological warfare agent [18] (Figure 18.1b).

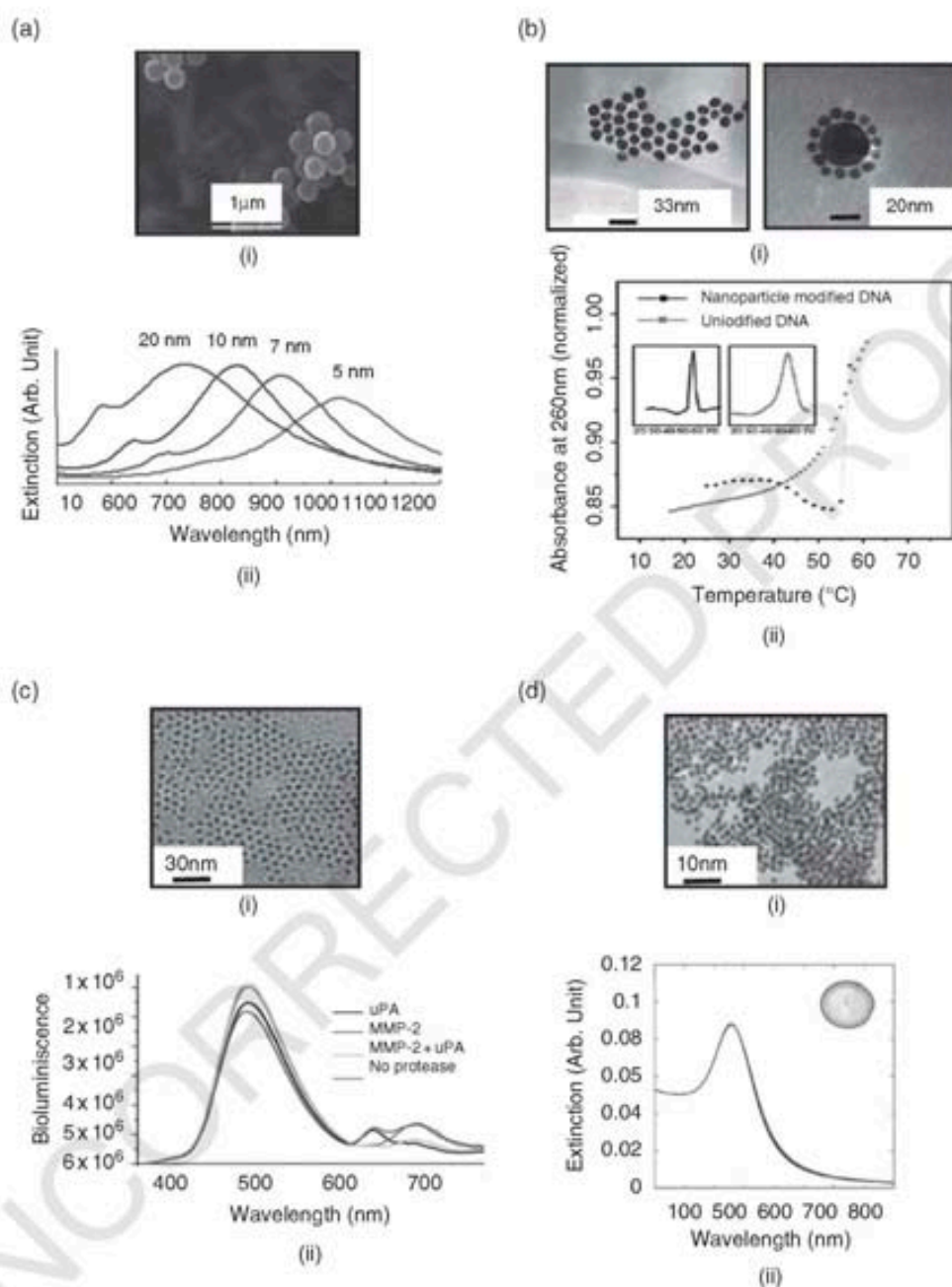


Figure 18.1 Optical nanosensors. (a) TEM image of core (gold)-shell (silicon) nanoparticles (i) and optical resonances of gold shell-silica core nanoshells as a function of their core/shell ratio (ii) (adapted with permission from Reference [16]). (b) TEM image of gold nanoparticles modified with a polypeptide-base (i) and absorbencies of gold nanoparticles modified or not with DNA (ii) (adapted with permission from Reference [18]). (c) TEM image of quantum dots (QDs) (i) and two-plex detection of matrix metalloproteinase-2 (MMP-2), $1 \mu\text{g ml}^{-1}$ and/or urokinase-type plasminogen activator (uPA) $10 \mu\text{g ml}^{-1}$ via the bioluminescence resonance energy transfer (BRET) sensitized photoluminescence (PL) of QDs with peak emission at 655 and 705 nm, respectively (ii) (adapted with permission from Reference [23]). (d) TEM images of hybrid nanoparticles (i), absorbance of the binding of the enzyme to the particles sterically (b) (adapted with permission from Reference [27])

An interesting recent work demonstrates that by using a colourimetric method, a proteinase assay could be developed by exploiting the colour shift upon aggregation of functionalized AuNPs. This aggregation is observed by means of a colour change from red to purple. Researchers used UV spectroscopy to quantify proteinase in future biosensing platforms [19].

Another example is the use of AuNPs to elucidate the mechanism using a unique structure of the monoazacrown ether moieties, useful to detect Pb(II) in aqueous solution at ambient temperatures. These modified AuNPs were shown to be selective to Pb²⁺ ions as the colour changes from brown to purple. This method doesn't use enzymatic reaction or light-sensitive dye molecules and it doesn't require time consuming protocols or sophisticated instrumentation [20].

On the other hand, a silver nanoparticles-on-plastic sensor was recently developed. This sensor is based in polyethylene terephthalate (PET) films chemically modified with *silver nanoparticles* (AgNPs) and it represents a very sensitive platform to monitor protein-protein interactions and biotin-avidin binding by simply changing the surface functionality [21].

Other attractive particles are the *quantum dots* (QDs); crystals with a size of a few nanometres that when appropriately excited, emit light with a colour depending on their size [22]. These nanostructures seem to have a great potential in the cancer cells detection. Companies like the Quantum Dots Corporation produce commercially these crystalline structures, which are used for cancer diagnosis [23] (Figure 18.1c).

QDs are highly sensitive and their versatility in changing their optical properties according to the size and surface modification is especially interesting. A recent application is the QDs-dopamine-peptide bioconjugates coupled pH sensors [24].

New nanostructures used for optical detection are *magnetic fluorescent microspheres* in the evanescent field [25], *upconversion nanoparticles* in biological labelling, imaging and therapy where their operation principle refers to non-linear optical processes that convert two or more low-energy pump photons to a higher-energy output photon [26] and some other hybrid nanoparticles with optical properties [27] (Figure 18.1d).

Bioconjugations of *silicon nanoparticles* (SiNPs) with DNA/RNA molecules can provide unique biofunctionalities. These nanoparticles usually exhibit very high luminescence and photostability, within a broad size range from 5 to 400 nm. Furthermore, dye-doped silica NPs have been extensively used in bioimaging and biochemical analysis due to their advantages such as signal enhancement, photostability and surface modification availability for the immobilization of biomolecules [28].

18.2.2 Electrochemical nano(bio)sensors

Nanotechnology has a great impact on the development of electrochemical biosensors bringing new alternatives for their designs/constructions and modifications. Nanomaterials have been useful to promote electrochemical reactions, improving the sensibility in the measurement thus the specific recognition events [29]. Several electrochemical routes (voltammetric, potentiometric, conductometric, impedimetric and scanning electrochemical microscope-based methods) have been exploited for the sensitive detection of these NP tags in bioassays [30] (Figure 18.2a).

There are many nanoparticles with electrical properties that in combination with micro and nanotechnologies are useful for developing different kinds of electrical based biosensing systems. For example, *metallic nanoparticles* (NPs) modified by bioconjugation present excellent electrochemical activity. It has given rise to their extensive use as labels in nanobiosensors in recent years.

NP-based amplification schemes have improved the sensitivity of bioelectronic assays by several orders of magnitude. In 2001, Wang's [31] and Limoges' [32] groups both pioneered the use of *AuNPs* tags for electronic detection of DNA hybridization. Their protocols are based on capturing the NPs to the hybridized target, followed by highly sensitive anodic stripping electrochemical measurement of the metal tracer.

Other strategies based on the use of *inorganic nanocrystals* offering an electrodiverse population of electrical tags as needed for designing electronic coding have been reported. Three encoding NPs (ZnS, CdS

and PbS) have been used in this way to differentiate the signals of three ssDNA target strands in connection with a sandwich hybridization assays and stripping voltammetry of the corresponding metals [33].

Nanostructured metal oxides are known for their high mechanical, chemical, physical, thermal, electrical, optical, magnetic and also specific surface area properties, which make them really interesting nanostructures for nanoelectronics, nanophotonics, nanobiomaterials, nanobiolabels, and so on [34] (Figure 18.2b). Some examples of these nanostructures are ZnO, TiO₂, ZrO₂, SnO₂, CeO₂, MnO₂, Fe₃O₄ and SiO₂ with interest in applications such as optics, optoelectronics, catalysis, as sensors and actuators [35].

Inorganic-organic hybrid nanocomposites represent other kinds of nanomaterials with electrical properties. They have attracted many scientists over the last few years because of their potential for combining the different physical properties of their organic and inorganic components within a single molecular composite application in the catalysis field, as well as electronics and optics [36]. An example of the use of this material is in the field of electrochemical immunosensors. In the mentioned work, the developed sensor was fabricated by using a CNPs-doped chitosan organic-inorganic hybrid composite membrane as a matrix. This nanocomposite has low toxicity, high conductivity due to the presence of carbon nanoparticles and high compatibility due to the presence of chitosan as a matrix. These nanocomposites used as bionanoparticles displayed high electrochemical responses in comparison to the conventional label methods. Various tumour markers; including carcinoma antigen 125 (CA125), carcinoembryonic antigen (CEA), cancer antigen 19-9 (CA 19-9) and prostate-specific antigen (PSA), obtaining detection limits of 2 ng ml⁻¹ to 0.05 ng ml⁻¹ respectively without any interference from other agents, have been studied [37].

Other nanomaterials such as *carbon nanotubes* (CNTs) being used as carriers for several thousand enzyme tags has been reported allowing the detection of DNA and proteins down to 80 copies (5.4 aM) and 2000 protein molecules (67 aM), respectively [38] with future interest in environmental monitoring.

The electrochemical qualities of carbon-based materials are significantly dependent on the surface properties, such as the creation of specific functional groups on the surface (especially oxygen-containing groups) that can considerably increase the rate of electron transfer. All these properties are the reason which makes this nanomaterial so attractive and versatile to be implemented in sensors and biosensors [39].

(a) Electrochemical sensors



(b) Field effect transistor

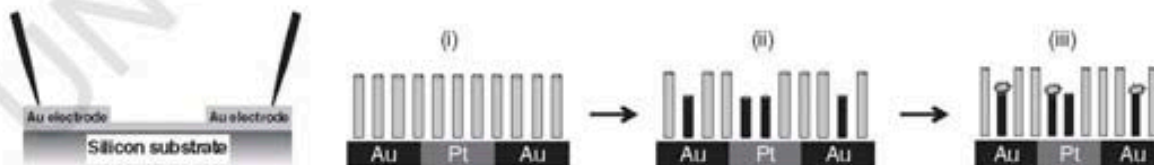


Figure 18.2 Some examples of electrochemical nanosensors. (a) Electrochemical sensors: absorption of AuNPs (open circuit) (i), electrochemical oxidation (+1.25V, 120s) (ii), electrochemical reduction (DPV) (iii) (adapted with permission from Reference [34]). (b) Field effect transistor: nanowires (i), nanowires + MEA (ii), MEA molecules coupled with rhodamine B isothiocyanate (iii) (adapted with permission from Reference [30])

Recent studies have demonstrated that CNTs exhibit strong electrocatalytic activity for a wide range of compounds, such as neurotransmitters, hydrogen peroxide, ascorbic and uric acid, cytochrome c, hydrazines, hydrogen sulfide, amino acids and deoxyribonucleic acid (DNA). Their potential applications in electrochemical sensors and biosensors due to their high conductivity are also reported [40].

Finally, an emergent nanomaterial is *graphene*, constituted by a single-atom-thick and two-dimensional carbon material. It has attracted great attention for being a novel alternative to carbon nanotubes in biosensing, as it had demonstrated its capabilities in many applications. An example of its application is the glucose sensor where the glucose or glutamate molecules were detected by the change of graphene conductance in a transistor platform showing exceptional electronic properties [41]. Some variation in the sensing platform such as a transistor with suspended gate modified with graphene could improve the signal and decrease the noise [42].

18.2.3 Other detection principles

Electrochemiluminescence (ECL) is an optical and electrical phenomenon in which a material emits light in response to an electric current or electrical field. One important application of ECL is in enzyme biosensors based on cadmium sulfide nanocrystals (CdS NCs) in situ formed onto the surface of multi-walled carbon nanotubes (MWCNTs). The MWCNT-CdS can react with H_2O_2 generating strong and stable ECL emission in neutral solution [43] (See Figure 18.3a). By following the same procedure,

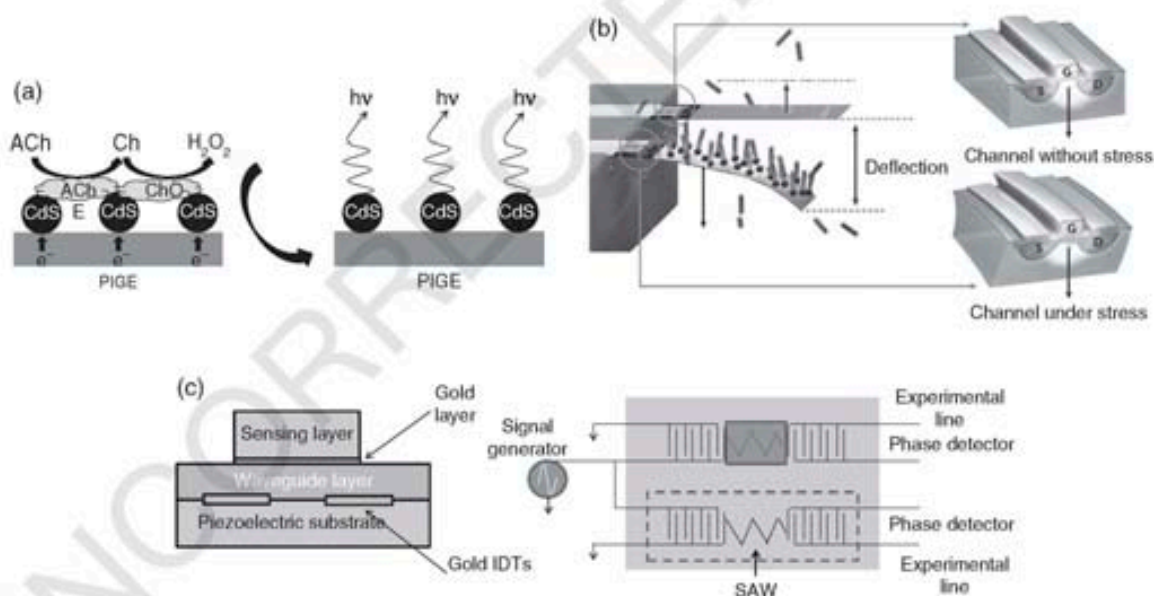


Figure 18.3 Some examples of other detection alternatives. (a) *Electroluminescence*: Schematic diagram of the multi-wall carbon nanotubes (MWCNT): Cadmium sulfide (CdS), acetylcholine esterase (AChE), ECL biosensor for detection of neurotransmitter acetylcholine (ACh) (adapted with permission from Reference [43]); (b) schematic of an embedded metal-oxide semiconductor field-effect transistor (MOSFET) cantilever system (adapted with permission from Reference [46]); and (c) surface acoustic wave sensor (SAW): a sinusoidal voltage is applied to the input (input interdigitated transducer - IDT), which develops an alternating electric field that is translated into a mechanical SAW by the piezoelectric effect. The velocity of the SAW is affected by mass loading, fluid viscosity and temperature on the surface of the substrate (adapted with permission from Reference [45])

the biosensors based on CdS-graphene, had shown promising results to detect H_2O_2 with acceptable linear response from $5\ \mu\text{M}$ up to $1\ \text{mM}$ with a detection limit of $1.7\ \mu\text{M}$ [44].

Electromechanical detection is another interesting detection technique. It is especially interesting for *surface acoustic wave sensors* (SAW), where the mechanical vibration that propagates just below the surface of piezoelectric solids is excited by an electrical signal at the resonant frequency. The velocity of a SAW is sensitive to mass changes applied to the active area, the viscosity of the material applied to the active area and the surface temperature [45] (see Figure 18.3c).

Finally another interesting detection alternative is based on the use of nanowires or nanotubes as mass detectors. One example is the development of a nanocantilever-based sensor with a field effect transistor as a transducer (see Figure 18.3b) where the signal on the gate changes when the cantilever is deflected due to specific binding of biomolecules on its surface [46].

18.3 Lab-on-a-chip (LOC) technology

18.3.1 Miniaturization and nano-/microfluidics

One of the trends in the analytical chemistry field is oriented to the miniaturization, integration and automation of all the analytical steps into a single system. The integration of analytical operations such as filtration, extraction, mixing, separation and detection lead to lab-on-a-chip systems (LOC) or total analysis microsystems (μTAS) [47].

The first LOCs were gas chromatography systems, created in 1975 by S.C. Terry [48], of Stanford University. However, its high growth was in the 1990s with the development of micropumps, flow sensors and the concept of the integrated systems probing the possibility to integrate all steps of treatment, separation and sample cleaning, obtaining a whole analysis in a one single device [49].

Major advantages of micrototal analysis systems (μTAS) are the possibility to reduce the sample and reagents volumes (down to picolitres) and the reaction times as molecular diffusion lengths are of the order of the microchannel dimensions. Another advantage is the large surface-to-volume ratio providing a wide range of possibilities in surface-based assays due its compatibility with microfluidics.

Most common microfluidic system devices consist on microchannel networks made in flat galls or plastic substrates, in which solutions are displaced using pneumatic micropumps or by applying an electric field.

Nanofluidics involves the fluid motion studies in channels with less than $100\ \text{nm}$ in one or more direction. The introduction of this concept was raised due to necessity to replace polymer gels used for DNA separations with solid-state materials. Nanofluidic devices can be designed according to the application requirements, advances in nanofabrication techniques, availability of new tools to investigate and understanding fluid behaviour on the nanoscale finally allowing the prediction of new phenomena at this scale [50].

The design and fabrication of nanofluidic devices requires some previous considerations such as the use of very high pressure gradient to drive fluids. Some applications combine micro and nanochannels inside the geometry [51]. In addition, some other parameters like the introduction of the liquid sample must be considered. It is not an easy process; therefore it had been widely studied. *Capillarity* considers the Young-Laplace relationship and viscous pressure drop [52]. Hibara's group fabricated nanometre-sized channels and performed fluorescence measurements of aqueous solutions [53]. Fluid transport in fused silica nanochannels with diameters between $330\ \text{nm}$ and $850\ \text{nm}$, by capillary action, results in fluid velocity four times lower than the theoretical model, maybe because of the increase of viscosity through the channel. Other alternative to introduce the fluid inside the nanochannel is *dissolution of gas in liquid* based on the high solubility of CO_2 in water, reducing the pressure inside during the fluid introduction [54]. Finally, another studied option is the

pressure-driven flow, demonstrating that the Navier Stokes approach is still available while local shear rate at the interface is lower than the critical shear rate [55].

18.3.2 Micro- and nanofabrication techniques

18.3.2.1 Chip fabrications

Several chip fabrication methodologies that allow the obtaining of different geometries according to the micro- and nanofluidics have been reported. A brief description of the most important technologies is given in the next sections.

Photolithography is an optical methodology that allows transferring of patterns onto certain substrates. It is essentially the same process used in lithographic printing. This technique consists in transferring a landlord from a photomask to the surface of a substrate. Three-dimensional structures fabricated using this process have potential applications in MEMS sensors/actuators, optical devices and microfluidics [56].

Soft Lithography is a manufacturing technique using elastomers, moulds and conformable photomasks. 'Soft' is called because elastomeric materials are used, especially poly(dimethylsiloxane) (PDMS) and recently poly[(3-mercaptopropyl)-methylsiloxane] (PMMS), demonstrating the successful pattern replication from the micrometre to sub-100nm scale [57]. Generally, it is used to build devices at micro- and nanoscale. The process includes technology of impression by microcontact, moulding by replica, moulding by micro transference and micromoulding in capillaries [58].

Micro manufacturing is based on the use of a cutting tool to obtain predefined material geometries [59]. Although the sizes obtained by this technique are not as small as those obtained using lithography, it allows the fabrication of platforms for the integration with smaller devices.

Ink-printing technology was initially used for computer science and decorative objects. Now it is widely used to print on different surfaces, such as aluminium, glass, plastic and paper. Nowadays, special inks like graphite inks, silver, carbon nanotubes inks and polymer inks, among others are used. These allow printing geometries with certain thicknesses and roughness to create three-dimensional structures, without using masks [60].

Polymerization based prototyping is a layer-by-layer fabrication technique through a computer aided design (CAD). Resin is deposited in crud and then using laser traces or an agglutinant cartridge it is polymerized and solidified onto the surface. It allows the construction of 3D structures and assembled pieces [61].

Other processes used to fabricate microfluidic systems are: X-ray lithography [62], moulding by high precision, hot embossing [63], micro-injection moulding⁶⁴, and roll-to-roll embossing [65]. This technology allows building three-dimensional complex structures with a great variety of materials.

18.3.2.2 Electrode/detector fabrication methods

Screen-printed technology is based on the sequential transfer of different conductive or non-conductive inks on a variety of inert substrates through a mask with the desired geometry. Nowadays, screen-printing microfabrication technology is a well-established technology for mass production of thick film electrodes and it is widely applied to build biological or chemical sensors [66]. Screen-printed electrodes (SPE) represent one of the most important products of this technology because these are high mass production and low cost.

Generally, inert substrates used in screen-printed processes are ceramic or polymeric ones. In case of polymeric substrates, polyester substrate is the most commonly used for its durability, thermal and hydroscopic stability, clarity and stiffness. Exact composition of printing inks is uncertain, as they are commercial and patented.

Ink-jet printing is also being used as an alternative to screen-printing technology. Other micro and nanofabrication techniques based on photolithography and other 'micro' and 'nano' imprinting techniques are also extended for electrode/detector fabrication.

18.4 LOC applications

Systems based on nanomaterials-based sensors, lab-on-a-chip technology and micro/nanofabrication techniques have been used to detect different analytes of interests as: cells, proteins, DNA fragments, and so on. Lab-on-a-chip platforms for optical, electrochemical and other detection systems have been reported.

18.4.1 LOCs with optical detections

Biomolecules and nanoparticles with optical properties in order to realize optical detection in a microfluidic system have been reported. Some examples are: (a) the development of a platform with 3D microfluidics used to culture metastatic prostate cancer cells. In addition a microchannel with side-chamber design to keep the spheroids in a stationary way is built. This device was designed with the purpose to evaluate the effect of drugs in the mentioned cells culture using fluorescence dyes for the detection step [67] (Figure 18.4a); (b) use of pillars geometry inside the channel, where circulating tumour cells (CTs) have been identified in peripheral blood from cancer patients. This kind of analytical system can be a potential alternative to invasive biopsies as source of cancer detection through an optical technique [68] (Figure 18.4b); (c) use of a passive mixer, without external forces [69]. The authors studied the hydrodynamics inside the channels at different geometries and did experimental tests using gold nanoparticles and CuSO_4 solutions to visualize the mixing tendencies. The results were coherent with the theoretical calculus exhibiting a good alternative to integrate this system into a lab-on-a-chip system (Figure 18.4c); (d) another example using optical detection is the integration of QDs into a modular microfluidic biosensor for the quantification of biomarkers such as: carcinoembryonic antigen (CEA), cancer antigen 125 (CA125), and Her-2/Neu (C-erbB-2). This detection was applied for both serum and whole saliva specimens [70] (see Figure 18.4d).

18.4.2 LOCs with electrochemical detectors

Electrochemical detectors inside the microfluidic channels for different applications are also described in the literature. Some examples include: (a) paper microfluidics, where micropaper-based microfluidic electrochemical devices (μ PEDs) patterned by photolithography or wax printing, and electrodes screen-printed from conducting inks [71]. This device is applied in the heavy metal detection or glucose in aqueous solutions showing a low-cost alternative for analytical applications in environmental monitoring and public health respectively (Figure 18.5a); (b) a microfluidic system with an integrated control and microelectrochemical modules for detection of urinary proteins was reported. This system has shown a high sensitivity in the urinary proteins detection, including lysozyme and albumin, demonstrating a good alternative for (bio) chemical detections [72] (Figure 18.5b); (c) an amperometric glucose sensor based on glucose oxidase enzyme encapsulated into a sol-gel derived zirconia/Nafion matrix to demonstrate its biosensing capability is also reported. The amperometric measurements were carried out using a three-electrode system. The microchannel was fabricated using SU8 epoxy over the electrode layer and the enzyme was immobilized by sealing with a PDMS membrane [73] (Figure 18.5c); (d) a label-free immunosensor for detection of *E. coli* O157:H7 cells using faradic impedance spectroscopy with an interdigitated microelectrodes array was developed [74] (Figure 18.5d).

The developed electrochemical and LOC based systems show advantages in terms of a better system integration due to the easy miniaturization of the detectors and their compatibility with the detection platform.

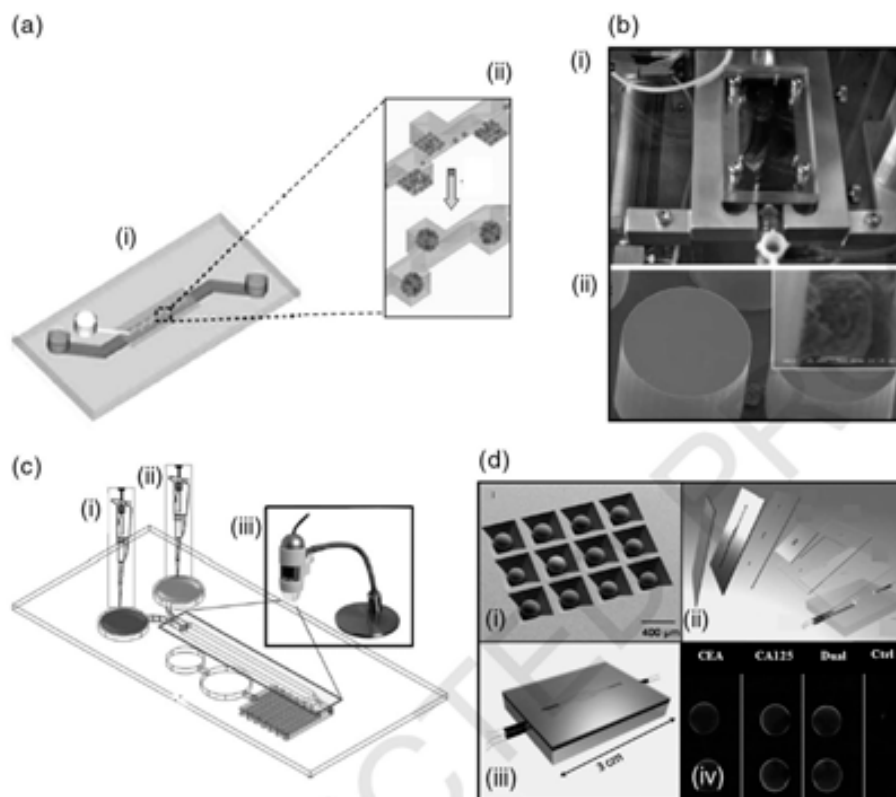


Figure 18.4 Some examples of LOCs with optical detection. (a) 3D PDMS microfluidic for cell culture. Detection using fluorescence dyes (i), co-culture spheroids within 1 day of culture (ii) (adapted with permission from Reference [67]); (b) whole blood flowing through the microfluidic device (i), scanning electron microscope image of a captured NCI-H1650 lung cancer cell spiked into blood. The inset shows a high magnification view of the cell (ii) (adapted with permission from Reference [68]); (c) sample introduction (i), reagents introduction (ii), optical visualization (iii) (adapted with permission from Reference [69]); (d) TEM image of biosensing device (i), layer of the whole microdevice (ii), integration of the microfluidic system (iii), and fluorescence image of each channel using quantum dots as biomarkers (adapted with permission from Reference [70])

18.4.3 LOCs with other detections

Hybrid or multiple detection based LOC systems have also been developed. Figure 18.6 shows some typical examples using: (a) an array of ion sensitive field effect transistors, where the gate of the transistor is open and in contact with the solution to be detected. As a result of this work a microfluidic purification chip for capturing of multiple biomarkers from blood samples is presented. The selective and quantitative detection of two model cancer antigens in less than 20 min was demonstrated [75] (Figure 18.6a); (b) CMOS-compatible approach to fabricate silicon nanowires (SiNW) array biosensor is represented, capable of sensing human cardiac troponin-TcTnT in a buffer solution. Measurements taken were conductance changes, thus providing a method of label-free detection of biomolecular species [76]

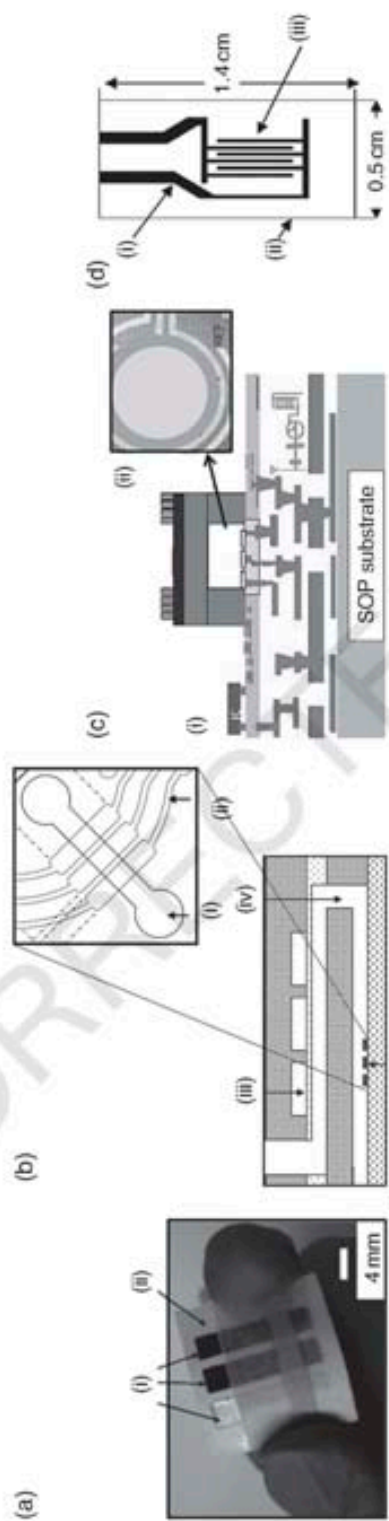


Figure 18.5 Some examples of LOCs with electrochemical detection. (a) Paper-based microfluidic system; electrodes (i), paper channel (ii), paper (iii), tape (iv), hydrophobic barrier (v) (detection using fluoresce dyes) (adapted with permission from Reference [71]). (b) Microfluidic channel (i), electrochemical electrodes (ii), air chamber (iii), microchannel (iv) (adapted with permission from Reference [72]). (c) Amperometric glucose sensor (i), TEM lithography electrode (adapted with permission from [73]). (d) Impedance interdigitated electrode; ITO coating (i), glass substrate (ii), 25 pairs of finger electrodes with $15\ \mu\text{m}$ of digit and interdigit width (iii) (adapted with permission from Reference [74])

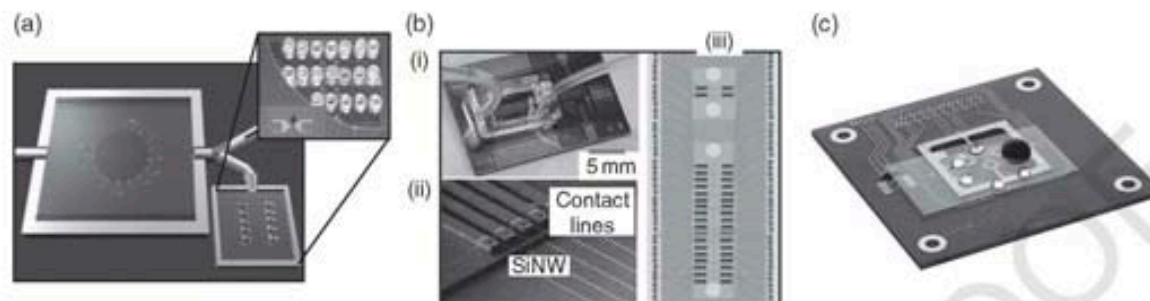


Figure 18.6 (a) Whole blood is injected into the chip with the valve set to the waste compartment (black arrow shows the direction of fluid flow) and, if present in the sample, biomarkers bind their cognate antibodies (adapted with permission from Reference [75]); (b) clockwise from top; image of SiNW device array chip, integrated with microfluidic system for fluid exchange, used in experiments (i), SEM image of a cluster of nanowires (ii), each nanowire is individually addressable by oxide-passivated metal contact lines running out to the external edge of the chip (iii) (adapted with permission from Reference [76]); and (c) example of a contactless microsystem for influenza virus detection including sample preparation and RT-PCR on a disc developed by Pippier and colleagues (adapted with permission from Reference [77])

(Figure 18.6b); contactless detection using an electrode to measure the change of impedance when the influenza virus concentration change is also reported [77] (See Figure 18.6c).

18.5 Conclusions and future perspectives

Micro- and nanomaterials based detection systems applied in lab-on-a-chip technology are showing to be interesting alternative devices for Green Analytical Chemistry. Their benefits in relation with the system integration are being combined with the greatly reducing of the waste amount of solvents and samples provided by the LOC systems. The developed systems provide both environmental and cost/efficiency benefits making the analytical procedures more sustainable.

The micro- and nanomaterial based detection systems integrated into LOC show several advantages in comparison to the classical analytical methods. Nanomaterials are showing to be of particular interest in developing high sensitive (bio)detection devices with multidetection capability and compatibility with LOCs. Various detection techniques ranging from optical, electrochemical and mass changes can be applied. They offer different advantages in terms of the (bio)assay formats, sensitivity, selectivity, linear range of response beside the reproducibility of measurements. Some of the techniques (i.e. electrical/electrochemical) are inherently prone to a better miniaturization in comparison to optical/spectroscopic techniques which make the first one the 'highest' of integrated systems.

The efforts in the development of this novel generation of analytical techniques are related with the breakthroughs in microelectronics and micro/nanotechnology. This synergy is allowing the development of powerful analytical devices that are contributing to the Green (bio) Analytical Chemistry due to the minimization of hazardous substances consumption and the amount of waste generated during assays.

Problems such as the application of some rather complicated fabrication and measuring technologies probably not in agreement with mass production and user-friendly technologies need to be resolved so as to bring these devices to end-users interested in green analytical processes. Overcoming this and other drawbacks (i.e. detection limits, sensibility etc.) of the systems would bring new benefits for our society: better point-of-care diagnostics for healthcare, safety and security beside other applications.

Acknowledgements

Ministerio de Ciencia e Innovación. MICIN (Madrid) for the Project MAT2008-03079/NAN is acknowledged.

References

1. Koel, M. and Kaljurand, M. (2006) Application of the principles of Green Chemistry in analytical chemistry, *Pure Appl. Chem.*, **78**, 1993–2002.
2. Valcárcel, M.; Simonet, B. and Cárdenas, S. (2008) Analytical nanoscience and nanotechnology today and tomorrow, *Anal. Bioanal. Chem.*, **391**, 1881–1887.
3. Merkoçi, A.; Aldavert, M.; Marín, S. and Alegret, S. (2005) New materials for electrochemical sensing. V. Nanoparticles for DNA labelling, *Trends in Anal. Chem.*, **24**, 341–349.
4. de la Escosura-Muñiz, A.; Parolo, C. and Merkoçi, A. (2010) Immunosensing using nanoparticles, *Materials Today*, **13**, 24–34.
5. Aragay, G.; Pons, J.; Ros, J. and Merkoçi, A. (2010) Aminopyrazole based ligand induces gold nanoparticle formation and remains available for heavy metals sensing. A simple 'mix and detect' approach, *Langmuir*, **26**, 10165–10170.
6. Merkoçi, A. (2010) Nanoparticles-based strategies for DNA, protein and cell sensors, *Biosens. Bioelectron.*, **26**, 1164–1177.
7. Ronkainen, N.J.; Halsall, H.B. and Heineman, W.R. (2010) Electrochemical biosensors, *Chem. Soc. Rev.*, **39**, 1747–1763.
8. de la Escosura-Muñiz, A.; Ambrosi, A. and Merkoçi, A. (2008) Electrochemical analysis with nanoparticle based biosystems, *Trac-Trend. Anal. Chem.*, **27**, 568–584.
9. Suni, I.I. (2008) Impedance methods for electrochemical sensors using nanomaterials, *Trac-Trend. in Anal. Chem.*, **27**, 604–6011.
10. Masadome, T.; Yada, K. and Wakida, S.I. (2006) Microfluidic Polymer Chip Integrated with an ISFET Detector for Cationic Surfactant Assay in Dental Rinses, *Anal. Sci.*, **22**, 1065–1069.
11. Tsai, H.H.; Lin, C.F.; Juang, Y.Z.; Wang, I.L.; Lin, Y.C.; Wang, R.L. and Lin, H.Y. (2010) Multiple type biosensors fabricated using the CMOS BioMEMS platform, *Sensor. Actuator. B*, **144**, 407–412.
12. Waleed Shinwari, M. and Jamal Deen, M. (2008) Optimization of DNA Detection Using FETs, *IEEE*, 185–188.
13. Strambini, E.; Piazza, V.; Pingue, P.; Biasiol, G.; Sorba, L. and Beltram, F. (2010) Cantilever deflection measurement and actuation by an interdigitated transducer, *Appl. Phys. Lett.*, **96**, 173505–173508.
14. Son, A.; Dosev, D.; Nichkov, M.; Ma, Z.; Kennedy, I.M.; Scow, K.M. and Hristov, K.R. (2007) Quantitative DNA hybridization in solution using magnetic/luminescent core-shell nanoparticles, *Anal. Biochem.*, **370**, 186–194.
15. Averitt, R.D.; Westcott, S.L. and Halas, N.J. (1999) Linear optical properties of gold nanoshells, *J. Opt. Soc. Am. B*, **16**, 1824–1832.
16. Loo, C.; Lin, A.; Hirsch, L.; Lee, M.-H.; Barton, J.; Halas, N.; West, J. and Drezek, R. (2004) Nanoshell-enabled photonics-based imaging and therapy of cancer, *Technol. Cancer Res. Treat.*, **3**, 33–40.
17. I. El-Sayed, H.; Huang, X. and El-Sayed, M.A. (2005) Surface plasmon resonance scattering and absorption of anti-EGFR antibody conjugated gold nanoparticles in cancer diagnostics: Applications in oral cancer, *Nano Letters*, **5**(5), 829–834.
18. Mirkin, C.A. (2000) Programming the assembly of two- and three-dimensional architectures with DNA and nanoscale inorganic building blocks, *Inorg. Chem.*, **39**, 2258–2272.
19. Chuang, Y.C.; Li, J.C.; Chen, S.H.; Liu, T.Y.; Kuo, C.H.; Huang, W.T. and Lin, C.S. (2010) An optical biosensing platform for proteinase activity using gold nanoparticles, *Biomaterials*, **31**, 6087–6095.
20. Alizadeh, A.; Khodaei, M.M.; Karami, Ch.; Workentin, M.S.; Shamsipur, M. and Sadeghi, M. (2010) Rapid and selective lead (II) colorimetric sensor based on azacrown ether-functionalized gold nanoparticles, *Nanotechnology*, **21**, 315503–315511.

21. Fan, M.; Thompson, M.; Andrade, M.L. and Brolo, A.G. (2010) Silver nanoparticles on a plastic platform for localized surface plasmon resonance biosensing, *Anal. Chem.*, **82**, 6350–6352.
22. Michalet, X.; Pinaud, F.F.; Bentolila, L.A.; Tsay, J.M.; Doose, S.; Li, J.J.; Sundaresan, G.; Wu, A.M.; Gambhir, S.S. and Weiss, S. (2005) Quantum dots for live cells, in vivo imaging, and diagnostics, *Science*, **28**, 538–544.
23. Algar, W.R. and Krull, U.J. (2010) New opportunities in multiplexed optical bioanalyses using quantum dots and donor–acceptor interactions, *Anal. Bioanal. Chem.*, **398**, 2439–2449.
24. Medintz, I.L.; Stewart, M.H.; Trammell, S.A.; Susumu, K.; Delehanty, J.B.; Mei, B.C.; Melinger, J.S.; Blanco-Canosa, J.B.; Dawson, P.E. and Mattoussi, H. (2010) Quantum-dot/dopamine bioconjugates function as redox coupled assemblies for in vitro and intracellular pH sensing, *Nature Materials*, **9**, 676–684.
25. Bijamov, A.; Shubitidze, F.; Oliver, P.M. and Vezenov, D.V. (2010) Optical response of magnetic fluorescent microspheres used for force spectroscopy in the evanescent field, *Langmuir*, **26**, 12003–12011.
26. Wang, K.; Liu, Q.; Wu, X.Y.; Guan, Q.M. and Li, H.N. (2010) Graphene enhanced electrochemiluminescence of CdS nanocrystal for H₂O₂ sensing, *Talanta*, **82**, 372–376.
27. Aili, D. and Stevens, M.M. (2010) Bioresponsive peptide–inorganic hybrid nanomaterials, *Chem. Soc. Rev.*, **39**, 3358–3370.
28. Knopp, D.; Tang D. and Niessner, R. (2009) Review: bioanalytical applications of biomolecule-functionalized nanometer-sized doped silica particles, *Anal. Chim. Acta*, **647**, 14–30.
29. Pumera, M.; Sánchez, S.; Ichinose, I. and Tang, J. (2007) Electrochemical nanobiosensors, *Sensor. Actuator. B: Chem.*, **123**, 1195–1205.
30. de la Escosura-Muñiz, A.; Ambrosi, A. and Merkoçi, A. (2008) Electrochemical analysis with nanoparticle-based biosystems, *TrAC-Trend. Anal. Chem.*, **27**, 568–584.
31. Wang, J.; Xu, D.; Kawde, A.N. and Polsky, R. (2001) Metal nanoparticle-based electrochemical stripping potentiometric detection of DNA hybridization, *Anal. Chem.*, **73**, 5576–5581.
32. Authier, L.; Grossiord, C. and Brossier, P. (2001) Gold nanoparticle-based quantitative electrochemical detection of amplified human cytomegalovirus DNA using disposable microband electrodes, *Anal. Chem.*, **73**, 4450–4456.
33. Wang, J.; Liu, G. and Merkoçi, A. (2003) Electrochemical coding technology for simultaneous detection of multiple DNA targets, *J. Am. Chem. Soc.*, **125**, 3214–3215.
34. Wanekaya, A.K.; Chen, W.; Myung, N.V. and Mulchandani, A. (2006) Nanowire-based electrochemical biosensors. *Electroanalysis*, **18**, 533–550.
35. Ansari, A.A.; Solanki, P.R.; Kaushik, A. and Malhotra, B.D. (2009) Recent advances in nanostructured metal oxides based electrochemical biosensors for clinical diagnostics, in *Nanostructured Materials for Electrochemical Biosensors*. Nova Science Publishers.
36. Shchipunov, Y.A.; Karpenko, T.Y. and Krekoten, A.V. (2005) Hybrid organic–inorganic nanocomposites fabricated with a novel biocompatible precursor using sol–gel processing, *Compos. Interface.*, **11**, 587–607.
37. Tang, J.; Su, B.; Tang, D. and Chen, G. (2010) Conductive carbon nanoparticles-based electrochemical immunosensor with enhanced sensitivity for α -fetoprotein using irregular-shaped gold nanoparticles-labeled enzyme-linked antibodies as signal improvement, *Biosens. Bioelectron.*, **25**, 2657–2662.
38. Munge, B.; Liu, G.; Collins, G. and Wang, J. (2006) Multiple enzyme layers on carbon nanotubes for electrochemical detection down to 80 DNA copies, *Anal. Chem.*, **77**, 4662–4666.
39. Hu, C. and Hu, S. (2009) Carbon nanotube-based electrochemical sensors: Principles and applications in biomedical systems, *Journal of Sensors* (on-line publication).
40. Pérez, B. (2007) *Carbon Nanotubes for Electrochemical (Bio)Sensing*. Universidad Autónoma de Barcelona. Ph.D Thesis. Chemistry Department. Science Faculty, Barcelona-Spain.
41. Huang, Y.; Dong, X.; Shi, Y.; Li, C.M.; Li, L.J. and Chen, P. (2010) Nanoelectronic biosensors based on CVD grown grapheme, *Nanoscale*, **2**, 1485–1488.
42. Cheng, Z.; Li, Q.; Li, Z.; Zhou, Q. and Fang, Y. (2010) Suspended graphene sensors with improved signal and reduced noise, *Nano Lett.*, **10**, 1864–1868.
43. Wang, X.F.; Zhou, Y.; Xu, J.J. and Chen, H.Y. (2009) Signal-on electrochemiluminescence biosensors based on CdS–carbon nanotube nanocomposite for the sensitive detection of choline and acetylcholine, *Adv. Funct. Mater.*, **19**, 1444–1450.

44. Wang, F.; Banerjee, D.; Liu, Y.; Chen, X. and Liu, X. (2010) Upconversion nanoparticles in biological labeling, imaging, and therapy, *Analyt.*, **135**, 1839–1854.
45. Arruda, D.L.; Wilson, W.C.; Nguyen, C.; Yao, Q.W.; Caiazzo Jr, R.J.; Talpasanu, I.; Dow, D.E. and Liu, B.C.S. (2009) Microelectrical sensors as emerging platforms for protein biomarker detection in point-of-care diagnostics, *Expert Rev. Mol. Diagn.*, **9**, 749–755.
46. Cheng, M.M.C.; Cuda, G.; Bunimovich, Y.L.; Gaspari, M.; Heath, J.R.; Hill, H.D.; Mirkin, C.A.; Nijdam, A.J.; Terracciano, R.; Thundat, T. and Ferrari, M. (2006) Nanotechnologies for biomolecular detection and medical diagnostics, *Curr. Opin. Chem. Biol.*, **10**, 11–19.
47. Dittrich, P.S.; Tachikawa, K. and Manz, A. (2006) Micro Total Analysis Systems. Latest advancements and trends, *Anal. Chem.*, **78**, 3887–3908.
48. Terry, S.C. (1975) A gas chromatographic air analyzer fabricated on silicon wafer using integrated circuit technology. PhD. Dissertation Stanford University.
49. Manz, A.; Graber, N. and Widmer, H.M. (1990) Miniaturized total chemical analysis systems: A novel concept for chemical sensing, *Sensor. Actuator. B1*, 244–248.
50. Sparreboom, W.; van den Berg, A. and Eijkel, J.C.T. (2009) Principles and applications of nanofluidic transport, *Nature nanotechnology*, **4**, 713–720.
51. Tamaki, E.; Hibara, A.; Kim, H.B.; Tokeshi, M. and Kitamori, T. (2006) Pressure-driven flow control system for nanofluidic chemical process, *J. Chromatogr. A*, **1137**, 256–262.
52. Tas, N.R.; Mela, P.; Kramer, T.; Berenschot, J.W. and van den Berg, A. (2003) Capillarity induced negative pressure of water plugs in nanochannels, *Nano Letters*, **3**, 1537–1540.
53. Hibara, A.; Saito, T.; Kim, H.B.; Tokeshi, M.; Ooi, T.; Nakao, M. and Kitamori, T. (2002) Nanochannels on a fused-silica microchip and liquid properties investigation by time-resolved fluorescence measurements, *Anal. Chem.*, **74**, 6170–6176.
54. Phan, V.N.; Nguyen, N.T.; Yang, C.; Joseph, P.; Djeghla, L.; Bourrier, D. and Gue, A.M. (2010) Capillary filling in closed end nanochannels, *Langmuir*, **26**, 13251–13255.
55. Zhang, Z.Q.; Zhang, H.W. and Ye, H.F. (2010) Pressure-driven flow in parallel-plate nanochannels, *Appl. Phys. Lett.*, **95**, DOI: 154101_1-154101_3.
56. Richards Grayson, A.C.; Shawgo, R.S.; Johnson, A.M.; Flynn, N.T.; Li, Y.; Cima, M.J. and Langer, R. (2004) A BioMEMS Review: MEMS technology for physiologically integrated devices, *Proceedings of the IEEE*, **92**, 6–21.
57. Campos, L.M.; Truong, T.T.; Shim, D.E.; Dimitriou, M.D.; Shir, D.; Meinel, I.; Gerbec, J.A.; Hahn, H.T.; Rogers, J.A. and Hawker, C.J. (2009) Applications of photocurable PMMS thiol-ene stamps in soft lithography, *Chem. Mater.*, **21**, 5319–5326.
58. Lomas, T.; Mongpraneet, S.; Wisitsoraat, A.; Jaruwongrunsee, K.; Sappat, A.; Maturros, T.; Chevasuvit, F. and Tuantranont, A. (2009) Low cost hot Embossing process for plastics microfluidic chips fabrication, *6th International Conference on Electrical Engineering/Electronics, Computer, Telecommunications and Information Technology*, 462–464.
59. Shiu, P.P.; Knopf, G.K. and Ostojic, M. (2010) Fabrication of metallic micromolds by laser and electro-discharge micromachining, *Microsyst. Technol.*, **16**, 477–485.
60. Roy, S. (2007) Fabrication of micro- and nano-structured materials using mask-less processes, *J. Phys. D: Appl. Phys.*, **40**, 413–426.
61. Nath, P.; Fung, D.; Kunde, Y.A.; Zeytun, A.; Branch, B. and Goddard, Rapid prototyping of robust and versatile microfluidic components using adhesive transfer G. (2010) tapes, *Lab. Chip*, **10**, 2286–2291.
62. Mongpraneet, S.; Wisitsora, A.; Phatthanakun, R.; Chomnawang, N. and Tuantranont, A. (2010) Low-cost X-ray mask based on micropattern sputtered lead film for X-ray lithography, *American Vacuum Society*, **27**, 1299–1303.
63. Greener, J.; Li, W.; Ren, J.; Voicu, D.; Pakhareenko, V.; Tang, T. and Kumacheva, E. (2009) Rapid, cost-efficient fabrication of microfluidic reactors in thermoplastic polymers by combining photolithography and hot embossing, *Lab. Chip*, **10**, 522–524.
64. Choi, S.H.; Kim, D.S. and Kwon, T.H. (2009) Microinjection molded disposable microfluidic lab-on-a-chip for efficient detection of agglutination, *Microsyst. Technol.*, **15**, 309–316.
65. Yeo, L.P.; Huan, S.; Wang, Z.; Wang, Z. and Frans, N. (2009) Micro-fabrication of polymeric devices using hot roller embossing, *Microelectron. Eng.*, **86**, 933–936.

66. Fanjul-Bolado, P.; Hernández-Santos, D. and Lamas-Ardisana, P.J. (2008) Electrochemical characterization of screen-printed and conventional carbon paste electrodes, *Electrochim. Acta*, **53**, 3635–3642.
67. Hsiao, A.Y.; Torisawa, Y.S.; Tung, Y.C.; Sud, S.; Taichman, R.S.; Pienta, K.J. and Takayama, S. (2009) Microfluidic system for formation of PC-3 prostate cancer co-culture spheroids, *Biomaterials*, **30**, 3020–3027.
68. Nagrath, S.; Sequist, L.V.; Maheswaran, S. *et al.* (2007) Isolation of rare circulating tumour cells in cancer patients by microchip technology, *Nature*, **450**, 1235–1241.
69. Jeon, W. and Shin, C.B. (2009) Design and simulation of passive mixing in microfluidic systems with geometric variations, *Chem. Eng. J.*, **152**, 575–582.
70. Jokerst, J.V.; Raamanathan, A.; Christodoulides, N. *et al.* (2009) Nano-bio-chips for high performance multiplexed protein detection: Determinations of cancer biomarkers in serum and saliva using quantum dot bioconjugate labels, *Biosens. Bioelectron.*, **24**, 3622–3629.
71. Nie, Z.; Nijhuis, C.A.; Gong, J.; Chen, X.; Kumachev, A.; Martinez, A.W.; Narovlyanskya, M. and Whitesides, G.M. (2010) Electrochemical sensing in paper-based microfluidic devices, *Lab. Chip*, **10**, 477–483.
72. Liu, G.; Wang, J.; Kim, J. and Jan, M.R. (2003) Electrochemical coding for multiplexed immunoassay of proteins, *Anal. Chem.*, **76**, 7126–7130.
73. Huang, C.J.; Chen, Y.H.; Wang, C.H.; Chou, T.C. and Lee, G.B. (2007) Integrated microfluidic systems for automatic glucose sensing and insulin injection, *Sensors Actuator B-Chem.*, **122**, 461–468.
74. Yang, L.; Li, Y. and Erf, G.F. (2004) Interdigitated array microelectrode-based electrochemical impedance immunosensor for detection of escherichia coli O157:H7, *Anal. Chem.*, **76**, 1107–1113.
75. Stern, E.; Vacic, A.; Rajan, N.K.; Criscione, J.M.; Park, J.; Ilic, B.R.; Mooney, D.J.; Reed, M.A. and Fahmy, T.M. (2010) Label-free biomarker detection from whole blood, *Nature Nanotechnology*, **5**, 138–142.
76. Chua, J.H.; Chee, R.E.; Agarwal, A.; Wong, S.M. and Zhang, G.J. (2009) Label-Free Electrical Detection of Cardiac Biomarker with Complementary Metal-Oxide Semiconductor-Compatible Silicon Nanowire Sensor Arrays, *Anal. Chem.*, **81**, 6266–6271.
77. Schulze, H.; Giraud, G.; Crain, J. and Bachmann, T.T. (2009) Multiplexed optical pathogen detection with lab-on-a-chip devices, *J. Biophoton.*, **2**, 199–211.

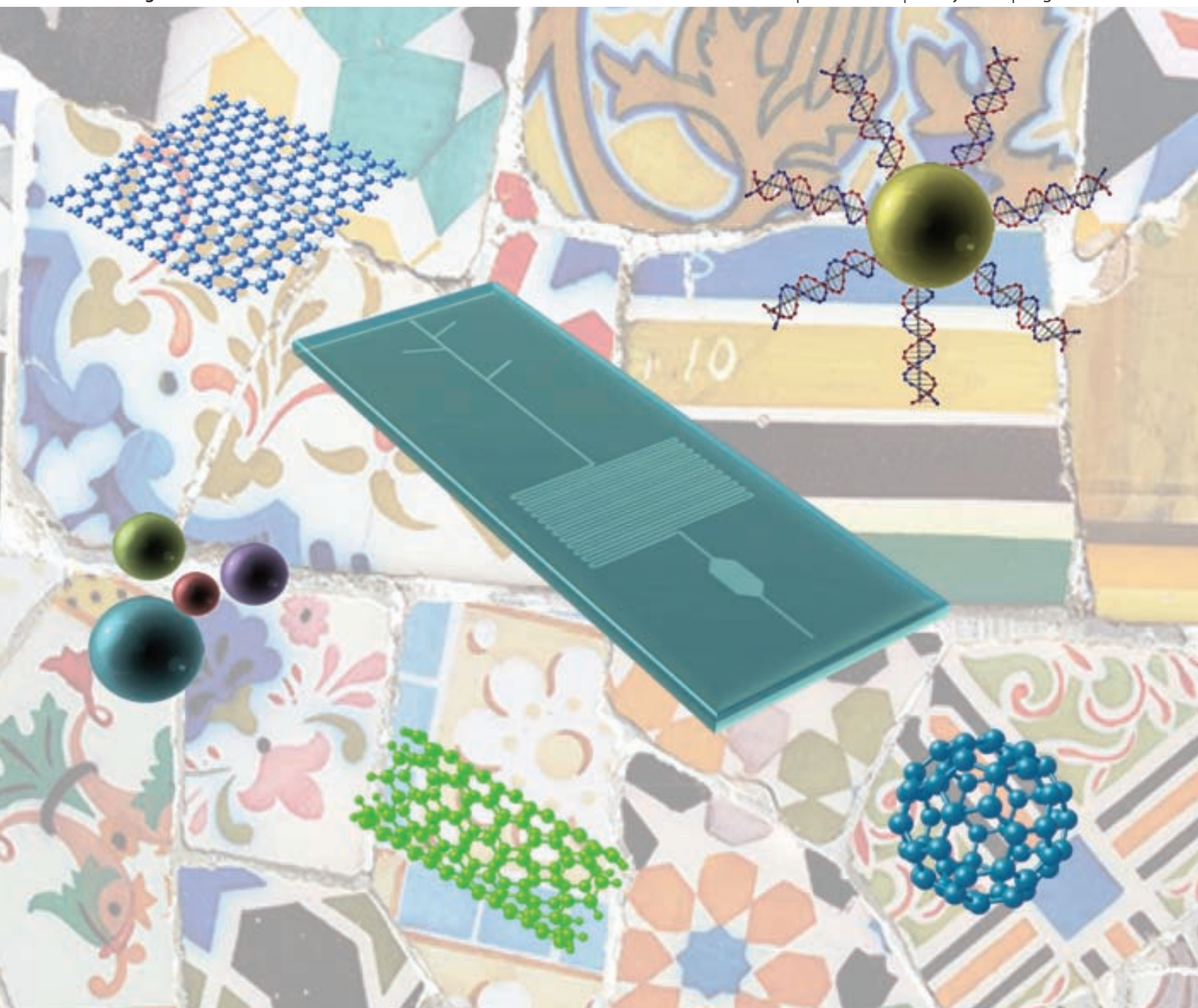
UNCORRECTED PROOF

Lab on a Chip

Miniaturisation for chemistry, physics, biology, materials science and bioengineering

www.rsc.org/loc

Volume 12 | Number 11 | 8 May 2012 | Pages 1905–2076



ISSN 1473-0197

RSC Publishing

CRITICAL REVIEW

Arben Merkoçi *et al.*

Nanomaterials and lab-on-a-chip technologies

Cite this: *Lab Chip*, 2012, 12, 1932–1943

www.rsc.org/loc

CRITICAL REVIEW

Nanomaterials and lab-on-a-chip technologies†

Mariana Medina-Sánchez,^{ab} Sandrine Miserere^{ab} and Arben Merkoçi^{*abc}

Received 13th January 2012, Accepted 19th March 2012

DOI: 10.1039/c2lc40063d

Lab-on-a-chip (LOC) platforms have become important tools for sample analysis and treatment with interest for DNA, protein and cells studies or diagnostics due to benefits such as the reduced sample volume, low cost, portability and the possibility to build new analytical devices or be integrated into conventional ones. These platforms have advantages of a wide set of nanomaterials (NM) (*i.e.* nanoparticles, quantum dots, nanowires, graphene *etc.*) and offer excellent improvement in properties for many applications (*i.e.* detectors sensitivity enhancement, biolabelling capability along with other in-chip applications related to the specificities of the variety of nanomaterials with optical, electrical and/or mechanical properties). This review covers the last trends in the use of nanomaterials in microfluidic systems and the related advantages in analytical and bioanalytical applications. In addition to the applications of nanomaterials in LOCs, we also discuss the employment of such devices for the production and characterization of nanomaterials. Both framed platforms, NMs based LOCs and LOCs for NMs production and characterization, represent promising alternatives to generate new nanotechnology tools for point-of-care diagnostics, drug delivery and nanotoxicology applications.

1. Introduction

While the term “nanotechnology” is widely used, its definition due to involvement of many research fields is rather open. Nanotechnology is the technical capability to manipulate and

modify the matter with the possibility to produce new materials through the re-organization or self-assembly of atoms and molecules, in order to obtain functional structures on a nano-scale.¹

There is a strong relation between nanotechnology and miniaturized (bio)analytical or biosensing systems. The advantages of miniaturized (bio)systems include the reduction of the volumes of samples and reagents consumed, detection facility, minimal handling of hazardous materials and parallel multiple sample detection. It is well known that nanomaterials (NMs) are bringing a series of advantages in the improvement of biosensing systems. DNA,^{2–4} proteins,^{5,6} and even cell detection⁷ using electrochemical, optical and other techniques have been reported

^aNanobioelectronics & Biosensors Group, Institut Català de Nanotecnologia, Campus UAB, Bellaterra, Barcelona-Spain

^bUniversitat Autònoma de Barcelona (UAB), Campus UAB, Bellaterra, Spain

^cICREA, Barcelona, Spain. E-mail: arben.merkoci@icn.cat; Fax: +34935868020; Tel: +34935868014

† Published as part of a themed issue in collaboration with the III International Workshop on Analytical Miniaturization and NANOTEchnologies, Barcelona, 2012.



Mariana Medina-Sánchez

Mariana Medina received her Engineering degree in Mechatronics at San Buenaventura's University and then her Master of nanotechnology at the University Autonomous of Barcelona. Currently, Mariana is a Ph.D student in biotechnology at the same university and a researcher in the Nanobioelectronics and Biosensors Group at the Catalan Institute of Nanotechnology, Barcelona, Spain. Her areas of work are: microfabrication, nanosensing, microfluidics, electronics and mechanics.



Sandrine Miserere

Sandrine Miserere studied analytical chemistry (in Paris, France) and joined the Curie Institute to do her PhD on microfluidics and DNA separation which she received in 2009. She is currently a postdoctoral fellow in the Nanobioelectronics & Biosensors Group at the Catalan Institute of Nanotechnology. Her current projects deal with the integration of electrochemical detection based on nanoparticles in microfluidics.

to gain impressive advantages by using NMs. Micro and nanomaterials have recently been shown to be important building blocks for the improvement of environmental monitoring systems, such as those for heavy metals analysis.⁸ Given the advantages of NMs in the design of novel biosensing systems or improvements of the existing ones, it is logical to see a strong interaction between these novel materials and lab on a chip (LOC) platforms. NMs are being used in microfluidic platforms as detectors (or detectors modifiers),⁹ tools for microreactors,¹⁰ and others. In addition, LOCs are being used for NMs synthesis.^{11,74,86}

Several NM based accessories for flow control, such as particle positioning platforms (*i.e.* an optical method to manipulate nanosized particles in suspensions within confined microfluidic devices¹²), have also been reported.

LOC technology is already an established research field where scientists of different areas of knowledge are working together to achieve new synergies of this technology with nanotechnology in general and NMs in particular. This is a continuous growing field where the development of novel “nanobiosensors” is opening the way to cost-effective devices that would be the perfect candidate to be integrated into LOC systems.

Pumera has recently put emphasis on the mutual benefits of microfluidics and nanomaterials. His paper is focused on in-chip separation and detection of analytes, microfluidics use for synthesis and as platform for nanomotors and other applications.¹³ In this review we provide an overview of the various strategies related to the use of nanoparticles and nanostructures for microfluidics, as well as of microfluidic platforms for synthesis, toxicity studies and characterization of NMs. The integration of NMs into analytical devices for both detection and in-chip process improvement will also be discussed.

2. Nanomaterials in LOC technologies

2.1. Transducers involving nanomaterials

The application of nanomaterials (NMs) in the development of sensors and biosensors represents one of the main focuses of current research in nanotechnology. Their interesting optical and

electrical properties are making NMs new building blocks for the design of various kinds of sensing and biosensing devices with improved performance. In the past decade, NMs have been very attractive for the modification of transducers which are the most important part of the (bio)sensing systems to be integrated into LOCs. The transducer's modification through NMs can improve the electrochemical (amperometric, impedimetric, potentiometric), optical (light absorbance, dispersion, fluorescence) or other mixed signals (*i.e.* electrochemiluminescence) based measurements. This work is discussed in the following sections.

2.1.1. Electrochemical detection. Various NMs based electrochemical detectors integrated within the LOC systems have been reported. Among these, carbon nanotubes (CNTs) are the most extensively studied.^{14–17} Indeed they present interesting properties such as extraordinary thermal and electrical conductivity, as well as excellent mechanical resistance. CNTs can be easily deposited or grown onto different surfaces through simple dropping, chemical vapour deposition (CVD) or plasma enhanced CVD. The CNTs modified transducers have a larger surface area which increases the current density, as well as offering an increased surface for biomolecule attachment. This can improve the current stability and increase the sensitivity of the detector. The electrical behaviour of such platforms depends on CNTs chirality, the number of carbon layers, defects and their functionalization, which must be carefully considered during their application. All these CNTs properties are useful in catalysis,¹⁸ enzyme immobilization,¹⁹ protein detection²⁰ and metal detection.²¹

Okuno *et al.* have developed a label-free immunosensor modified with CNTs to enhance the detection of total prostate-specific antigen (T-PSA) (Fig. 1A).²² An array of platinum microelectrodes was modified by CVD with single-wall carbon nanotubes (SWCNTs). CNTs allow a better electron transfer, improving the limit of detection (LOD) in relation to the non-modified electrodes, obtaining a LOD of 0.25 ng mL⁻¹.

CNTs are widely used in the fabrication of field effect transistors (FET); Javey *et al.* have obtained a CNTs based FET by combining ohmic metal-tube contacts, high dielectric constant films as gate insulators, and electrostatically doped nanotube segments as source/drain electrodes.²³ This approach looks like those of MOSFETs (metal oxide semiconductor field effect transistor) and can provide excellent ON-OFF states to nanotube based FETs under aggressive vertical scaling.

Tey *et al.* described a liquid gate field effect transistor (LG-FET) that integrates SWCNTs.²⁴ The electrical detection was performed by using CNTs as contact electrodes and semiconductive channels. A limit of detection of 1 pM of poly-L-lysine was achieved. The SWCNTs were used as “channel modulation labels” to sense changes in their immediate environment as a result of specific interactions with biomolecules. In this design the electrolyte replaces the dielectric in normal operation. Also, the electrical double layer capacitance created by the electrolyte and high surface area of the SWCNT network yields a total gate capacitance which is increased by an order of magnitude in comparison to typical Si/SiO₂ bottom gate configuration.

A non-enzymatic carbon nanotube sensor for sugar detection was developed by Vlandas *et al.*²⁵ The sensor was also assembled as a LG-FET (liquid gate field effect transistor). The



Arben Merkoçi

Prof. Merkoçi is the head of the Nanobioelectronics & Biosensors Group at ICN (Institut Català de Nanotecnologia) in Barcelona. His research is focused on the integration of biological molecules (DNA, antibodies, cells, and enzymes) and other receptors with micro- and nanostructures as they apply to the design of novel sensors and biosensors. He is the author of over 150 manuscripts, special journal issues, and books on nanomaterials and biosensors and lastly serves also as an Editor of the Nanoscience and Nanotechnology Encyclopedic Series launched by John Wiley & Sons.

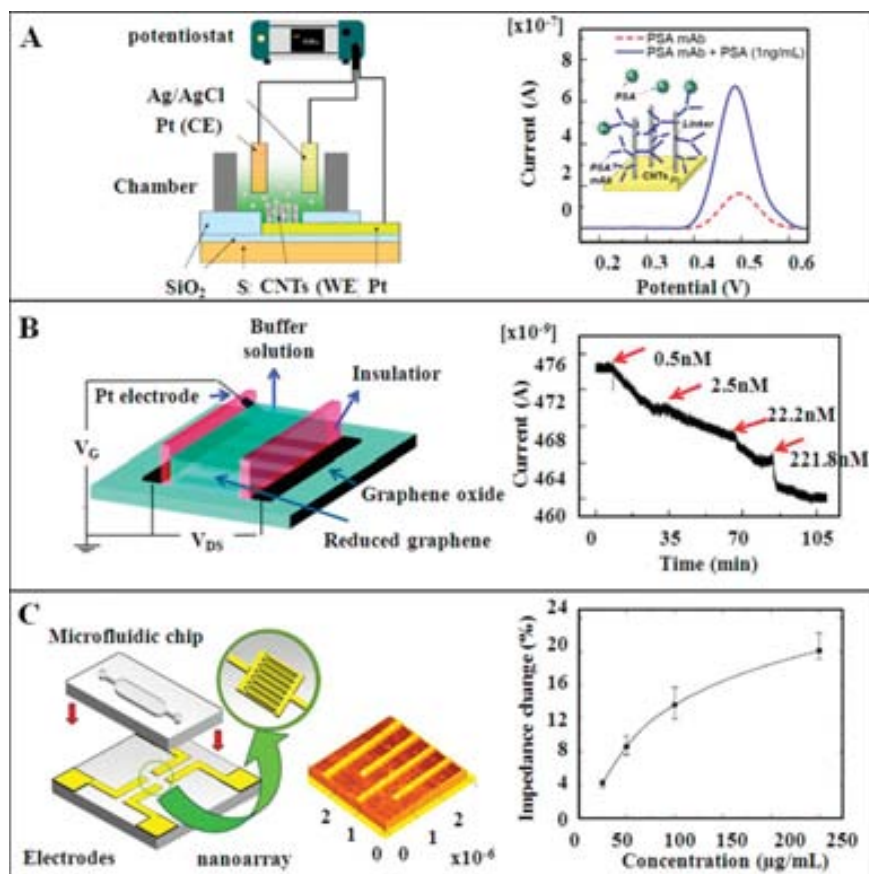


Fig. 1 Electrochemical readout technologies. A. Amperometric sensor modified with SWCNTs for PSA detection; B. Bio-field effect transistor (BioFET) fabricated with graphene oxide (source–drain contacts) and reduced graphene (conductive channel) integrated into microfluidic system for fibronectin detection; C. Impedimetric gold nanoelectrodes array for protein detection. Adapted with permission from ref. 22, 30 and 32 respectively.

semiconductive channel is based on SWCNTs functionalized with boronic acid receptors. This sensor is capable of detecting glucose in a range of concentration from 5 to 30 mM by measuring the change of impedance at different frequencies and gate voltages, which is in the range of physiological glucose detection. However, the conventional impedance detector, based on the use of screen printed electrodes (SPEs) modified with bimetallic nanowires, has been able to achieve a limit of detection of 20 μM ,²⁶ being an excellent alternative for lab-on-a-chip applications.

LG-FET with CNTs to detect herbicides *via* competitive immunoassay was also reported.²⁷ This system could detect concentrations lower than 500 fM of 2,4-dichlorophenoxyacetic acid herbicides by conductimetric methods by reading the current in the drain contact. Graphene is another interesting NM which has recently attracted significant attention due to its interesting input for electrochemical detection. It offers higher electron transference and is easy to be functionalized with (bio) molecules. This material, which is easy to produce from graphite,²⁸ seems to be much cheaper than CNTs and consequently a good alternative.

Chua *et al.* reported a microfluidic graphene oxide based amperometric detector which showed higher peak sensitivity, resolution and separation efficiency than the same device without modification.²⁹ Fig. 1B represents a graphene FET-based device³⁰ where the drain and source pads were made with graphene oxide and the channel with reduced graphene (rGO).

The detection of fibronectin was demonstrated as proof of concept, with a detection limit of 0.5 nM. Finally, nanoelectrodes and nanostructured electrodes are attracting the attention for biological sample analysis at very low concentrations where the reduction of the sensor size seems to facilitate the detection of reaction products at a similar scale.³¹

Ahn's group reported the functionalization of nano interdigitated electrodes array fabricated onto cyclic olefin copolymer (COC) substrate for direct bio-affinity sensing (see Fig. 1C).³² The protein immobilization was based on the self-assembly of alkanethiol groups on the electrode surface. Different concentrations of mouse monoclonal anti-rabbit immunoglobulin were used as the analyte for biomolecular binding sensing tests. The protein was covalently immobilized on the alkanethiols SAMs which recognize the amino groups of the protein. Finally, the variations of impedance to the electrode were measured for different protein concentrations. In this example, the scale and thickness of the electrode play an important role due to the possibility of being integrated in microfluidic platforms, as well as improving the sensitivity when the analyte is detected at the same scale as the detection platform.

These kinds of electrodes could also be modified with nanoparticles, as Lee *et al.*³³ reported in 2011. Indium oxide and silica nanoparticles (SNP) were selectively assembled onto multi-site channel area of the resistors, using layer-by-layer

self-assembly. Glucose oxidase was immobilized onto the SNPs layer and glucose detection was performed by conductivity. A current dependence upon different glucose concentrations with a sensitivity that depends on the channel and resistors dimensions was observed. The sensitivity for glucose detection was 4–12 nA mM⁻¹.

In general, modifying transducing platforms with nanoparticles allows generating really high-conductive surface area interfaces that enables the sensitive/catalytic detection of ionic, molecular and biomolecular analytes. These high sensitive sensors are easy to be integrated and become good candidates for LOCs.

2.1.2. Optical detections. The integration of photonics and microfluidics is a well-known strategy that provides enhanced sensing and simplification of microsystems. Various optofluidic detections such as those based on surface enhanced Raman spectroscopy (SERS), fluorescence and absorbance and related with the use of NMs modified detectors have been reported. SERS is a surface-sensitive technique that enhances Raman scattering by molecules adsorbed onto rough metal surfaces. For this reason, the use of NMs provides a wide range of possibilities for sensitive detection.

The use of gold nanowires (NWs) (diameter of 170 nm) synthesized by an electrocrystallization method into a poly-

carbonate microchannel has been reported.³⁴ Gold nanowires produce large increases in a Raman cross-section. This kind of SERS-active dielectric polymer/NWs itself is a good candidate for in-microchip integration (Fig. 2A). An increased sensitivity was also observed by detection of isonicotinic acid in perchloric acid due to the higher surface to volume ratio.

Different SERS spectra for a microfluidic separation chip with an integrated chromatographic column based on pillar arrays were evaluated.³⁵ Diffusive mixing of silver nanoparticle (AgNPs) solution with the eluent stream in a laminar flow to induce SERS signals due to their advantages as relative easy preparation, manipulation and possibility to have high SERS reproducibility has been reported. Interesting information about complex mixtures without complete resolution of chromatography bands was obtained. Analysis of the mixing kinetics effect on efficiency was also performed.

The combination of localized surface plasmon resonance (LSPR) and SERS has also been reported by Astilean's group.³⁶ LSPR provides detection of molecular adsorption in both transmission and reflectivity modes, and SERS gives the analysis of the adsorbed molecule and its structure and orientation on the metal surface. The optical and spectroscopy properties of regular arrays of subwavelength holes in a thin gold film by combining SPR and SERS was demonstrated by the binding of the *p*-ATP monolayer, observing a shift in SPR. A change in SERS related

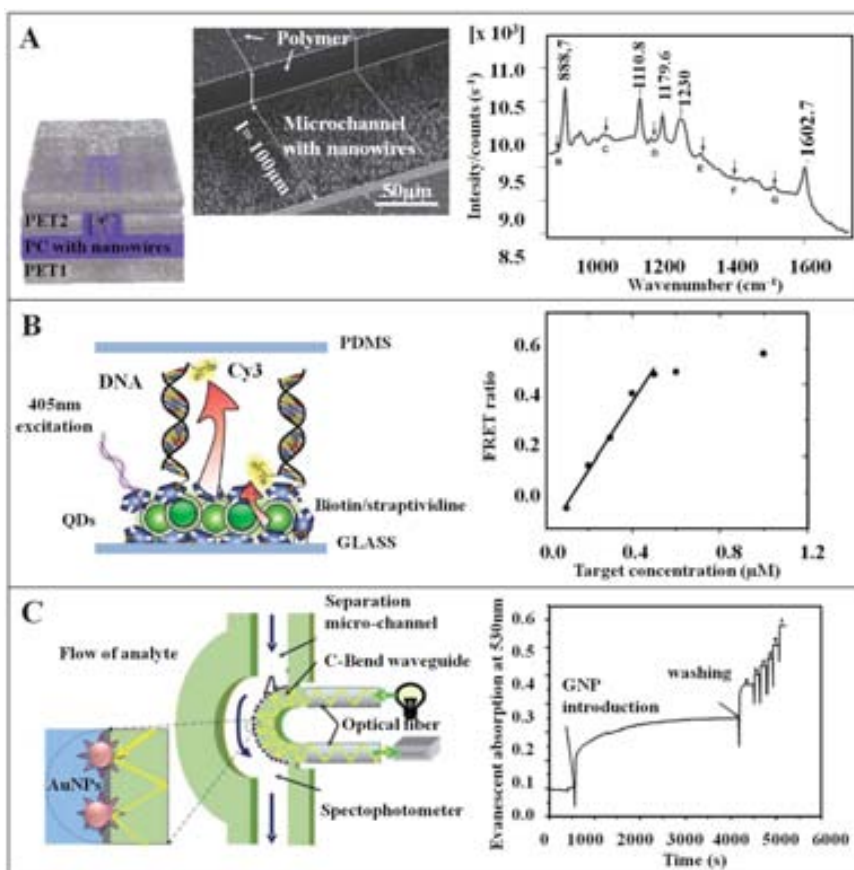


Fig. 2 Optical readout technologies. A. Schematic and SEM images of a microchannel with embedded gold nanowires and the corresponding typical SERS response. B. Assay for the transduction of nucleic acid hybridization using FRET and CdSe/ZnS QDs. C. Scheme of optical set-up with gold nanoparticles (GNPs) modified waveguide coupled microchannel and its typical curves of absorbance vs. time. Adapted with permission from ref. 34, 37 and 40.

to the orientation of the absorbed molecule, with a greater sensitivity of 300 nm/RIU and spectral shift of 16 nm was also observed.

The glass surface of a glass-PDMS microfluidic channel was modified by immobilization of QDs to develop a solid-phase assay for nucleic acid determination (Fig. 2B).³⁷ QDs served as energy donors in fluorescence resonance energy transfer (FRET) for transduction of nucleic acid hybridization. A selective detection of femtomole quantities of the target using 20% formamide was reported.

A novel alternative for fluorescence detection by using on-chip superlocalization and super-resolution imaging of single molecules and nanoparticles under different microscopy modes was reported by Luo *et al.*³⁸ The detection was performed by using epi-fluorescence and differential interference contrast (DIC) modes at the same time. The performance was validated by precisely mapping micronecklaces made of fluorescent microtubules and gold nanoparticles (40 nm of diameter) and by demonstrating the activation and excitation cycles of single Alexa Fluor 647 dyes for direct stochastic optical. In chip measurements of light absorbance have also been reported by Demming *et al.* They demonstrate that nanoparticles can be used to modify the index of reflection of the material, thus increasing the obtained signal.³⁹ A PDMS matrix involving copper nanoparticles (CuNPs) and silver nanoparticles (AgNPs) for microfluidic devices was also performed. These nanoparticles were suspended in PDMS to obtain a permanent modification. The antiseptic behaviour of the different nanoparticles was studied by observing the absorption of *Saccharomyces cerevisiae* culture cells.

Gold nanoparticles (AuNPs) embedded in a polymeric waveguide for localized surface plasmon resonance (Fig. 2C), capable of capturing minor variations in the refractive index of its microenvironment, have been demonstrated.⁴⁰ A linear behaviour of refractive index changes of SU8 waveguide bound to gold nanoparticles was also observed. Optical characterization should also be performed in microfluidic platforms, mainly by SERS detection. Qu *et al.*, reported the development of disposable screen printed SERS arrays by using silver nanoparticles ink (AgNPs). This nanostructured surface was characterized by detecting rhodamine 6G with a LOD of 1.6×10^{-13} M.⁴¹

The combination between quantum dots labeled nerve growth factor (QDs-NGF), microfluidic chambers for neuronal culture, and pseudo total internal reflection (TIRF) microscopy provided a single molecule detection and analysis.⁴² Chu's group developed a platform to detect retrograde axonal transport of NGF signals which is critical for the survival, differentiation, and maintenance of peripheral sympathetic and sensory neurons and basal forebrain cholinergic neurons. QD-NGF was used to track the movement of NGF in real time in compartmentalized culture of rat dorsal root ganglion (DRG) neurons. They obtained quantitative analysis at the single molecule level demonstrating that the majority of NGF containing endosomes had only a single NGF dimer. Electron microscopic analysis of axonal vesicles carrying QD-NGF confirmed this finding. Kuyper *et al.* proposed real-time nanoparticles synthesis (quantum dots, gold colloids, fluorescent and non-fluorescent beads) allowing the possibility to optimize reactions on the basis of real-time readout of particle dimensions.⁴³ Confocal correlation spectroscopy

(CCS) for on chip sizing of both fluorescent and nonfluorescent nanoparticles was used. This technique can be an advantageous powerful tool to characterize colloids, polymer beads, and biological particles such as vesicles, viruses, and DNA molecules.

In summary, optical detection is the most common detection method in microfluidic analyses. Fluorescence-based detection can be considered more usual for its facility to be integrated onto microfluidic devices (*i.e.* fluorescence excitation and detection components), as well as its ability to detect low volume samples. SERS technique is also a potential tool to carry out qualitative and quantitative characterization of analytes, however its integration with microfluidic devices still needs more research. In the same way, fluorescence and absorbance detection are moving towards information-improving techniques, such as fluorescence lifetime imaging microscopy or multicolor analyses. NMs are play an increasingly important role as labelling and surface modification materials in fluorescence imaging in order to improve the sensitivity and the sensibility of existing methods.

2.1.3. Other detection methods. Other detection methods, such as electrochemiluminescence (ECL) and mass detection using nanoresonators, are also applied in lab-on-a-chip technologies. Electrochemiluminescence is a kind of luminescence produced during electrochemical reactions in which a material emits light in response to an electric current or electrical field (see Fig. 3A).

Nanoparticles could be used to improve the sensitivity of ECL. An enzymatic biosensor based on MWCNT surface modified with cadmium sulfide nanocrystals (CdS NCs) (Fig. 3B).⁴⁴ The MWCNT-CdS can react with H₂O₂, generating strong and stable ECL emission in neutral solution. By following the same procedure, a biosensor based on CdS-graphene has shown promising results for H₂O₂ sensing with an acceptable linear response from 5 μ M up to 1 mM and a detection limit of 1.7 μ M.⁴⁵

Nanomechanical biosensors^{46–48} can also be integrated into microfluidics. A variation of the mass onto the cantilever will produce a change in the length by material deformation. This deformation can be detected by different transducers (*i.e.* optical, piezoelectrical, electrical by field effect transistor principle, *etc.*) (Fig. 4A).

Waggoner *et al.* were able to detect concentrations of 1–100 fM of PSA in serum, using a gold nanoparticle-based mass-labelling sandwich assay.⁴⁹ A reduced time of analysis with microfluidic assay was observed. Such a platform using nanoparticles allows multiplexed protein analysis with a very high sensitivity, offering many new alternatives of applications in clinical and biological studies for the early detection of diseases (Fig. 4B).

Nanowires or nanotubes could also be employed as mass detectors. Hwang *et al.* have developed a nanocantilever-based sensor with a field effect transistor as a transducer. The signal from the gate changes when the cantilever is deflected due to specific binding of biomolecules on its surface.⁵⁰

2.2. Nanoparticles as labels in microfluidics

Biomarkers related to various diseases are present at very low concentrations. For this reason, enhancement strategies such as nanoparticle-labelling, besides labelling with fluorescence dyes,

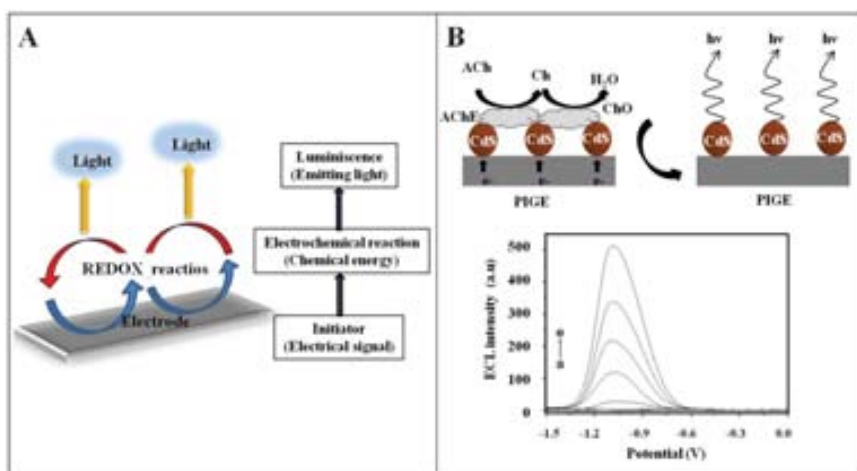


Fig. 3 Electroluminescence (ECL) based measurement. A. Principle of operation. B. Schematic diagram of multi wall carbon nanotubes (MWCNT)–cadmium sulfide (CdS) modified with acetylcholine esterase (AChE). This ECL biosensor is used for the detection of the neurotransmitter acetylcholine. Adapted with permission from ref. 44.

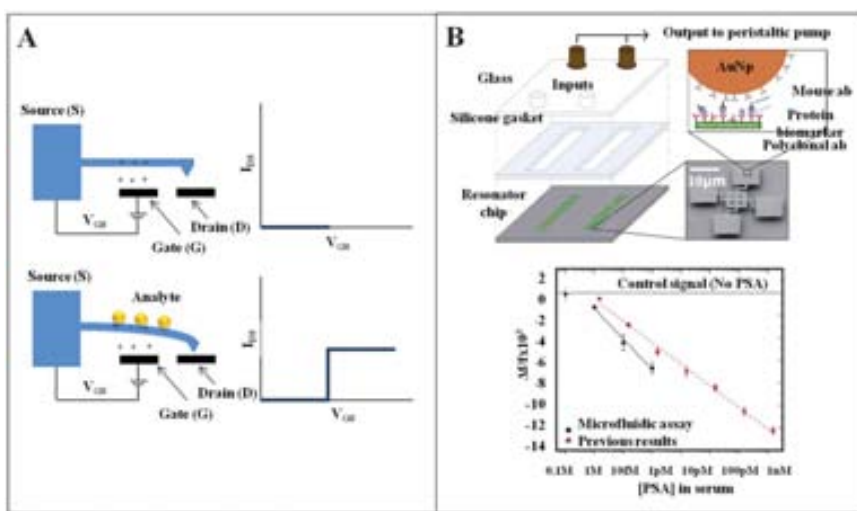


Fig. 4 Schematic of a microfluidic-resonator device with its respective graph of frequency shifts for detection of PSA in serum. Adapted with permission from ref. 49.

Table 1 Nanomaterials as labels in lab-on-a-chip applications

Nanomaterial as label	Analyte	Detection mode	LOD	Reference
CdSe/ZnS QDs	Carcinoembryonic antigen (CEA)	Fluorescence	0.02 ng mL ⁻¹	54
CdSe/ZnS QDs	Hepatitis B virus (HBV) in serum samples	Fluorescence	1000 copies mL ⁻¹	55
CdSe/ZnS QDs	Marine fish iridovirus	Fluorescence	22 ng mL ⁻¹	56
CdSe/ZnS QDs	Cotinine	Electrochemical	1 ng mL ⁻¹	57
Gold nanoparticles	Prostate specific antigen (PSA)	Fluorescence	10 fM	58
Gold nanoparticles	Proteins	Electrochemical	50 ng mL ⁻¹	59
Magnetic nanoparticles	DNA strands	Magnetoresistance	20 pM	63
Magnetic nanoclusters	DNA strands	Magnetoresistance	20 mer single stranded DNA sequences	64
PbS nanoparticles	Carcinoembryonic antigen (CEA)	Electrothermal vaporization inductively coupled plasma mass spectrometry	0.058 mg L ⁻¹	65

enzymes *etc.*, have been demonstrated with interest for lab-on-a-chip diagnostics applications. Some examples related to nanoparticles used as labels in different lab-on-a-chip applications are shown in Table 1.

Quantum dots are the most common nanoparticles used as labelling platforms in microfluidics. They could be attached to antibodies, aptamers, oligonucleotides, or peptides.⁵¹ The increased and stable fluorescence properties are of special interest to develop ultrasensitive and robust LOCs. Furthermore, they also have interesting electrochemical/electrocatalytic properties which could be very useful for the integration of electrochemical detection for lab-on-a-chip applications with high sensitivity and selectivity.

A nanoparticle-labelling based LOC platform involving different detection principles, including electrochemical detection by using QDs as biotracers/labels for tumour marker protein detection, is reported.⁵² Cadmium sulphide quantum dots (CdS QDs) were synthesized based on a modification of the procedure reported by Wang *et al.*,⁵³ with anti-carcinoembryonic antibody (α CEA) and detected by square wave anodic stripping voltammetry (SWASV). The electrode surface was modified with carbon nanoparticles enhancing the performance of the electrochemical reaction while the QDs labels allow the amplification of the signal, improving the sensitivity and selectivity of the detection system.

Another interesting application involving QDs as biomarkers is the development of nano-bio-microfluidic chips for multiplexed protein detection in serum and saliva.⁵⁴ Fluorescence detection of carcinoembryonic antigen (CEA), cancer antigen 125 (CA125) and Her-2/Neu (C-erbB-2) was achieved. The platform used to capture the antigen is a microporous agarose bead array where an antibody labelled with QDs is captured. An amplification of 30 times higher in comparison to the standard molecular fluorophores is observed. In addition, the use of different sized QDs with a wide range of wavelength emissions for multiple detection is also possible.

Zhang *et al.* reported the use of QDs as fluorescent labels for virus detection and genotyping.⁵⁵ The device could detect 1000 copies mL^{-1} of hepatitis B virus in clinical serum samples using *in vitro* transcribed RNA as the target molecules. Based on DNA hybridization with quantum dots labels, on-chip virus genotyping was also described.

A study for virus detection was performed by Ang's group.⁵⁶ A microfluidic platform for immunofluorescent detection using quantum dots was employed. The LOD was improved from 360 ng mL^{-1} (ELISA assay) to 22 ng mL^{-1} using these QDs based microfluidic system. An immunochromatographic strip based on nanoparticle probe was also demonstrated.⁵⁷ This platform allows the determination of cotinine in human serum. In this case, the QDs serve as signal vehicles for electrochemical readout with a linear range from 1 ng mL^{-1} to 100 ng mL^{-1} of cotinine and a detection limit of 1 ng mL^{-1} . This sensor provides a rapid, accurate, and quantitative tool for cotinine detection and shows great promise for in-field and point of care (POC) quantitative screening of tobacco smoke exposure.

Gold nanoparticles (AuNPs) are also good labels candidates. They are easy to produce in a variety of sizes and are also easy to functionalize. AuNP can be used for both fluorescence and electrochemical detections. Prostate specific antigen (PSA) in the

samples was detected by using AuNPs as labels at concentrations ranging from 40 pM to 40 fM.⁵⁸ The reported detection limit of this assay is 10 fM, with the entire assay, from sample injection to final data analysis, being completed in eighty minutes. Lei *et al.* also developed a biochip for protein detection involving AuNPs.⁵⁹ AuNPs indicate the presence of a protein. The concentration of protein was related to the resistance between interdigitated electrodes, achieving a limit of detection of 50 ng mL^{-1} .

Another detection principle applied in relation to labelling is the magnetoresistance, where the sensor is a magnetic field transducer that exhibits a linear change in electrical resistance under an external field.^{60,61} An integrated microfluidic system incorporating spin valve (SV) sensors has been fabricated, allowing cell detection and counting.⁶² This detection system can be used as a flow chip cytometer having the same efficiency for high concentration samples as the hemocytometer method, with approximately half the error (4.5% in comparison to 8.5%). Germano *et al.* reported a platform for biomolecular recognition detection using magnetic nanoparticles (250 nm), achieving a robust detection of up to 20 pM of DNA (20 mer single stranded DNA oligonucleotides hybridization).⁶³ The signal between complementary and non-complementary controls was possible to be discriminated.

Freitas' group developed a biochip portable platform for bioassays using a DNA–DNA oligonucleotides hybridization model,⁶⁴ where 130 nm magnetic nanoparticles (MNPs) were used for their magnetic resonance contribution, allowing the detection in real-time of 20 mer single stranded DNA sequences. The same MNPs were used by Chen *et al.* for both capturing and labelling.⁶⁵ Their device enabled the determination of carcinoembryonic antigens (CEA) in human serum samples. Briefly, the immunoassay was performed by immobilizing the CEA onto magnetic NPs modified with the 1st Ab-CEA. Then, 2nd Ab-CEA labelled with PbS NPs was added. A limit of detection of 0.058 $\mu\text{g L}^{-1}$, suitable for CEA determination in human serum samples, was achieved.

NMs as labels give a wide range of possibilities to improve sensibility and selectivity. They have also been shown to be of particular interest in developing high sensitive (bio)detection devices with multidetection capability and compatibility with LOCs. Various detection techniques ranging from optical, electrochemical and mass changes can be applied in LOCs while using NMs based labelling technologies.

2.3. Nanomaterials for process improvement

NMs could also be employed to improve analytical processes. Electrophoresis separation, capture and cell sorting between others are some of the reported examples improved through the use of NMs. Concerning electrophoresis, a microchannel used for separation purposes could be modified with nanoparticles in order to control the electro-osmotic flow (EOF). Wang *et al.* modified microfluidic channels by citrate-stabilized gold nanoparticles after coating a layer of linear polyethylenimine (LPEI).⁶⁶ This modification was successfully used to separate dopamine and pinephrine, which were difficult to separated from the baseline in native and hybrid PDMS microchannels. Measurements by in-channel amperometric detection with a

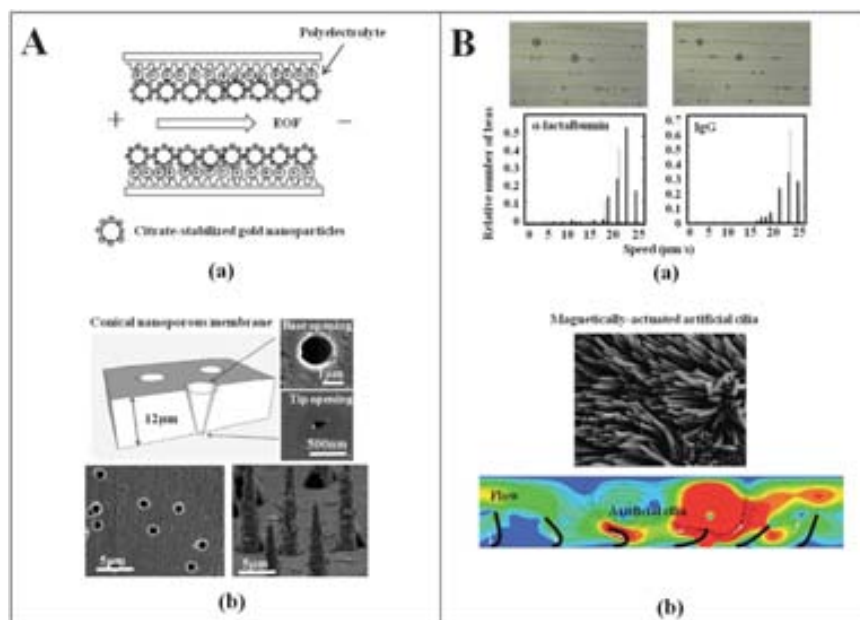


Fig. 5 Process improving by using nanomaterials: A. Sorting tasks: PDMS–PDMS modification by using gold nanoparticles (13 nm of diameter). (a), schematic of the channel and (b) SEM images of conical nanopore array in PET used to trap cyanobacteria; B. Capturing and mixing tasks: magnetic bead velocity distribution of protein coated beads (α -lactalbumin, f IgG) (a) and magnetically controlled nano-cilia for flow mixing with their respective simulation (b). Figures adapted with permission from ref. 66, 67, 71 and 72.

single carbon fibre cylindrical electrode were performed. Linear responses from 25 to 600 μM for both compounds with detection limits of 2 μM for dopamine and 5 μM for epinephrine, respectively, were obtained. (Fig. 5A,a)

The use of nanopore arrays is also extended for the capture and release of bacteria, as described by Zare's group. In this work, conical nanopores on membranes inside a microfluidic device was developed,⁶⁷ demonstrating the optimal capture of cyanobacteria, (one bacteria per pore) in a defined orientation with viabilities as high as 100%. The platform can discriminate cyanobacteria from a mixed suspension of cyanobacteria and chlamydomonas with a 90% selectivity (Fig. 5A,b).

For filtering and/or capturing processes, nanoporous elements have been integrated into microfluidics in order to manipulate bioparticles. Porous materials have been limited to membranes sandwiched between microchannel layers and polymer monoliths, but Chen *et al.* reported the use of micropatterned carbon-nanotubes confined inside microfluidic channels for mechanically and/or capturing particles ranging over three orders of magnitude in size.⁶⁸ Nanoparticles with a size below the internanotube spacing can penetrate inside the forest and interact with the large surface area of carbon nanotubes. To validate this platform, specific biomolecular interactions were demonstrated by using cells, bacteria and viral-sized particles.

Carbon nanotubes for lab-on-a-chip applications, especially their integration into microfluidic devices to improve super-lubricating, microchannels, filtering and separation processes, have also been studied by Choong *et al.*⁶⁹ The use of nanoassembled graphene oxide appears as a novel capture alternative. Yoon *et al.* reported the circulating tumour cell isolation by using this strategy, showing a selective and sensitive detection of cells.⁷⁰ The functionalized GO can self-assemble on patterned gold surfaces *via* electrostatic interactions between

functional groups on GO and gold surfaces. This material is attractive for their 2D and 3D electrical conductivity, large surface area, mechanical flexibility, and high chemical and thermal stability.

Magnetic nanoparticles used as labels in magnetoresistive sensors are also used as a molecule transport controller in order to preconcentrate the sample on the detector chamber. Oscarsson's group reported a magnetic microchip for the controlled transport of an attomole level of proteins. The activity of proteins immobilized on the beads was also demonstrated by injecting antibodies into the channel. Parameters like the sticking forces between beads and substrate during transportation of proteins and the charge interaction in comparison with the hydrophobic forces were also optimized. The performance of the platform was tested by detecting a solution of fluorescein iso-thiocyanate (FITC) labelled anti-HSA, achieving a LOD of 0.02 mg mL^{-1} by fluorescence methods (Fig. 5B,a).⁷¹ Another interesting application for process improvement is microfluidic propulsion by using magnetically-actuated artificial cilia, fabricated using thin polymer films with embedded magnetic nano-particles. These artificial cilia were fabricated using thin polymer films with embedded magnetic nanoparticles. Onck's group studied their deformation under different external magnetic fields and flows (Fig. 5B,b).⁷²

3. In-chip production and characterization of nanomaterials

3.1. Synthesis

As already seen in the previous section of this review, NMs are really powerful tools to improve the sensitivity of microfluidic

devices, but the contrary is also true. Nanoparticles are usually produced by batch chemical syntheses which are designed for mass production, however these methods are time consuming and suffer from poor control of the homogeneity and monodispersity. Furthermore, they require high volumes of reagents which doesn't make them environmental friendly. Also, for biological and medical applications, the quality and the homogeneity of the NPs is much more important than the amount of NPs produced. The rapid chemical reactions and efficient mixing of microfluidics allows better control of the synthesis parameters, such as the size and properties of the nanoparticles. The flexibility of the wide variety of device substrates available is also an important property in the solvent employed for the NPs fabrication. Synthesis of a wide range of polymeric and inorganic particulate materials has already been investigated in microfluidics.⁷³

Semiconductors like QDs have been produced by continuous flow. In this case the reaction occurs at the interface of two liquids. Thus CdS,⁷⁴ CdSe^{75–77} and CdSe–ZnS syntheses have been reported. A better distribution could be obtained by using segmented techniques like droplet based flow synthesis and reactor's features. Droplets are assimilated as microreactors of nanoliters (nL) volumes size solutions. QDs with better controlled sizes have been produced by this method,^{78,79} even at high temperature.^{80,81}

In 2011, Zhao *et al.* generated multifunctional quantum dot barcode particles.⁸² Indeed, the QDs were entrapped in a hydrogel. By melting different QDs or different sized QDs, it is possible to obtain an infinite range of barcodes. The authors also demonstrated the possibility to have two delimited compartments inside these particles, one of QDs for the detection and one of magnetic particles for magnetic separation and manipulation.

Colloidal nanoparticles synthesis in lab-on-a-chip platforms have been also reported for applications in optical coating, displays, chromatography, and catalysts.⁸³ The use of microreactors for nanoparticles synthesis allows the flexibility for reagent manipulation and therefore has the possibility to use multichannels depending of the synthesis requirements. Gijs's group reported the synthesis of silica nanoparticles with controllable shape and size, taking advantage of the high monodispersity of on-chip generated microdroplets to produce nanoparticles assemblies with narrow size distribution.⁸⁴ By rolling the droplets over a hydrophobic substrate they were able to obtain pillar-like assemblies which could be used as a support for catalytic precipitation reactions of fluorescent dyes.

The synthesis of magnetic iron oxide nanoparticles (4 nm of diameter) were also demonstrated in a microfluidic system by Frenz, *et al.* The novelty of this work is that the entire reaction occurs within the microdroplets. In this way, it is possible to reduce the time of reaction and is therefore more efficient.⁸⁵ During microreactors formation, it is also possible to integrate a functionalization step for biocompatibility, drug anchoring and cell targeting, giving a better control of synthesis conditions determining their properties. Jensen *et al.* described basic principles of operation of microfluidic reactors for synthesis of colloidal silica nanoparticles, controlling the particle size, changing the linear velocity and mean residence time.⁸⁶ For a given laminar flow reactor design, monodisperse particle distributions are only feasible under conditions that minimize axial dispersion (Fig. 6A).

New nanomaterial-conjugated polymer dots were synthesized in a microfluidic platform, leading to a new class of fluorescent nanoprobe with the possibility to be used in the subcellular labelling and sensor fields. That is the case for the preparation of highly monodisperse, sub-micrometre conjugated polymer

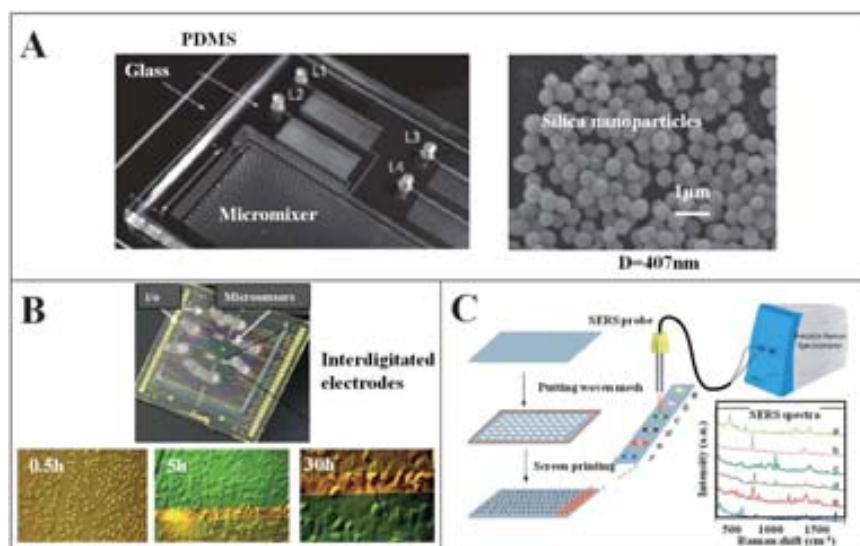


Fig. 6 In-chip production and characterization of nanomaterials: A. PDMS–glass based chip that includes a micromixer used for the in-chip synthesis of nanoparticles. Are shown SEM images of silica nanoparticles from the Stober process developed in a gas-liquid segmented microflow. B. Toxicity studies using a microfluidic biochip consisting of PDMS microchannels bonded to a glass bottom substrate, which includes four sample inlets and wastes as well as contactless dielectric microsensors located underneath monitoring chambers. Pictures taken after 0.5 h, 5 h and 30 h after cell seeding show NHDF seeding density, adhesion and spreading processes during cell cultivation are included. C. A schematic diagram of a nanoparticle detecting microfluidic chip. Adapted with permission from ref. 86, 90 and 94.

particles reported by Weitz's group.⁸⁷ Particle size is tuned between 150 to 2 nm by emulsification of a conjugated polymer solution on a microfluidic chip, followed by solvent evaporation. The obtained particles represent a novel class of photonic materials with a wide spectrum for applications such as coatings, photonic crystals, *etc.* Other polymeric materials were also developed by Schütze, *et al.*⁸⁸ Stable fluorescent nanoparticles (between 30 to 60 nm) from controlled mixing of a tetrahydrofuran (THF) solution of poly(fluorene ethynylene)-block-poly(ethylene glycol) in a microfluidic laminar flow cross junction were obtained. Due to different conjugation lengths and energy transfer to lower-energy chromophores, fluorescence emission of conjugated polymer nanoparticles is commonly red-shifted compared to polymer solutions in organic solvents.

3.2. Toxicity

NMs, even when made of inert elements like gold, become highly active at nanometer dimensions. Nanotoxicological studies are intended to determine whether and to what extent these properties may pose a threat to the environment and to human beings. For instance, some work involving microfluidic platforms have brought an interesting solution to study the NMs behaviour in presence of biological elements, taking advantage of the small volume consumed, lower time of analysis and sensitivity enhancement. NMs have many potential biomedical applications, therefore, *in vitro* studies should be performed to analyse and optimize the interaction between these nanoparticles and biological entities.

In 2005, Faronkhzad, *et al.* studied the interaction of polymeric nanoparticles conjugated with aptamers that recognized the transmembrane prostate specific membrane antigen (PSMA), with cells seeded in microchannels. The binding of particles to cells that expressed or did not express the PSMA (LNCaP or PC3, respectively) were evaluated with respect to changes in fluid shear stress, PSMA expression on target cells, and particle size. The presence of ligands on vehicle surface, size of vehicles, and amount of shear stress generated during fluid flow that can affect the *in vitro* targeting efficiency of these vehicles was demonstrated.⁸⁹ Also, the shear stress generated from fluid flow can have a significant effect on the binding characteristics. Richter *et al.* developed a microfluidic tool to study cell–nanoparticle interactions and nanoparticle accumulation effects in small cell populations.⁹⁰ Results of the study showed a 20% and 95% reduction of collagen production following 4 h exposure to 10 and 1 mg mL⁻¹ of gold and silver nanoparticles (diameter of 10 nm), respectively (Fig. 6B).

In 2010, Rhee's group evaluated the cytotoxicity effects of surface-modified QDs on neuron-like PC12 cells cultured inside microfluidic devices.⁹¹ The results suggest that QDs can induce toxicity to neurons depending on the stability of surface ligands on their surface. CTAB/TOPO-QDs were highly toxic to neurons, whereas MPA-QDs were non-toxic. Through the use of the microfluidic neuronal device, the axonal degeneration induced by CTAB/TOPO-QDs was related to the neuronal cell death, as well as of direct axonal toxicity. The results indicated that oxidative stress could be a leading cause of QD toxicity. Moreover, the microfluidic neuronal device, which is providing distinguished benefits over the conventional platforms, can be

efficiently utilized to study the mechanisms of axonal growth and degeneration and the protection of axons.

A study carried out by Safi *et al.* was focused on interactions between magnetic nanowires and living cells, their toxicity and degradation.⁹² The toxicity studies were based on mitochondrial activity, cell proliferation and the production of reactive oxygen species, showing that the wires don't display acute short-time (<100 h) toxicity towards the cells. In relation to the nanowires, the cells are able to degrade them and transform them in aggregates in short time periods (days). This degradation is likely to occur as a consequence of the internal structure of the wires, which is that of a noncovalently bound aggregate.

3.3. Characterization

Few works regarding microfluidic for NMs characterization are reported, however, this could be a good approach to understand optical, electrochemical and mechanical behaviour of NMs under flow conditions, with interest for further applications in (micro)analytical assays.

One characterization device found in the literature is the CMOS-hall-effect sensor for characterization and detection of magnetic nanoparticles⁹³ for biomedical applications. This technique was proposed by Liu *et al.* in contrast with the conventional characterization technique, magnetic resonance (MRX). They improved the time of measurement due to the fast magnetic relaxation within a short time-frame of 64 ns. Three different commercial magnetic nanoparticles were tested with this system showing different times of relaxation, allowing the implication of samples with different magnetic properties. The chip is easy to be integrated with microfluidics for point-of-care applications.

Resistive pulse sensor (RPS) with a submicron sensing gate and dual detecting channels-two stage differential amplifier was also proposed to characterize nanoparticles.⁹⁴ This device can achieve a high sensitivity allowing the detection of nanometer size particles. This method is able to detect nanoparticles of 490 nm and 220 nm using a microfluidic chip. The RPS chip can be divided into an upstream section, sensing gate, downstream section, and two detecting channels. The upstream channel, sensing gate, and downstream channel form the main channel between inlet and outlet reservoirs at the two ends. The detecting channels also have two reservoirs at the end of each channel for inserting the sensing electrodes, so when a non-conducting particle passes through a small sensing gate, the resistance of the sensing gate as well as its resistance change (Fig. 6C).

4. Other applications

Other nanostructured platforms have been reported for applications in cell therapy/tissue engineering, cell and developmental biology. Gallego-Pérez *et al.*, developed a micro-nanofabricated platform, consisting of microwells structurally bonded to a sheet of electrospun fibers.⁹⁵ Human hepatocytes were used as model cells to demonstrate the ability of the platform to allow controlled cluster formation. The recent use of nanostructures (*i.e.* vesicles, micelles, bilayers) as encapsulation agents for the eventual release of drugs, flavors, and fragrances has been well reported. Micelle-vesicle transition studies were performed by Lee *et al.* by the development of an integrated microfluidic

chip/cryogenic transmission electron microscopy (cryo-TEM) unit,⁹⁶ in order to characterize this phenomenon in specific amphiphilic system where micellar solutions of cetyltrimethylammonium bromide (CTAB) and dodecylbenzene sulfonic acid (HDBS) are mixed to form vesicles. This tool can be applied broadly to study transient structures in nanoscale systems under highly controlled conditions provided by microfluidics.

5. Conclusions and future perspectives

Nanomaterials (NM)-based lab-on-a-chip technology is showing to be an interesting alternative for a wide range of (bio)analytical devices applications. The integration of NMs into LOC systems seems to bring additional advantages in relation to the system sensitivity and miniaturization, besides the versatility of the designs and applications possibilities. NMs application as detectors or detector modifiers is improving the performance of conventional LOCs. In particular, the use of carbon nanotubes and graphene is bringing significant advances in electrical or optical detections. NMs applications as microchannel modifiers for separation enhancement are offering novel functionalization possibilities for improvements in sample pretreatment or separation processes.

Microfluidic platforms are also being used as a novel strategy for the production and characterization of NMs, opening new routes for encapsulation and homogenous shell-particle synthesis. Of notable progress are the synthesis of QDs and nanowires using microfluidic devices. Very good reproducibility, reducing of the preparation time and the reagents consumed, are some of the advantages of in-chip NMs preparation and applications. NMs are also involved in microanalytical process enhancement. NMs can be used for filtering, sorting, biomolecule capturing and other actuations, with the possibility for various applications. The in-chip NM application spectra also include applications such as tissue nano-scaffolds and drugs delivery systems. This is a challenging field for future nano drug delivery platforms.

Finally, problems such as the application of complicated fabrication and measuring technologies are probably not suitable for mass production and user-friendly technologies need to be designed in order to bring these devices to the end-users interested in microdevices.

Acknowledgements

We acknowledge E.U.'s support for the project FP7 contract number 246513 "NADINE" and MICINN (Madrid) for MAT2011-25870 and PIB2010JP-00278 projects.

References

- 1 S. C. Currall, E. B. King, N. Lane, J. Madera and S. Turner, *Nat. Nanotechnol.*, 2006, **1**, 153–155.
- 2 C. M. Niemeyer, *Angew. Chem., Int. Ed.*, 2001, **40**, 4128–4158.
- 3 N. L. Rosi and C. A. Mirkin, *Chem. Rev.*, 2005, **105**, 1547–1562.
- 4 A. Merkoçi, *Biosens. Bioelectron.*, 2010, **26**, 1164–1177.
- 5 A. de la Escosura-Muñiz, C. Parolo and A. Merkoçi, *Mater. Today*, 2010, **13**, 24–34.
- 6 A. de la Escosura-Muñiz, A. Ambrosi and A. Merkoçi, *TrAC, Trends Anal. Chem.*, 2008, **27**, 568–584.
- 7 M. Perfezou, A. Turner and A. Merkoçi, *Chem. Soc. Rev.*, 2012, **41**, 2606.
- 8 G. Aragay, J. Pons and A. Merkoçi, *Chem. Rev.*, 2011, **111**(5), 3433–3458.
- 9 O. A. Sadik, A. L. Zhou, S. Kikandi, N. Du, Q. Wang and K. Varner, *J. Environ. Monit.*, 2009, **11**(10), 1782–1800.
- 10 Y. Liu, Y. Xue, J. Ji, X. Chen, J. Kong, P. Yang, H. H. Girault and B. Liu, *Molecular and cellular proteomics*, 2007, 1428–1436.
- 11 C. H. Weng, C. C. Huang, C. S. Yeh and G. B. Lee, *2007 7th IEEE Conference on Nanotechnology (IEEE NANO)*, 2007, 462–466.
- 12 P. B. Abdallah, A. O. Moctar, B. Ni, N. Aubry and P. Singh, *J. Appl. Phys.*, 2006, **99**, 094303–1–6.
- 13 M. Pumera, *Chem. Commun.*, 2011, **47**, 5671–5680.
- 14 C. L. Choong, W. I. Milne and K. B. K. Teo, *Int. J. Mater. Form.*, 2008, **1**, 117–125.
- 15 A. G. Crevillén, M. Pumera, M. C. González and A. Escarpa, *Lab Chip*, 2009, **9**, 346–53.
- 16 K. Maehashi and K. Matsumoto, *Sensors*, 2009, **9**, 5368–5378.
- 17 J. N. Tey, I. P. M. Wijaya, J. Wei, I. Rodriguez and S. G. Mhaisalkar, *Microfluid. Nanofluid.*, 2010, **9**, 1185–1214.
- 18 P. Serp and E. Castillejos, *Chem. Cat. Chem.*, 2010, **2**, 41–47.
- 19 W. Feng and P. Ji, *Biotechnol. Adv.*, 2011, **29**(6), 889–895.
- 20 Q. Z. Zhang, B. Zhao, J. Yan, S. P. Song, R. Min and C. H. Fan, *Anal. Chem.*, 2011, **83**(23), 9191–9196.
- 21 J. Morton, N. Havens, A. Mugweru and A. K. Wanekayaa, *Electroanalysis*, 2009, **21**(14), 1597–1603.
- 22 J. Okuno, K. Maehashi, K. Kerman, Y. Takamura, K. Matsumoto and E. Tamiya, *Biosens. Bioelectron.*, 2007, **22**, 2377–81.
- 23 A. Javey, J. Guo, D. B. Farmer, Q. Wang, D. Wang, R. G. Gordon, M. Lundstrom and H. Dai, *Nano Lett.*, 2004, **4**(3), 1319–1322.
- 24 J. N. Tey, I. P. M. Wijaya, Z. Wang, W. H. Goh, A. Palaniappan, S. G. Mhaisalkar, I. Rodriguez, S. Dunham and J. A. Rogers, *Appl. Phys. Lett.*, 2009, **94**, 073704–1–3.
- 25 A. Vlandas, T. Kurkina, A. Ahmad, K. Kern and K. Balasubramanian, *Anal. Chem.*, 2010, **82**, 6090–6097.
- 26 C. Mayorga-Martinez, M. Guix, R. E. Madrid and A. Merkoçi, *Chem. Commun.*, 2012, **48**, 1686–1688.
- 27 I. P. M. Wijaya, T. J. Nie, S. Gandhi, R. Boro, A. Palaniappan, G. W. Hau, I. Rodriguez, C. R. Suri and S. G. Mhaisalkar, *Lab Chip*, 2010, **10**, 634–638.
- 28 W. S. Hummers and R. E. Offeman, *J. Am. Chem. Soc.*, 1958, **80**(6), 1339–1339.
- 29 C. K. Chua, A. Ambrosi and M. Pumera, *Electrochem. Commun.*, 2011, **13**, 517–519.
- 30 Q. He, S. Wu, S. Gao, X. Cao, Z. Yin, H. Li, P. Chen and H. Zhang, *ACS Nano*, 2011, **5**(6), 5038–5044.
- 31 B. J. Plowman, S. K. Bhargava and A. P. O'Mullane, *Analyst*, 2011, **136**, 5107–5119.
- 32 Z. Zou, J. Kai, M. Rust, J. Han and C. Ahn, *Sens. Actuators, A*, 2007, **136**, 518–526.
- 33 D. Lee, J. Ondrake and T. Cui, *Sensors*, 2011, **11**, 9300–9312.
- 34 J. Gamby, A. Rudolf, M. Abid, H. H. Girault, C. Deslouis and B. Tribollet, *Lab Chip*, 2009, **9**, 1806–1808.
- 35 L. C. Taylor, T. B. Kirchner, N. V. Lavrik and M. J. Sepaniak, *Analyst*, 2012, **137**, 1005–1013.
- 36 V. Canpean and S. Astilean, *Lab Chip*, 2009, **9**, 3574–3579.
- 37 A. J. Tavares, M. O. Noor, C. H. Vannoy, W. R. Algar and U. J. Krull, *Anal. Chem.*, 2012, **84**(1), 312–319.
- 38 Y. Luo, W. Sun, C. Liu, G. Wang and N. Fang, *Anal. Chem.*, 2011, **83**, 5073–5077.
- 39 S. Demming, A. Hahn, A. Edlich, E. Franco-Lara, R. Krull, S. Barcikowski and S. Büttgenbach, *Phys. Status Solidi A*, 2010, **207**, 898–903.
- 40 A. Prabhakar and S. Mukherji, *Lab Chip*, 2010, **10**, 3422–3425.
- 41 L. L. Qu, D. W. Li, J. Q. Xue, W. L. Zhai, J. S. Fossey and Y. T. Long, *Lab Chip*, 2012, **12**, 876–881.
- 42 B. Cui, C. Wu, L. Chen, A. Ramirez, E. L. Bearer, W. P. Li, W. C. Mobley and S. Chu, *Proc. Natl. Acad. Sci. U. S. A.*, 2007, **104**(34), 13666–13671.
- 43 L. C. Kuyper, K. L. Budzinski, R. M. Lorenz and D. T. Chiu, *J. Am. Chem. Soc.*, 2006, **128**, 730–731.
- 44 X. F. Wang, Y. Zhou, J. J. Xu and H. Y. Chen, *Adv. Funct. Mater.*, 2009, **19**, 1444–1450.
- 45 K. Wang, Q. Liu, X. Y. Wu, Q. M. Guan and H. N. Li, *Talanta*, 2010, **82**, 372–376.
- 46 Y. R. Lu, S. M. Peng, D. Luo and A. Lal, *Nat. Commun.*, 2011, **2**, 578, DOI: 10.1038/ncomms1587.

- 47 A. Y. Joshi, S. C. Sharma and S. P. Harsha, *Sens. Actuators, A*, 2011, **168**(2), 275–280.
- 48 I. Mehdipour, A. Barari and G. Domairry, *Computational Science*, 2011, **50**(6), 1830–1833.
- 49 P. S. Waggoner, C. P. Tan and H. G. Craighead, *Sens. Actuators, B*, 2010, **150**, 550–555.
- 50 K. S. Hwang, S. M. Lee, S. K. Kim, J. H. Lee and T. S. Kim, *Annu. Rev. Anal. Chem.*, 2009, **2**, 77–98.
- 51 M. K. Wagner, F. Li, J. Li, X. F. Li and X. C. Le, *Anal. Bioanal. Chem.*, 2010, **397**, 3213–24.
- 52 J. A. Ho, Y. C. Lin, L. S. Wang, K. C. Hwang and P. T. Chou, *Anal. Chem.*, 2009, **81**, 1340–1346.
- 53 S. Wang, N. Mamedova, N. A. Kotov, W. Chen and J. Studer, *Nano Lett.*, 2002, **2**, 817–822.
- 54 J. V. Jokerst, A. Raamanathan, N. Christodoulides, P. N. Floriano, A. a Pollard, G. W. Simmons, J. Wong, C. Gage, W. B. Furmaga, S. W. Redding and J. T. McDevitt, *Biosens. Bioelectron.*, 2009, **24**, 3622–3629.
- 55 H. Zhang, T. Xu, C. W. Li and M. Yang, *Biosens. Bioelectron.*, 2010, **25**, 2402–2407.
- 56 W. T. Liu, L. Zhu, Q. W. Qin, Q. Zhang, H. Feng and S. Ang, *Lab Chip*, 2005, **5**, 817–820.
- 57 H. Nian, J. Wang, H. Wu, J. G. Lo, K. H. Chiu, J. G. Pounds and Y. Lin, *Anal. Chim. Acta*, 2012, **713**, 50–55.
- 58 E. D. Goluch, S. I. Stoeva, J.-S. Lee, K. A. Shaikh, C. A. Mirkin and C. Liu, *Biosens. Bioelectron.*, 2009, **24**(8), 2397–2403.
- 59 K. F. Lei, *Measurement Science and Technology*, 2011, **22**(105802), 1–7.
- 60 X. Zhi, Q. Liu, X. Zhang, Y. Zhang, J. Feng and D. Cui, *Lab Chip*, 2012, **12**, 741.
- 61 P. P. Freitas, H. A. Ferreira, D. L. Graham, L. A. Clarke, V. Amaral, L. Martins, J. S. Fonseca, J. S. Cabral, Ed. M. Johnson, Elsevier Inc., Oxford, UK, 2004, 331–374.
- 62 J. Loureiro, P. Z. Andrade, S. Cardoso, C. L. da Silva, J. M. Cabral and P. P. Freitas, *Lab Chip*, 2011, **11**, 2255–2261.
- 63 J. Germano, V. C. Martins, F. a Cardoso, T. M. Almeida, L. Sousa, P. P. Freitas and M. S. Piedade, *Sensors*, 2009, **9**, 4119–4137.
- 64 V. C. Martins, J. Germano, F. a Cardoso, J. Loureiro, S. Cardoso, L. Sousa, M. Piedade, L. P. Fonseca and P. P. Freitas, *J. Magn. Magn. Mater.*, 2010, **322**, 1655–1663.
- 65 B. Chen, B. Hu, P. Jiang, M. He, H. Peng and X. Zhang, *Analyst*, 2011, **136**, 3934–42.
- 66 A. J. Wang, J. J. Xu, Q. Zhang and H. Y. Chen, *Talanta*, 2006, **69**(1), 210–215.
- 67 P. Guo, E. W. Hall, R. Schirhagl, H. Mukaibo, C. R. Martin and R. N. Zare, *Lab Chip*, 2012, **12**(3), 558–561.
- 68 G. D. Chen, F. Fachin, M. Fernandez-Suarez, B. L. Wardle and M. Toner, *Small*, 2011, **7**, 1061–1067.
- 69 C. L. Choong, W. I. Milne and K. B. K. Teo, *Int. J. Mater. Form.*, 2008, **1**, 117–125.
- 70 H. J. Yoon, K. Lee, Z. Zhang, T. M. Pham and S. Nagrath, *Most*, 2011, 1098–1100.
- 71 L. Johansson, K. Gunnarsson, S. Bijelovic, K. Eriksson, A. Surpi, E. Göthelid, P. Svedlindh and S. Oscarsson, *Lab Chip*, 2010, **10**, 654–661.
- 72 S. N. Khaderi, C. B. Craus, J. Hussong, N. Schorr, J. Belardi, J. Westerweel, O. Prucker, J. Rühle, J. M. J. den Toonder and P. R. Onck, *Lab Chip*, 2011, **11**, 2002–2010.
- 73 J. Park, A. Saffari, S. Kumar, A. G. Unther and E. Kumacheva, *Annu. Rev. Mater. Res.*, 2010, **40**, 415–443.
- 74 J. B. Edel, R. Fortt, J. C. De Mello and A. J. De Mello, *Chem. Commun.*, 2002, 1136–7.
- 75 E. M. Chan, R. A. Mathies and A. P. Alivisatos, *Nano Lett.*, 2003, **3**, 199–201.
- 76 H. Nakamura, Y. Yamaguchi, M. Miyazaki, M. Uehara, H. Maeda and P. Mulvaney, *Interface*, 2002, 1072–1073.
- 77 H. Nakamura, Y. Yamaguchi, M. Miyazaki, H. Maeda, M. Uehara and P. Mulvaney, *Chem. Commun.*, 2002, 2844–2845.
- 78 L.-H. Hung, K. M. Choi, W.-Y. Tseng, Y.-C. Tan, K. J. Shea and A. P. Lee, *Lab Chip*, 2006, **6**, 174–8.
- 79 I. Shestopalov, J. D. Tice and R. F. Ismagilov, *Lab Chip*, 2004, **4**, 316–21.
- 80 E. M. Chan, a P. Alivisatos and R. a Mathies, *J. Am. Chem. Soc.*, 2005, **127**, 13854–61.
- 81 B. K. H. Yen, A. Günther, M. a Schmidt, K. F. Jensen and M. G. Bawendi, *Angew. Chem., Int. Ed.*, 2005, **44**, 5447–51.
- 82 Y. Zhao, H. C. Shum, H. Chen, L. L. a Adams, Z. Gu and D. a Weitz, *J. Am. Chem. Soc.*, 2011, **133**, 8790–8793.
- 83 G.-R. Yi, T. Thorsen, V. N. Manoharan, M.-J. Hwang, S.-J. Jeon, D.J. Pine, S. R. Quake and S.-M. Yang, *Adv. Mater.*, 2003, **15**, 1300–1304.
- 84 J. B. Wacker, V. K. Parashar and M. A. M. Gijs, *Transducers*, 2011, 2940–2943.
- 85 L. Frenz, A. E. Harrak, M. Pauly, S. Bégin-Colin, A. D. Griffiths and J. C. Baret, *Microfluidics*, 2008, **47**, 6817–6820.
- 86 S. A. Khan, A. Günther, M. A. Schmidt and K. F. Jensen, *Langmuir*, 2004, **20**(20), 8604–8611.
- 87 A. J. C. Kuehne and D. A. Weitz, *Chem. Commun.*, 2011, **47**, 12379–12381.
- 88 F. Schütze, B. Stempfle, C. Jüngst, D. Wöll, A. Zumbusch and S. Mecking, *Chem. Commun.*, 2012, **48**, 2104–2106.
- 89 O. C. Farokhzad, A. Khademhosseini, S. Jon, A. Hermmann, J. Cheng, C. Chin, A. Kiselyuk, B. Teply, G. Eng and R. Langer, *Anal. Chem.*, 2005, **77**, 5453–5459.
- 90 L. Richter, V. Charwat, C. Jungreuthmayer, F. Bellutti, H. Brueckla and P. Ertl, *Lab Chip*, 2011, **11**, 2551–2560.
- 91 S. K. Mahto, T. H. Yoon and S. W. Rhee, *BioChip J.*, 2010, **4**, 82–88.
- 92 M. Safi, M. Yan, M.-A. Guedeau-Boudeville, H. Conjeaud, V. Garnier-Thibaud, N. Boggetto, A. Baeza-Squiban, F. Niedergang, D. Averbeck and J.-F. Berret, *ACS Nano*, 2011, **5**, 5354–64.
- 93 P. Liu, K. Skucha, M. Megens and B. Boser, *IEEE Trans. Magn.*, 2011, **47**, 3449–3451.
- 94 Y. Song, H. Zhang, C. H. Chon, X. Pan and D. Li, *Sens. Actuators, B*, 2011, **155**, 930–936.
- 95 D. Gallego-Perez, N. Higuera-Castro, S. Sharma, R. K. Reen, A. F. Palmer, K. J. Gooch, L. J. Lee, J. J. Lannutti and D. J. Hansford, *Lab Chip*, 2010, **10**, 775–82.
- 96 J. Lee, A. K. Jha, A. Bose and A. Tripathi, *Langmuir*, 2008, **24**(22), 12738–12741.

On-chip electrochemical detection of CdS quantum dots using normal and multiple recycling flow through modes†‡

Mariana Medina-Sánchez,^{ab} Sandrine Miserere,^{ab} Sergio Marín,^{ab} Gemma Aragay^{ab} and Arben Merkoçi^{*abc}

Received 3rd January 2012, Accepted 23rd April 2012

DOI: 10.1039/c2lc00007e

A flexible hybrid polydimethylsiloxane (PDMS)–polycarbonate (PC) microfluidic chip with integrated screen printed electrodes (SPE) was fabricated and applied for electrochemical quantum dots (QDs) detection. The developed device combines the advantages of flexible microfluidic chips, such as their low cost, the possibility to be disposable and amenable to mass production, with the advantages of electrochemistry for its facility of integration and the possibility to miniaturize the analytical device. Due to the interest in biosensing applications in general and particularly the great demand for labelling alternatives in affinity biosensors, the electrochemistry of cadmium sulfide quantum dots (CdS QDs) is evaluated. Square wave anodic stripping voltammetry (SWASV) is the technique used due to its sensitivity and low detection limits that can be achieved. The electrochemical as well as the microfluidic parameters of the developed system are optimized. The detection of CdS QDs in the range between 50 to 8000 ng mL⁻¹ with a sensitivity of 0.0009 $\mu\text{A}/(\text{ng mL}^{-1})$ has been achieved. In addition to the single in-chip flow through measurements, the design of a recirculation system with the aim of achieving lower detection limits using reduced volumes (25 μL) of sample was proposed as a proof-of-concept.

Introduction

The microfluidic know-how for itself has been oriented to develop new products and solutions in different areas, such as biotechnology, environmental science, medical and pharmaceutical industries.¹ The operations that can be developed in these microsystems are basically for analysis and sample treatment, including cells, proteins and viruses, due to advantages such as the reduction of sample and reagent volumes, the decrease of analysis time, the possibility of portability and the integration of conventional analytical techniques.

Microfluidic chips must be inexpensive, disposable and amenable to mass production. That is why polymers are increasingly replacing traditional substrates such as glass and silicon. The kinds of substrate, as well as the detection methods in microfluidics, are critical points to be considered for further integration.²

Furthermore, amplification strategies to achieve low detection limits are being considered for in-chip measurements, especially

by using nanomaterials. In this context, quantum dots (QDs) have been reported as promising probes for ultrasensitive in-chip detection of biological targets such as cancer biomarkers, among others, using mainly optical techniques due to their high quantum yields, easy and diverse surface modification and flexibility.³

The use of QDs in biosensing applications has emerged as a very promising alternative for various optical or electrochemical sensing strategies.^{4–6} Of special interest has been the consideration of QDs bioconjugates as alternatives to isotopes or dyes. Advantages in comparison to organic dyes (*i.e.* rhodamine) in terms of being 20 times brighter and 100 times more stable against photobleaching, besides having a narrower spectral linewidth, are making QDs a very interesting material in biosensing.⁷ Beside their optical properties, their metal composition core along with easy electrochemical detection has led to various interesting applications, including DNA⁸ and protein⁹ sensing. The high sensitivity, selectivity, and low detection limits of electrochemical analysis of QDs already demonstrated in batch techniques would be of great interest if applied to low-cost microfluidic devices.

With this in mind, we present a hybrid polydimethylsiloxane–polycarbonate (PDMS–PC) microfluidic platform with an integrated screen-printed-electrode (SPE). This is an easy to fabricate and low cost platform for QDs detection. Carbon (working and counter) and silver electrodes were printed by screen-printing technology onto a polycarbonate substrate. A slab of PDMS with a simple channel was bonded to it without

^aNanobioelectronics & Biosensors Group, Institut Català de Nanotecnologia, Bellaterra, Barcelona-Spain

^bUniversitat Autònoma de Barcelona, Bellaterra, Spain

^cICREA, Barcelona, Spain. E-mail: arben.merkoci@icn.cat; Fax: +34935868020; Tel: +34935868014

† Published as part of a themed issue in collaboration with the III International Workshop on Analytical Miniaturization and NANOTEchnologies, Barcelona, 2012.

‡ Electronic supplementary information (ESI) available. See DOI: 10.1039/c2lc00007e

showing any leakage. In order to evaluate the performance of the developed chip, cadmium sulfide (CdS) QDs were prepared and used for SWASV measurements.¹⁰

In addition, the design of a recirculation system with the aim of achieving lower detection limits using reduced volumes of sample (25 μL) was proposed as a proof-of-concept. Despite the great number of publications involving in-chip QDs detection using fluorescence techniques,¹¹ to the best of our knowledge the electrochemical detection of such nanoparticles in a microfluidic platform has not yet been reported.

Experimental

Microfluidic device and screen printed electrodes fabrication.

Microchips were fabricated by rapid prototyping and PDMS technologies as described previously.¹² Briefly, a 4 inch silicon wafer was spin coated with a negative photoresist (SU-8 from Microchem) and patterned by photolithography. PDMS was poured onto the resulting mold and cured at 65 $^{\circ}\text{C}$ for 2 h. The channels were 500 μm wide by 50 μm depth and 5 cm long (Fig. 1A(a)).

The electrochemical detector consists of a set of three electrodes of 500 μm width separated by 500 μm with an approximate thickness of 4 μm (Fig. 1A(a)). They were produced by screen printing technology using a screen-printing machine (DEK 248). Graphite ink (Electrodag 423SS) was used for the working (WE) and counter electrode (CE), and silver/silver chloride ink (Electrodag 6037SS) for the reference electrode (RE). All the inks were purchased from Acheson Industries. The fabrication process involved two steps. In the first step the graphite layer (WE, CE) was printed onto a polycarbonate sheet

and cured at 60 $^{\circ}\text{C}$ for 20 min. The RE was obtained by printing a second layer of silver/silver chloride ink which was cured under the same conditions.

Finally, the PDMS channel and the PC substrate were assembled using a previously reported protocol.¹³ The polycarbonate substrate was treated by air-plasma for 1 min and then immersed into a 2% (v/v) 3-aminopropyltriethoxylane (APTES) (Sigma Aldrich) solution in water for 1 h in order to functionalize the surface with amino groups. The surface of the PDMS channel was also activated for 1 min by plasma, and put into contact with the PC sheet to achieve irreversible bonding (ESI†). Finally, a homemade connector was used for the electrical connection (see Fig. 1A(b)).

CdS QDs electrochemical detection

3 nm CdS QDs were synthesized by arrested precipitation using water-dispersed cadmium chloride and hexamethyldisilathiane (HMSDT) as a sulfide precursor (Fig. 1B).¹⁴

The procedure for CdS QDs detection has been previously described by our group.¹⁵ It involves adsorption of CdS QDs onto the surface of the working electrode and the further reduction of Cd^{2+} ions from the QDs surface onto the WE. The further reoxidation of Cd^0 to Cd^{2+} gives the electrochemical response. The electrochemical detection was performed in acetate buffer 0.2 M (NaCl 0.05 M, pH 4.6).

The CdS QDs concentrations were determined by SWASV. In order to get maximum sensitivity, the voltammetric parameters (deposition time, conditioning potential, conditioning time and frequency) were optimized using a solution of 1 $\mu\text{g mL}^{-1}$ of CdS QDs in acetate buffer. The flow-through conditions were used during the conditioning and the deposition step, whereas the equilibration step and the square wave scan were performed in a static solution. Before each analysis, SPE were pretreated by cyclic voltammetry between -0.8 V and 0.8 V in acetate buffer solution (previously mentioned), for 10 cycles.

Results and discussion

In this work, a simple and low cost microfluidic platform for CdS QDs electrochemical detection was fabricated. It consists of a PDMS channel and a polycarbonate sheet onto the surface of which the carbon and silver/silver chloride electrodes were screen-printed. Screen-printing is a well-known technique to produce low cost electrodes at an industrial level. Combining the advantages of PDMS technology and screen-printing allows the production of reliable and low-cost microdevices. As shown in Fig. 1A(a), SPE are thick electrodes of around 5 μm which could be a problem during the assembly of the chip and some leakage between the electrodes could appear. This problem can be solved if the width of the electrode remains smaller than the width of the channel.

Out of chip and in-chip cyclic voltammetry studies of SPE detectors

In order to validate the use of SPE as a detector in a chip, we first investigated the cyclic voltammetry responses of the working electrode before and after the bonding procedure (in static and flow through modes). Fig. 2A shows typical voltammograms

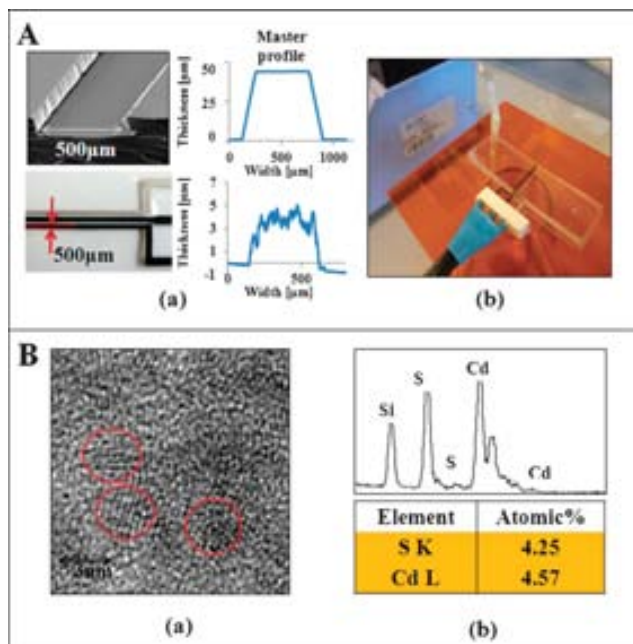


Fig. 1 (A) Microfluidic platform system: scanning electron microscopy images of microchannel cross section, optical image of SPE and their respective profiles (a) and microfluidic set-up (b). (B) CdS QDs: transmission electron microscopy images of CdS QDs (a) and the corresponding microanalysis data (b).

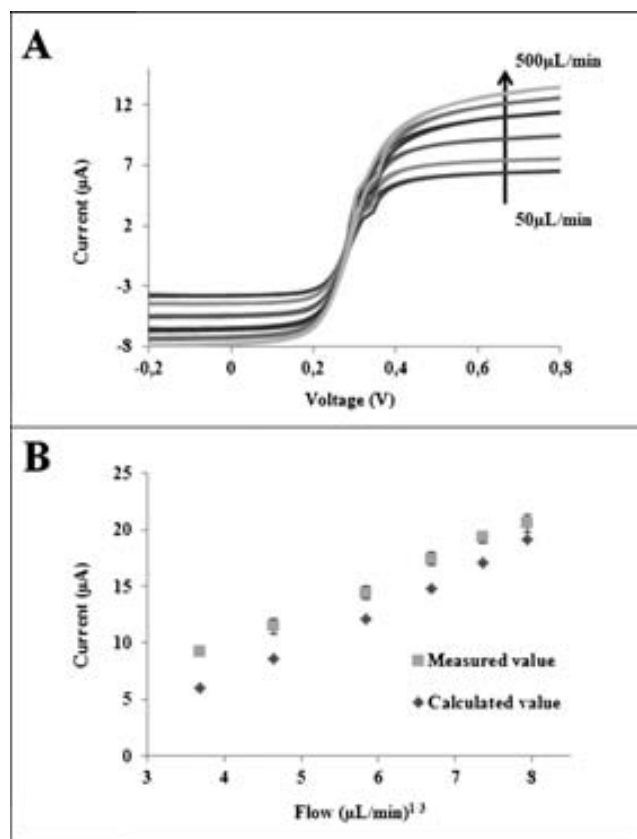


Fig. 2 Cyclic voltammetry curves recorded at different flow rates (50, 100, 200, 300, 400, 500 $\mu\text{L}/\text{min}$) (A), and comparison between the calculated and the measured values of ferrocyanide/ferricyanide using cyclic voltammetry (B). Range of the measurement from -0.2 V to 0.8 V and scan rate 50 mV/s .

obtained with a solution of 5 mM ferrocyanide/ferricyanide in 0.1 M KCl. The obtained electrodes were characterized in order to observe their repeatability and reproducibility. The repeatability studies were performed by studying the electrochemical response of three different electrodes in three consecutive measurements. The electrochemical conditions for the electrodes characterization were: $V_{\text{ini}} = -0.2$ V; $V_1 = 0.8$ V; $V_2 = -0.2$ V; scan rate of 50 mV/s .

The current data can be interpreted according to Levich's equation.^{16,17} For SPE inside a channel with a rectangular cross-section, it can be expressed as:

$$I = 0.925nF cw(x_e D)^{2/3} \left(\frac{U}{h^2 d} \right)^{1/3} \quad (1)$$

where n is the number of exchanged electrons, F is the Faraday constant (96485 C/mol), c and D are the concentration and the diffusion coefficient of the electroactive species, respectively, d is the channel width, h is half the height of the channel, x_e and w are the length and the width of the electrode, respectively, and U is the flow rate. In our case, the values used for the diffusion coefficients of ferrocyanide and ferricyanide¹⁸ were, in both cases, $D = 7.63 \times 10^{-10}$ m^2/s . The electrode dimensions were set to be approximately $w = 500$ μm , $x_e = 500$ μm , and the channel dimensions to $d = 500$ μm and $2h = 50$ μm , according to

the SEM images. The experimental data represented for each flow rate correspond to the average limiting current value from at least six consecutive cyclic voltammograms. The experimental limiting current values present a linear dependence with the cubic root of the flow rate, as predicted by the Levich equation, with a standard deviation between the measured values (in laminar flow regime) and calculated values around 1.72 μA . See Fig. 2B.

The presented results prove that the screen-printed electrodes integrated into the microfluidic platform show good performance in aqueous media and their behavior is in good agreement with Levich's predictions, demonstrating that the bonding process does not affect the electrodes. The developed integrated system shows good adhesion of screen printed electrodes with high resistance to high flow values of the measuring solution.

QDs detection. Until now, our group has demonstrated the electrochemical detection of CdS QDs in batch measurements using commercial electrodes,¹⁸ which are mercury-modified carbon electrodes. These electrodes, combined with stripping methods, lead to really high sensitivities but nowadays, the development of alternative methods less toxic and more environmental friendly than the ones using mercury are a subject of interest. This is why we have focused this work on the use of a "non-toxic" carbon electrode detector. However, as can be seen in Fig. 3, we are not able to discriminate the QDs signal from the blank. Indeed, with commercial electrodes, a mercury-cadmium amalgam is created during the deposition step, which helps with the deposition of cadmium on the electrodes. When the detection is done in chip (in flow) an increase of the signal was observed.

This increase is related to a faster redox process that occurs in chip in comparison to drop measurement that should be related to the channel dimensions and the more controllable environmental conditions. (Fig. 4(A)). Furthermore, as the deposition of QDs is done under flow conditions we are not limited by the diffusion which leads to a higher enrichment to the electrode.

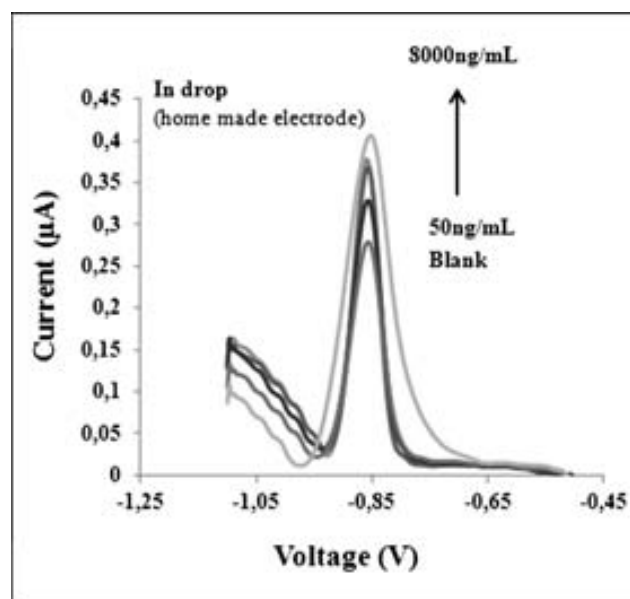


Fig. 3 Typical voltammetric peak of CdS QDs re-oxidation in batch measurements with homemade carbon screen printed electrodes.

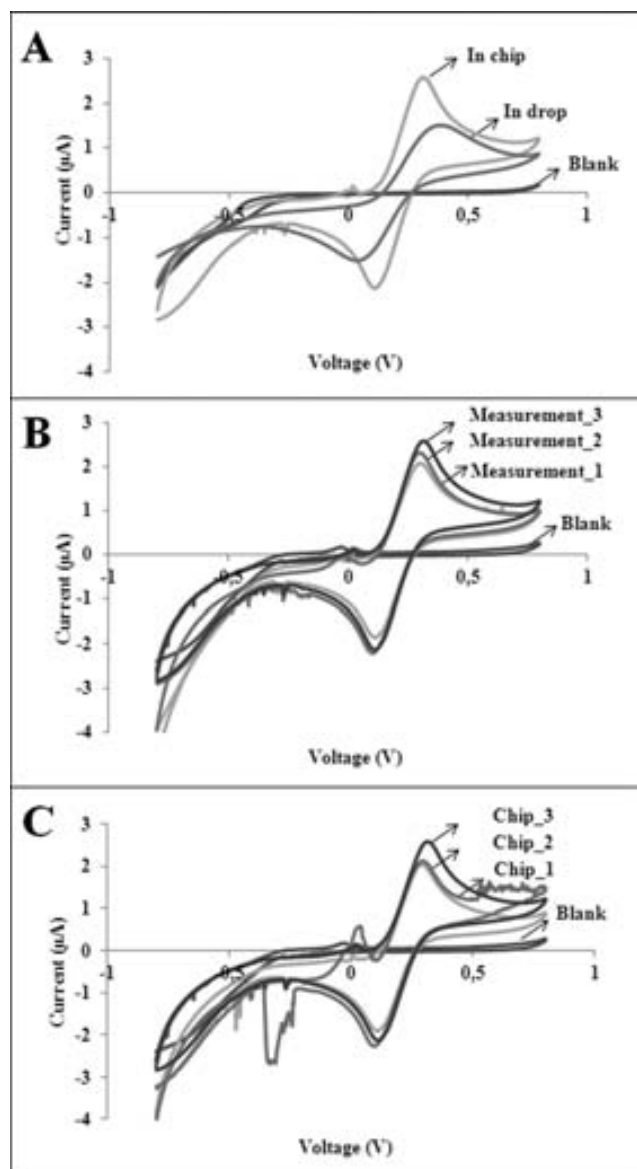


Fig. 4 Cyclic voltammograms in a solution of 5 mM ferrocyanide/ferricyanide in 0.1 M KCl. Comparison between in chip and in drop measurements (A), three consecutive measurements by using the same chip (B), and with three different chips (C). The scan rate for all CVs was 50 mV s⁻¹.

The repeatability between measurements using one single electrode was studied so as to see its operation behavior. Similar responses in three consecutive measurements with a standard deviation of 2.4 µA (Fig. 4(B)) were obtained. In addition, the reproducibility between electrodes (chips) was studied giving rise to very similar responses using three different chips with a standard deviation of 2.9 µA (Fig. 4(C)).

Electrochemical stripping parameters optimization

The electrochemical stripping detection of QDs was studied in different mediums such as phosphate buffer, acetate buffer or HCl (results not shown). Acetate buffer 0.2 M + NaCl 0.05 M (pH 4.5) was selected taking into account the lower detection limits achieved.

In Fig. 5, the different optimizations of the analytical parameters are shown. The best signal to noise relation and the highest sensitivity of the detection were the choice criteria. Based on this study, the optimal conditions were: conditioning potential: -0.15 V; conditioning time: 60 s; deposition voltage: -1.3 V; deposition time: 120 s; equilibrium time: 30 s; frequency: 10 Hz, and scan rate: 5 mV s⁻¹.

Calibration curve and repeatability studies

The calibration curve for different CdS QDs concentrations in acetate buffer (0.2 M, pH 4.5) was obtained using the polycarbonate based platform achieving a linear range of detection between 50 and 8000 ng QDs mL⁻¹ (see Fig. 6A, B). The results show a well-defined stripping peak at -0.83 V in concordance with the Cd⁰ oxidation potential.

Three replicate determinations of each concentration were carried out with a maximum RDS of 6.5%. Thanks to this device, we can achieve a sensitivity of 0.0009 µA/(ng mL⁻¹) which is similar to the sensitivity obtained in static mode with commercial electrodes (with a working electrode area 50 times bigger than the chip electrode), as can be seen in Fig. 6C.

The obtained range of response demonstrates that this device shows promising potential for its integration in biosensing systems for future applications in immunosensors and DNA sensors using QDs as labels.

The repeatability of the device was also studied using a second polycarbonate chip. The reproducibility and the sensitivity (results not shown) were in the same range as the first device. The flow-through conditions allow the concentration of QDs to remain constant during the deposition step so the process is not limited by the diffusion. In addition, the peak current can be increased due to the continuous renewed solution during deposition time.

QDs response increased by flow-recycling mode

A flow-through recycling system based on a close-loop system by using a peristaltic micropump (Fig. 7A) is designed and studied with the aim of improving the electrochemical signal, decreasing

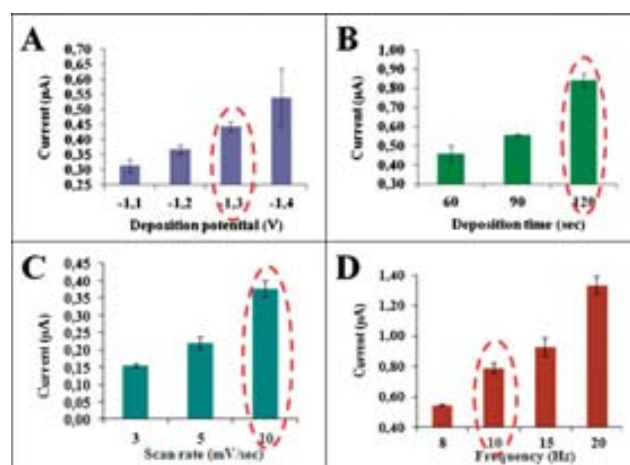


Fig. 5 Optimization of electrochemical parameters for in chip CdS QDs detection: deposition potential (A), deposition time (B), scan rate (C) and frequency (D). Experimental conditions were as described in the text.

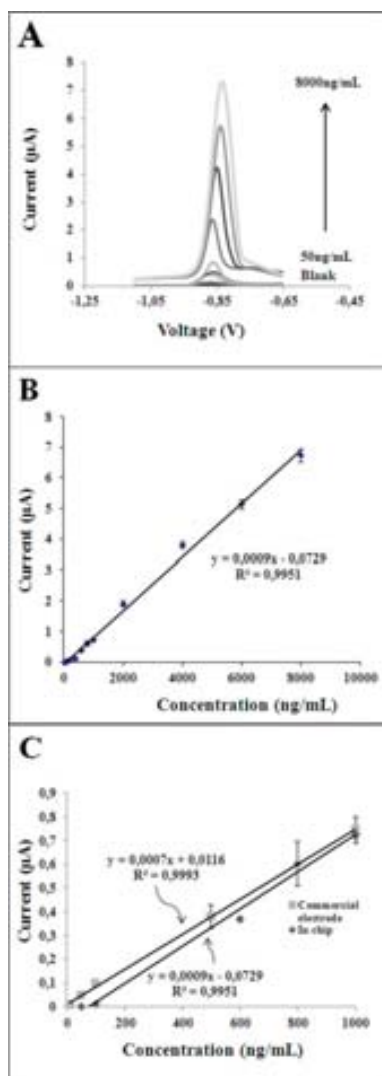


Fig. 6 Calibration curve of CdS QDs electrochemical detection “in-chip” platform. Typical voltammetric peak of CdS QDs re-oxidation in batch measurements with homemade carbon screen printed electrodes. (A) Typical voltammetric peak of CdS QDs re-oxidation in chip measurements with homemade carbon screen printed electrodes. (B) The linear calibration curve. (C) Comparison of calibration curves between batch measurements with commercial SPEs and in chip measurements with homemade CSPEs. Blanks and curves with increasing peaks from 50 ng mL^{-1} to 8000 ng mL^{-1} are shown.

the detection limit and reducing the sample volume used in each measurement.

The flow recycling mode was applied after filling the electrochemical flow cell with $25 \mu\text{L}$ of a sample of CdS QDs (500 ng mL^{-1}) in acetate buffer. Maintaining the same electrochemical parameters (e.g. deposition time, 120 s; deposition potential, -1.3 V ; flow rate, $50 \mu\text{L min}^{-1}$), an increase of around 6 times of the cadmium stripping peak was achieved with the flow recycling mode (2 turns) in comparison to the normal in-chip flow-through mode without the need of increasing the deposition time. Such recycling mode reported earlier for trace metals detection using ASV technique was found to be an efficient method for ion detection.¹⁹ Fig. 6B shows the

voltammetric responses corresponding to three consecutive measurements of a CdS QDs suspension (500 ng mL^{-1} in acetate buffer) using the flow-recycling system (one single turn for each measurement). An increase of the stripping peak was observed repeatedly (Fig. 7B), which might be due to the QDs accumulation on the surface of the WE after each measurement and the impossibility of cleaning during the duration of the applied conditioning time. For that reason, the conditioning time was increased from 60 s to 150 s ($V_{\text{cond}} = -0.15 \text{ V}$) in order to achieve a better cleaning of the electrode surface prior to the deposition step. Fig. 7C shows the voltammetric stripping responses of three consecutive measurements using the new conditioning parameters.

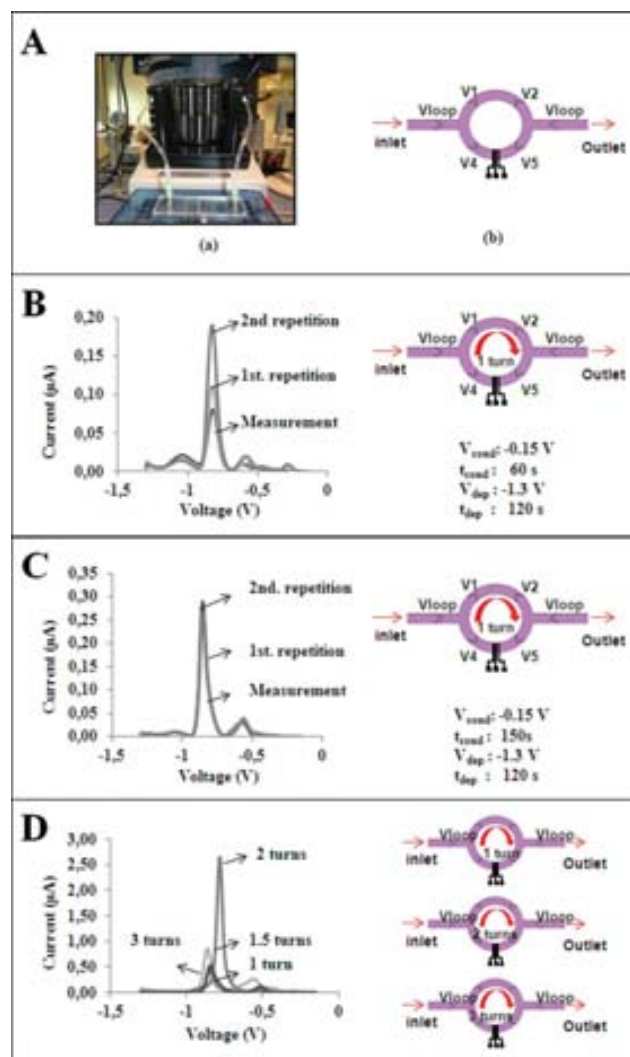


Fig. 7 (A) Recycling platform set-up picture (a) and schematic (b). (B) Voltammetric responses of three consecutive measurements of CdS QDs (500 ng mL^{-1}) using in flow-recycling mode with a conditioning time of 60 s. (C) Voltammetric responses of three consecutive measurements of CdS QDs (500 ng mL^{-1}) using in flow-recycling mode with a conditioning time of 150 s. (D) Voltammetric responses of CdS QDs (500 ng mL^{-1}) using different flow rates corresponding to 1 single turn ($50 \mu\text{L min}^{-1}$), 1.5 turns ($75 \mu\text{L min}^{-1}$), 2 turns ($100 \mu\text{L min}^{-1}$) and 3 turns ($125 \mu\text{L min}^{-1}$).

A good reproducibility was obtained between the three consecutive measurements (RDS 9.8%) showing that a higher conditioning time at -0.15 V allows a complete re-oxidation of the Cd^0 accumulated onto the WE surface and consequently giving reproducible peak after each measurement.

After achieving good reproducibility between measurements, the flow rate of the recirculation process was studied in order to evaluate the effect of the number of turns during which the sample passes through the WE toward the response of the chip. The initial flow rate used for the reproducibility study ($50 \mu\text{L min}^{-1}$) represents one single turn of the sample through the electrode. Other flow rates to obtain 1.5, 2 and 3 turns of the sample through the system were tested ($75 \mu\text{L min}^{-1}$, $100 \mu\text{L min}^{-1}$, and $125 \mu\text{L min}^{-1}$, respectively) (see Fig. 7D).

The results (Fig. 7D) show a correlation between the intensity of the peak current and the flow rate when working between $50 \mu\text{L min}^{-1}$ and $100 \mu\text{L min}^{-1}$. However, the use of higher flow rates ($125 \mu\text{L min}^{-1}$) provokes a decrease on the electrochemical response which might be caused by the short time that QDs have to be in contact with the WE owing the higher flow rate not allowing their efficient reduction and further detection. The obtained results are of interest for further applications, for example this device could also be applied to the detection of heavy metals in water.

The integration of a peristaltic pump into microfluidic channel to allow the fluid recirculation through the channel, thus reducing the dead volumes (tubes), will be a subject of further studies. Some preliminary designs for recycling platform as well as new geometries for QDs bioconjugation in microfluidic chip for electrochemical detection are being developed (ESI†).

Conclusions

The fabrication of a hybrid PDMS-PC microfluidic chip with integrated SPE electrodes has been demonstrated. SPEs have been integrated into an SWASV detector and shown to be a simple alternative for easy to use, low cost and mass produced chips.

The electrochemical parameters of the in-chip CdS QDs detection such as scan rate, deposition potential, deposition time, frequency, and flow rate, in order to obtain the best relation electrochemical response vs. noise using the developed microfluidic platform, have been optimized.

In-chip flow recycling allows an increase in the QDs electrochemical signals without increasing the need of larger

sample volumes and even using lower sample volumes (*i.e.* $25 \mu\text{L}$) compared to the normal flow through chip (from $50 \mu\text{L}$ to $100 \mu\text{L}$).

The developed in-chip QD detection in addition to the integration of other operations such as microreactions, pre-concentrations, separations, and bioconjugations, can open the way to the design of various biosensing platforms. These operations, in addition to the high sensitivity of the detector, will open the way to future applications of the developed device in diagnostics between other applications.

Acknowledgements

We acknowledge E.U. support for the project FP7 contract number 246513 “NADINE”. MICINN (Madrid) for MAT2011-25870, PIB2010JP-00278 and NATO 53042013 projects is also acknowledged.

References

- 1 S. Haeberle and R. Zengerle, *Lab Chip*, 2007, **7**(9), 1094–1110.
- 2 R. P. Baldwin, *Electrophoresis*, 2000, **21**, 4017–4028.
- 3 J. Wang, G. Liu and A. Merkoçi, *J. Am. Chem. Soc.*, 2003, **125**(11), 3214–3215.
- 4 C. J. Murphy, *Anal. Chem.*, 2002, **74**(19), 520–526.
- 5 C. M. Niemeyer, *Angew. Chem., Int. Ed.*, 2001, **40**, 4128–4158.
- 6 N. L. Rosi and C. A. Mirkin, *Chem. Rev.*, 2005, **105**, 1547–1562.
- 7 W. C. W. Chan and S. Nie, *Science*, 1998, **281**, 2016–2018.
- 8 A. Merkoçi, M. Aldavert, S. Marín and S. Alegret, *TrAC, Trends Anal. Chem.*, 2005, **24**, 341–349.
- 9 G. Liu, J. Wang, K. Kim and M. Jan, *Anal. Chem.*, 2004, **76**, 7126–7130.
- 10 A. Merkoçi, S. Marín, M. T. Castañeda, M. Pumera, J. Ros and S. Alegret, *Nanotechnology*, 2006, **17**, 2553–2559.
- 11 J. V. Jokerst, A. Raamanathan, N. Christodoulides, P. N. Floriano, A. A. Pollard, G. W. Simmons, J. Wong, C. Gage, W. B. Furmaga, S. W. Redding and J. T. McDevitt, *Biosens. Bioelectron.*, 2009, **24**, 3622–3629.
- 12 Y. Xia and G. M. Whiteside, *Annu. Rev. Mater. Sci.*, 1998, **28**, 153–84.
- 13 L. Tang and N. Yoon Lee, *Lab Chip*, 2010, **10**, 1274–1280.
- 14 Ch. Barglik-Chory, D. Buchold, M. Schmitt, W. Kiefer, C. Heske, C. Kumpf, O. Funchs, L. Weinhardt, A. Stahl, E. Umbach, M. Lentze, J. Gerts and G. Müller, *Chem. Phys. Lett.*, 2003, **379**, 443–451.
- 15 S. Marín and A. Merkoçi, *Nanotechnology*, 2009, **20**, 055101–055107.
- 16 R. G. Compton, A. C. Fisher, R. G. Wellington, P. J. Dobson and P. A. Leigh, *J. Phys. Chem.*, 1993, **97**, 10410–10415.
- 17 X. Illa, O. Ordeig, D. Snakenborg, A. Romano-Rodríguez, R. G. Compton and J. P. Kutter, *Lab Chip*, 2010, **10**, 1254–1261.
- 18 I. Palchetti, S. Majid, A. Kicela, G. Marraza and M. Mascini, *Int. J. Environ. Anal. Chem.*, 2003, **83**, 701–711.
- 19 S. Armalis and G. Johansson, *Anal. Chim. Acta*, 1997, **339**, 155–159.

INKJET PRINTED FET FOR BIOSENSING APPLICATIONS

M. Medina-Sánchez¹, C. Martínez-Domingo², E. Ramon², S. Miserere¹, A. Alcalde-Aragonés², J. Carrabina² & A. Merkoçi^{1,3}.

¹*Nanobioelectronics & Biosensors Group, Catalan Institute of Nanotechnology (ICN), Universitat Autònoma de Barcelona, Spain*

²*Centre for Accessibility and Ambient Intelligence of Catalonia, Universitat Autònoma de Barcelona, Catalonia, Spain.*

³*ICREA, Barcelona, Spain*

ABSTRACT

The developed bio-field effect transistor (BioFET) consists in nano-silver ink printed source and drain electrodes, a polymeric organic semiconductor, dielectric layer based on methyl methacrylate (MMA) and finally the reference electrode of silver-silver chloride ink. The thickness of dielectric layer was optimized and characterized by Scanning Electron Microscopy (SEM) as well as by electrical measurements to characterize the dielectric breakdown and the semiconductor dielectric interface. The electrical characterization was also performed using different electrolytic solutions. Finally some preliminary results about the FET functionalization onto dielectric layer so as to obtain a BioFET are shown.

KEYWORDS: Inkjet, organic transistor, biosensor, BioFET, EISFET, surface functionalization, protein.

INTRODUCTION

The development of Organic Thin Film Transistors (OTFTs) has opened an interesting research field in biosensing applications by replacing the gate by an electrolyte and a reference electrode [1]. By functionalizing field effect transistor (FET) with biological materials, a BioFET is obtained. The main advantage of this FET based biosensor is the possibility to get an all-integrated, portable and low cost system, compatible with the “single-use sensor” concept. In addition, these devices can be fabricated by different deposition techniques, which require low temperatures, are environment friendly and easily adaptable to mass fabrication processes [2]. To overcome these issues an inkjet based FET for biosensing applications is proposed.

BioFETs to be used as biomedical devices require specific interactions between biological molecules used as receptors and the analyte contained in the sample fluid. Up to date the fabrication of such biosensors has involved the assembly of many parts making them expensive and non-reproducible. Recently, the production of BioFETs has moved to fabrication and production processes with high throughput and integration level. Indeed traditional silicon-based semiconductor electronics tend to be replaced by organic, hybrid and flexible printed electronic methodologies. Between examples of biosensors fabricated with these new technologies are the development of electrochemical biosensor based on gold electrodes by inkjet printing onto polyimide (PI) substrate, for detection of a cancer biomarker such as interleukin-6 (IL-6) in serum [3]. Organic field effect transistors are also used for glucose detection. A simple poly(3,4-ethylene dioxythiophene)/poly(styrene sulfonic acid) based transistor was used for glucose detection through a mechanism that involves sensing of hydrogen peroxide [4].

Regarding the deposition of organic materials several technologies such as inkjet-printing, screen-printing, microcontact-printing, gravure and flexography beside lithography's such as scanning probe, photo and e-beam and laser printing are already known. Between these various deposition technologies, inkjet printing has become one of the most promising techniques capable of manufacturing devices by using small volumes of ink, in a rapid and additive procedure, achieving high pattern precision and resolution with greater reproducibility. This method doesn't require any mask which makes it easier and cheaper in comparison to other ones [5].

The purpose of this work is to develop a simple, low cost and miniaturized BioFET to determine biomarkers (i.e. for Alzheimer, cancer etc.) based on the use of specific antibodies immobilized onto the transducer surface of a field effect transistor. The quick and sensible detection of biomarkers in a point-of-care application will allow an early diagnosis achieving prompt treatments of patients.

PRINCIPLE OF BIOFET OPERATION

BioFET is based on the electrolyte-insulator-semiconductor field-effect transistor (EISFET) that provides means of electrical detecting of biomolecular interactions by the capacitive coupling between interacting species and the organic semiconductor. A simplified scheme of the BioFET is shown in Figure 1. It consists of a conventional FET structure that includes source, drain and gate. However, in the BioFET, the gate contact is replaced by an electrolytic solution, an antibody-protein conjugate and a reference electrode. The amount of accumulated charge on the dielectric gate in the BioFET can result in an increase (or decrease) of the Source-Drain current. This would create variations in the transistor responses (I-V curves) that are proportional to the amount of the introduced charge. If the change of the electrical charge is related to the interaction between biological molecules, then it can be used to monitor this process quite effectively and with very high sensitivity.

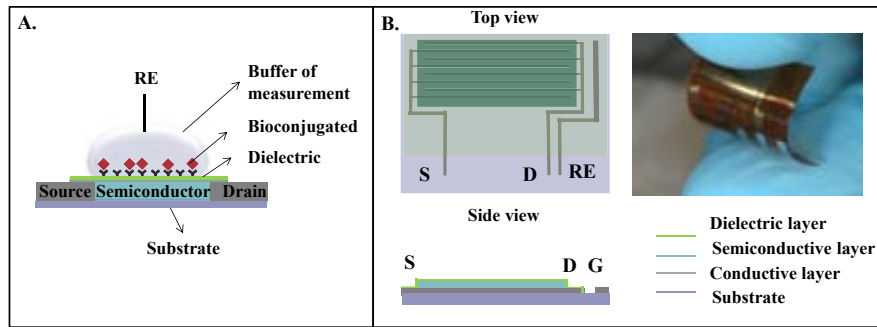


Figure 1. Scheme of BioFET components (A), and top and side views (B) representing each layer of the BioFET including a picture of the flexible printed device.

RESULTS AND DISCUSSIONS

Homemade BioFETs were fabricated by using an R&D inkjet printing machine (Dimatix DMP2831) which especially printed the silver contacts and the semiconductive layer (OSC layer) Figure 2B. The dielectric layer was obtained by an optimized deposition of methyl methacrylate (MMA) using spin coating process (Figure 2A). I-V results were obtained for different number of layers as well their thickness, in order to select the properly thickness to decrease the current leakages (Figure 2C and 2D).

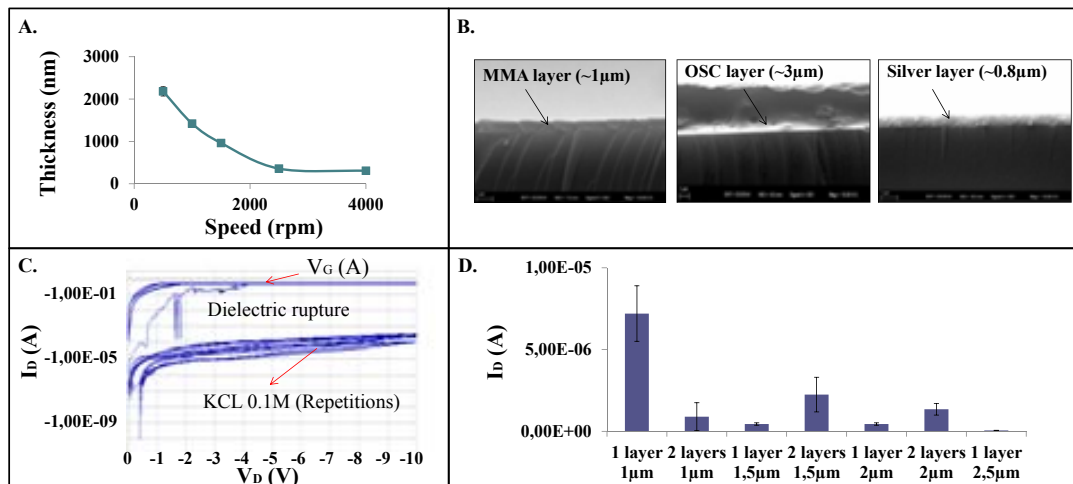


Figure 2. Dielectric layer studies that include thickness optimization (A), SEM images of the various layers are also shown (B), dielectric rupture studies (C), and study of current at different dielectric thickness (D).

MMA functionalization allowing the immobilization of proteins onto gate surface was performed. It consists in plasma oxidation of the MMA layer followed by an incubation using 3-aminopropyltriethoxysilane (APTES). Different concentrations of amino-groups were compared and characterized by colorimetric method for quantification of amine groups by using acid orange II dye (Figure 3A). 1% of APTES was chosen as a suitable concentration that does not affect the physical properties of the material, obtaining an adhesion of $0.18 \mu\text{M}\cdot\text{cm}^2$ amine groups. Fluorescence characterization of the bovine serum albumin (BSA) labeled with a fluorophore (ALEXA 555) by using epifluorescence microscope confirmed the selective adhesion of the analyte onto the device (Figure 3B). Atomic Force Microscopy (AFM) study was also performed. AFM images (Figure 3C) show a clear phase change and roughness increase after APTES and BSA immobilization.

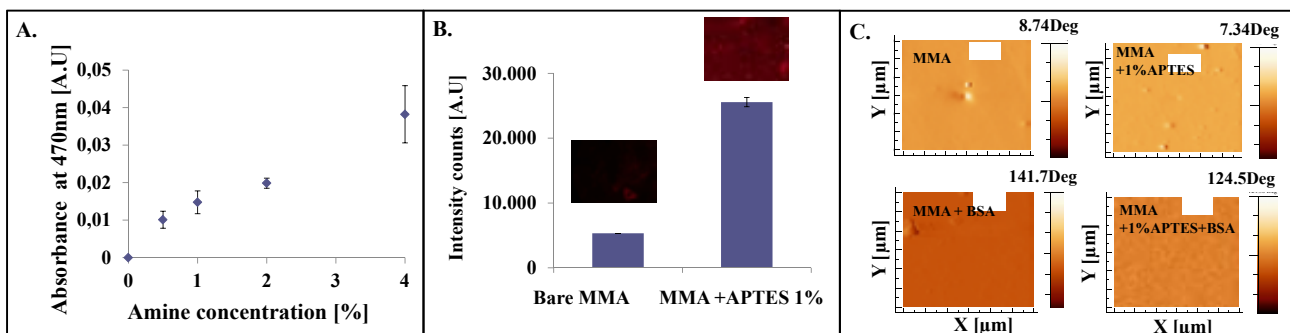


Figure 3. MMA layer functionalization. Absorbance studies at different APTES percentages, equivalent to 0, 0.13, 0.18, 0.24, and $0.41 \mu\text{M}/\text{cm}^2$ (A), Fluorescence images (B), and Phase-atomic force microscopy (AFM) images (C).

To evaluate the detection of the immobilized protein BSA [$1\mu\text{g/mL}$], two kinds of capacitive structures were fabricated. The structures are based on buffer electrolyte PBS- MMA dielectric functionalized- semiconductor with and without BSA protein onto the dielectric surface. The capacitance-voltage (C-V) measurements were performed at 1kHz frequency at room temperature. This technique allows to know the response of surface states, surface accumulation and layer thickness beside others. Figure 4A shows the C-V characteristics of electrolyte-insulator-semiconductor for the case of (a) structure functionalized and (b) structure functionalized with immobilized protein BSA. The capacitance depends on bias voltage and have three regions of accumulation-depletion-inversion indicating the modulation of the carriers. The capacitance remains constant under forward bias, although above the threshold gradually increases to reach the maximum peak value and then decreases with a higher bias. This phenomena is explained by short-circuited parallel capacitance and it is based on the model RC circuit. As shown in Figure 4A a significant difference of peak heights of capacitance for (a) and (b) is observed. The capacitance ranges from 100nF to 280nF with low variability for different devices shown in Figure 4B. Confocal and interferometry images are shown in Figure 4C with (a) functionalization and (b) with immobilized protein structures. Surface of immobilized protein shows a higher roughness comparatively to the functionalized. The high scale values compared to AFM images ($1\times 1\mu\text{m}^2$) is due to large area ($600\times 400\mu\text{m}^2$) taken by the confocal.

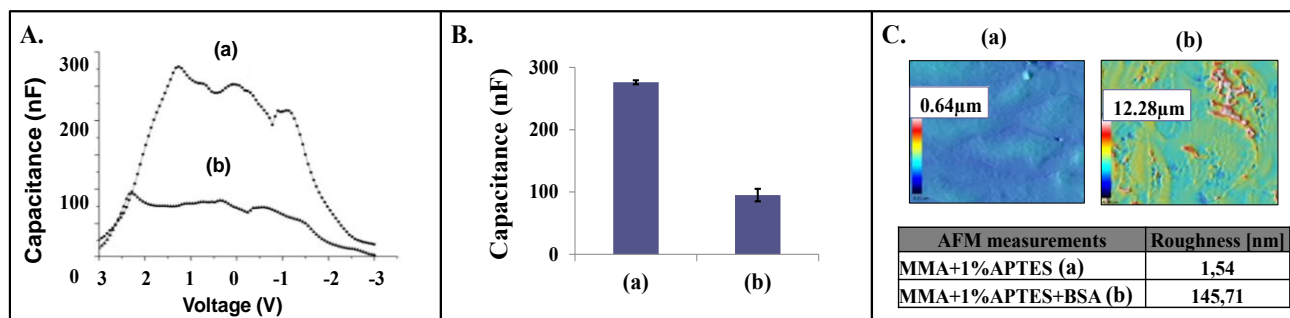


Figure 4. Capacitance-voltage with electrolyte (PBS) onto dielectric-semiconductive-conductive structure functionalized with APTES 1% (a) and functionalized with immobilized protein BSA [$1\mu\text{g/mL}$](b); Characteristic curves (A), repeatability with different devices (B), and confocal images with functionalization and with immobilized protein (C).

CONCLUSIONS

An all integrated and functional BioFET by using organic materials mostly deposited by inkjet technology and spin-coating was designed and fabricated. Characterizations of the deposited layers by using SEM and profilometry were performed. Dielectric rupture evaluation at different thicknesses (one and two layers of MMA dielectric layer) was also performed. MMA surface functionalization (with interest for future biological applications) study through colorimetric assay to determine the quantity of amine groups onto FET surface, fluorescence measurements and AFM images to confirm the selective adhesion of proteins onto BioFET surface were also carried out. Detection of the immobilized protein BSA was performed by means of C-V measurement. Moreover, we present the repeatability with different devices. Finally, confocal and interferometry images was undertaken to assess the roughness of functionalized and immobilized protein structures.

REFERENCES:

- [1] M. Singh, H. M. Haverinen, P. Dhagat, and G. E. Jabbour, *Inkjet printing-process and its applications*, Advanced materials, 22, 673 (2010).
- [2] Y. Wen, Y. Liu, Y. Guo, G. Yu, and W. Hu, *Experimental Techniques for the Fabrication and Characterization of Organic Thin Films for Field-Effect Transistors*, Chemical Reviews, 111(5), 3358 (2011).
- [3] G. C. Jensen, C. E. Krause, G. A. Sotzingab and J. F. Rusling, *Inkjet-printed gold nanoparticle electrochemical arrays on plastic. Application to immunodetection of a cancer biomarker protein*, Phys. Chem. Chem. Phys., 13, 4888 (2011).
- [4] E. Tekin, P. J. Smith, and U. Schubert, Inkjet printing as a deposition and patterning tool for polymers and inorganic particles, *Soft Mater.*, 4, 703 (2008).
- [5] L. Tang and N. Y. Lee, *A facile route for irreversible bonding of plastic-PDMS hybrid microdevices at room temperature*, Lab on a chip, 10, 1274 (2010).

CONTACT:

*arben.merkoci@icn.cat

We acknowledge MICINN (Madrid) for the project MAT2011-25870 and the E.U.'s support under FP7 contract number 246513 "NADINE".

This work is also partly supported by the Spanish Ministry MICINN project ASPEC (TEC2011-29800-C03-01) and the Catalan Government Grant Agency Ref. 2009SGR700.

ANNEX 2

Articles in preparation

M. Medina-Sánchez, S. Miserere, and A. Merkoçi. “Design and fabrication of a recycling flow micro-system for immunoassay based on quantum dots as electrochemical labels”. Technical communication.

M. Medina-Sánchez, C. Mayorga-Martínez, Y. Honda, T. Watanabe, T. A. Ivandini, Y. Einaga and A. Merkoçi. “On-chip sensitive electrochemical analysis of pesticides by magneto-immunoassay strategy with boron-doped diamond electrode modified with platinum nanoparticles”.

C. Martínez-Domingo, M. Medina-Sánchez, A. Alcalde-Aragonés, J. Carrabina, H. L. Gomes, A. Merkoçi and E. Ramon. “Material characterization and electrochemical performance for inkjet printed organic ISFET-based biosensor”.

M. Medina-Sánchez, E. Ramon, A. Alcalde-Aragonés, S. Miserere, C. Martínez-domingo, J. Carrabina, and A. Merkoçi. “Double ate inkjet Bio-OTFT transistor for label-free protein detection”.

Articles in collaboration

C. Parolo, M. Medina-Sánchez, H. Montón, A. de la Escosura and A. Merkoçi. “Paper-based electrodes for nanoparticles detection”. *Part. Part. Syst. Charact.* **2013**, 30, 662–666.

“Simple paper architecture modifications lead to enhanced sensitivity in nanoparticle based lateral flow immunoassay”, C. Parolo, M. Medina-Sánchez, A. de la Escosura and A. Merkoçi, *Lab Chip*, 2013, 13, 386-390.

“Nano/micromotor Enhanced Microarray Technology for Protein Detection”, E. Morales-Nárvaez, Maria Guix, Mariana Medina-Sánchez, C. Mayorga-Ramírez. *Submitted*, **2013**.

Simple paper architecture modifications lead to enhanced sensitivity in nanoparticle based lateral flow immunoassay†

Cite this: *Lab Chip*, 2013, 13, 386

Claudio Parolo,^a Mariana Medina-Sánchez,^a Alfredo de la Escosura-Muñiz^a and Arben Merkoçi^{*ab}

Received 11th October 2012,
Accepted 25th October 2012

DOI: 10.1039/c2lc41144j

www.rsc.org/loc

Lateral flow immunoassays (LFIA) are ideal biosensors to detect proteins, but their lack of sensitivity hinders their extensive use. We report a strategy that yields up to an 8-fold improvement in the sensitivity of a gold nanoparticles-based LFIA by changing the sizes of the pads. Theoretical flow simulations of the developed LFIA architectures are in accordance with the experimental results.

Introduction

Sensitive methods for the detection of proteins are of tremendous interest in everyday diagnostics, since many proteins are biomarkers of diseases.¹ Early detection of such biomarkers could allow treatment to start in the early stages of a disease, making it possible to save many lives. This is particularly important in third world countries, where advanced and expensive technologies are unavailable to most people.^{2,3} The same situation can be found in remote or dangerous regions or on battlefields, where the conditions do not allow the use of complicated devices and trained personnel cannot be present. For these reasons, it is of extreme importance to develop biosensors which fulfil the requirements of an ASSURED biosensor:⁴ affordable, sensitive, specific, user-friendly, rapid and robust, equipment free and deliverable to end-users.

Lateral flow immunoassays (LFIA) can be considered as biosensors which fit the definition of ASSURED technology. Since the first pregnancy test was sold in the mid-1970s, LFIAs have gained much more importance in the field of biosensing.⁵ However, some limitations have prevented their wide adoption by other fields, where quantitative analysis together with better sensitivity are required. In order to answer these demands, the integration of several nanomaterials into paper based biosensors has already been investigated.^{6,7} Taking advantage of the outstanding properties of nanometer-scale materials, it is possible to improve the performance of the biosensors.^{8–11} Examples of nanomaterials used in lateral flow assays are gold nanoparticles (AuNPs),^{12–15} quantum dots,^{16,17}

carbon nanotubes,¹⁸ magnetic nanoparticles,^{19,20} and liposomes,^{21,2} amongst others.

In this article, we show both theoretically and experimentally how simple changes in the architecture of an AuNP based LFIA, such as the width of the sample and conjugation pads, can be translated into an increase in sensitivity and an improved detection limit for this analytical device.

Materials and methods

Chemicals and equipment

All the materials used for the production of the strips were purchased from Millipore (Billerica MA 08128, USA): sample and absorbent pads (CFSP001700), conjugation pad (GF00080000), detection pad (SHF2400425) and backing card (HF000MC100). The membranes were characterized using Scanning Electron Microscopy (SEM) (ZEISS MERLIN FE-SEM). Human IgG whole molecule (HIgG) (I2511), antibody anti-human IgG (α HIgG) whole molecule (produced in goat; I1886), antibody anti-human IgG γ chain specific biotinylated (produced in goat; B1140) and all the chemical reagents (analytical grade) used for the preparation of AuNPs and buffer solutions were purchased from Sigma Aldrich (Spain). Anti-goat IgG (α GIgG) (produced in chicken; ab86245) was purchased from Abcam (UK). The stirrer used was a TS-100 Thermo shaker (BioSan, Latvia). A thermostatic centrifuge (Sigma 2-16 PK, Fisher Bioblock Scientific, France) was used to purify the AuNP-antibody conjugates. An IsoFlow reagent dispensing system (Imagene Technology, USA) was used to dispense the detection and control lines. A strip reader (COZART, SpinReact, UK) was used for quantitative measurements. A guillotine (Dahle 533, Germany) was used to cut the strips. mQ water, produced using a Milli-Q system (>18.2 M Ω cm⁻¹) purchased from Millipore (Sweden), was used for the preparation of all solutions.

^aNanobioelectronics & Biosensors Group, Institut Català de Nanotecnologia, CIN2 (ICN-CSIC), Campus UAB, Barcelona, Spain

^bICREA, Barcelona, Spain. E-mail: arben.merkoci@icn.cat

† Electronic supplementary information (ESI) available. See DOI: 10.1039/c2lc41144j

The mathematical simulations were done using the chemical reaction engineering module of Comsol Multiphysics 3.4 software, taking advantage of the equations of transport in porous media.

Preparation and modification of gold nanoparticles

AuNPs of 20.99 ± 2.72 nm in diameter were synthesized according to the citrate reduction of HAuCl_4 (as pioneered by Turkevich *et al.*²²); details of the synthesis can be found in the ESI† together with the experimental procedure for the functionalization of AuNPs with αHIgG γ chain specific. The AuNPs modified with antibodies were concentrated 5 times in 2 mM borate buffer pH 7.4 containing 10% of sucrose after a centrifugation step.

Preparation of LFIA strips

The sample pad was pre-treated by dipping it into 10 mM PBS buffer pH 7.4, containing 5% BSA and 0.05% Tween20 and then drying it for 30 min at 60 °C. The conjugation pad was dipped into the AuNP solution and then dried for 1 h under vacuum. The control and the detection lines were obtained by dispensing αHIgG whole molecule and αGIgG respectively onto the detection pad. The antibody solutions (1 mg mL^{-1} in 10 mM phosphate buffer pH 7.4) were dispensed at a rate of $1 \mu\text{L cm}^{-1}$ using an IsoFlow reagent dispensing system. The pad was then dried at 37 °C for 30 min. After that, the different pads were laminated on the backing card in the following order: first, the detection pad, then the absorbent pad at the end of the backing card and overlapping the detection pad, next, the conjugation pad overlapping the detection pad and finally the sample pad on the beginning of the backing card and overlapping the conjugation pad (see Fig. 1A). All of the overlaps were around 1 mm.

After lamination, the strips were cut using a guillotine to define the external edges and then with a manual cutter to define the internal ones. In order to study the effects of the sample and conjugation pad sizes, two different setups were used: one where only the sample pad size was changed and another where both the sample and the conjugation pad sizes were changed. In both cases the surface area studied was $1 \times$, $2 \times$ and $3 \times$ the original one.

Assay procedure

For the 1X, 2X and 3X strip sizes, the assays were performed by pipetting 200, 400 and 600 μL of the HIgG solution respectively onto the bottom of the sample pad. A blank and three different concentrations of HIgG were studied: 6, 60 and 600 ng mL^{-1} in 10 mM PBS pH 7.4. The assay took around 10 min to develop the color of the lines and 10 min for the washing step, performed by pipetting the same amount of buffer onto the sample pad. The strip was finally cut to a uniform width of 8 mm in order to be read by the strip reader.

The assay follows an immunosandwich format: the αHIgG (γ -chain specific) antibodies, attached to the AuNPs, recognize the γ -chain of the HIgG of the sample. The AuNP- αHIgG (γ -chain specific)-HIgG conjugates are stopped by the αHIgG (whole molecule) antibodies which are fixed at the detection line. The stronger the red color of the AuNPs at the detection line, the higher the concentration of the analyte (HIgG)

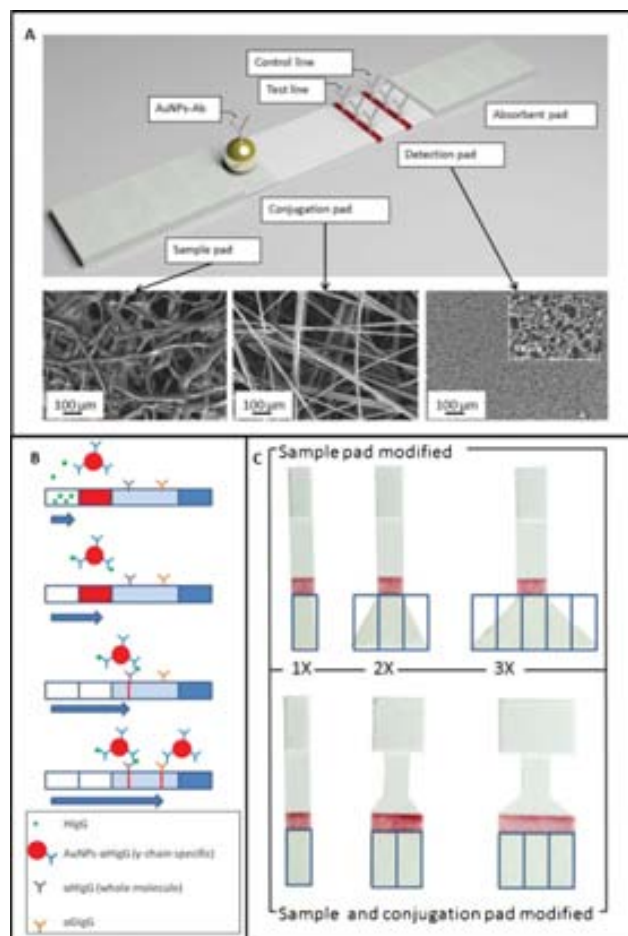


Fig. 1 (A) Scheme, not to scale, of a LFIA strip based on a sandwich format (above) and SEM images of the different pads (below). (B) Scheme of the formation of the immune-complex during the flow. (C) Different setups for LFIA: with only the sample pad 1X, 2X and 3X (above) and with both the conjugation and sample pads 1X, 2X and 3X (below).

present in the sample (Fig. 1B). Furthermore the αGIgG at the control line recognizes αHIgG (γ -chain specific) in the complexes which are not stopped at the detection line, confirming that the assay worked properly.

Mathematical simulations

The flow in strip membranes is usually described by the Navier–Stokes equation (pore-free region) and the Brinkman equations (porous region). The most common way to deal with pore-free and porous media flow in a system is to couple Darcy's law, which does not account for viscous effects, with the Navier–Stokes equations. However, depending on the pore size distribution of the porous media and the fluid's properties, it is not always appropriate to neglect viscous effects. The Brinkman equations account for momentum transport through viscous effects and through pressure gradients in porous media, and can be considered an extension of Darcy's law, which is a derived constitutive equation that describes the flow of a fluid through a porous medium (see eqn (1)).²³

$$Q = \frac{kA}{\mu} \left(\frac{dP}{dL} \right) \quad (1)$$

where Q is the flow rate (in units of volume per time unit), k is the relative permeability (typically in millidarcys), A is the cross sectional area (in square meters), μ is the viscosity of the fluid (in centipoises), L is the length of the porous media (in meters) and dP/dL is the pressure change per unit length. The constants for the different pads were calculated empirically measuring the volume of water absorbed by each pad. In this way it was possible to estimate the porosity and the permeability of the different pads (see ESI†).

The initial conditions defined for the simulation were: porosity and permeability of the membranes (empirically calculated, as detailed at the ESI†) and the viscosity and density of the fluid (water). On the other hand, for the boundary conditions the initial velocity was calculated from the volume of the liquid introduced into the membrane (200, 400, and 600 μL for the 1X, 2X and 3X strips respectively), the cross sectional area and the time necessary to absorb the respective volume. So for the 1X, 2X and 3X strips, the velocities were 1.47×10^{-3} , 2.94×10^{-3} and $4.41 \times 10^{-3} \text{ m s}^{-1}$ respectively.

Results and discussion

Effect of the architecture of the sample pad

A scheme of the LFIA used for the detection of HlgG as a model analyte is shown in Fig. 1B. Firstly, the effect of changing the sample pad size on the sensitivity of the LFIA was evaluated. The sample pads were designed to have a trapezoid shape to facilitate the flow. In order to obtain the sample pads with areas 2 and 3 times larger, the shorter base of the trapezoid (the one in contact with the conjugation pad) was fixed at 8 mm wide, whereas the longer base was increased to 24 mm and 40 mm respectively, as detailed in Fig. 1C. The strip reader outputs % values corresponding to the intensity of the lines: the weaker the intensity of the line, the higher the % value. The blank of each strip was subtracted from the results obtained in order to compensate for possible non-specific interactions.

In Fig. 2A it is possible to see how the strips looked following an assay with 60 ng mL^{-1} of HlgG. There are no clear differences in sensitivity for the different geometries used. In fact as shown in Fig. 2B there are two opposing effects that influenced the assay: the amount of analyte and the speed of the flow. Using bigger sample pads it is possible to use a greater volume of sample, and consequently more analyte is available, but this induces an increase in the speed of the flow, which reduces the time that the AuNP labels have to bind the analyte. The flow is also faster in the detection pad, decreasing the time to recognize the immuno-complexes formed by the antibodies of the test and control lines. As represented by the arrows in the figure, in the 1X format the AuNP speed is low giving enough time to have good recognition of the analyte, but the analyte amount is not high. The 2X format has a higher

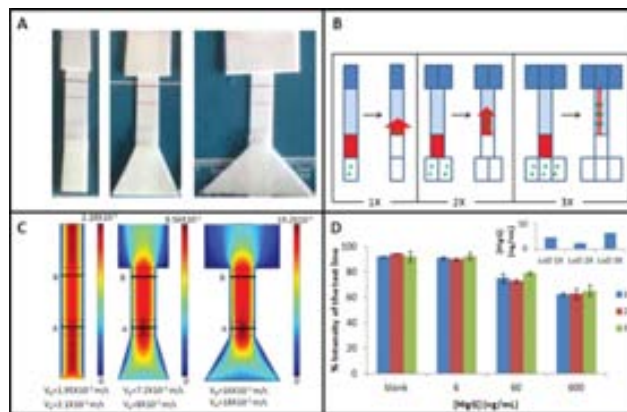


Fig. 2 (A) Photos of LFIA with different sample pad architectures for 60 ng mL^{-1} HlgG. (B) Scheme of the two opposite effects: the amount of analyte vs. the speed of the flow for the LFIA using a bigger sample pad. The red arrows represent the speed of the AuNPs in the flow and the green point stated for the analyte. (C) Results of the flow speed simulations for sample pads with different sizes. (D) Effect of the relative size of the sample pad on the quantitative measurement of different HlgG concentrations and the corresponding LODs obtained (inset).

flow speed than the 1X but is still not fast enough to compromise the interaction between the antibodies and the analyte; furthermore the amount of analyte is larger, increasing the possibility of recognition by the AuNPs. Finally, in the 3X format the flow is very fast, not giving enough time for the AuNP complexes to interact with the antigen, consequently decreasing the sensitivity of the assay even though the quantity of analyte is larger.

These phenomena were also evaluated using mathematical simulations (see Fig. 2C). For each geometry the flow speed was calculated at the level of the conjugation pad and the test line. For the 1X geometry, the speeds were calculated to be 2.1×10^{-3} and $1.95 \times 10^{-3} \text{ m s}^{-1}$ respectively. For the 2X, they were 8×10^{-3} and $7.2 \times 10^{-3} \text{ m s}^{-1}$ and for the 3X they were 18×10^{-3} and $16 \times 10^{-3} \text{ m s}^{-1}$.

The graph in Fig. 2D shows the results obtained with the strip reader. They are in accordance with the theoretical calculations. In fact, there is no clear positive effect on the sensitivity of the LFIA when changing only the sample pad size. For the strips with a 2 times bigger sample pad, it was possible to observe a slight increase in the sensitivity of the assay, probably due to the higher volume of sample, which implies a higher amount of analyte. However, the results obtained using the strips with the 3 times larger sample pad show that the sensitivity of the assay is lower than with the sample pad of the original size. This can be explained considering that in the 3X configuration, the flow has a speed of approximately one order of magnitude higher than the 1X. Furthermore, the AuNPs are re-suspended by a fixed amount of liquid and they are dragged by it. This means that only the analyte present in this volume of liquid can be recognized by the AuNP labels, showing that use of an excess sample volume is not useful.

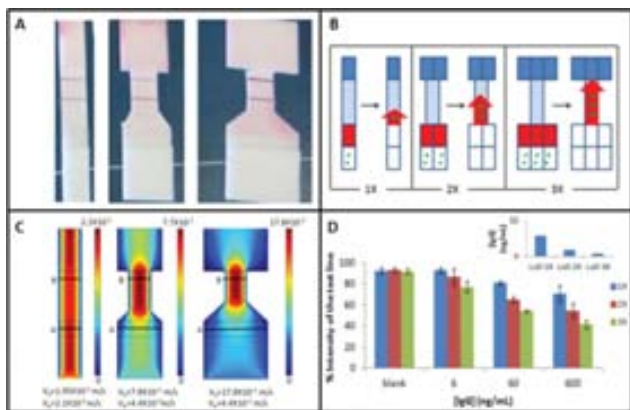


Fig. 3 (A) Photos of LFIA with different sample and conjugation pad architectures after 60 ng mL^{-1} HIgG assays. (B) Scheme of the two opposite effects: the amount of analyte vs. the speed of the flow for the LFIA using bigger sample and conjugation pads. The red arrows represent the speed of the AuNPs in the flow and the green point stated for the analyte. (C) Results of the flow speed simulations for sample and conjugation pads with different sizes. (D) Effect of the relative sizes of the sample and conjugation pads on quantitative measurements for different HIgG concentrations and the corresponding LODs obtained (inset).

Effect of different architectures for both sample and conjugation pad

In the second study, both the conjugation and the sample pads were changed. Here, the shapes of the sample and conjugation pads remain rectangular, so they were simply made 2 and 3 times bigger (Fig. 1C). Fig. 3A shows how the strips look after an assay using 60 ng mL^{-1} of HIgG. An increase in the intensity of the band is evident with increasing the sizes of sample and conjugation pads. In fact, as shown in Fig. 3B, using these configurations, the flow speed in the conjugation pad does not change significantly, giving enough time for the AuNPs labels to recognize the analyte. In addition, using a larger volume meant that there were more analyte molecules to be detected and since the conjugation pad was bigger, more AuNPs could be used as labels. This enabled the formation of a higher number of immuno-complexes. When the flow passed to the detection pad, there was an increase in the flow speed, but this phenomenon was compensated by the larger number of labels, which recognized the analyte. This theory was confirmed by the mathematical simulations (Fig. 3C): for the conjugation pad, the speed values were of the same order: 2.1×10^{-3} , 4.4×10^{-3} and $4.4 \times 10^{-3} \text{ m s}^{-1}$ for 1X, 2X and 3X respectively. However for the detection pad, a large increase is observed when increasing the size, with values of 1.95×10^{-3} , 7.8×10^{-3} and $17.8 \times 10^{-3} \text{ m s}^{-1}$ respectively. The results obtained with the strip reader (Fig. 3D) confirmed all of the previous data, showing the limits of detection for the 1X, 2X and 3X strips to be 5.89, 1.83 and 0.7 ng mL^{-1} respectively. This means that a 3-fold increase in the width of the conjugation and sample pads gives an 8-fold improvement in the limit of quantification.

These results could be further improved by increasing the difference in width between the detection pad and the conjugation and sample pads. This can be achieved by making

the conjugation and sample pads wider and/or making the detection pad smaller. However, some drawbacks are envisaged: with bigger conjugation and sample pads, a greater volume of sample as well as a larger amount of label is required. Furthermore, smaller detection pads would not be compatible with the strip reader. Another point to be considered is the shape of the strips: longer strips would allow a softer pre-concentration, which would probably produce more reproducible results. This can also be achieved placing the detection line closer to the end of the detection pad.

Conclusions

We have demonstrated that very simple changes to the LFIA architecture, such as increasing the size of both the conjugation and the sample pads, can improve its performance in terms of the sensitivity of the assay. Flow speed simulations also corroborate the experimental results and represent useful tools in designing novel lateral flow architectures. The proposed designs can be easily applied to any type of LF strip without changing the fabrication method; moreover it is simple and cheap, enabling its use in point-of-care applications, even at the doctor's surgery or in undeveloped countries. Studies using a different method of detection, based on the use of a camera, and the use of a wax printer, in order to define better the shape of the LFIA, have already started in our lab and they will enable further decreases in the size of the detection pad, allowing greater improvements in the sensitivity of the device.

Acknowledgements

We acknowledge MEC (Madrid) for the project MAT2011-25870, the EU's support under FP7 contract number 246513 "NADINE" and the NATO Science for Peace and Security Programme's support under the project Sfp 983807.

References

- 1 D. Mabey, R. W. Peeling, A. Ustianowski and M. D. Perkins, *Nat. Rev. Microbiol.*, 2004, **2**, 231–240.
- 2 P. Yager, T. Edwards, E. Fu, K. Helton, K. Nelson, M. R. Tam and B. H. Weigl, *Nature*, 2006, **442**, 412–418.
- 3 A. K. Ellerbee, S. T. Phillips, A. C. Siegel, K. a Mirica, A. W. Martinez, P. Striehl, N. Jain, M. Prentiss and G. M. Whitesides, *Anal. Chem.*, 2009, **81**, 8447–8452.
- 4 R. W. Peeling, K. K. Holmes, D. Mabey and A. Ronald, *Sex. Transm. Infect.*, 2006, **82**, v1–6.
- 5 G. a Posthuma-Trumpie, J. Korf and A. van Amerongen, *Anal. Bioanal. Chem.*, 2009, **393**, 569–582.
- 6 S. Song, Y. Qin, Y. He, Q. Huang, C. Fan and H.-Y. Chen, *Chem. Soc. Rev.*, 2010, **39**, 4234–4243.
- 7 C. Parolo and A. Merkoçi, *Chem. Soc. Rev.*, 2013, DOI: 10.1039/c2cs35255a.

- 8 G. Aragay, J. Pons and A. Merkoçi, *Chem. Rev.*, 2011, **111**, 3433–3458.
- 9 M. Perfézou, A. Turner and A. Merkoçi, *Chem. Soc. Rev.*, 2012, **41**, 2606–2622.
- 10 A. de la Escosura-Muñiz, C. Parolo and A. Merkoçi, *Mater. Today*, 2010, **13**, 24–34.
- 11 M. Medina-Sánchez, S. Miserere and A. Merkoçi, *Lab Chip*, 2012, **12**, 2000–2005.
- 12 Y. He, S. Zhang, X. Zhang, M. Baloda, A. S. Gurung, H. Xu, X. Zhang and G. Liu, *Biosens. Bioelectron.*, 2011, **26**, 2018–2024.
- 13 S. Lou, J.-Y. Ye, K.-Q. Li and A. Wu, *Analyst*, 2012, **137**, 1174–1181.
- 14 W. Zhao, M. M. Ali, S. D. Aguirre, M. A. Brook and Y Li, *Anal. Chem.*, 2008, **80**, 8431–8437.
- 15 C. Parolo, A. de la Escosura-Muñiz and A. Merkoçi, *Biosens. Bioelectron.*, 2013, **40**, 412–416.
- 16 X. Zhu, L. Chen, P. Shen, J. Jia, D. Zhang and L. Yang, *J. Agric. Food Chem.*, 2011, **59**, 2184–2189.
- 17 Z. Zou, D. Du, J. Wang, J. N. Smith, C. Timchalk, Y. Li and Y. Lin, *Anal. Chem.*, 2010, **82**, 5125–5133.
- 18 A. Abera and J.-W. Choi, *Anal. Methods*, 2010, **2**, 1819–1822.
- 19 S. Puertas, M. Moros, R. Fernández-Pacheco, M. R. Ibarra, V. Grazú and J. M. de la Fuente, *J. Phys. D: Appl. Phys.*, 2010, **43**, 474012.
- 20 D. Tang, J. C. Saucedo, Z. Lin, S. Ott, E. Basova, I. Goryacheva, S. Biselli, J. Lin, R. Niessner and D. Knopp, *Biosens. Bioelectron.*, 2009, **25**, 514–518.
- 21 S. Shukla, H. KimLeem and M. Kim, *Anal. Bioanal. Chem.*, 2011, **401**, 2581–2590.
- 22 J. Turkevich, J. Stevenson and P. Hillier, *Discuss. Faraday Soc.*, 1951, **11**, 55–75.
- 23 S. Chen and G. D. Doolen, *Annu. Rev. Fluid Mech.*, 1998, **30**, 329–364.

Paper-Based Electrodes for Nanoparticle Detection

Claudio Parolo, Mariana Medina-Sánchez, Helena Montón, Alfredo de la Escosura-Muñiz, and Arben Merkoçi*

In general, the success of a sensor depends not only on the efficient recognition of the analyte, but it is also affected by the detection method and the platform used.^[1] In this context, the development of sensitive, robust, and cheap electrodes is essential for the progress of electrochemical based (bio)sensors. Many different kinds of electrodes, used as a sensing platform, are reported: glassy carbon electrodes, gold electrodes, micro-electrodes, screen-printed carbon electrodes (SPCEs), etc.^[2] In our opinion, the integration of SPCEs in a point of care platform, such as lateral flow sensor, is easier, and the resulting device easy to be used.^[3,45] In addition, due to their small sizes, low cost, fast, and versatile fabrication, using screen printing technology, the resulting device is cheaper in comparison with other types of electrodes, such as those based on sputtering or other micro and nanofabrication technologies. SPCEs are usually printed on polymeric materials, such as polyester, due to overall the mechanical properties of this platform, beside their low cost. These materials have two main drawbacks: they are not safely disposable and the sample to be analyzed needs pretreatments (i.e., incubations, washings, labeling etc.) outside the electrode. These problems can be overcome by the use of paper as a platform for the production of SPCEs, instead of plastic materials.^[6,8] In fact, paper electrodes can be safely disposed by burning them. Their inherent microfluidic capability combined with an easy insertion of sample pretreatment pads including electrochemical detectors makes these devices the best candidate in terms of full integration of all the steps required for the detection of a sample.^[9,10]

Paper-based nanobiosensors are showing to be the best sensing platforms for point of care applications.^[11] They combine the advantages of the paper with those of nanomaterials, in general and especially of nanoparticles. The paper-based nano-biosensors, developed so far, are based mainly on optical detection of gold nanoparticles (AuNPs) plasmon signal.^[12] Although such detection technologies are successfully applied for DNA,^[13] proteins,^[14] or cells,^[15] there is still a big demand to improve the sensitivity and decrease the detection limits. Given the simplicity and robustness of electrochemical detection, its integration with lateral flow seems to be the best choice. The

efforts to achieve such integration are usually limited to a simple mechanical approximation of electrochemical detector with lateral flow paper platform. In fact, it is possible to develop paper-based sensors (such as lateral flow assays, microfluidic paper-based devices, etc.), where the paper SPCEs can be easily integrated and the entire device can be easily burned after use.^[16] Furthermore, the sensitivity of such electrodes is generally expected to be higher than the others, because the surfactants of the inks can be absorbed by the paper, making the conductive material more exposed. In addition, they have a bigger electroactive surface available, since the matrix of the paper has a porous 3D structure.^[17] To clarify such phenomena, characterizations of paper SPCEs and polyester SPCEs by scanning electron microscopy (SEM), confocal laser scanning microscopy (CLSM), and the studies of their hydrophobicity and porosity are firstly discussed. Then, the results obtained using paper SPCEs are compared with those obtained with polyester SPCEs for the detection of AuNPs and CdSe@ZnS quantum dots (QDs) with different electrochemical techniques. These very sensitive paper SPCEs are produced by combining screen printing, wax printing, and plasma cleaner.

First, we characterized the surface of the electrodes by SEM. Figure 1A,B shows the images of the paper and polyester platforms before printing any ink. A higher porosity of the paper can be clearly observed. In Figure 1C,D, it is possible to see the carbon-based working electrodes (WE) of polyester SPCE and paper SPCE respectively. In the paper SPCE, it is observed that in addition to the higher porosity of the substrate, the carbon ink is also printed on a microporous like pattern of around 185 μm , which apparently increases the roughness of the WE and, in addition, may allow free space for an easy penetration of the sample. Such structures, in addition to the porous nature of the paper, make the WE having an enhanced electroactive surface easily accessible by the analyte. These ink-printed structures are observed only after printing (they are not present in Figure 1B) and are due to the nitrocellulose properties. We suggest that during the screen-printing process, when the ink is squeezed out of the mesh, the surfactants are quickly absorbed by the paper, making the carbon material accumulated into certain areas ordered according to the micropore distribution in the used mask. Such ordered carbon areas cannot be observed when the same ink is printed onto polyester, due to the fact that the ink, once is getting out from the mesh, keeps containing the same amount of solvent and consequently the same fluidity, causing an almost uniform coverage with carbon. As expected, the printed WE onto the polyester surface (SPCE) is very flat compared with the one of paper SPCE. This difference in the WE structure is probably one of the most important factors in the better electrochemical behavior of paper SPCEs

C. Parolo, M. Medina-Sánchez, H. Montón,
Dr. A. de la Escosura-Muñiz, Prof. A. Merkoçi
Nanobioelectronics & Biosensors Group
Institut Català de Nanotecnologia, CIN2 (ICN-CSIC)
CampusUA B, Barcelona, Spain
E-mail: arben.merkoci@icn.cat
Prof. A. Merkoçi
ICREA, Barcelona, Spain



DOI: 10.1002/ppsc.201200124

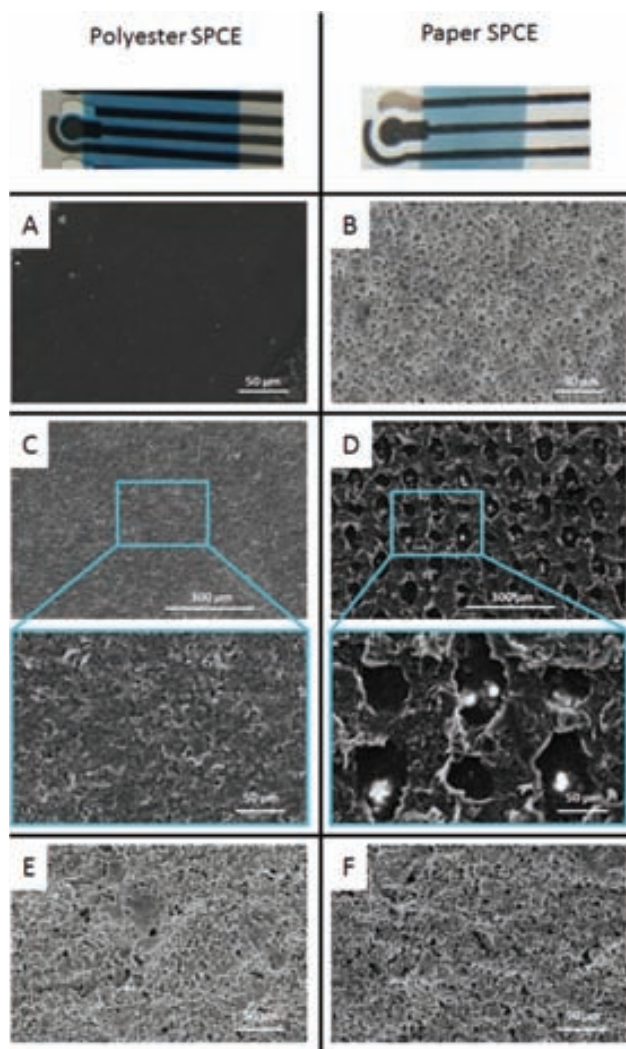


Figure 1. Microscopy images of polyester and paper-based SPCEs and SEM characterizations of: A) polyester sheet, B) nitrocellulose membrane (paper), C) carbon ink printed onto polyester, D) on paper at two different magnifications, E) silver ink printed onto polyester, and F) on paper.

compared with the polyester ones, as will be shown below. In the case of the silver layers, no observable differences are noticed between polyester and paper, as shown in Figure 1E,F, due to the different behavior (more fluidity) in comparison with the carbon ink.

CLSM $\times 10$ – 12 Mas used to confirm such observations by scanning the depth of the electrode along the z-axis using the reflection mode and z-stacks (Figure 2A,B). The periodic pattern in the WE of the paper SPCE and the much more homogeneous surface of the WE in polyester are evidenced in the plan view. Moreover, in order to see in depth the X and Y profiles of the WEs, a cross-section of the z-stack was performed (the dashed cross represents the exact site where the virtual cuts are performed). It is possible to see the periodic changes in the surface both in the X and Y profiles of the paper SPCE, while in the polyester one no remarkable changes of the surface can be observed.

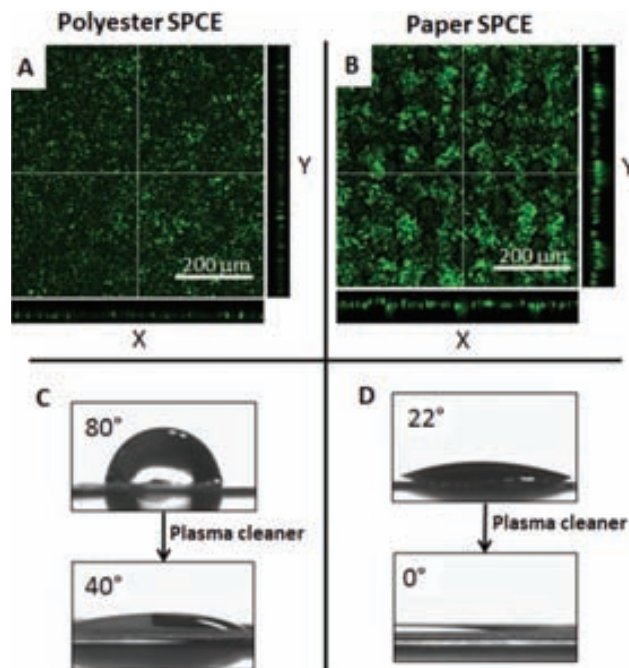


Figure 2. CLSM and hydrophilicity characterizations of the carbon WE printed onto polyester (left column) and on paper (right column). A,B) CLSM plan views and cross-section of the z-stack and C,D) contact angle study before (up) and after (down) plasma treatment.

The study of the hydrophilicity, of both carbon-printed surfaces, was also performed after plasma exposition (see Figure S2, Supporting Information). This plasma treatment is applied in order to introduce hydroxyl groups. The presence of such groups increases the hydrophilicity of the surface, causing a better and faster entrance of the sample into the porous surface of the WE, and increasing the contact area between the WE and the analyte. The increment in the humectability was confirmed by contact angle studies, as shown in Figure 2C,D. As expected, the untreated polyester is more hydrophobic than the untreated paper, as shown by the resulting contact angles of $80 \pm 0.5^\circ$ and $22 \pm 0.5^\circ$, respectively. After the plasma treatment (1 min of exposure), the contact angle for the polyester decreased to $40 \pm 0.5^\circ$, whereas the paper value could not be measured, because the liquid was immediately absorbed. The obtained results indicate that the plasma treatment is effective in making the paper SPCE more hydrophilic, enabling its application in water medium sensing (see Figure S2, Supporting Information).

The improved characteristics of the paper SPCEs was evaluated for the electrochemical detection of gold nanoparticles (AuNPs) and CdSe@ZnS quantum dots (QDs), which are of great interest for further applications in bioassays, where these NPs will be used as electroactive labels. To obtain a better sensing performance, all the electrochemical measurements were performed using the electrodes treated with plasma. The detailed experimental conditions for the detection of each NPs are detailed in the Supporting Information.

In the case of the AuNPs, two different methods, previously optimized on polyester SPCEs for the detection of these

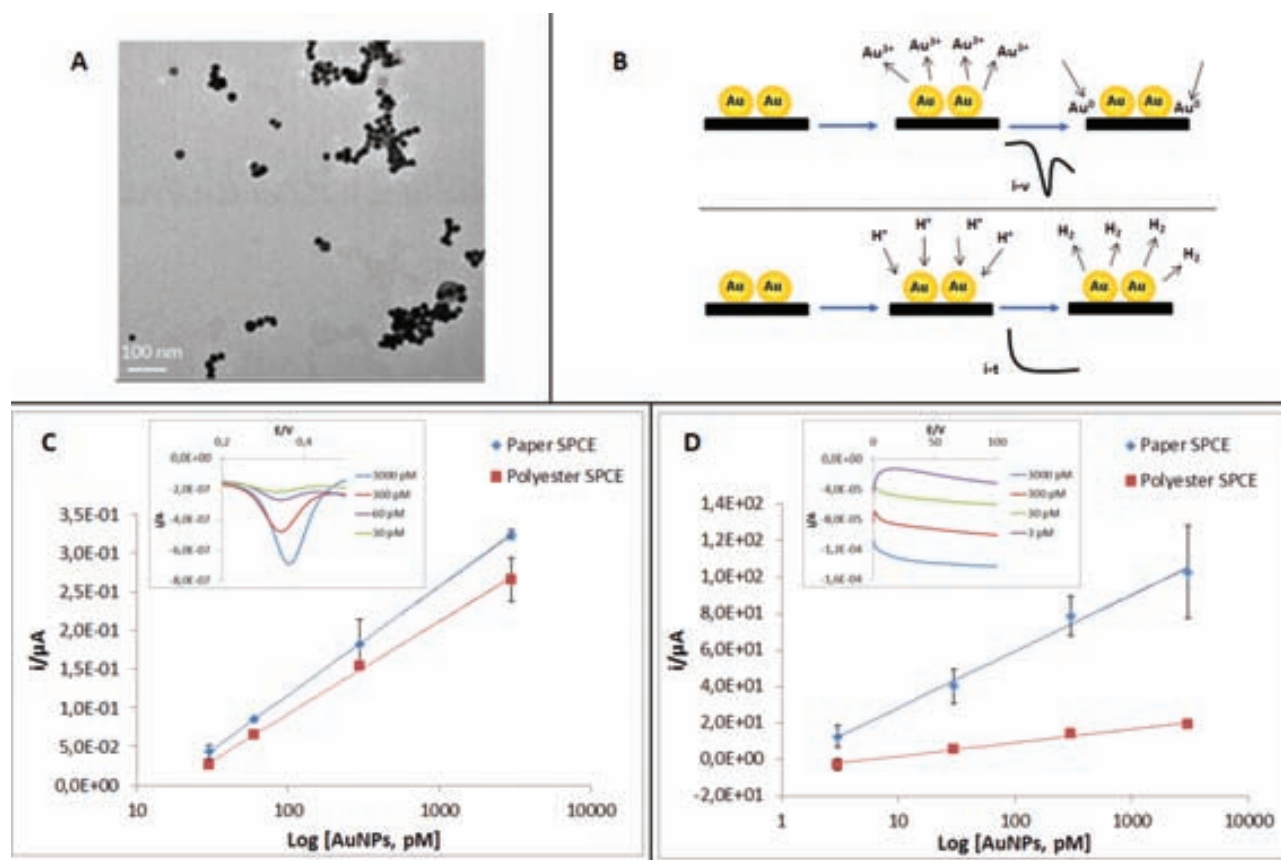


Figure 3. A) Transmission electron microscopy (TEM) images of AuNPs. B) Electrochemical principles for the detection of AuNPs: Direct voltammetric detection (top) and catalytic detection of AuNPs through the hydrogen evolution reaction (HER; bottom). C) Calibration curves of direct voltammetric detection of AuNPs, obtained measuring the peak values; in the inset representative signals obtained with paper SPCE at different concentration of AuNPs. D) Calibration curves of catalytic detection of AuNPs, obtained considering the current values at 100 s; in the inset representative signals obtained with paper SPCE at different concentration of AuNPs are shown.

NP labels in immunoassays, were tested with the two kinds of electrodes. Firstly, suspensions of 20 nm AuNPs of different concentrations were voltammetrically detected following a previously optimized method.^[18] It consists in the electrochemical oxidation of the Au(0) to AuCl_4^- , followed by the differential pulse voltammetric (DPV) reduction back to Au(0) (Figure 3B), which generates a peak of current directly related with the quantity of AuNPs. The results obtained, shown in Figure 3C, demonstrate that also with paper SPCEs was possible to directly detect AuNPs, obtaining sensitivity and reproducibility values of the same order of magnitude of polyester SPCEs, noticing even a slightly better sensitivity in the case of the paper. In particular, the limits of detection for paper SPCEs and polyester SPCEs were respectively 15×10^{-12} M and 25×10^{-12} M of AuNPs.

The second method tested was based on the hydrogen evolution reaction (HER) catalyzed by AuNPs and was followed chronoamperometrically. The value of the current registered at a 100 s is related with the quantity of AuNPs. This method leads to an efficient indirect detection of AuNPs by measuring the current produced during H_2 formation catalyzed by AuNPs (Figure 3D). This AuNP quantification technique is known to be more sensitive than the direct voltammetric detection and has been used in many biosensors ranging from protein^[19]

to cancer cell^[20,21] detections. The results show a clear increment in the signal using paper SPCEs. The limits of detection obtained were respectively 3×10^{-12} M and 24×10^{-12} M for paper SPCEs and polyester SPCEs. The bigger improvement obtained using paper instead of polyester, respect the direct detection of gold, can be related to the 3D structure of the WE, which allows an easier flow of protons toward the electrode area, pushing forward the H_2 evolution (hydrogen gas also escape faster through the generated micropores) reaction. This makes the paper SPCE an excellent platform to perform the whole catalytic cycles, with interest for an efficient AuNP quantification.

Finally, the last application of paper SPCEs was the direct voltammetric detection of CdSe@ZnS QDs in PBS buffer, without the need of a previous acidic dissolution of the NPs. This methodology has also been previously reported for QD detection on polyester SPCEs.^[22] It consists in the electrochemical reduction of the Zn(II), contained in the NP, to Zn(0) followed to a square wave voltammetric (SWV) oxidation back of the Zn(0) to Zn(II), which generates a peak of currents at -0.9 V, which is related with the quantity of these NPs (Figure 4B). The results showed a very good trend, reaching a limit of detection of 11×10^{-6} M of QDs in a PBS solution (Figure 4C) using paper SPCEs. In this experiment, the data obtained with polyester SPCE are

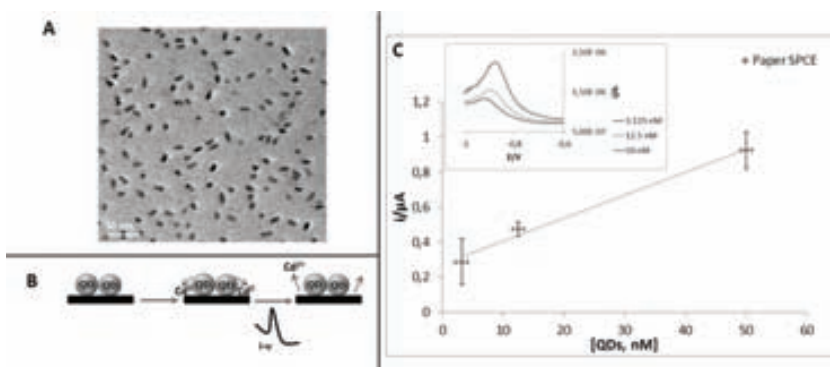


Figure 4. A) TEM images of CdSe@ZnS QDs. B) Electrochemical principle for the direct voltammetric detection of QDs. C) Calibration curve of direct voltammetric detection of QDs; in the inset representative signals obtained with paper SPCE at different concentration of QDs are shown. The response of polyester SPCE were not representative.

not shown, because such electrodes could not detect even the highest concentration of QDs evaluated.

In conclusion, we have developed very sensitive paper SPCEs by combining screen printing, wax printing, and plasma cleaner. This complete integrated paper-based SPCE shows a better response in comparison with state-of-the-art screen-printed platforms, such as polyester. We have also clarified such better response, due to the 3D structure of the electrode and the formation of microporous structures, which allowed a higher surface interaction between the nanoparticles and the WE. Furthermore, the use of plasma exposition makes the surface more hydrophilic. The detections of AuNPs and CdSe@ZnS QDs demonstrate that paper SPCEs can be used with a wide range of electrochemical techniques. Finally, the better electrochemical responses, compared with those obtained with polyester SPCE, make evident that the paper SPCE can be integrated in many biosensing platforms for several applications, where nanoparticles are used as labels either for DNA, protein, or even cell detection. In addition, fast and sensitive detection of electroactive nanoparticles with interest for environmental control can be done.

The developed paper-based sensor may improve, in a significant mode, the lateral flow-based devices, and opens the way to new real world applications of electrochemical sensing technology, which is still lacking from the separation between sample introduction, pretreatment, and incubations (immuno-reactions, DNA reactions) with detection. Having the electrochemical detector well integrated within paper microfluidics will further strengthen the efficiency of the resulting biosensing technologies. We envisage that, given the easy deposition of electrodes onto paper, combined with the flexibility and variability of paper platforms and wax printing, paper-based electrodes and sensors will be strong devices, with interest, not only in (bio)sensing, but also energy related applications,^{[23][25]} where efficient green solutions are always welcome.

Experimental Section

Paper SPCEs Fabrication: The nitrocellulose membrane HF240 was purchased from Millipore. A first insulating/hydrophobic layer of wax

was printed on it using a Xerox ColorQube 8570 wax printer (Xerox Corp., USA). Then, the membrane was heated at 150 °C for 30 s on a hot plate (VWR, USA). Finally, when the membrane was cooled to room temperature, the carbon ink and the Ag/AgCl ink were screen printed onto the paper. After each printing, the membrane was heated at 90 °C for 15 min.

Polyester SPCE Fabrication: On a polyester sheet, purchased by Mac Dermid Autotype, UK, three different layers were printed, in order: first the carbon ink, then the silver ink, and finally an insulating ink. For carbon and silver, the procedure was the same of the paper SPCEs, whereas the insulating ink was cured at 120 °C for 15 min.

Plasma Cleaner. All the electrodes were treated with plasma (from Harrick Plasma, E. U). First 3 min of vacuum were applied and then 1 min of plasma (30 W).

NPs Preparations: AuNPs of 20 nm of diameter were prepared according with the citrate reduction of HAuCl₄, method pioneered by Turkevich,^[26] as stated in the Supporting Information.

CdSe@ZnS QDs were purchased from (Invitrogen, USA).

Assay Procedure: The direct electrochemical detection of AuNPs was performed by placing 25 μL of the AuNPs solution on the working electrode area and leaving the AuNPs to adsorb during 2 min. After that, 25 μL of a HCl 0.2 M solution were added, covering the three electrodes area. A pre-concentration step to oxidize AuNPs to AuCl₄⁻ was performed at +1.25 V (vs Ag/AgCl) for 120 s in a non-stirred solution. Immediately after the electrochemical oxidation, DPV was performed by scanning from +1.25 V to 0.0 V (step potential 10 mV, modulation amplitude 50 mV, scan rate 33.5 mV s⁻¹, non-stirred solution), resulting in an analytical signal due to the reduction of AuCl₄⁻ at +0.45 V.

The chronoamperograms, of the electrocatalytic detection of AuNPs, were obtained placing a mixture of 25 μL of 2 M HCl and 25 μL of the AuNP solution (different concentrations) onto the surface of the electrodes and, subsequently, holding the working electrode at a potential of +1.35 V for 1 min and then a negative potential of -1.00 V for 100 s.

The direct voltammetric detection of CdSe/ZnS QDs were obtained placing a drop of 50 μL of the desired QD in PBS concentration was suspended on the surface of the electrode and a potential of -0.15 V was applied for 60 s (conditioning step). Later, in the accumulation step, a deposition potential of -1.5 V for 120 s was applied to promote the electrochemical reduction of Zn²⁺ ions contained in the shell structure of QD to Zn⁰. Then, the reduced zinc is oxidized back to zinc ions by SWV scanning from -1.5 V to -0.15 V (step potential 3 mV, modulation amplitude 30 mV and frequency 15 Hz), resulting in an analytical signal.

Supporting Information

Supporting Information is available from the Wiley Online Library or from the author.

Acknowledgements

M.M.-S. and H.M. contributed equally to this work. The authors acknowledge MEC (Madrid) for the project MAT2011-25870.

Received: November 12, 2012

Revised: April 7, 2013

Published online: June 5, 2013

- [1] A. de la Escosura-Muñiz, C. Parolo, A. Merkoçi, *Mater. Today* **2010**, 13, 24.
- [2] D. W. Kimmel, G. LeBlanc, M. E. Meschievitz, D. E. Cliffl, *Anal. Chem.* **2012**, 84, 685.
- [3] L. Ge, J. Yan, X. Song, M. Yan, S. Ge, J. Yu, *Biomaterials* **2012**, 33, 1024.
- [4] P. Wang, L. Ge, M. Yan, X. Song, S. Ge, J. Yu, *Sens. Bioelectron.* **2012**, 32, 238.
- [5] Z. Nie, C. A. Nijhuis, J. Gong, X. Chen, A. Kumachev, A. W. Martinez, M. Narovlyansky, G. M. Whitesides, *Lab Chip* **2010**, 10, 477.
- [6] W. Dungchai, O. Chailapakul, C. S. Henry, *Anal. Chem.* **2009**, 81, 5821.
- [7] R. F. Carvalhal, M. S. Kfoury, M. H. D. O. Piazzetta, A. L. Gobbi, L. T. Kubota, *Anal. Chem.* **2010**, 82, 1162.
- [8] D. Zang, L. Ge, M. Yan, X. Song, J. Yu, *Chem. Commun.* **2012**, 48, 4683.
- [9] S. Ge, L. Ge, M. Yan, X. Song, J. Yu, J. Huang, *Chem. Commun.* **2012**, 48, 9397.
- [10] X. Liu, M. Mwangi, X. Li, M. O'Brien, G. M. Whitesides, *Lab Chip* **2011**, 11, 2189.
- [11] C. Parolo, A. Merkoçi, *Chem. Soc. Rev.* **2013**, 42, 450.
- [12] K. Saha, S. S. Agasti, C. Kim, X. Li, V. M. Rotello, *Chem. Rev.* **2012**, 112, 2739.
- [13] P. Lie, J. Liu, Z. Fang, B. Dun, L. Zeng, *Chem. Commun.* **2012**, 48, 236.
- [14] C. Parolo, A. de la Escosura-Muñiz, A. Merkoçi, *Biosens. Bioelectron.* **2012**, 40, 412.
- [15] C.-Z. Li, K. Vandenberg, S. Prabhulkar, X. Zhu, L. Schnepfer, K. Methee, C. J. Rosser, E. Almeida, *Biosens. Bioelectron.* **2011**, 26, 4342.
- [16] Z. Nie, F. Deiss, X. Liu, O. Akbulut, G. M. Whitesides, *Lab Chip* **2010**, 10, 3163.
- [17] D. Zang, L. Ge, M. Yan, X. Song, J. Yu, *Chem. Commun.* **2012**, 4683.
- [18] A. de la Escosura-Muñiz, C. Parolo, F. Maran, A. Mekoçi, *Nanoscale* **2011**, 3, 3350.
- [19] M. Maltez-da Costa, A. de la Escosura-Muñiz, A. Merkoçi, *Electrochem. Commun.* **2010**, 12, 1501.
- [20] M. Maltez-da Costa, A. de la Escosura-Muñiz, C. Nogués, L. Barrios, E. Ibáñez, A. Merkoçi, *Nano Lett.* **2012**, 12, 4164.
- [21] M. Maltez-da Costa, A. de la Escosura-Muñiz, C. Nogués, L. Barrios, E. Ibáñez, A. Merkoçi, *Small* **2012**, 8, 3605.
- [22] M. Medina-Sánchez, S. Miserere, S. Marín, G. Aragay, A. Merkoçi, *Lab Chip* **2012**, 12, 2000.
- [23] N. K. Thom, K. Yeung, M. B. Pillion, S. T. Phillips, *Lab Chip* **2012**, 12, 1768.
- [24] L. Yuan, X. Xiao, T. Ding, J. Zhong, X. Zhang, Y. Shen, B. Hu, Y. Huang, J. Zhou, Z. L. Wang, *Angew. Chem. Int. Ed.* **2012**, 51, 4934.
- [25] L. Ge, P. Wang, S. Ge, N. Li, J. Yu, M. Yan, J. Huang, *Anal. Chem.* **2013**, 85, 3968.
- [26] J. Turkevich, P. C. Stevenson, P. Hillier, *Discuss. Faraday Soc.* **1951**, 11, 55.

ANNEX 3

1. Set-up for microperistaltic pump control (LABVIEW)

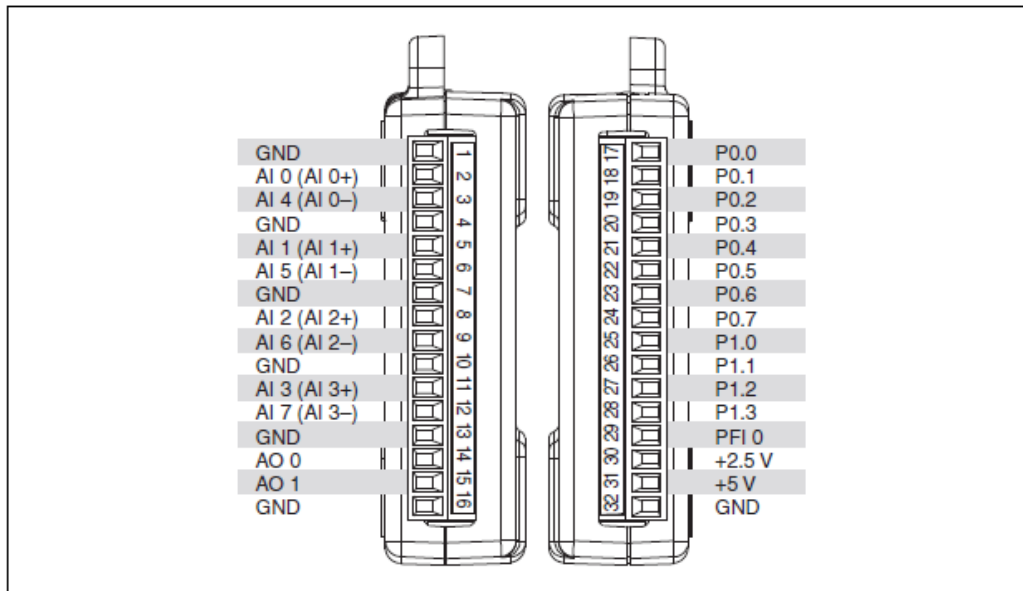
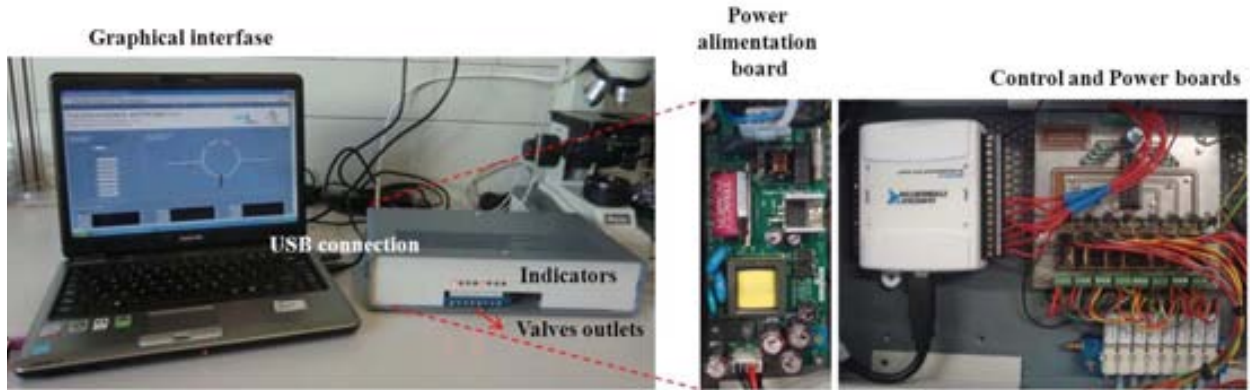
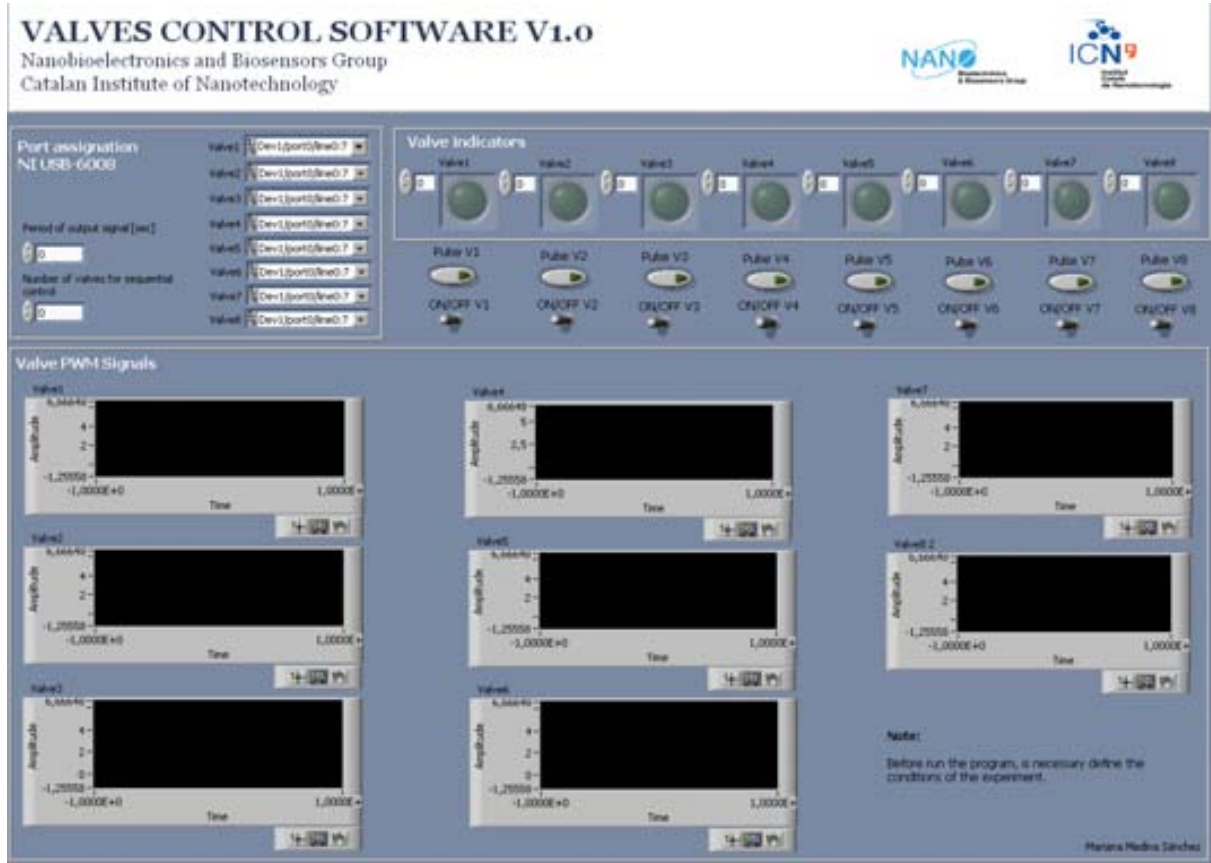


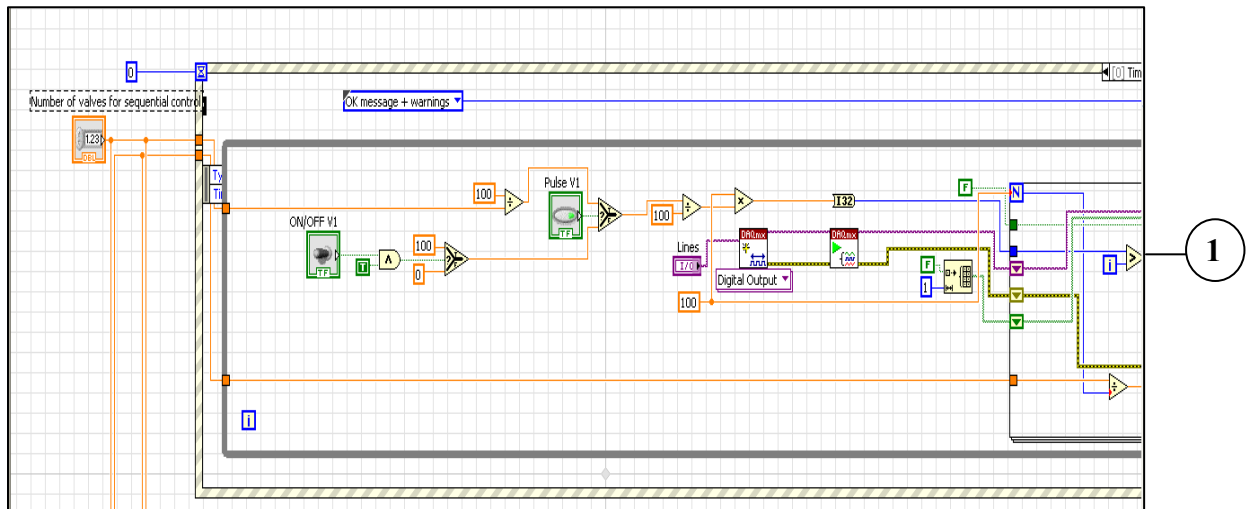
Figure 6. NI USB-6008/6009 Pinout

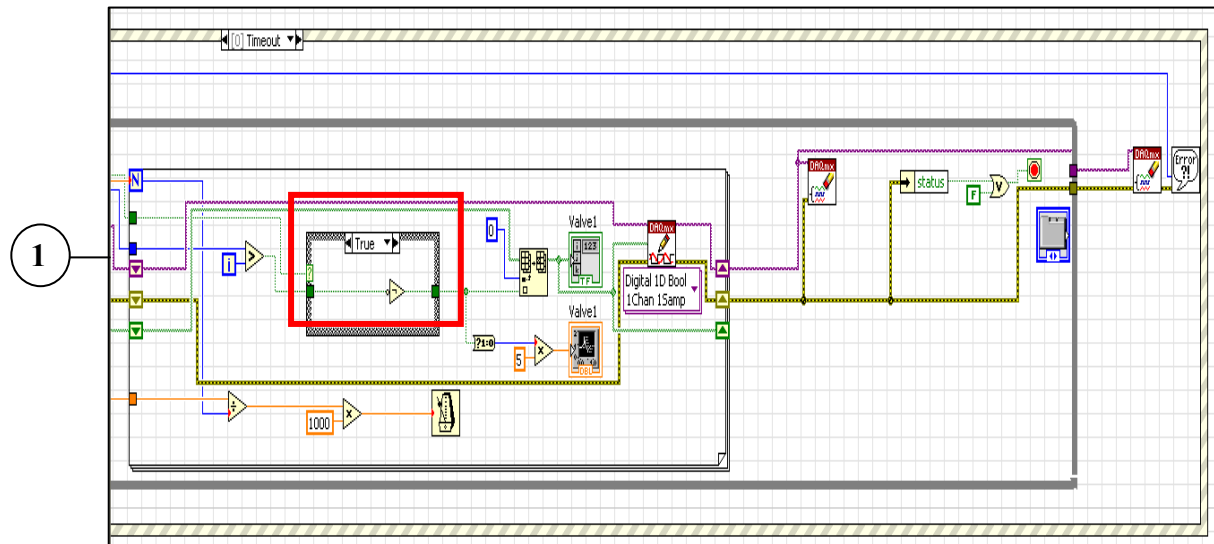
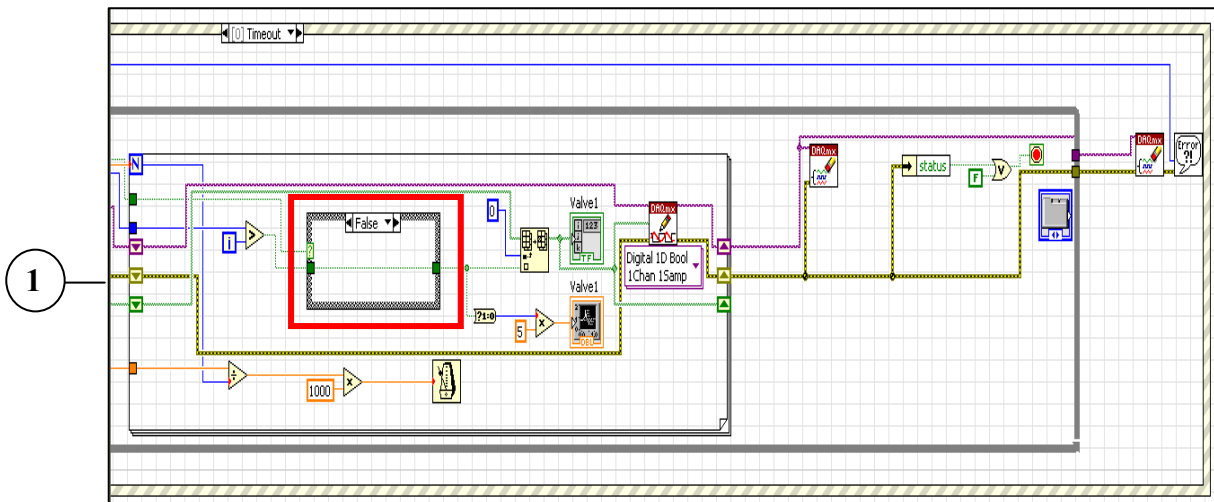
2. General purpose software for 8-valves control

2.1. Graphical interface



2.2. Flow diagram. (This program is repeated n-times according with the number of valves).





3. Recycling flow control

3.1. Graphical interface

VALVES CONTROL SOFTWARE V1.0
Nanobioelectronics and Biosensors Group
Catalan Institute of Nanotechnology

NANO Nanobioelectronics & Biosensors Group
ICN⁹ Institut Català de Nanotecnologia

Port assignation
NI USB-6008

Period of output signal [ms]
0

Lines definition

Valve1	Dev1 (port0)line0.7
Valve2	Dev1 (port0)line0.7
Valve3	Dev1 (port0)line0.7
Valve4	Dev1 (port0)line0.7
Valve5	Dev1 (port0)line0.7

Valve configuration
Manual control

Valve PWM Signals

Valve1

Valve2

Valve3

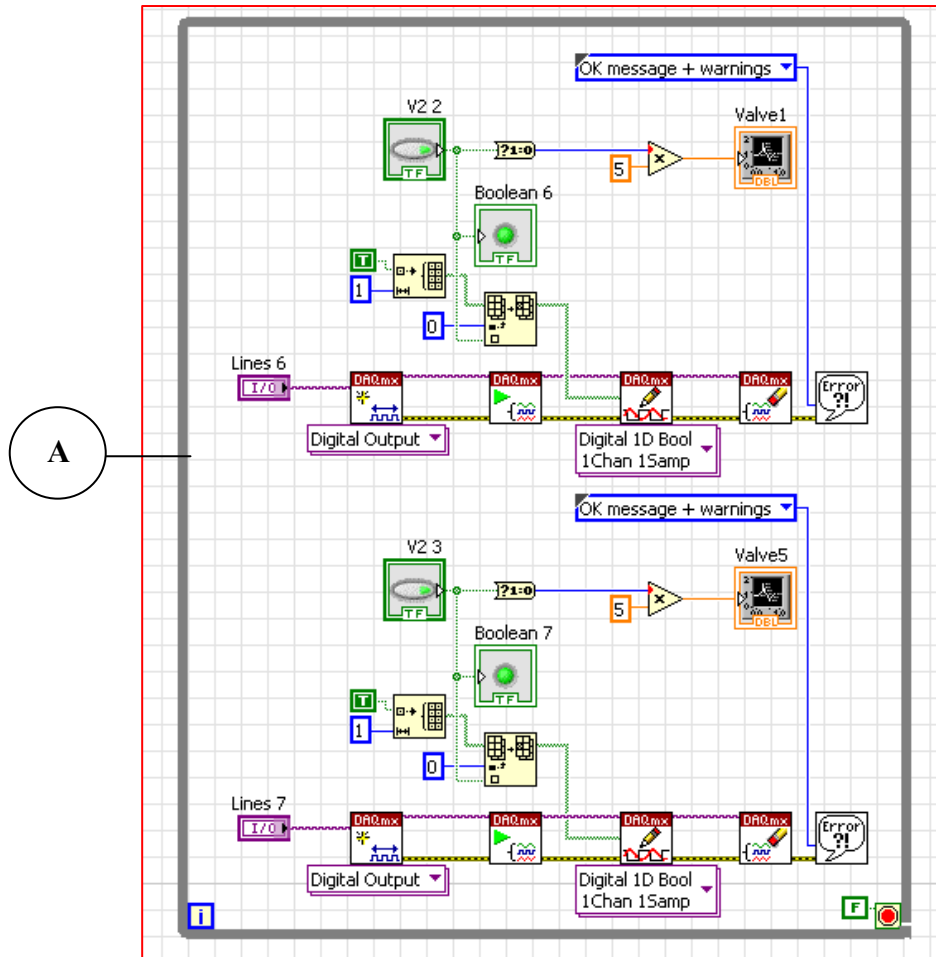
Valve4

Valve5

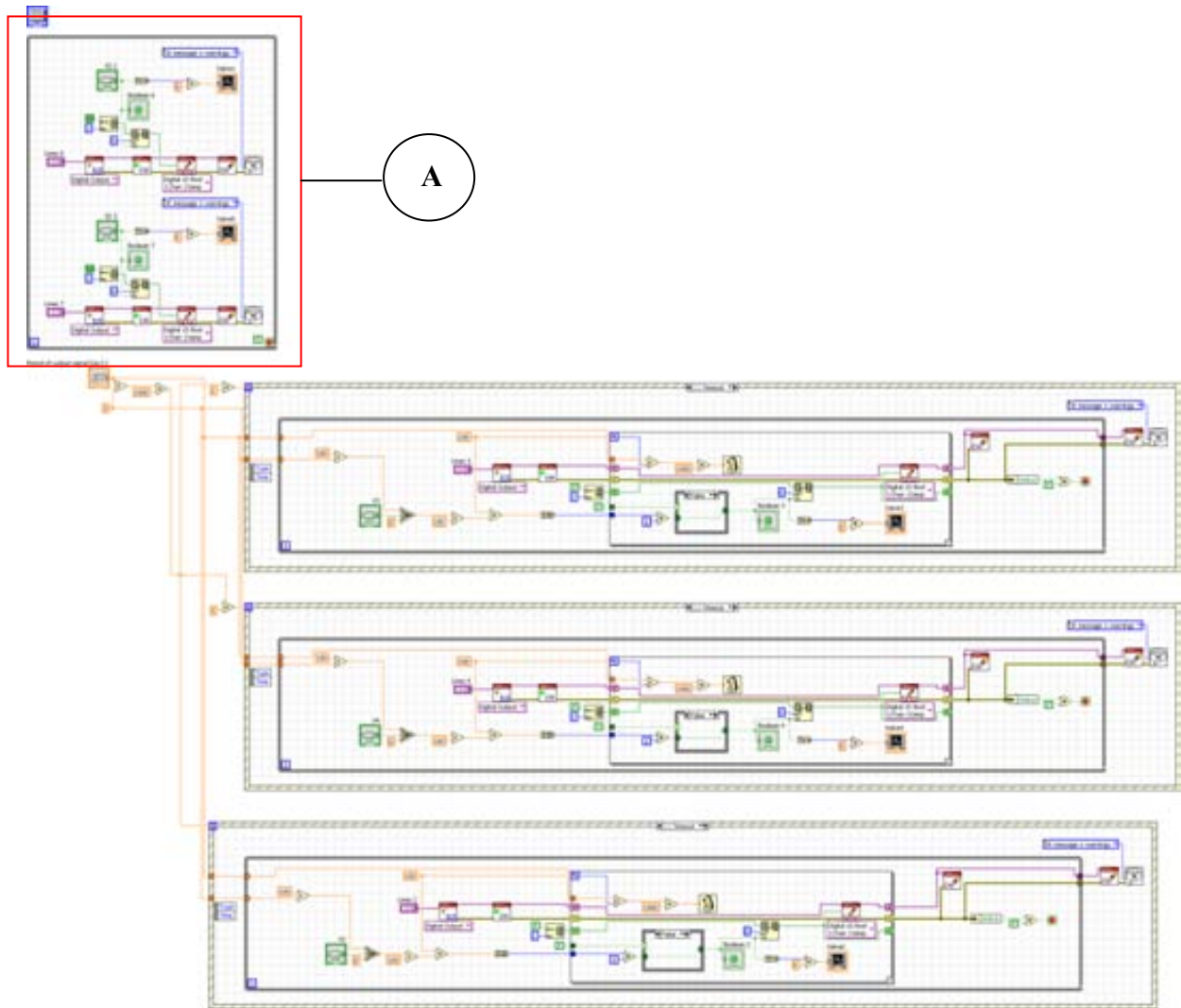
Manuela Medina Sánchez

3.2. Diagram flow

Initial conditions



Complete sequence



4. Arduino UNO program for 3-valve controlling

```
// Pin 13 has an LED connected on most Arduino boards.
// give it a name:
int led1 = 13;
int led2 = 12;
int led3 = 11;
// the setup routine runs once when you press reset:
void setup() {
  // initialize the digital pin as an output.
  pinMode(led1, OUTPUT);
  pinMode(led2, OUTPUT);
  pinMode(led3, OUTPUT);
}
// the loop routine runs over and over again forever:
void loop() {
  digitalWrite(led1, HIGH);
  digitalWrite(led3, HIGH);
  digitalWrite(led2, LOW);
  // second step of the sequence
  delay(500);      // wait for a second
  digitalWrite(led1, LOW);
  digitalWrite(led3, LOW);
  digitalWrite(led2, HIGH);
  // third step of the sequence
  delay(500);
  digitalWrite(led1, LOW);
```

```
digitalWrite(led3, HIGH);  
digitalWrite(led2, LOW);  
  // turn to the first step of the sequence  
delay(500);  
}
```


ANNEX 4

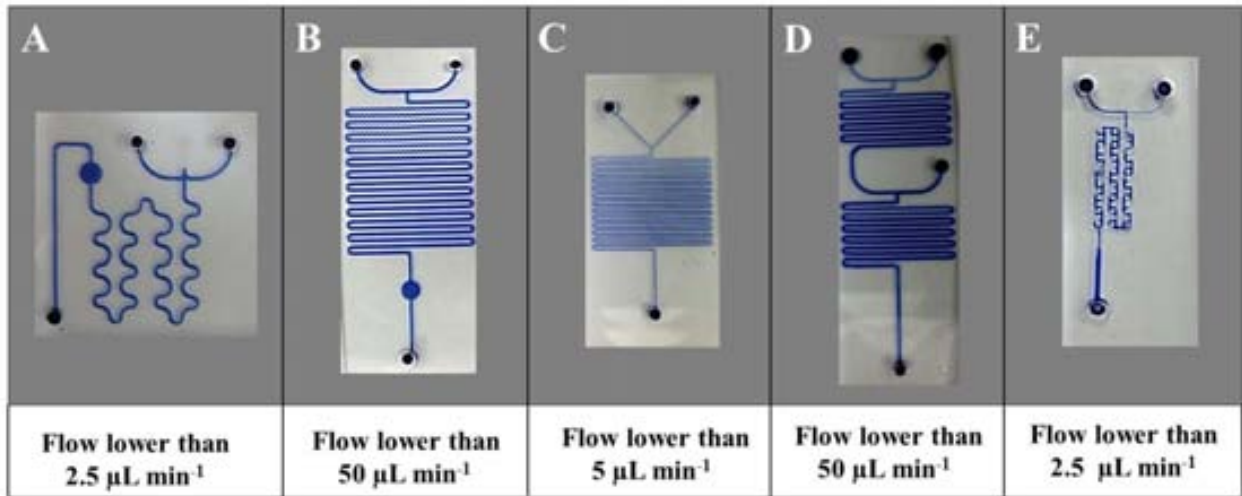


Figure 1. Different mixers with the respective minimum flow need to obtain an optimal mixing at the end of the channel.

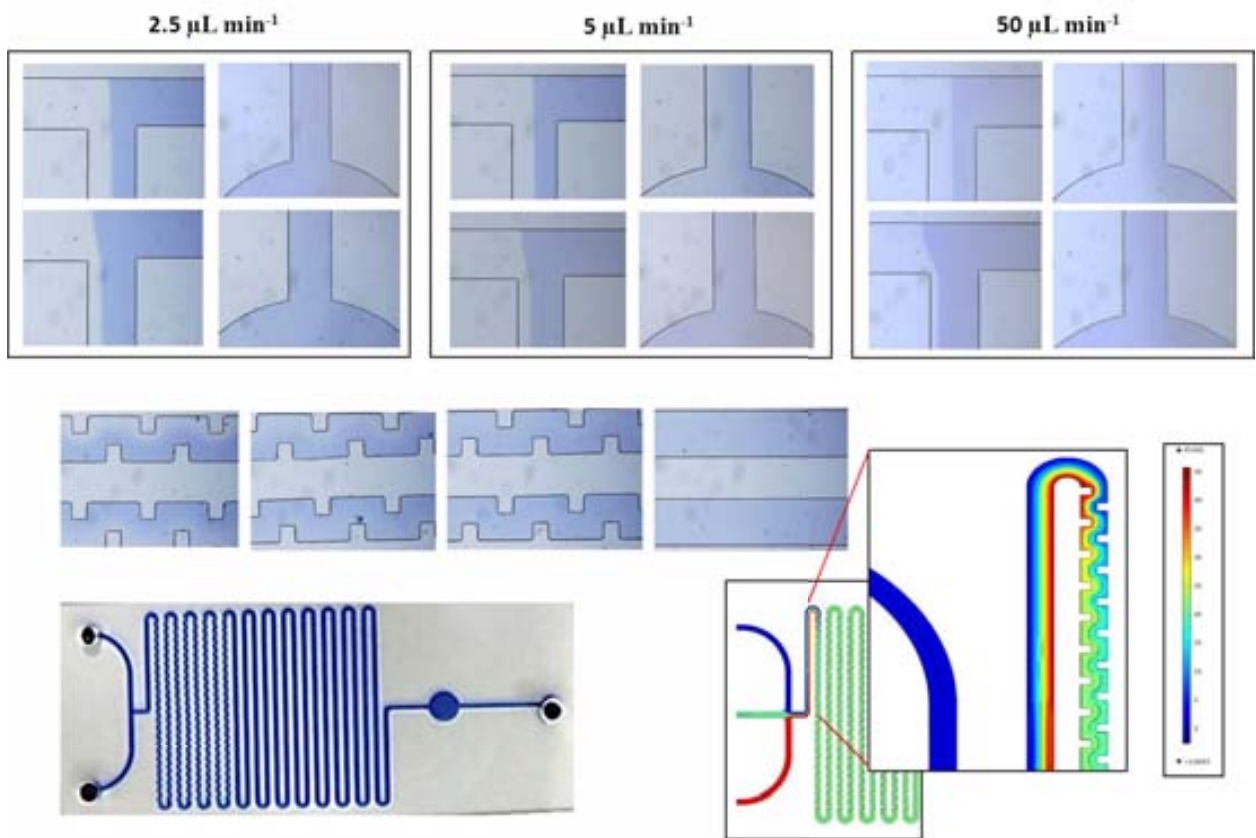


Figure 2. The chosen mixer, its performance at different flow rates, as well as its respective simulation.

